Aix*Marseille université
Socialement engagée

NNT : 0000AIXM0000

THÈSE DE DOCTORAT

Soutenue à Aix-Marseille Université
le 15 décembre 2023 par

Pamela FIERRO GONZÁLEZ

Structure and functioning of zooplankton communities in the Mediterranean Sea and Tunisian coasts: Contributions of two oceanographic campaigns in spring-summer 2019

Discipline

SCIENCES DE L'ENVIRONNEMENT

Spécialité
Océanographie

École doctorale

ED 251- SCIENCES DE L'ENVIRONNEMENT

Laboratoire/Partenaires de recherche
Institut Méditerranéen d'Océanologie (MIO)

Composition du jury

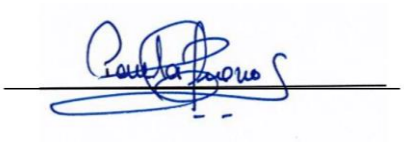
Dr. Maria Grazia Mazzocchi Stazione Zoologica Anton Dohrn	Rapporteur
Pr. Habib Ayadi Université de Sfax	Rapporteur
Dr. Camila Fernández LOMIC, Observatoire Océanologique de Banyuls	Examinatrice
Dr. France Van Wambeke MIO, Aix-Marseille Université	Présidente
Dr. François Carlotti MIO, Aix-Marseille Université	Directeur de thèse
Dr. Marc Pagano MIO, Aix-Marseille Université	Co-directeur de thèse

mio Mediterranean Institute of Oceanography

Affidavit

I, undersigned, Pamela Fierro González , hereby declare that the work presented in this manuscript is my own work, carried out under the scientific supervision of Dr. François Carlotti of thesis director and Dr. Marc Pagano of co-thesis director, in accordance with the principles of honesty, integrity and responsibility inherent to the research mission. The research work and the writing of this manuscript have been carried out in compliance with both the French national charter for Research Integrity and the Aix-Marseille University charter on the fight against plagiarism.

This work has not been submitted previously either in this country or in another country in the same or in a similar version to any other examination body.



Marseille, Octobrer 06, 2023

Cette œuvre est mise à disposition selon les termes de la Licence Creative Commons Attribution - Pas d'Utilisation Commerciale - Pas de Modification 4.0 International.

Liste de publications et/ou brevets et participation aux conférences

1) Liste des publications et/ou brevet [1] réalisées dans le cadre du projet de thèse :

1. **Fierro-González, P.**, Pagano, M., Guilloux, L., Makhlouf Belkahia, N., Tedetti, M., Carlotti, F., 2023. Zooplankton biomass, size structure, and associated metabolic fluxes with focus on its roles at the chlorophyll maximum layer during the plankton-contaminant MERITE-HIPPOCAMPE cruise. Marine Pollution Bulletin 193 (2023) 115056 https://doi.org/10.1016/j.marpolbul.2023.115056

2. Tesán-Onrubia, J.A., Tedetti, M., Carlotti, F., Tenaille, M., Guilloux, L., Pagano, M., Lebreton, B., Guillou, G., **Fierro-González, P.**, Guigue, C., Chifflet, S., Garcia, T., Boudriga, I., Belhassen, M., Bellaaj-Zouari, M., Bănaru, D., 2023. Spatial variations of stable isotope compositions and biochemical content of size-fractionated plankton in the Mediterranean Sea (MERITE-HIPPOCAMPE campaign). Marine Pollution Bulletin, 189 (2023) 114787 https://doi.org/10.1016/j.marpolbul.2023.114787

3. Tedetti, M., Tronczynski, J., Carlotti, F., Pagano, M., Sammari, C., Bel Hassen, M., Ben Ismail, S., Desboeufs, K., Poindron, C., Chifflet, S., Abdennadher, M., Amri, S., Bănarua, D., Ben Abdallah, L., Bhairy, N., Boudriga, I., Bourin, A., Brach-Papa, C., Briant, N., Cabrol, L., Chevalier, C., Chouba, L., Coudray, S., Daly Yahia, M.N., de Garidel-Thoron, T., Dufour, A., Dutay, J.-C., Espinasse, B., **Fierro-González, P.**, Fornier, M., Garcia, N., Giner, F., Guigue, C., Guilloux, L., Hamza, A., Heimbürger-Boavida, L.-E., Jacquet, S., Knoery, J., Lajnef, R., Makhlouf Belkahia, N., Malengros, D., Martinot, P.L., Bosse, A., Mazur, J.-C., Meddeb, M., Misson, B., Pringault, O., Quéméneur, M., Radakovitch, O., Raimbault, P., Ravel, C., Rossi, V., Rwawi, C., Sakka Hlaili, A., Tesán Onrubia, J.A., Thomas, B., Thyssen, M., Zaaboub, N., Zouari, A., Garnier, C., 2023. Contamination of planktonic food webs in the Mediterranean Sea: Setting the frame for the MERITE-HIPPOCAMPE oceanographic cruise (spring 2019). Marine Pollution Bulletin, 189 (2023) 114765 https://doi.org/10.1016/j.marpolbul.2023.114765

[1] Cette liste comprend les articles publiés, les articles soumis à publication et les articles en préparation ainsi que les livres, chapitres de livre et/ou toutes formes de valorisation des résultats des travaux propres à la discipline du projet de thèse. La référence aux publications doit suivre les règles standards de bibliographie et doit être conforme à la charte des publications d'AMU.

4. Carlotti, F., Gerigny, O., Bienvenu, D., Ravel, C., **Fierro-González, P.**, Guilloux, L., Makhlouf Belkahia, N., Tesán-Onrubia, J.A., Pagano, M., 2023. Microplastics in the maximum chlorophyll layer along a north-south transect in the Mediterranean Sea in comparison with zooplankton concentrations. Marine Pollution Bulletin, (accepted)

2) Participation aux conférences[2] et écoles d'été au cours de la période de thèse :

1. 29ème congress **"**Ecole Doctorale des sciences de l'environnement de l'Université Aix-Marseille" - 5 - 6 May 2022, Marseille, France. « Comparative zooplankton structure and functioning in epipelagic layers of different mediterranean regions during the HIPPOCAMPE cruise". **Fierro-González, P.**, Pagano, M., Guilloux, L., Makhlouf Belkahia, N., Carlotti, F. Oral format.

2. 2nd meeting of the IBERIAN Ecological Society (SIBECOL), 3-8 July 2022, Aveiro, Portugal. "Structure and functioning of mediterranean zooplankton communities". **Fierro-González, P.**, Pagano, M., Guilloux, L., Makhlouf Belkahia, N., Carlotti, F. Poster format.

[2] Le terme « conférence » est générique. Il désigne à la fois « conférence », « congrès », « workshop », « colloques », « rencontres nationales et/ou internationales » … etc.

Résumé

Cette étude se concentre sur l'analyse des communautés zooplanctonique dans la mer Méditerranée occidentale (MMO), en utilisant les données de deux campagnes en 2019. La première, MERITE-HIPPOCAMPE s'est déroulée en avril-mai, le long d'un transect nord-sud des côtes françaises à tunisiennes, dans le but de fournir des informations sur le transfert de contaminants au sein du réseau trophique planctonique. Ce projet s'est particulièrement concentré sur la collecte d'échantillons de plancton dans la couche du maximum de chlorophylle (CMC), ainsi qu'en surface et dans la colonne d'eau, en utilisant des filets à zooplancton de différentes mailles. MOOSE-GE 19, en juin-juillet, a couvert la majeure partie du nord de MMO. Elle s'inscrit dans le cadre d'une observation annuelle des paramètres physiques, chimiques et biologiques visant à identifier et caractériser les réponses de l'écosystème au changement climatique et aux influences anthropogéniques.

Nos analyses comprenaient des mesures d'abondance, de biomasse, de diversité et de distribution de tailles du zooplancton. Les outils d'imagerie numérique FlowCam et ZOOSCAN ont été utilisés de manière complémentaire pour couvrir les gammes de taille allant du petit zooplancton (60 µm-200µm) au mésozooplancton (> 200 µm). Le biovolume, la biomasse et les flux trophiques et métaboliques ont été dérivés de relations allométriques. La microscopie classique a été utilisée pour obtenir une résolution taxonomique plus fine.

La stratégie Hippocampe a permis de comparer les communautés de zooplancton échantillonnées par des filets verticaux classiques dans la couche épipélagique (max 200m), avec celles échantillonnées par des filets horizontaux à la surface et au CMC, ce dernier étant également ciblé pour les études sur les contaminants par le consortium Hippocampe. Les échantillons prélevés au filet horizontal ont montré des spécificités dans les communautés de ces strates : hyponeuston en surface, organismes agrégés (nauplii, petits copépodes) ou évitants (appendiculaires) les fortes accumulations détritiques au CMC. Les différences de composition du zooplancton entre classes de taille successives considérées pour l'analyse des contaminants suggèrent un changement trophique progressif allant de l'herbivorie dominante dans les fractions les plus petites à une structure trophique plus contrastée (incluant la carnivorie) dans les fractions les plus grandes, donnant des informations pertinentes pour la compréhension des flux de contaminants.

Le regroupement des observations des filets verticaux de MOOSE et d'Hippocampe a permis d'évaluer les patrons d'abondance, de structure de communauté et d'importance fonctionnelle du zooplancton dans l'ensemble de la MNO. Les différences spatiales ont mis en évidence une séparation claire à la bordure méridionale du front des Baléares. La contribution décroissante des copépodes du nord au sud est compensée par celles des

organismes gélatineux et crustacés en haute mer, ou celles des ptéropodes et du méroplancton sur la marge tunisienne.

Dans le Bassin Provençal, la zone centrale profonde qui inclut la zone de convection profonde, présente une communauté zooplanctonique dominée par des copépodes herbivores qui se maintenant au printemps et en été, et s'étendant jusqu'à la Mer Ligure. La périphérie de cette zone, comprenant la zone des accores du plateau du Golfe du Lion - au nord - et la branche de retour du gyre cyclonique de MNO - à l'ouest et au sud -, héberge une communauté plus mature avec une plus grande diversité trophique. Au sud, les stations de la marge orientale tunisienne et du bassin algérien étaient relativement similaires en termes de zooplancton et de variables environnementales, liées par les eaux atlantiques de surface. L'impact estimé du broutage sur le phytoplancton était le plus élevé dans cette région méridionale. Nos résultats suggèrent que le zooplancton pourrait être pris en compte dans des analyses de régionalisation plus fines.

Mots clés : Métazooplancton, Distribution spatiale, Mer Méditerranée nord-occidentale, Lien avec les structures environnementales, Flux trophiques.

Abstract

This study focuses on analyzing the dynamics of zooplankton communities in the western Mediterranean Sea (WMS), using data collected during two expeditions in 2019. The first cruise, MERITE-HIPPOCAMPE occurred between April and May, along a north-south transect from French to Tunisian coasts, with the goal to provide information on the transfer of contaminants within the planktonic food web. This project specifically focused on collecting plankton samples at the chlorophyll maximum layer (CML), along with surface and water column samples, using zooplankton nets of different mesh sizes. The MOOSE-GE 19 expedition, conducted between June and July, covered most of the northern WMS. This is part of an annual monitoring effort of physical, chemical and biological observations for identifying and characterizing ecosystem responses in the context of climate change and anthropogenic influences. There, zooplankton sampling was realized through water column with different size-mesh (60 and 120 µm).

Our analyses included measurements of zooplankton abundance, biomass, diversity and size distribution. The digital imaging tools FlowCam and ZOOSCAN were complementary used to cover size ranges from small zooplankton (60 µm-200 µm) to mesozooplankton (> 200 µm). The treated data allowed to derive biovolume, biomass and trophic and metabolic fluxes from allometric relationships. In addition, classical microscopy was used to get a finer resolution of taxonomic description.

The MERITE-HIPPOCAMPE strategy made it possible to compare the characteristics of zooplankton communities sampled by classical vertical net tows in the epipelagic water column (max 200m), with those sampled by horizontal nets at the surface and at the CML, the latter being also targeted for the contaminant studies by the MERITE-HIPPOCAMPE consortium. Horizontal net samples showed specificities in the communities of these strata : hyponeuston at the surface, organisms aggregated to (nauplii, small copepods) or repelled by (appendicularians) strong detrital accumulations at the CML. Differences in zooplankton composition between the successive size classes considered for contaminant analyses suggested a progressive trophic shift from dominant herbivory in the smallest fractions to more contrasted trophic structure (including carnivory) in the largest fractions, giving relevant information for understanding contaminant fluxes.

Coupling MOOSE-GE 19 and MERITE-HIPPOCAMPE observations of vertical nets allowed us to assess patterns of abundance, community structure and functional importance of zooplankton across the WMS in comparison with previous studies. Spatial differences were highlighted with a clear separation at the level of the Balearic - South Sardinia line which corresponds to the southern rim of the Balearic front. The zooplankton composition showed a decreasing copepod contribution from North to South, compensated by an increasing contribution of either gelatinous or other crustacean organisms in the open sea, or pteropods and meroplankton organisms on the Tunisian margin.

In the Provencal basin, the deep-sea central zone that includes the deep convection area presented a zooplankton community dominated by herbivorous copepods which maintained over the two observed seasons (spring-summer) and extended from the Gulf of Lion to the Ligurian Sea. The periphery of this central zone, comprising the shelf break zone of the Gulf of Lion - in the north - and the return *branch* of the cyclonic gyre in the north WMS - in the west and south -, hosted a more mature community with a greater diversity of trophic groups. In the south, the stations of the Tunisian eastern margin and the Algerian basin were relatively similar both in terms of zooplankton communities and environmental variables, possibly with an effect of the circulation of Atlantic waters. The estimated grazing impact on phytoplankton was the highest in this southern region.

Finally, our results suggest that zooplankton, could be taken into account in finer regionalization analyses.

Key words: Metazooplankton, Spatial distribution, North Western Mediterranean Sea, Linkage with environmental structures, Trophic fluxes.

Acknowledgements

I would like to thank my two supervisors, Dr. François Carlotti and Dr. Marc Pagano, for their guidance, support throughout the development of my doctoral thesis, and for giving me the opportunity to advance my career in this place. François Carlotti, I want to thank you for the time, the knowledge you shared. Marc Pagano, I am thankful for the didactic scientific training you provided whenever possible and your willingness to always assist me, even in personal matters as a foreigner.

I extend my thanks to Dr. Maria Grazia Mazzocchi, Pr. Habib Ayadi, Dr. Camila Fernández, and Dr. France Van Wambeke for agreeing to be part of my thesis defense. Marc Tedetti, Daniela Barnau, and Camila Fernández, I appreciate your unfailingly friendly disposition and the valuable feedback during our annual committee meetings throughout the progress of this project, both professionally and personally.

I would also like to acknowledge the team of individuals involved in collecting samples for the campaigns: MERITE-HIPPOCAMPE (support by the French Oceanographic Fleet, CNRS/INSU, IFREMER, IRD, the Tunisian Ministry of Agriculture, Water Resources and Fisheries and the Tunisian Ministry of Higher Education and Scientific Research) and MOOSE-GE 19 (Supported by the MISTRALS- MERMEX and MOOSE programs of CNRS-INSU). Thanks to the MIM platform for providing the imaging facilities. Special thanks to Loïc Guilloux for his kindness, patience, and help in laboratory matters. For teaching me how to use ZOOSCAN and his help in image processing using ZOOPROCEES and Ecotaxa. His taxonomic classification of MOOSE-GE 2019 samples was also immensely valuable. I would also like to thank Nouha Makhlouf for her taxonomic identification on the MERITE-HIPPOCAMPE samples, and Guillermo Feliú for teaching me how to use FlowCAM. Thanks to Becas-Chile N ◦ 72190675 PhD scholarship from the Agencia Nacional de Investigación y Desarrollo (ANID), Gobierno de Chile.

I am grateful to my friends who made these years much more welcoming: Lydvina for her immense and genuine solidarity and concern, for saving me countless times from bureaucracy. To my friends and compatriots Claudia, Mercedes, and Pablo, for all those good times.

A special thanks to Ángel and Feña for being my family in every sense of the word, for surviving a pandemic together with cheese, good wine, and movies. Mario Hugo, the best support dog I've ever known. You've left an indelible mark on my life. To my friends who continue to be there despite the distance, I feel your enormous affection: Carolina Burgos, Sonia, Belén, Iris, Selim, and Carolina Pérez.

I thank my family in Chile, Dad and Seba, for believing in my abilities and supporting me so generously on this journey. Mom, you're always in my thoughts. I love you.

Finally, to my Chipi chipi, the void you left will always be felt in the places you inhabited.

Table of contents

Affidavit 3
Liste de publications et/ou brevets et participation aux conférences 5
Résumé 7
Abstract 9
Acknowledgements 11
Table of contents 13
List of figures 15
List of tables 17
1. General Introduction 19
1.1. The Mediterranean Sea 19
1.1.1. Water masses and basin circulation in the Mediterranean Sea 20
1.1.2. Characteristics of main regions in the Mediterranean Sea considered is 23
1.1.3. The region of deep convection 24
1.1.4. Observed modifications in biodiversity linked to global changes 33
1.2. Zooplankton in the Mediterranean Sea 36
1.2.1. Zooplankton community in the North Western Mediterranean Sea 37
1.2.2. The zooplankton size spectrum 38
1.2.3. The importance of small metazooplankton 40
1.3. Roles of zooplankton in the ecosystems 40
1.4. Objective of this thesis 43
2. Materials and Methods 45
2.1. Study area 45
2.2. Environmental data 46
2.2.1. CTD profiles and Nutrients for MERITE-HIPPOCAMPE and MOOSE-GE 46
2.2.2. Mixed layer depth calculations 47
2.3. Zooplankton sampling 47
2.3.1. Sample analysis and image treatment 48
2.3.2. Data analysis of plankton abundance and community structure 55
2.3.3. Data analysis of plankton group biomass and fluxes 57
2.4. Statistical analysis 59
3. The MERITE-HIPPOCAMPE campaign. 61
3.1. Introduction about MERITE-HIPPOCAMPE program 61
3.1.1. Objectives of the campaign 61
3.1.2. Design of the campaign 62
3.1.3. Importance to characterize biota and zooplankton 63
3.2. Zooplankton biomass, size structure, and associated metabolic fluxes with focus on its roles at the chlorophyll maximum layer during the plankton-contaminant MERITE-HIPPOCAMPE cruise. Fierro-González et al., 2023 64
3.2.1. Introduction 64
3.2.2. Material and methods 65

3.2.3. Results 70
3.2.4. Discussion 86
3.2.5. Conclusion 92
3.3. General conclusion on the role of zooplankton for MERITE-HIPPOCAMPE 93
3.3.1. Additional information provided for the study of the biochemistry and isotope ratios of zooplankton size fractions 93
3.3.2. Major inputs of Zooplankton analyses for contaminants 96
4. Zooplankton structure and functioning during MOOSE-GE 2019 campaign 99
4.1. Introduction 99
4.2. Materials and Methods 101
4.3. Results 104
4.3.1. Spatial patterns in the environment 104
4.3.2. Spatial patterns of zooplankton from imagery treatment 107
4.3.3. Spatial patterns of zooplankton from microscopy analysis 112
4.3.1. Fluxes through zooplankton 121
4.4. Discussion 124
4.4.1. Environmental context 124
4.4.2. Zooplankton abundance, biomass, community structure, and diversity during the MOOSE-GE 2019 cruise 125
4.5. Conclusion 131
5. General discussion and perspectives 133
5.1. General discussion on the Mediterranean zooplankton characteristics across the Western Mediterranean Sea 133
5.1.1. Patterns of abundance and community structure of zooplankton across the Western Mediterranean Sea 133
5.1.2. Functional importance of zooplankton across the Western Mediterranean Sea in terms of biomasses and fluxes 138
5.2. How our results on environment and zooplankton can characterize different regions in the western Mediterranean Sea? 141
5.2.1. Grouped data analyses of the two campaigns 141
5.2.2. How the results fit with proposed models of regionalization? 143
5.3. Concluding remarks and perspectives 145
References 146
ANNEXES 163
Annexes for Chapter 2 163
Annexes for Chapter 3 165
Annexes for Chapter 4 171
Annex : Publication 179

List of figures

Figure 1.1. Domain and bathymetry of the Mediterranean Sea 19
Figure 1.2. Circulation of Atlantic Waters in the Mediterranean Sea 20
Figure 1.3. Circulation of the Modified Atlantic Water for the Western basin 22
Figure 1. 4. Circulation of the Levantine Intermediate Water from the Easter basin 23
Figure 1.5. Maps from three regionalization of the Mediterranean Sea 24
Figure 1.6. Map of the area of deep convection in the Western Mediterranean Sea 25
Figure 1. 7. Sea surface temperature in the Mediterranean Sea 27
Figure 1.8. Deep convection depths from 2007-2022 in the North-Western Mediterranean 28
Figure 1.9: Spatial distributions of nutrient concentrations averaged from 1999 to 2004 30
Figure 1.10: Sea surface chlorophyll distribution in the Mediterranean Sea 32
Figure 1.11: Phytoplankton type-based ecoregions of the Mediterranean Sea 32
Figure 1.12: Map of the cumulated anthropogenic pressures in the Mediterranean 35
Figure 1.13. Summary of spatial distributions of zooplankton in Mediterranean Sea 37
Figure 1.14: Dominant copepod in the Mediterranean Sea from Siokou Frangou et al., (2010) 38
Figure 1.15 Planktonic composition within large size-fractions 39
Figure 1.16: Main pathways involving zooplankton in the cycling and export of carbon in oceanic ecosystem 41
Figure 1.17: Processes involved in carbon consumption and metabolism by zooplankton. 42
Figure 2.1. Map showing the sampling stations during the cruises 46
Figure 2.2. The zooplankton nets employed during the cruises 48
Figure 2.3. Representation of the methodology for sample collections and treatments during the cruises 49
Figure 2.4. Protocol steps outline for processing a zooplankton sample in FlowCAM. 51
Figure 2.5. Methodology employed for zooplankton sample analysis 52
Figure 2.6. Protocol steps outline for processing a zooplankton sample in ZOOSCAN. 52
Figure 2.7. Image analysis process conducted using ZOOPROCESS 55
Figure 2.8. Two RFD with linear regressions for the first 4 ranks and the other ranks 57
Figure 3.1. Map of sampled stations during the two legs of the MERITE-HIPPOCAMPE cruise 66
Figure 3.2. Principal component analysis of environmental indicators and Nonmetric Multi-Dimensional Scaling on zooplankton taxa relative biomass 72
Figure 3.3. Cumulated percentages an total of zooplankton taxa biomasses sampled at each station in the different strata 74
Figure 3.4. Vertical profiles of oceanographic variables 78
Figure 3.5. Plankton and detritus biomasses collected at Chlorophyll Maximum layer 80
Figure 3.6. Plankton and detritus biomasses collected at water column 83
Figure 3.7. Estimation of zooplankton carbon demand, nitrogen excretion and DIN stock 85
Figure 3.8. Contributions size-fractions and zooplankton to the zooplankton carbon demand 86
Figure 3.9. Biomass distribution of detritus, algae, and zooplankton by different size-fractions 94
Figure 3.10. Biomass distribution of zooplankton taxonomic groups by different size fractions 95

Figure 3.11. Mean biomass percentages of detritus, algae, and zooplankton and of zooplankton groups within different zooplankton size-fractions 96
Figure 4.1. Deep convection in the in the northwestern Mediterranean Sea 100
Figure 4.2. The MOOSE observation system with its diverse monitoring tools 101
Figure 4.3. Map of the stations sampled during MOOSE-GE 2019 102
Figure 4.4. Size spectrum of St15 as an example, obtained by FlowCAM and ZOOSCAN 103
Figure 4.5. Hierarchical clustering of environmental variables and map of the stations identified by clustering 105
Figure 4.6. Boxplots for the environnemental variables in the water column 106
Figure 4.7. Vertical distribution profiles of environnemental variables grouped by clusters 106
Figure 4.8. Spatial distributions of zooplankton variables during MOOSE-GE 2019 108
Figure 4.9. Zooplankton abundance and biomass by taxa groups 109
Figure 4.10. Zooplankton abundance and biomass cumulated by ESD size-classes 110
Figure 4.11. Zooplankton biomass percentage by taxa groups for each ESD size-classes 111
Figure 4.12. Comparison between abundances from microscope and FlowCAM + ZOOSCAN 112
Figure 4.13. Rank frequency diagrams grouped by regions 115
Figure 4.14. Linear regression between Adults/Copepodites ratio and p1/p2 ratio 116
Figure 4.15. Spatial distributions of P1/P2 ratio and Adult/Copepodite ratio ; Species richness and Shannon diversity index from microscopic treatment 117
Figure 4.16. Co-inertia analysis 118
Figure 4.17. Spatial distributions of Phytoplankton stock and Zooplankton stock 122
Figure 4.18. Grazing and metabolic rates of zooplankton during MOOSE-GE 2019 123
Figure 5.1. Map of the MERITE-HIPPOCAMPE cruise and the MOOSE-GE 19 expedition 134
Figure 5.2. Joint analyses of environmental and zooplankton variables during the cruises 142
Figure 5.3. Tentative synthesis of our multivariate analysis of environmental variables and zooplankton variables, in regards with proposed ecoregions 143

List of tables

Table 2.1. Summary of the zooplankton groups within the various size fractions 54
Table 3.1. Stations sampled during the MERITE-HIPPOCAMPE cruise 67
Table 3.2. Treatments of the various size-fractions from the three nets used during the MERITE-HIPPOCAMPE cruise 68
Table 3.3. Summary of the biomass for plankton and detritus, and size fractions 82
Table 4.1. Percentages of abundances of all the taxauring MOOSE-GE 2019 113
Table 4.2. Values of diversity indices for all stations based on microscopic counts 114
Table 4.3. Mean abundance of rare and abundant taxa per environmental cluster 119
Table 4.4. Average similarity and dissimilarity, and main contributing taxa 120
Table 4.5. Phytoplankton stock in C, zooplankton stock in C, grazing impact of zooplankton on phytoplankton stock per day, zooplankton carbon demand, zooplankton production and zooplankton P/B ratio by region during MOOSE-GE 2019 121
Table 4.6. Zooplankton nitrogen and phosphorous excretion rates 124
Table 4.7 Comparison of mean values of zooplankton abundance, biomass and taxonomic diversity between MOOSE-GE 2019 and MOOSE-GE 2017 cruises 127
Table 5.1. Comparison of zooplankton abundance and Shannon index in the Mediterranean Sea 137
Table 5.2. Comparison of zooplankton biomass and grazing impact 139
Table 5.3. Phytoplankton stock in C, zooplankton stock in C and Zooplankton/Phytoplankton ratio, in different areas of the Mediterranean Sea during MOOSE-GE 19 cruise 140

1. General Introduction

1.1. The Mediterranean Sea

The Mediterranean Sea is a semi-enclosed basin, connected to the Atlantic Ocean through the Strait of Gibraltar, where depths range from 300 to 900 m. The Strait of Gibraltar is a connection vital for maintaining the delicate balance of freshwater and salt budgets within the Mediterranean (Ciavatta et al., 2019; Criado-Aldeanueva et al., 2012). Additionally, the Mediterranean links to the Black Sea through the Dardanelles / Marmara Sea / Bosphorus system. Nevertheless, the average depth of the entire Mediterranean Sea is approximately 1500 m (Figure 1.1). However, there are areas of even greater depth, notably in the eastern area, where depths can overcome a maximum of 5000 m in the Matapan trench in the Ionian Sea (Cramp et al., 1987).

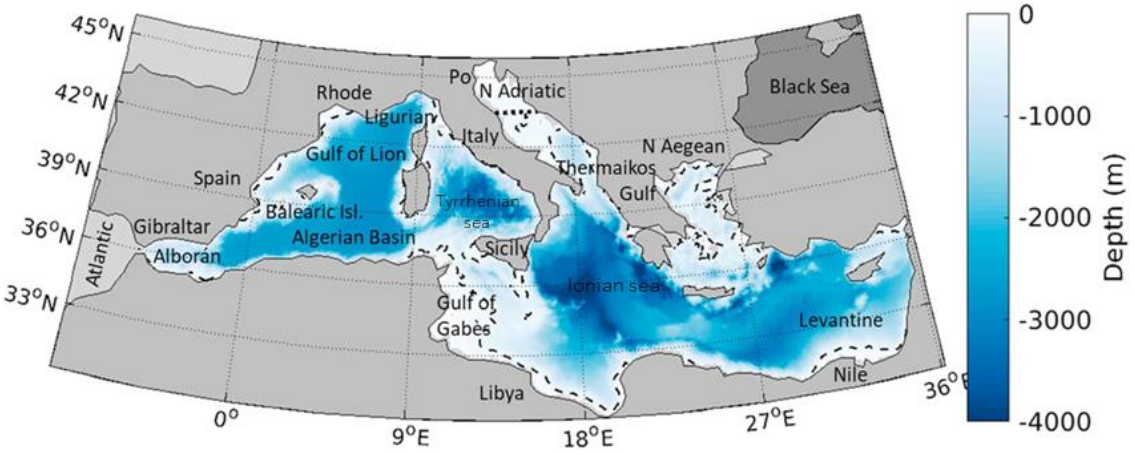


Figure 1.1. Domain and bathymetry of the Mediterranean Sea. The dashed line represents the 200-m isobaths. Figure from Ciavatta et al.(2019).

Geographically, the Mediterranean Sea can be divided into two major sub-basins. The Western Mediterranean consists of several sub-sea basins, which include the Alboran Sea, Algerian Basin, Tyrrhenian Sea, Liguro Provençal basin, Catalan sea and Balearic Sea. It also encompasses the Gulf of Lions. On the other hand, the Eastern Mediterranean comprises two primary sub-sea basins: the Ionian Sea and the Levantine Basin, with the northern region encompassing the Adriatic and Aegean Seas. These two large sub-basins are interconnected through the Sicily Strait, notable for its shallow sill. This feature plays a crucial role in delineating the hydrodynamic and ecological conditions between these two sub-basins (Crise et al., 1999; El-Geziry and Bryden, 2010; Adloff et al., 2015).

1.1.1. Water masses and basin circulation in the Mediterranean Sea

The Mediterranean Sea represents a distinctive and complex ecosystem, often likened to a miniature ocean, featuring a complex water circulation system influenced by various factors (Millot, 1999). It is distinguished by its unique circulation patterns, where both atmospheric and thermohaline elements exert significant influence over the dispersion of water masses and the flow of seawater throughout the basin.

Millot and Taupier-Letage (2005) provided a comprehensive description of the circulation of water masses in the Mediterranean Sea, offering a complete picture of the complex hydrological processes prevailing in the Western Mediterranean. At the Strait of Gibraltar, surface Atlantic Waters (**AW**) enter with temperatures averaging 15.5°C and a relatively low salinity level of 36.2 PSU. These AW follow a path that leads them along the continental slope of the northern African coast up to the Levantine basin (Figure 1.2). As they journey through the Mediterranean, they undergo continuous modifications influenced by meanders and jets, which significantly alter the density structure of the upper-layer water column (Millot and Taupier-Letage, 2005a).

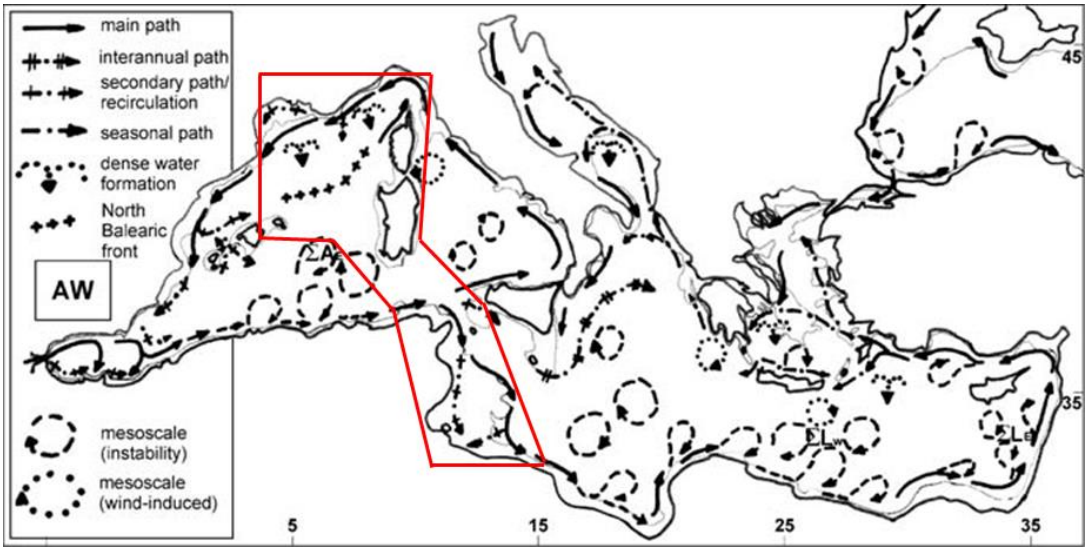


Figure 1.2. Circulation of Atlantic Waters (AW) in the Mediterranean Sea. The thin line represents the 200 m isobath. Figure from Millot and Taupier-Letage (2005). The red frame delineates the covered area of interest for the oceanographic campaigns studied in this thesis.

The circulation of AW in the Mediterranean Sea follows a counter-clockwise surface circuit, tracing the continental slopes of both the Western and Eastern Mediterranean basins(Millot and Taupier-Letage, 2005a). Upon reaching the Strait of Sicily, a shallow gateway that separates the deeper western and eastern basins, the flow bifurcates into two distinct paths: one proceeds northward along the Italian coasts, forming the North Current (Millot, 1999), while the other continues across the Strait of Sicily, eventually reaching the eastern Levantine basin (Gauchery et al., 2021). Along this intricate journey, the AW undergoes further transformations, including potential warming (up to 20–28°C) or cooling (reaching as low as approximately 13°C, or even less in localized areas), increased salinity (up to 38–39 PSU), and enhanced density (reaching up to 28–29).

These transformations ultimately lead to the formation of Modified Atlantic Water (**MAW**). As described by Millot (1999), this surface water creates a layer between 100 and 200 meters in thickness, characterized by increasing salinity levels due to evaporation and mixing. Salinity ranges from approximately 36.5 at Gibraltar to 38.0–38.3 in the North Western Mediterranean Sea (**NWMS**). The average temperature below the mixed layer typically falls between 14 and 15.8°C. It is worth noting that in the Alboran Sea, the recent MAW layer is generally thicker than 200 meters, although it exhibits notable variability over time and space. This encompasses the section of older MAW that concludes its counterclockwise circuit in this sea area, as well as the shallower intermediate waters that flow southward along the Spanish continental slope (Gauchery et al., 2021). At depths less than 200 meters, these waters intersect with the inflow of recent MAW and subsequently change course towards the east (Figure 1.3).

During winter, particularly in the northern part of the Western Mediterranean Sea when moderately strong and cold northwesterly winds prevail, MAW undergoes cooling without experiencing significant mixing with the underlying waters. This process gives rise to the formation of a distinctive water mass known as Winter Intermediate Water (**WIW**). WIW exhibits temperatures ranging from 12.5 to 13.08°C and salinities between 38.1 and 38.3. This water mass forms on the continental shelves, specifically in the Gulf of Lions and the Balearic Sea. Notably, WIW is typically located beneath the MAW in the Balearic Sea (Millot, 1999; see Figure 1. 3).

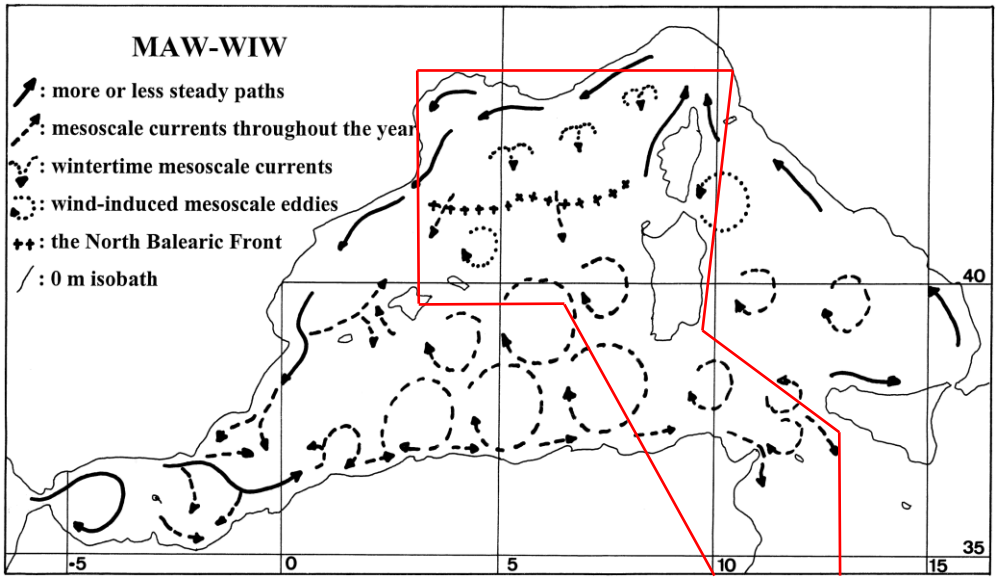


Figure 1.3. Circulation of the Modified Atlantic Water (MAW) and the Winter Intermediate Water (WIW) for the Western Mediterranean Basin. Figure from Millot (1999). The red frame delineates the area of interest for the oceanographic campaigns studied in this thesis.

During winter, air temperature variations increase evaporation, with surface water temperatures decreasing, sharply dropping to 12.5°C in the Northwestern Mediterranean Sea (**NWMS**), 11°C in the Adriatic Sea, and 14°C in the Northern Eastern Mediterranean (Millot and Taupier-Letage, 2005a). This variability triggers vertical mixing, initiating various deep convection processes within the Mediterranean basins. Consequently, different water masses, such as Levantine Intermediate Water (**LIW**) and Western Mediterranean Deep Water (**WMDW**), are formed during the winter convection processes in the region of the Gulf of Lions (Gauchery et al., 2021; Millot and Taupier-Letage, 2005a) (Figure 1. 4). More details about the deep convection process and the ecological impacts are given in section 1.1.3.

Deep waters in the Mediterranean form due to the mixing of cooled surface winter waters with LIW in the northern Adriatic Sea, resulting in Eastern Mediterranean Deep Water, and in the Gulf of Lions, giving rise to Western Mediterranean Deep Water (WMDW; Millot and Taupier-Letage, 2005).

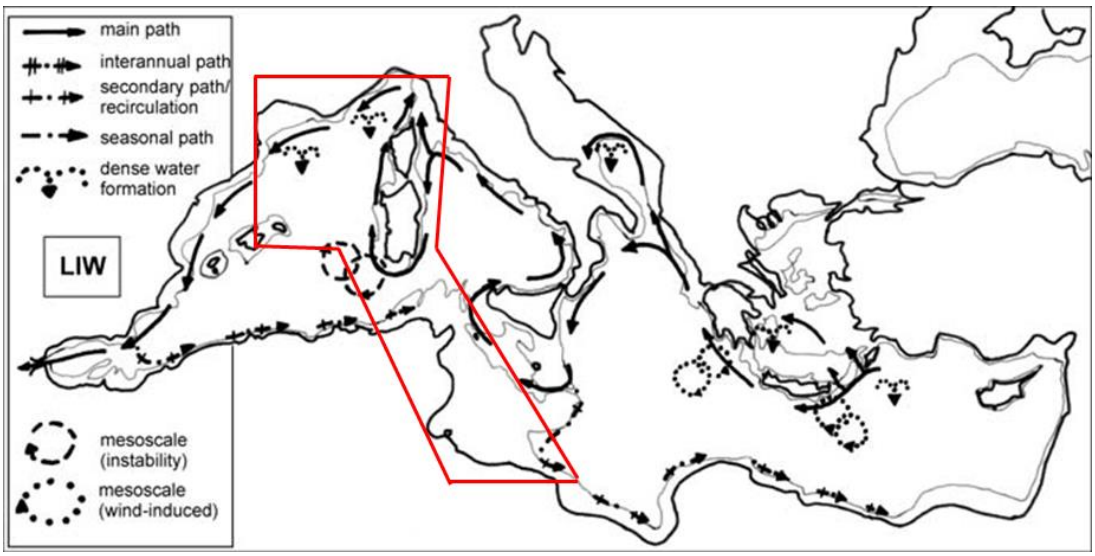


Figure 1. 4. Circulation of the Levantine Intermediate Water (LIW) from the Easter basin to the Western Basin. The thin line represents the 500-m isobath. Figure from Millot and Taupier-Letage (2005). The red frame delineates the area of interest for the oceanographic campaigns studied in this thesis.

1.1.2. Characteristics of main regions in the Mediterranean Sea considered in this thesis

Historically, the Mediterranean Sea has been divided into geographical entities based on features like straits or political boundaries (Ayata et al., 2018). The absence of a consensus on its geographical boundaries poses challenges in describing, managing, and conserving these ecosystems. Different criteria have been used by various authors, such as chlorophyll concentration, oceanic currents, hydrological properties, and organism distribution, to define ecosystem regions within the Mediterranean Sea (Bianchi and Morri, 2000; Coll et al., 2010; Durrieu de Madron et al., 2011; Lejeusne et al., 2010). However, a definitive consensus is yet to be reached, though there are some areas of agreement among the authors (D'Ortenzio and Ribera d'Alcalà, 2009; Mazzocchi et al., 2014).

To guide our discussion of results, we will draw upon the approaches employed by various authors. For instance, Berline et al. (2014) constructed a comprehensive grid covering the entire Mediterranean basin. Based on a hydrodynamics model, they conducted simulations of particle advection from each grid cell over the course of a year and subsequently calculated the average connection time between each pair of cells. Additionally, Mayot et al. (2017) focused on climatology with an emphasis on interannual variability based on sea surface satellite images. Furthermore, Reygondeau et al. (2014)

introduced an ecoregionalization approach that takes into account the biological aspects of ecosystems, specifically the pelagic ecoregionalization (Figure 1.5).

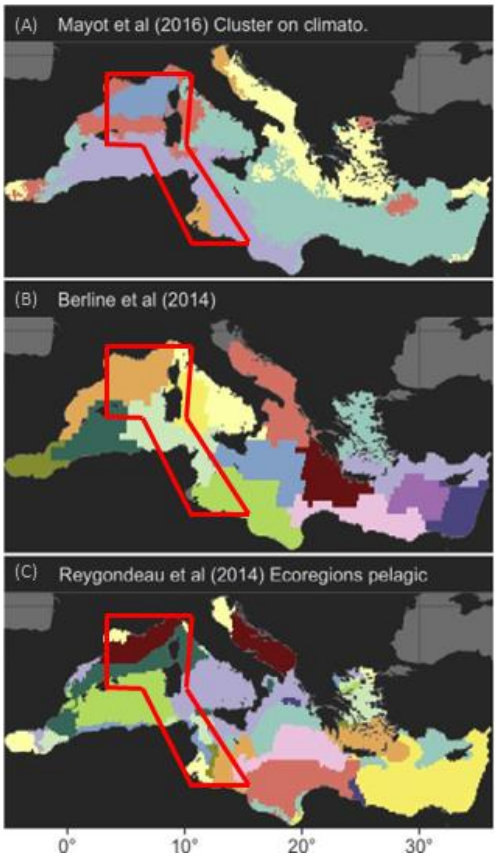


Figure 1.5. Maps from three different approaches employed for the regionalization of the Mediterranean Sea. Colors are used to differentiate regions. Figure from Ayata et al. (2018). From the top to bottom, ecoregion maps from: (A) Mayot et al. (2017), (B) Berline et al. (2014) and (C) Reygondeau et al. (2014). The red frame delineates the area of interest for the oceanographic campaigns studied in this thesis.

1.1.3. The region of deep convection

In the Northwestern Mediterranean Sea (**NWMS**), deep convection is a distinctive phenomenon that results in the formation of dense water extending from the Gulf of Lions to the Ligurian Sea. This process is primarily influenced by the northern gyre, bordered to the north by the Liguro-Provencal-Catalan Current (**LPCC**), also known as the Northern Current (**NC**), and to the south by the North Balearic Front (**NBF**) (see Figure 1.3). This delineation lies between the Modified Atlantic Water (**MAW**) from the Algerian basin and the colder waters of the Liguro-Provençal basin (Figure 1. 6; Schott et al., 1994). The Gulf

of Lion stands as the epicenter for the deepest convection, where the maximum mixed-layer depth ranges from a few hundred meters to 2500 meters during bottom-reaching events (MEDOC GROUP, 1970). According to Ulses et al. (2021), during autumn, the Northern Current and the Balearic Front combine to form a cyclonic gyre. This leads to the doming of isopycnals and upwelling of LIW near the surface (Millot, 1999; Millot and Taupier-Letage, 2005a). When winter arrives, the region experiences the influence of cold and dry northerly winds, such as the Mistral and Tramontane, from the Rhone Valley blowing southward over the Gulf of Lions. This results in a cooling effect, increased evaporation, and heightened density in surface waters. Additionally, there have been reports indicating that this instability may induce convective mixing, potentially giving rise to the formation of new deep waters, a phenomenon observed in 2004–2006, as noted by Schroeder et al. (2008)

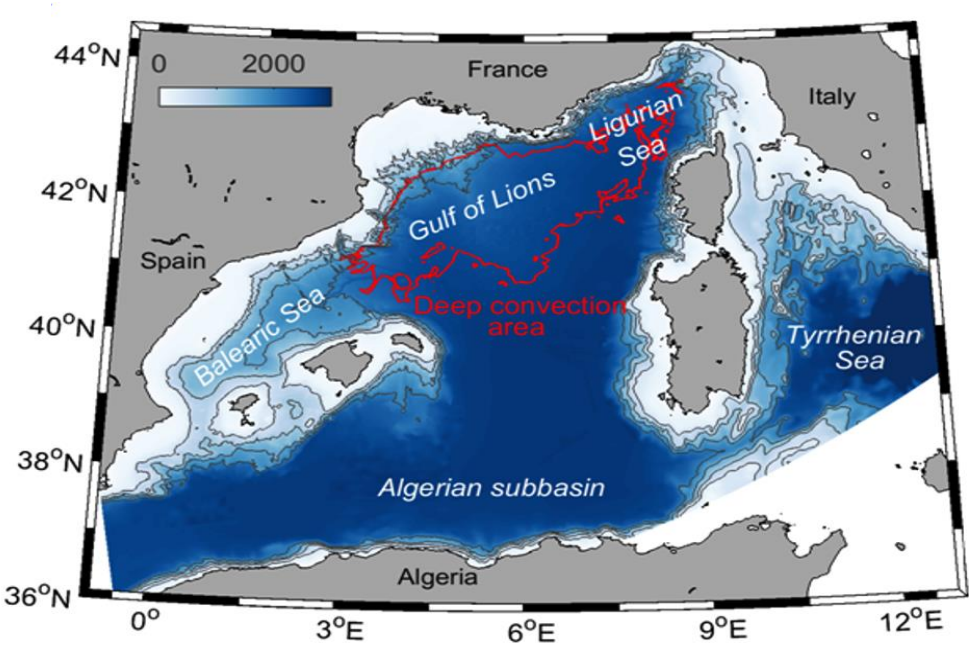


Figure 1.6. Map of the Western Mediterranean Sea, the area of deep convection is outlined within a red frame. Figure from Ulses et al. (2021).

Marshall and Schott (1999) delineated the deep convection process into three primary phases: preconditioning, deep convection, and lateral exchange. During the preconditioning phase, atmospheric forcing, combined with seasonal temperature reduction and strong winds, results in heat loss from the surface layer, leading to decreased temperature and increased salinity due to evaporation. This phase intensifies the mass density anomaly of the surface water. The deep convection phase involves an intensive mixing process that deepens the convection chimney. The subsequent lateral exchange and spreading phase encompasses the sinking and horizontal dispersion of mixed-water fragments, facilitating the stratification of the water column. Importantly, this deep convection profoundly influences the physical and chemical properties of the sea (Millot and Taupier-Letage, 2005), as well as marine productivity.

At the basin-wide scale, the Northwestern Mediterranean emerges as one of the most productive areas in the Mediterranean Sea. Here, deep convection plays a pivotal role in enriching the euphotic layer with nutrients, surpassing contributions from Atlantic, terrestrial, and atmospheric sources (Severin et al., 2014; Kessouri et al., 2017; Ulses et al., 2021).

1.1.3.1. Temperature gradients in the western Mediterranean Sea

As previously explained (Section 1.1.1), the exchange of heat in the Mediterranean Sea occurs through the Strait of Gibraltar with the Atlantic Ocean. Along its path, the AW undergoes a series of changes in properties, including temperature (Figure 1.7, top panel), with the warmest areas being recognized in the Eastern Mediterranean, especially in the southern Ionian Sea and the Levantine Basin. In contrast, the coldest waters are found in the Adriatic Sea, and in the northwestern basin, in the areas of the Ligurian Sea and the Gulf of Lions (Margirier et al., 2020). For the NWMS in the Gulf of Lion, the temperature of the epipelagic layer is substantially influenced by the deep convection, as previously described (Millot and Taupier-Letage, 2005a).

Throughout the year, variations in sea surface temperatures are observed (Figure 1.7, bottom panel). For example, in the western region, during the winter months, surface temperatures reach approximately 15°C in the north, while in the summer months they can rise to 26°C. On the other hand, in the southern zone, temperatures in winter are around 16°C, while in summer they reach 28°C. It is worth noting an increase in the occurrence of marine heat spikes (MHS) in recent years, which occur in different seasons (Juza and Tintoré, 2023).

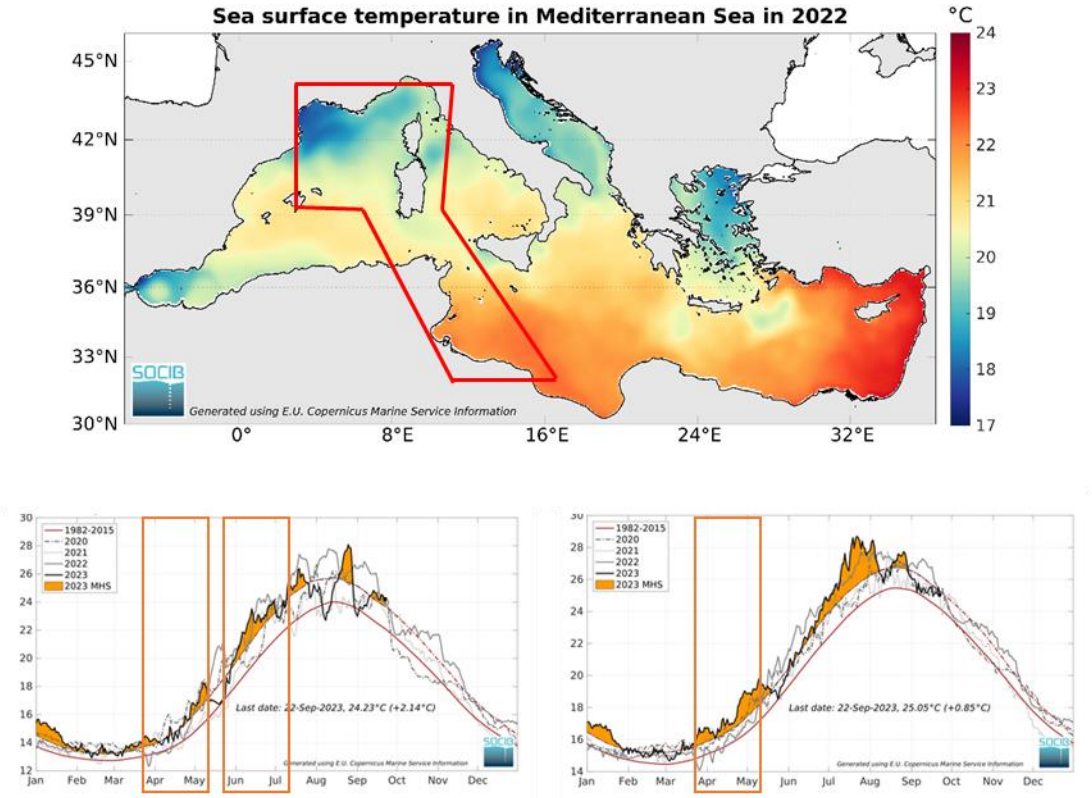


Figure 1.7. Sea surface temperature in the Mediterranean Sea. Top panel: map of the sea surface temperature distribution across the Mediterranean Sea in year 2022. Bottom panels: timeseries of the sub-regional daily sea surface temperature for the current year (2023) and the last 3 years, and the daily climatology from 1982-2015 for the North Western Mediterranean Sea (left panel) and the Algerian basin (right panel). Marine heat spikes (MHS, when values become higher than the climatological 90th percentile) are highlighted for the current year. From Juza and Tintoré, 2023. The red and orange frames delineate respectively the covered area and the periods of the oceanographic campaigns studied in this thesis.

The research conducted by Margirier et al. (2020) underscores the significant role of deep convection intensity in the Gulf of Lions from 2009 to 2013 (Figure 1.8, top panel). This process acted as a reservoir, influencing both surface and deeper layers, consequently leading to the warming and salinification of the WMDW with the propagation of LIW.

In the subsequent four years after 2013, as illustrated in Figure 1.8, a distinct lack of intense deep convection is evident. As per Margirier et al. (2020), this allowed the LIW to preserve its elevated temperature and salinity upon entering the basin. Consequently, the LIW infiltrated the intermediate layers of the Gulf of Lions, resulting in increased warmth and salinity. Notably, in the transitional winter of 2014, there were reduced cumulative monthly heat losses to the atmosphere compared to other years, potentially accounting for the absence of deep mixing.

Juza and Tintoré (2023) present an extended and thorough overview of the northwestern region, encompassing observations up to the year 2023(Figure 1.8, bottom panel. In 2018, deep convection events were documented, reaching depths of approximately 2000 meters. The subsequent year, 2019, which corresponds to the period of the oceanographic cruises examined in this thesis, witnessed deep convection recorded at around 500 meters in depth.

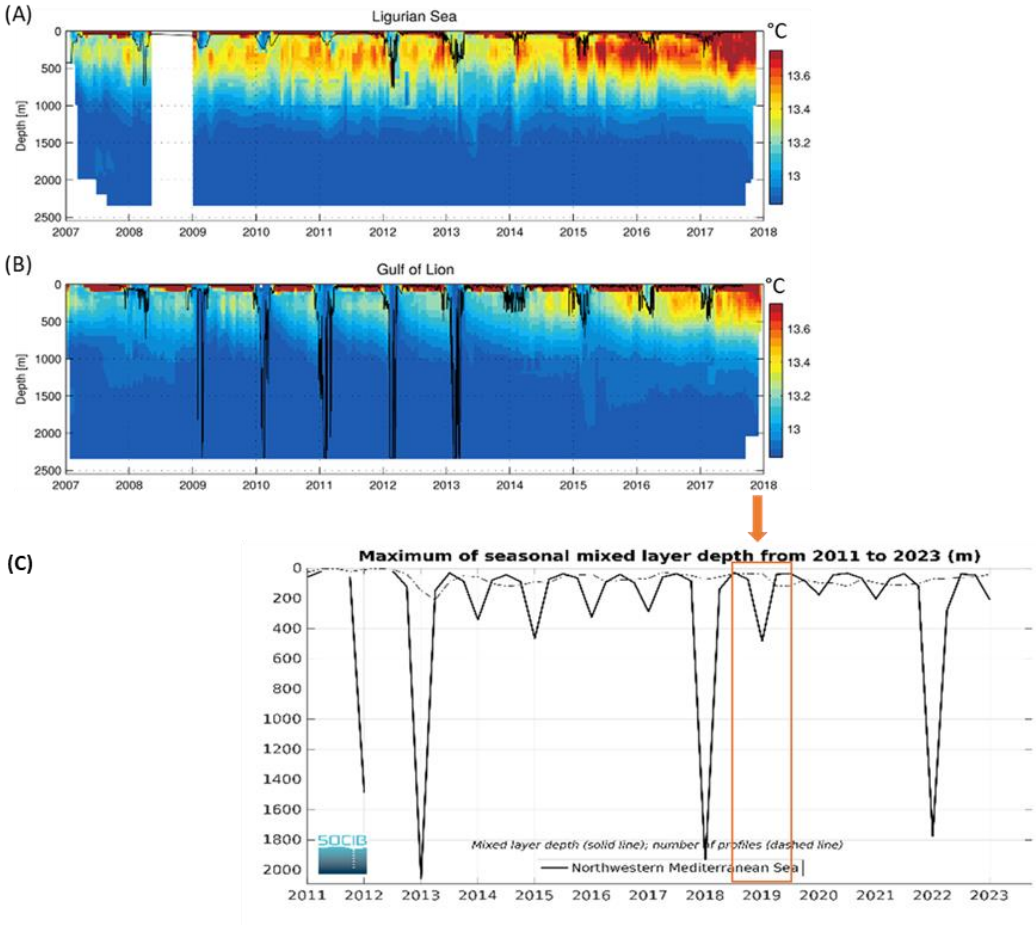


Figure 1.8. Deep convection depths from 2007 to 2022 in the North Western Mediterranean Sea. Top panels (A and B) deep convection depths from 2007 to 2017 (Figure from Margirier et al., 2020). Bottom panel (C) deep convection depths from 2011 to 2023 (Figure from Juza and Tintoré, 2023). Margirier et al. (2020) present depth-time temperature diagrams from two specific locations: (A) the Ligurian Sea (43.41° N 7.89° E) and (B) LION (42.04° N 4.68° E) for the Gulf of Lion. The mixed layer depth is indicated by the black contour. Profiles considered within a 15 km radius of the mooring site were combined with mooring line measurements (Juza and Tintoré, 2023). Timeseries of the maxima of the sub-regional seasonal distributions of the mixed layer depth from 2011 to the last available season. The orange frame delineates the year of the oceanographic campaigns studied in this thesis.

1.1.3.2. Nutrient gradients in the western Mediterranean Sea

The Mediterranean Sea demonstrates a distinct spatial gradient of declining nutrient concentrations, primarily driven by the inflow of nutrient-poor AW through the Strait of Gibraltar (Lazzari et al., 2016). Notably, the Mediterranean Sea is recognized for its disproportionately high nitrogen-to-phosphorus (N:P) ratio compared to the global ocean, particularly in its eastern area. This nutrient composition is attributed to the significant influence of terrestrial inputs, a phenomenon first identified by Redfield (1934).

In the top panel of Figure 1.9, specific regions, such as the Alboran Sea and the northwest Mediterranean, exhibit notably higher phosphate levels (0.10±0.03 and 0.04±0.02 mmol P m^{-3}, respectively). When examining vertical averages within the 0–50 meter range, consistent patterns emerge, showing elevated phosphate concentrations in the Tyrrhenian Sea compared to the eastern Mediterranean (Lazzari et al., 2016). On the other hand, in the Gulf of Gabés, phosphate concentrations were notably higer (0.06±0.02 µmol l^{-1}) (Drira et al., 2010).

Conversely, the vertical averages of nitrate in the 0-50 meter layer present distinct patterns when compared to phosphate. Interestingly, the east-west gradient is conspicuously absent, with only slightly lower nitrate concentrations observed in the Alboran Sea (0.83±0.21 mmol N m^{-3}), potentially influenced by conditions set at the Strait of Gibraltar. In contrast, a clear south-north gradient with heightened surface concentrations is evident along the northern coasts of the Mediterranean Sea (2.11±1.19 mmol N m^{-3}). It is worth noting that signals originating from the Rhone and Po rivers stand out prominently, providing a sharp contrast to the phosphate scenario(Lazzari et al., 2016). In the Gulf of Gabés, a significant presence of nitrate (1.45±0.21 µmol l^{-1}) is observed along the coastal areas (Drira et al., 2010).

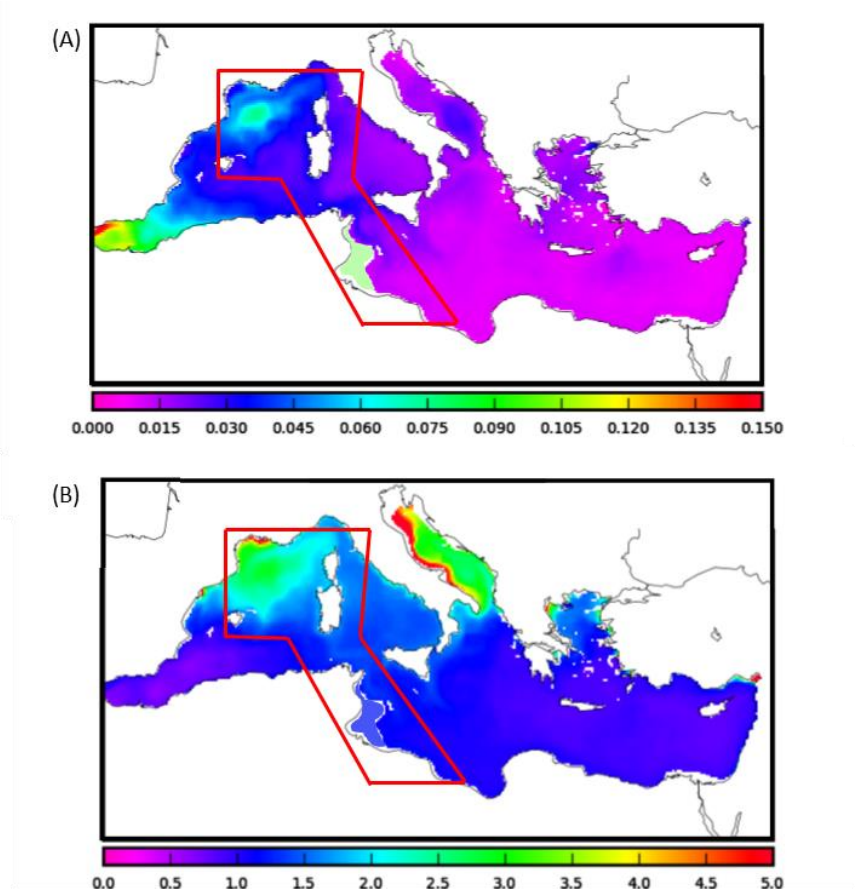


Figure 1.9. Spatial distributions of nutrient concentrations averaged from 1999 to 2004. The top panel depicts phosphate levels (mmol P m^{-3}) while the bottom panel illustrates nitrate concentrations (mmol N m^{-3}) over the 0–50 m layer. Modified from Lazzari et al., 2016, with aggregated information for the gulf gabes from Drira et al.(2010). The red frame delineates the area of interest for the oceanographic campaigns studied in this thesis.

1.1.3.3. Chlorophyll and phytoplankton gradients in the Western Mediterranean Sea

In this region, the deep convection fuels a significant marine life bloom during late winter and early spring. Specifically, this area showcases the highest chlorophyll-a (*Chl-a*) levels on a broad regional scale within the Mediterranean Sea, in contrast to observations in the eastern part of the basin, revealing an evident east-west gradient (Figure 1. 10, point A). Lavigne et al. (2015) conducted a basin-wide seasonal analysis of *Chl-a* concentrations in the Mediterranean Sea using satellite data. Their findings revealed that during winter, the Algero-Provencal Basin area (Figure 1.10, point B) displayed higher *Chl-a* concentrations compared to summer. This pattern is linked to the NO BLOOM regions as defined by D'Ortenzio and Ribera d'Alcalà (2009). Overall, *Chl-a* levels remain

consistently low in most parts of the basin, with the exception of the Liguro-Provençal region.

The vertical mixing linked to the deep convection promotes a large bloom at the end of the beginning of spring. The North-western Mediterranean presents the highest *Chl-a* values (up to 3 µg *Chl-a* l^{-1}) over a large regional scale (D'Ortenzio and Ribera d'Alcalà, 2009), with a typical massive increase in March in the deep convection areas (Figure 1.10, point A, from Lavigne et al. 2015). As described by Margirier et al. (2020), the deep chlorophyll maximum (DCM) is consistently located around the upper 100 m throughout the basin. However, during the deep mixing process in late winter, it has been documented to extend to depths of up to 1500 m. In addition, a distinctive and significant rise in *Chl-a* levels is evident from March onwards, particularly in the upper meters, where winter profiles exhibit relatively high *Chl-a* concentrations, often surpassing 0.5 mg m^{-3} (Lavigne et al., 2015). This pattern contrasts with the southwestern region (Figure 1.10, point B, from Lavigne et al. 2015), characterized by a consistent presence of the DCM in both winter and summer profiles, albeit not as deeply distributed (Letelier et al., 2004; Mignot et al., 2014). The combination of winter mixing and various environmental factors, including an extensive shelf, intermittent coastal upwelling, and significant fluvial inputs, establishes the NWMS as one of the most productive zones in the Mediterranean Sea.

The biological production decreases from north to south and west to east and west to east, and is inversely related to the increase in temperature and salinity (Siokou-Frangou et al., 2010a).

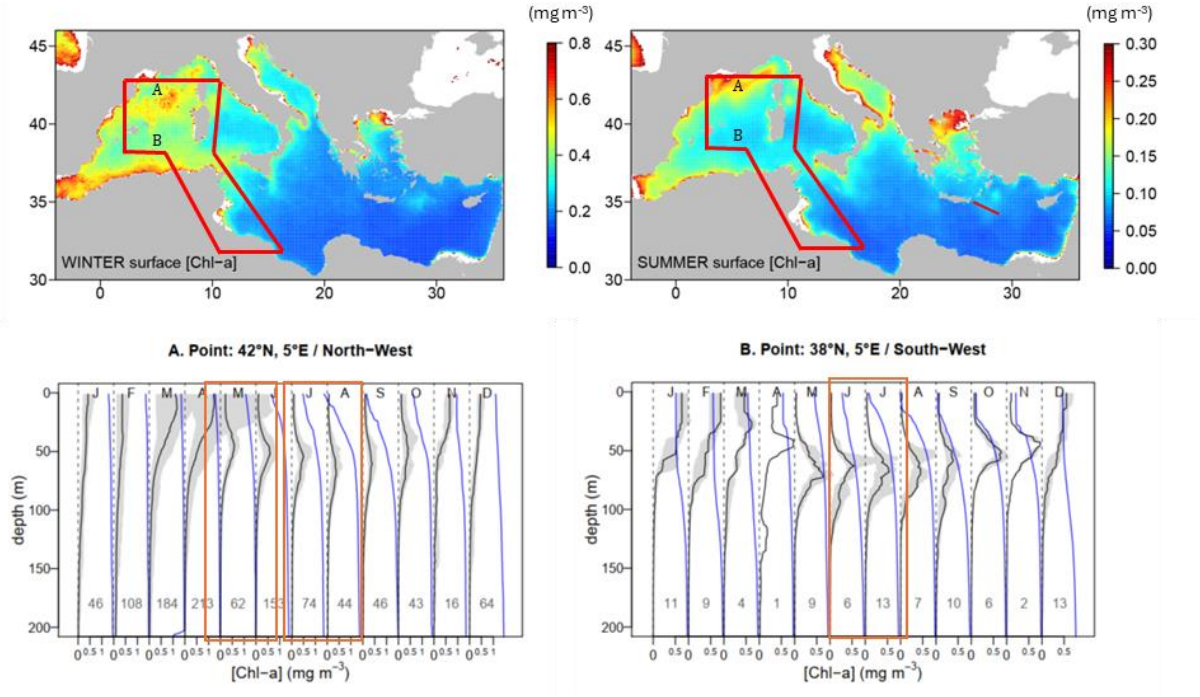


Figure 1.10. Sea surface chlorophyll distribution in the Mediterranean Sea in winter and summer and seasonal vertical distribution in Gulf of Lions (Point A, left panels) and Algerian basin (Point B, right panels). Figure from Lavigne et al., 2015. The upper panels depict surface *Chl-a* levels during both winter (left) and summer (right) in the Mediterranean Sea. It is noteworthy that the color scales vary between the two seasons. The lower panels illustrate the vertical *Chl-a* profiles (black lines) specifically in two stations, respectively in the North and the South of the Western Mediterranean Sea. The black line represents the median value for each month, while the shaded area denotes the 0.1-quantile to 0.9-quantile range. The numerical values below the climatological profiles indicate the quantity of available data profiles used in their computation. Additionally, normalized average water density profiles are superimposed and indicated by blue lines. The red and orange frames delineate respectively the covered area and the periods of the oceanographic campaigns studied in this thesis.

In relation to the structuring of the phytoplankton community and its role in productivity within ecoregions of the Mediterranean Sea, Ciavatta et al. (2019) conducted a study on the spatial variability of phytoplankton types, employing a combination of reanalysis data and satellite-derived ocean color products (Figure 1.11). The findings reveal that picophytoplankton is the dominant type in most open ocean waters, such as the Ligurian Sea, Gulf of Lions, and North Aegean Sea. Microphytoplankton, on the other hand, prevails in some highly productive coastal areas near large river mouths, notably in the North Adriatic and the Gulf of Gabès. It also extends along the Italian Adriatic coast, the Libyan coast, and the Nile Delta. Meanwhile, nanophytoplankton plays a significant role in moderately productive coastal areas along the Mediterranean coasts, especially in the Western Mediterranean, Adriatic Sea, and Levantine.

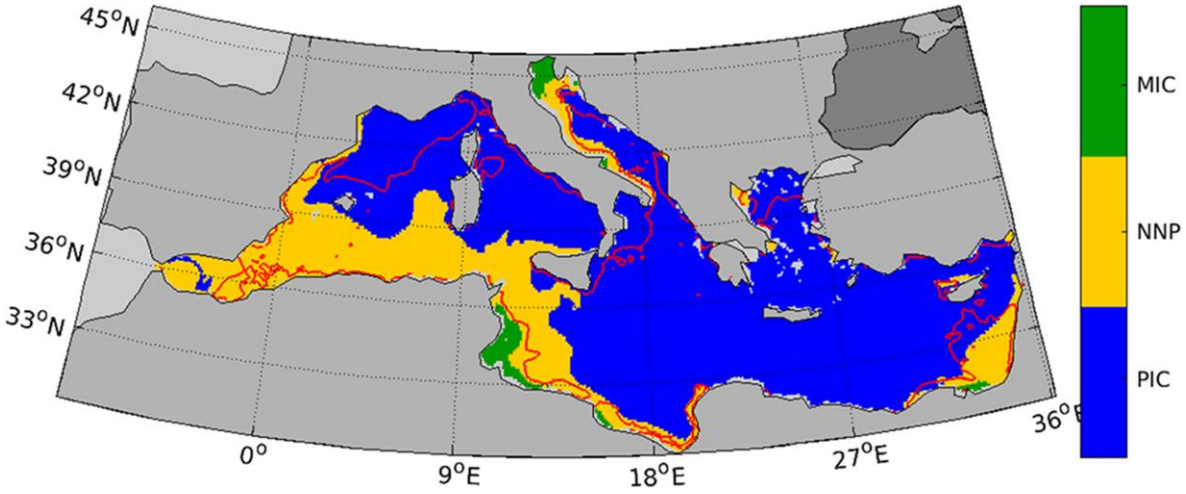


Figure 1.11. Phytoplankton functional type-based ecoregions of the Mediterranean Sea. Figure from Ciavatta et al. (2019). MIC = microphytoplankton; NNP = nanophytoplankton; PIC = picophytoplankton. The red line from the original figure, not be used present study.

1.1.4. Observed modifications in biodiversity linked to global changes

Despite covering only 0.82% of the global ocean surface and being considered oligotrophic, the Mediterranean Sea has a rich biodiversity, including a substantial proportion of endemic species (Durrieu de Madron et al., 2011; Aurelle et al., 2022). A notable feature is the relative isolation of its deep-sea communities, not only compared to those in the Atlantic but also between the eastern and western Mediterranean, thanks to the presence of the Sicilian strait. Furthermore, the Mediterranean Sea is characterized by unique geomorphological attributes, such as submarine canyons, seamounts, mud volcanoes, hypersaline anoxic environments, and deep trenches. These distinctive features make it one of the few warm deep-water basins in the world capable of supporting a diverse range of marine life, making it a biodiversity hotspot (Lejeusne et al., 2010).

However, this status is now under threat due to climate change. Reports highlight the Mediterranean Sea's pronounced and swift responses to climate-induced stress, underscoring its significance as a focal point for climate change research and a crucial region for studying its effects (Margirier et al., 2020). Similarly, Aurelle et al. (2022) emphasize the evident impact of climate change on biodiversity across various organizational levels, affecting genes, populations, species, ecosystems, and consequently, human livelihoods. This aligns with findings from studies by Burrows et al. (2014), Isbell et al. (2015), and Pecl et al. (2017).

One of the main stressors induced by climate change in the Mediterranean Sea is the rapid increase in temperatures, which are projected to change at rates similar to those observed at higher latitudes (Li et al., 2013; Micheli et al., 2013). If temperatures were to increase by 2 °C or more, substantial transformations would occur in Mediterranean ecosystems (Guiot and Cramer, 2016). Projections based on high emissions scenarios and the increasing impact of human activities predict significant changes in biodiversity, which could culminate in the disappearance of numerous species (Balzan et al., 2020). Reports state that marine heat wave incidents are becoming more frequent (Juza and Tintoré, 2023), extending beyond the summer season (Section 1.1.3.1 Figure 1.7).

Another vulnerability for Mediterranean Sea ecosystems arises from human activities. This encompasses rising demands for food and water resources, along with anthropogenic pressures like biological invasions, coastal migrations, and urbanization (Lipizer et al., 2022). The increase in coastal populations and shifts in fishing practices, spanning both traditional and recreational methods, have spurred the growth of sea fishing activities and subsequently led to heightened landings. This has resulted in the exploitation of previously overlooked species, driven by the gradual depletion of more commercially valued fish populations (Durrieu de Madron et al., 2011).

Reygondeau et al. (2014) presented a comprehensive assessment of anthropogenic pressures (Fishery activities, pollution and eutrophication index, climate change) across the different Mediterranean regions, as illustrated in Figure 1.12, where the values from the different categories were summed and normalize by the maximal value obtained a “new pressure layer”. Notably, the Gulf of Gabès emerges as a focal point, standing out as a critical ecoregion within the Mediterranean (Béjaoui et al., 2019a). This area holds immense significance in the context of fisheries resources for Tunisia, serving as a vital breeding ground for a diverse array of fish species. Research by Hattour et al. (1995), Derbel et al. (2012), and Enajjar et al. (2015) unequivocally affirm its pivotal role in the early life stages of several commercially prized fish. Industrial operations, particularly the discharge of phosphogypsum from phosphate production, have wrought severe consequences on the Gulf's biodiversity and fish populations, consequently leading to a discernible decline in water quality.

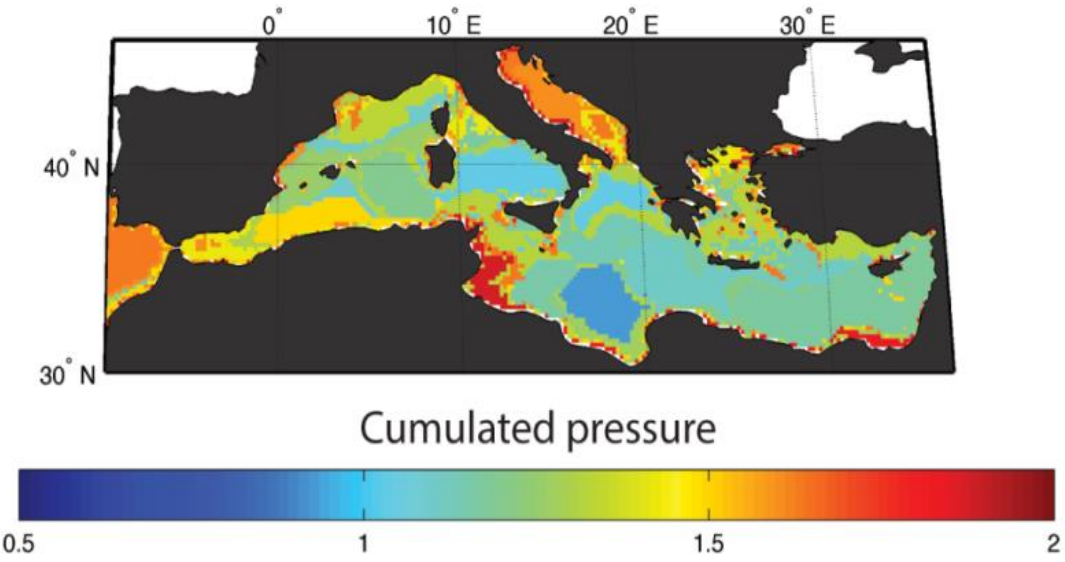


Figure 1.12: Map of the cumulated anthropogenic pressures in the Mediterranean. Figure from Reygondeau et al (2014).

In the realm of plankton, recognized as a pivotal component in trophic food webs, a consensus among several authors emphasizes the remarkable adaptability of phytoplankton and zooplankton species. Their large populations and rapid reproductive cycles enable them to swiftly respond to environmental shifts, employing diverse mechanisms like phenotypic plasticity, natural selection, and genetic adaptation (Colin and Dam, 2007; Dam, 2013; Reusch and Boyd, 2013; Aurelle et al., 2022).

The adaptability of some species belonging to zooplankton (mostly cosmopolitan) is underlined by their notable flexibility in terms of nutrition and trophic interactions with other planktonic organisms (Kiørboe et al., 2018). Additionally, as highlighted by Aurelle et al. (2022), their proficiency in vertical swimming empowers them to traverse diverse water layers characterized by distinct physical and chemical properties. This capability optimizes their growth in the face of dynamically changing environments (Carlotti and Nival, 1991; Svetlichny et al., 2000; Bonnet et al., 2005; Halsband-Lenk et al., 2001, 2002, 2004).

Several author's observations underscore the pivotal role of zooplankton in the processes of pollutant bioaccumulation and biomagnification, particularly concerning higher trophic levels (Durrieu de Madron et al., 2011; Foster et al., 2012; Tesán-Onrubia et al., 2023a). The air-water interface, often conditioned by physical changes, and subject to various transformations, has the potential to alter the general entry of contaminants into the water column, depending on climatic factors (Durrieu de Madron et al., 2011)

1.2. Zooplankton in the Mediterranean Sea

The composition and diversity of Mediterranean zooplankton have been shaped by geological events dating back to the Messinian Salinity Crisis around 5 million years ago. This period saw drastic climatic shifts due to a combination of glaciations and interglacial periods (Saiz et al., 2014a). Pérès (1985) and Fredj et al. (1992) pointed out that the current Mediterranean zooplankton community is a diverse blend originating from various sources, having undergone significant selective pressures and distinct evolutionary trajectories. The rich array of Mediterranean habitats, coupled with a history of colonization events, has contributed to species diversity (Bianchi and Morri, 2000; Mazzocchi et al., 2014). In general terms, it can be characterized as an Atlantic fauna, primarily consisting of subtropical species and species from northern regions, including a minority of boreal origin and a larger representation from temperate and cold areas. Additionally, there's an influence of oriental origin, notably in the Eastern Mediterranean (Bianchi and Morri, 2000; Saiz et al., 2014a). The distribution of species is significantly influenced by latitudinal and longitudinal temperature gradients. As a result, species of subtropical origin are predominantly found in the eastern basin and southern Mediterranean, where water temperatures are higher than average. On the other hand, cold-temperate species thrive in the northern areas such as the Gulf of Lions, Ligurian Sea, and northern Adriatic, where water temperatures are colder (Saiz et al., 2014).

Siokou-Frangou et al. (2010) observed a decrease in total zooplankton standing stock from west to east across the Mediterranean basin (Figure 1.13). And in this context, Mazzocchi et al. (2014) indicated that mesozooplankton are visibly influenced by food availability on a seasonal scale. While it is not always clear to observe a decreasing gradient from west to east in total stock, regional discontinuities can be identified. However, preferences towards the west or east were observed in the distribution of certain copepod species.

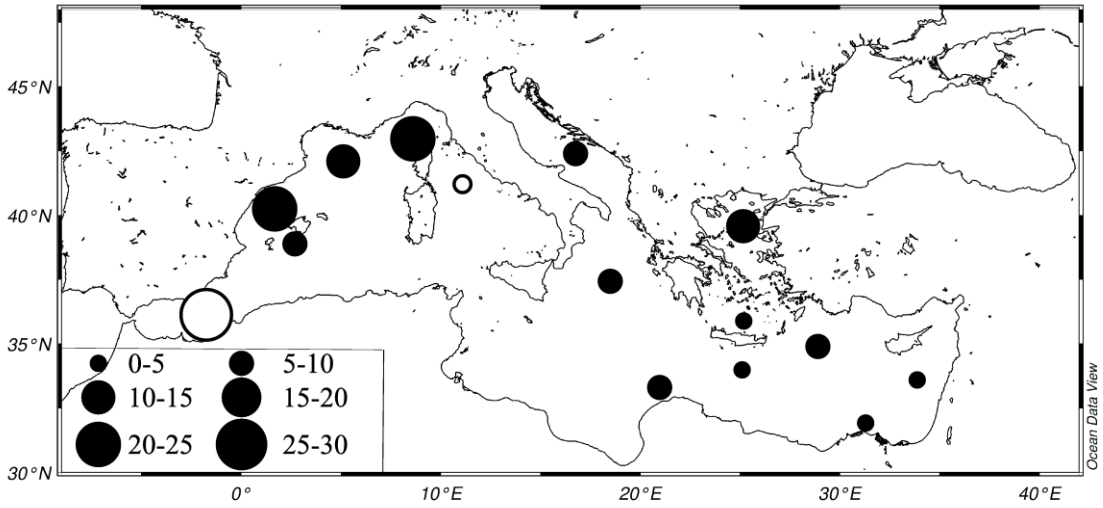


Figure 1.13. Summary of spatial distributions of zooplankton in Mediterranean Sea. Total mesozooplankton abundance (black circles) or total copepod abundance (open circles) (10^4 ind. m^{-2}) in spring time in the 0–200 layer of MS. Figure from Siokou-Frangou et al., (2010).

1.2.1. Zooplankton community in the North Western Mediterranean Sea

In the Northwestern Mediterranean, Champalbert (1996) and Calbet et al. (2001) described typically 2–3 seasonal peaks of zooplankton, occurring in late winter or spring and late summer. These observations regarding the standing stocks of zooplankton vary across different studies. For instance, Fernández de Puelles et al. (2007) noted the highest standing stocks in late winter-spring at the Mallorca channel. In contrast,Ribera d'Alcala et al. (2004) and Skovgaard and Saiz (2006) reported minimum values for winter standing stocks.

Copepods stand out as the predominant group within the zooplankton community, accounting for the highest levels of abundance roughly 55-65% of the total, with significant contributions during the winter and spring seasons (Champalbert, 1996; Calbet et al., 2001). Their dynamics play a central role in shaping the standing stocks of mesozooplankton, maintaining a consistent dominance year-round (Saiz et al., 2014a).

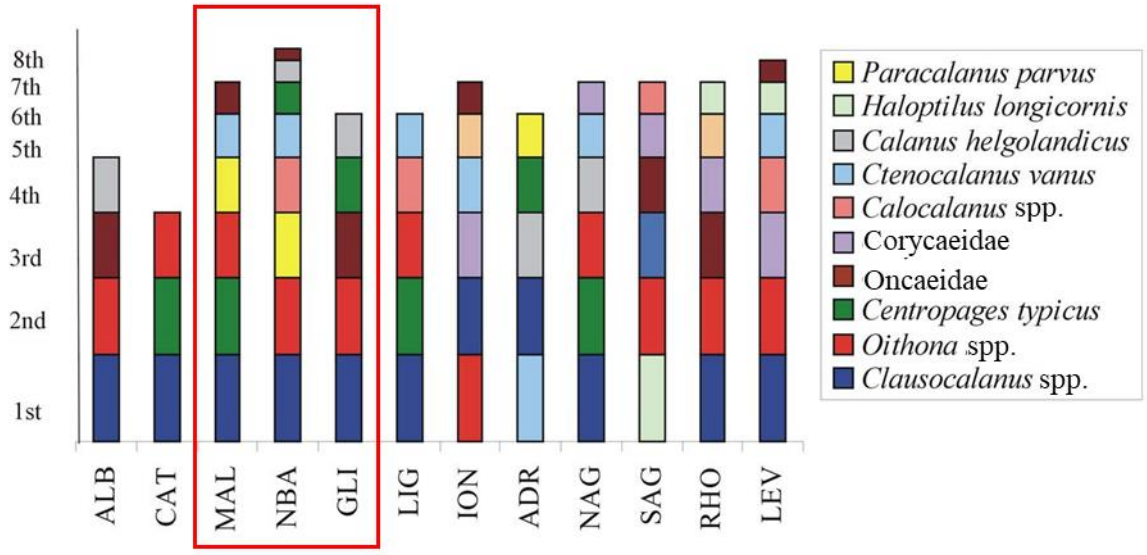


Figure 1.14: Dominant copepod taxa in the Mediterranean Sea from Siokou-Frangou et al., (2010). Rank order of dominant copepod species or genera in the 0–200m layer of several areas of the MS in spring. ALB: Alboran Sea, CAT: Catalan Sea, MAL: Mallorca Channel; NBA: North Balearic Sea; GLI: Gulf of Lions LIG: Ligurian Sea ADR: Adriatic Sea; ION: Ionian Sea; NAG: North Aegean Sea, SAG: South Aegean Sea; RHO: Rhodos cyclonic gyre, LEV: Central Levantine Sea. Red frame delineates the North Western Mediterranean Sea.

Siokou-Frangou et al. (2010) noted that there are fluctuations in dominant species of copepods both in terms of time and geographical location, exhibiting distinctions between the Western and Eastern Mediterranean Seas (Figure 1.14). For instance, in the Western Mediterranean, species such as *Centropages typicus* and *Temora stylifera* dominate (Saiz et al., 1999; Gaudy et al., 2003; Fernández de Puelles et al., 2007). Conversely, in the Eastern Mediterranean, *Calocalanus* spp., *Haloptilus longicornis*, Oncaeidae, and Corycaeidae make more substantial contributions to the overall copepod abundance compared to the Western Mediterranean (Weikert and Trinkaus, 1990; Mazzocchi et al., 2003; Ramfos et al., 2006; Siokou-Frangou et al., 2009).

1.2.2. The zooplankton size spectrum

Sheldon et al. (1972) conducted pioneering studies that revealed a well-balanced distribution of biomass across different size categories within the oceanic particle spectrum. These dynamics optimize energy transfer within the community, effectively bridging the gap between smaller and larger organisms. The introduction of a size-based fractionated system by Sieburth et al. (1978), continues to hold significance in contemporary studies, demonstrating its enduring influence in the field (Gluchowska et

al., 2016; Moriarty et al., 2013; Sieburth et al., 1978). This categorization delineates distinct plankton size fractions (Figure 1. 15). The smallest ones include pico- (0.2–2 µm), those represented by unicellular species such as cyanobacteria and microalgae, and nano- (2-20 µm) fractions, which comprises ciliates, heterotrophic flagellates, and nanophytoplankton, constituting the majority of phytoplankton. The micro-(20-200 µm) fraction encompasses protozoans such as sarcodinans and ciliates, along with early-stage metazooplankton, serving as primary grazers. Additionally, this category includes larger phytoplankton species, known as microphytoplankton. The meso- (0.2 to 20 mm) fraction encompasses various taxonomic groups such as copepods, cladocerans, tunicates, larvae of marine invertebrates, chaetognaths, and noctilucales. Finally, macrozooplankton comprises larger organisms, including crustaceans and gelatinous plankton. While Sieburth et al. (1978) defines it as above 20 mm, other authors, such as Feliú (2020), consider it as early as 2 mm or 5 mm.

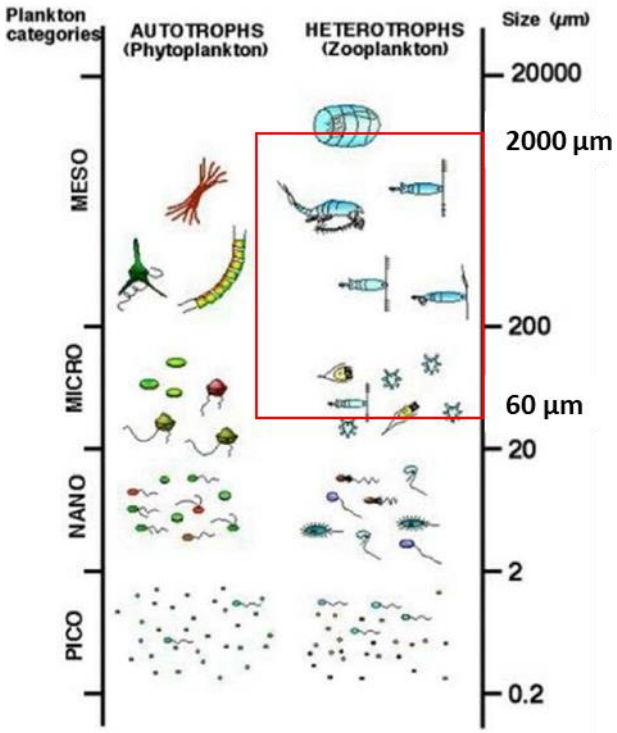


Figure 1.15 Planktonic composition within large size-fractions. Figure from Alcaraz and Calbet (2003). The division of plankton into size classes, functional groups, and major plankton organisms. The red frame represents the metazooplankton considered in the present thesis.

1.2.3. The importance of small metazooplankton

In the Mediterranean Sea, there has been extensive documentation of a notable abundance of small metazooplankton (*i.e.*, metazoan planktonic organisms) in the size fraction below 200 µm (see Figure 1. 15), including small copepods and copepod larval stages (nauplii and copepodites). They have previously been characterized as dominant in the zooplankton community. This dominance could be indicative of the type and size of available food, such as nanophytoplankton and/or diatoms, which may influence the presence of smaller or larger species (Siokou-Frangou et al., 2010; Nowaczyk et al., 2011; Feliú, 2020). Despite their relatively low biomass contribution in planktonic communities, small organisms exhibit rapid growth rates. Moreover, they can be significant contributors to the overall production. Given the substantial abundance of small-size zooplankton, their year-round presence, and high metabolic rates, they are likely pivotal actors in ocean carbon cycling (Zervoudaki et al., 2007; Nowaczyk et al., 2011; Svensen et al., 2011). These organisms play a critical role in the functioning of the pelagic ecosystem, especially in the oligotrophic areas of the Mediterranean, where they act as intermediaries between classical and microbial food webs (Siokou-Frangou et al., 2010a).

In this context, the study of size fractions of metazooplankton, particularly those corresponding to smaller organisms, is crucial. For instance, it helps establishing relationships between organism size classes and trophic levels, (Tesán-Onrubia et al., 2023a). Additionally, it offers another perspective for understanding the dynamics of planktonic food webs in the context of contaminant accumulation processes (Chifflet et al., 2023; Guigue et al., 2023a).

1.3. Roles of zooplankton in the ecosystems

The zooplankton community holds a pivotal role within the trophic network, serving as conduits for primary production and vital contributors to fish populations (Carlotti and Poggiale, 2010). Additionally, they act as key players in global biogeochemical cycles, facilitating the transport of matter to the deep ocean (Steinberg and Landry, 2017). Zooplankton exercise control over carbon production through diverse mechanisms, including predation and the conveyance of organic material to deeper layers, accomplished via fecal pellets (Turner, 2015), vertical migration (Ariza et al., 2015), or the sinking of carcasses (Figure 1.16).

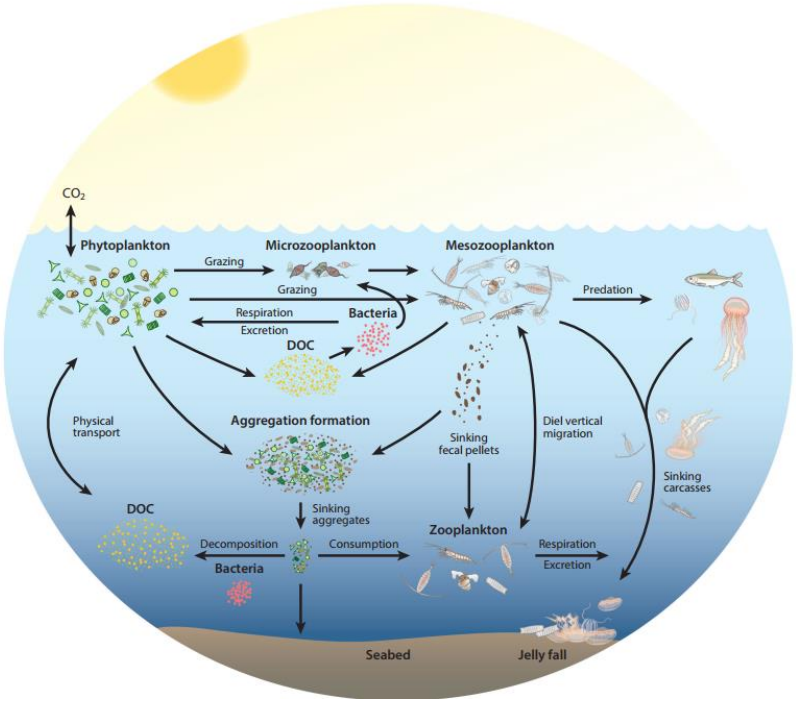


Figure 1.16: Main pathways involving zooplankton in the cycling and export of carbon in oceanic ecosystems. Figure from Steinberg and Landry (2017).

The grazing impact of zooplankton on phytoplankton and the trophic pathways in planktonic food webs vary spatially in response to phytoplankton resource availability. As carbon progresses through the food web, a substantial portion is respired. According to Steinberg and Landry (2017), zooplankton feed on particulate organic carbon (POC) derived from prey, which can encompass phytoplankton or other zooplankton. Due to the suboptimal feeding behavior of zooplankton, some dissolved organic carbon (DOC) within the prey is released into the surrounding water, while the remainder is ingested (Figure 1. 17). Consumers assimilate a fraction of the ingested POC. Unassimilated carbon is excreted as fecal pellets, including mini-pellets released by protists, which may subsequently leach DOC. Among the assimilated carbon, a portion is respired as CO_2, while the rest is allocated to the animal's growth and reproduction, constituting secondary production (Møller et al., 2003; Saba et al., 2009).

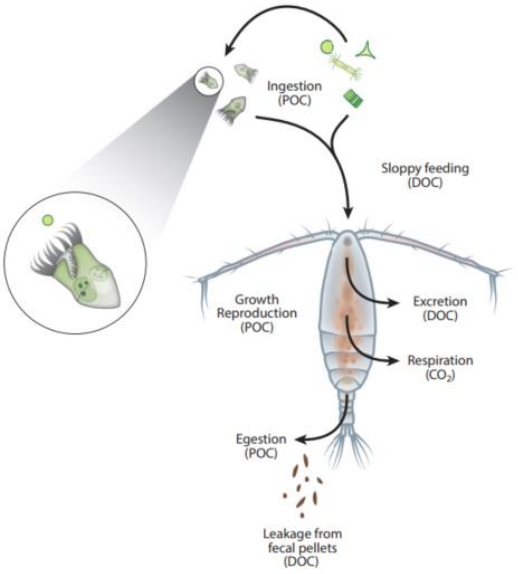


Figure 1.17: Processes involved in carbon consumption and metabolism by zooplankton. Figure from Steinberg and Landry (2017).

The body size of animals holds paramount importance in their biological and ecological functioning (Bachiller and Irigoien, 2013). Siokou-Frangou et al. (2010) reviewed the significance of the smaller fraction, which constitutes approximately 80% and 21% of the total community in terms of abundance and biovolume, respectively (Calbet et al., 2001; Siokou-Frangou et al., 2010a). Functionally, this size category plays a crucial role due to the inverse correlation between body size and metabolic rates. It exerts a grazing pressure on phytoplankton akin to that of larger zooplankton (>200 μm) (Almeda et al., 2011). Notably, when accounting for this size fraction, smaller copepod genera, particularly *Oithona*, *Oncaea*, and *Microsetella*, become significantly more prevalent (Calbet et al., 2001; Zervoudaki et al., 2007).

Siokou-Frangou et al. (2010) reviewed the variability of zooplankton respiration rates in the Mediterranean Sea, which are influenced by factors such as community composition and water mass characteristics. For instance, in the NWM, specifically in the Catalan Sea, the weight-specific respiratory carbon demand of zooplankton is slightly lower in winter-spring (0.180 d-1) compared to summer-autumn (0.219 d-1), although this difference does not reach statistical significance, as reported by Alcaraz et al. (2007). Conversely, a few years earlier, Gaudy et al. (2003) noted that respiration rates increase in spring in the Gulf of Lion, indicating heightened physiological activity in zooplankton genera, particularly in the growth and reproduction rates of most copepods.

Regarding zooplankton metabolic rates, Alcaraz et al. (2007) observed that weight specific excretion rates of ammonia in the Catalan Sea of the NWM were slightly higher in summer-autumn (averaging 0.111 d^{-1}) compared to winter-spring (0.082 d^{-1}). Similarly, orthophosphate excretion rates did not exhibit statistically significant differences between summer (0.0069 µg P µg C^{-1} d^{-1}) and winter (0.0022 µg P µg C^{-1} d^{-1}) periods (Alcaraz et al., 2007; Siokou-Frangou et al., 2010).

In the Gulf of Lion, it was calculated that zooplankton excretion played a role in supplying 31% of the nitrogen and 16% of the phosphorus required for primary production in spring. During winter, these contributions changed to 10% for nitrogen and 27% for phosphorus. Additionally, the nocturnal surface migration of copepods might enhance regenerated production above the DCM, thereby stimulating bacterial production (Christaki et al., 1998; Siokou-Frangou et al., 2010a). These observations emphasize the pivotal role of zooplankton in the nitrogen and phosphorous availability, also evidenced through analysis of protein-to-carbohydrate ratios in organisms (e.g. Tesán-Onrubia et al., 2023a). And this information proves vital for comprehending nutrient inputs and their repercussions on the trophodynamics of the ecosystem (Chen et al., 2019, 2021; Tedetti et al., 2023). Moreover, it acts as an indicator of nitrogen availability, especially in environments where nitrogen may be limited (Bhat et al., 1993.; Kim et al., 2019)

1.4. Objective of this thesis

This study examines zooplankton communities during two campaigns conducted in 2019: one in the northwestern Mediterranean Sea (MOOSE-GE 2019 cruise; July-August) and the other along a North-South Transect in the western Mediterranean Sea and on the Tunisian margin (MERITE-HIPPOCAMPE; April-May). Its aim is to define the structural variability of mesozooplankton in the western basin across different eco-regions of the western Mediterranean in relation to the environmental physical and biogeochemical processes during the spring and summer of the same year. This encompasses assessments of abundance, biomass, taxonomy, and size distribution, with a dedicated special focus on the small organisms of the zooplankton community (micro and mesozooplankton), which cannot always be included, often due to constraints in obtaining and analyzing samples from small zooplankton organisms. This detailed structural description, based on size spectra and trophic group distinctions, will be used to assess ingestion and metabolic fluxes in different habitats. These estimations will allow for the evaluation of potential impacts on phytoplankton due to grazing and nutrient regeneration. The structural and functional descriptions across the size spectrum also provide a basis for better understanding the transfer of contaminants in the planktonic trophic network.

Subsequent chapters will progressively unfold the thesis objectives, adopting the following structure:

Chapter 2: Outlines the methodology employed in the study, covering both the MERITE-HIPPOCAMPE and MOOSE-GE 19 cruises. It encompasses the description of the study area, environmental data collection (including CTD profiles and nutrient analysis), and the meticulous process of zooplankton sampling and analysis. This involves sample fractionation, image processing, and detailed size and structure analysis. Additionally, it explains the analytical techniques used to assess plankton group abundance and biomass, along with the statistical methods applied in the research.

Chapter 3: Concerns the MERITE-HIPPOCAMPE campaign, emphasizing its significance in biota and zooplankton characterization. The chapter includes a detailed article on zooplankton biomass, size-structure, and metabolic fluxes, with a focus on the Chlorophyll Maximum Layer. It sheds light on environmental variables, biomasses, and nutrient dynamics. This chapter underscores the key role of zooplankton analysis in biogeochemical processes and transfer of contaminants in the Mediterranean Sea.

Chapter 4: Deals with the MOOSE-GE 2019 campaign. The chapter presents results on spatial patterns in the environment, zooplankton abundance and diversity, as well as fluxes. It engages in discussion regarding the environmental context and zooplankton characteristics during the MOOSE-GE 2019 cruise.

Chapter 5: Summarizes zooplankton features in the Western Mediterranean, drawing from MOOSE-GE 2019, MERITE-HIPPOCAMPE 2019, and MOOSE-GE 2017 studies. It scrutinizes abundance, community structure, biomasses, and fluxes. The chapter also conducts a comparative analysis with works by Nowaczyk et al. (2011), Mazzocchi et al. (2014), Siokou-Frangou et al. (2019) and others. This provides a comprehensive view of zooplankton dynamics in the region, yielding valuable insights. The concluding chapter amalgamates the newfound insights from the research, offering a discussion on the recently identified traits of zooplankton communities in the northwestern Mediterranean Sea

2. Materials and Methods

2.1. Study area

The study area includes the sampling stations of two scientific cruises (Figure 2.1), MERITE-HIPPOCAMPE and MOOSE (Mediterranean Ocean Observation Multi-Sites on Environment), carried out in two different seasons. Most of the stations cover the north-western Mediterranean, with additional stations in southern Mediterranean Sea, located to the west off Sardinia and on the eastern plateau of Tunisia.

The MERITE-HIPPOCAMPE cruise, conducted from 13 April to 14 May 2019 during the spring phytoplankton bloom, includes 10 stations along a north-south transect from the French coast to the Tunisian coast aboard the French Research Vessel Antea. The MOOSE expedition (MOOSE-GE 2019) took place between June 06 to 01 July 2019 aboard the RV Thalassa, covering a track of 118 stations, including 18 dedicated to zooplankton sampling, distributed within a grid covering to the NWMS. The sampling regions encompass the Ligurian Sea (LS), Gulf of Lion Shelf Break (GLSB), Central Provencal Basin (CPB), Southern Provencal Basin (SPB), and Algero-Provencal Basin (APB) within the Western Mediterranean basin. And in the MERITE-HIPPOCAMPE also the Eastern Mediterranean, it includes the Tunisian Eastern Margin (TEM). These areas were operationally defined within the basin to facilitate our descriptions.

During the MERITE-HIPPOCAMPE cruise, three layers were sampled at each station: Surface, water column, and the Deep Chlorophyll Maximum (DCM), also known as the Chlorophyll Maximum layer (CML). The difference between DCM and CML is that while some variables can be measured directly at the depth of the second chlorophyll peak, such as those obtained by CTD, other variables do not always reach the exact depth. However, they do belong to this layer, such as the samples obtained by zooplankton nets. For the purposes of this thesis, both CML and DCM, will be treated as synonymous. On the other hand, during the MOOSE-GE 2019 cruise, the water column was sampled, approximately up to 200m depending on the bathymetry.

Further details regarding these regions and the sampling of zooplankton will be provided in chapters 3 and 4.

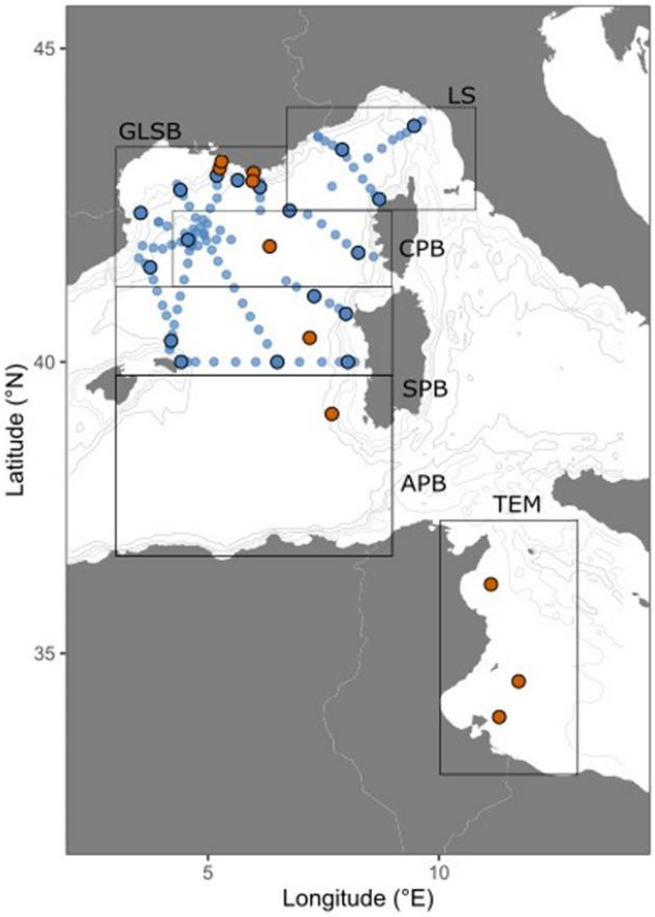


Figure 2.1. Map showing the sampling stations of the MERITE-HIPPOCAMPE cruise (red dots) and the MOOSE-GE 19 expedition (blue dots). Zooplankton stations in MOOSE : blue dots with dark circles, and other stations with CTD casts only. The black rectangles defined different areas: LS= Ligurian Sea, GLSB= Gulf of Lion Shelf Break, CPB= Central Provencal Basin, SPB= Southern Provencal Basin, APB= Algero-Provencal Basin, and TEM= Tunisian Eastern Margin.

2.2. Environmental data

2.2.1. CTD profiles and Nutrients for MERITE-HIPPOCAMPE and MOOSE-GE 2019 cruises

Hydrological variables were assessed through vertical profiles utilizing CTD-Rosette casts, which included measurements of temperature, salinity, dissolved oxygen, and fluorescence. During the MERITE-HIPPOCAMPE cruise, the CTD (Seabird SBE 911plus) was equipped with multiple sensors, including chlorophyll-a fluorimeter (Chl*a*; Aqua Tracka, Chelsea ctg). Nutrient concentrations such as nitrates (NO_3^-), nitrites (NO_2^-), and phosphates (PO_4^{3-}) were obtained from water samples collected at different depths within

the water column (Approximately within the upper 200 meters, depending on the bathymetry of each station). The Niskin bottles of the Rosette were employed in the water column. In the context of the MOOSE-GE 2019 expedition, the methodology was similar, additional data were collected from Niskin Rosette deployments, covering nutrient profiles including NO_3^- and NO_2^-, as well as PO_4^{3-}, which were subsequently utilized for comparing zooplankton N and P fluxes to N and P stocks.

2.2.2. Mixed layer depth calculations

The Mixed Layer Depth (MLD), defined as the surface layer exhibiting uniformity in salinity, temperature, and density, was determined through iterative testing of different values to ensure the best fit across all stations. Following the calculation method established by de Boyer Montégut et al. (2004), temperature differences between 0.5 and 1°C were tested at different layers (1, 5, and 10 meters). This approach was compared with observations from profile graphs of oceanographic variables to verify the results. Finally, the MLD was calculated using a criterion of a 0.5°C temperature difference relative to a reference temperature at a depth of 10 m. For details regarding this calculation, please refer to the annex, where you can find the MATLAB script.

2.3. Zooplankton sampling

MERITE-HIPPOCAMPE samples were collected using three distinct types of nets (Figure 2.2) designed for different strata within the water column (refer to Table 2 in Chapter 3). Logistical constraints, including factors like wind or ocean currents, may prevent a net from reaching the precise depth where the DCM is located. However, if it operates within a reasonably proximate depth range, it will be designated as the Chlorophyll Maximum Layer (**CML**). For horizontal sampling at the depth of the chlorophyll maximum layers (CML), a Multiple Plankton Sampler (Midi type, Hydro-Bios) with five successive nets of similar mesh-size of 60 µm, was utilized for horizontal sampling at the depth of the chlorophyll maximum layers (Figure 2.3 A). Surface sampling was conducted using a Manta net with a mesh size of 60 µm (Figure 2.3 B). Additionally, a steel frame with three circled-rings (Triple-net) equipped with 60, 120, and 200 µm mesh-size nets (0.6 m aperture diameter each) was vertically towed through the water column from a depth of 200 m (or near the bottom) up to the surface (Figure 2.3 C). The samples collected by the three different nets were fractionated into two equal parts using the motoda method and preserved according to distinct requirements, as detailed in next Chapter 3.

During the MOOSE-GE 2019 campaign, zooplankton samples were collected by vertically towing a Bongo net (0.6 m aperture diameter) with a mesh size of 120 µm from

a depth of 200 meters to the surface (refer to Figure 2.2 and Figure 2.3 D). It is important to note that the 200 µm net was not utilized in this study as it was reserved for analysis by the research group of VilleFranche.

Once the sampling process was completed, the collected zooplankton organisms were carefully transferred to 250 ml plastic bottles and preserved in a 4% borax-buffered water-formalin, as detailed in Chapter IV.



Figure 2.2. The zooplankton nets employed during the cruises: MERITE-HIPPOCAMPE (above) utilized Hydro-Bios, manta net, and triple net, while MOOSE-GE 19 (below) utilized the Bongo net.

2.3.1. Sample analysis and image treatment

2.3.1.1. Fractionation and sub-sampling

All the zooplankton samples collected for the MERITE-HIPPOCAMPE and MOOSE-GE 2019 were split by sieves into different size fractions (Figure 2.3). The fractionation procedure for one of the three nets used during the MERITE-HIPPOCAMPE cruise, specifically the Hydro-Bios net, was conducted on board, whereas, for the remaining nets used in this cruise and also for the MOOSE-GE 2019 cruise, the fractionation was carried out later in a laboratory setting.

For both cruises, zooplankton sample size fractions (in general < 500 µm) were subjected to processing using a FlowCAM of the Yokogawa Fluid Imaging Technologies Inc. Series VS-IV benchtop model, following the methodology outlined by Sieracki et al.

(1998). Alternatively, the remaining larger size fractions (in general> 500 µm) were analyzed using a ZOOSCAN as detailed by Gorsky et al. (2010). Image analysis procedures significantly reduced the time required for sample processing, following the methodology described by Feliú et al. (2020) (Figure 2.3).

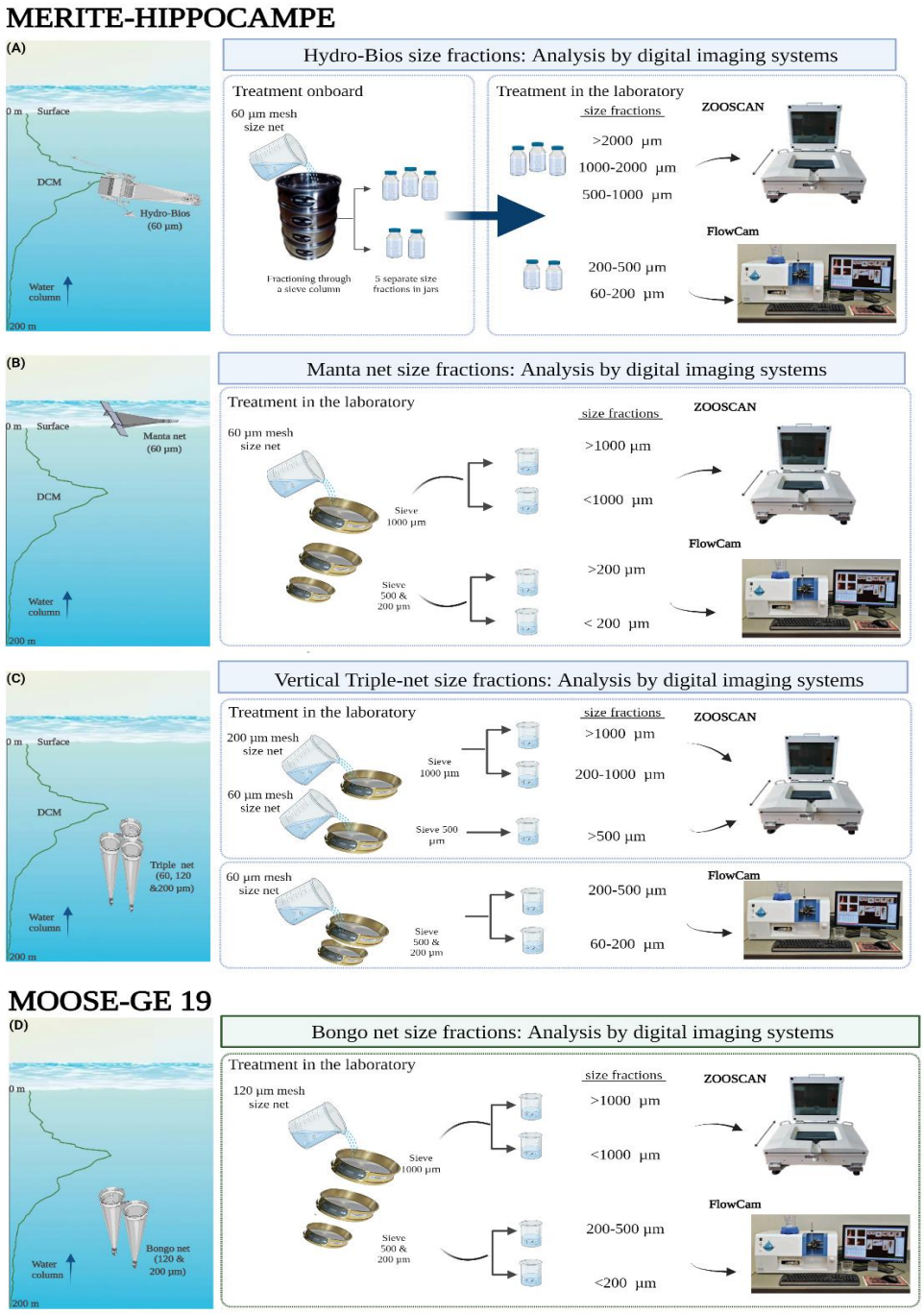


Figure 2.3. Schematic representation of the methodology for sample collections and treatments during the MERITE-HIPPOCAMPE and MOOSE-GE 2019 cruises. Illustration of the sampling depths in relation to the fluorescence profile, where zooplankton samples were collected using different nets (A) Hydro-bios net, (B) Manta net, (C) Triple net, and (D) Bongo net. Then size fractionation of samples and imagery treatment using FlowCAM and ZOOSCAN depending on the fractions.

For both cruises, zooplankton sample size fractions (in general < 500 μm) were subjected to processing using a FlowCAM of the Yokogawa Fluid Imaging Technologies Inc. Series VS-IV benchtop model, following the methodology outlined by Sieracki et al. (1998). The remaining larger size fractions (in general> 500 μm) were analyzed using a ZOOSCAN as detailed by Gorsky et al. (2010). Image analysis procedures significantly reduced the time required for sample processing, following the methodology described by Feliú et al. (2020) (Figure 2.3).

2.3.1.2. FlowCAM processing

The FlowCAM is an automated technique for particle enumeration. The instrument is able to detect particles ranging from 2 to 2000 μm, but it is primarily employed in the examination of unicellular microplankton (20-200μm), which includes marine photosynthetic organisms and ciliates (Buskey and Hyatt, 2006; Le Bourg et al., 2015; See et al., 2005; Zarauz et al., 2009). This means it is capable of capturing smaller organisms that ZOOSCAN cannot detect (<300 μm). The implementation of this zooplankton analysis methodology is relatively recent, leading to a limited number of published records regarding its use in studying the smaller size of metazooplankton communities, despite the developers of FlowCam considering it technically feasible. However, authors such as Álvarez et al. (2012) pointed out that nauplii were observed using FlowCAM. Furthermore, Le Bourg et al. (2015) conducted an assessment of the FlowCAM efficiency in identifying and enumerating small-size metazooplankton communities. They concluded that the FlowCAM system is well-suited for studying zooplankton communities, as it produced results similar to those obtained by microscopy for nearly all the organism groups considered in their study.

This method relies on the analysis of photographs taken from a water sample (aliquot) that is drawn through a glass chamber, known as a flow cell, by means of a peristaltic pump, a combination of flow cytometry and microscopy techniques. Subsequently, specialized software captures and records the size and shape information of each particle (Álvarez et al., 2012; Le Bourg et al., 2015; C. K. Sieracki et al., 1998).

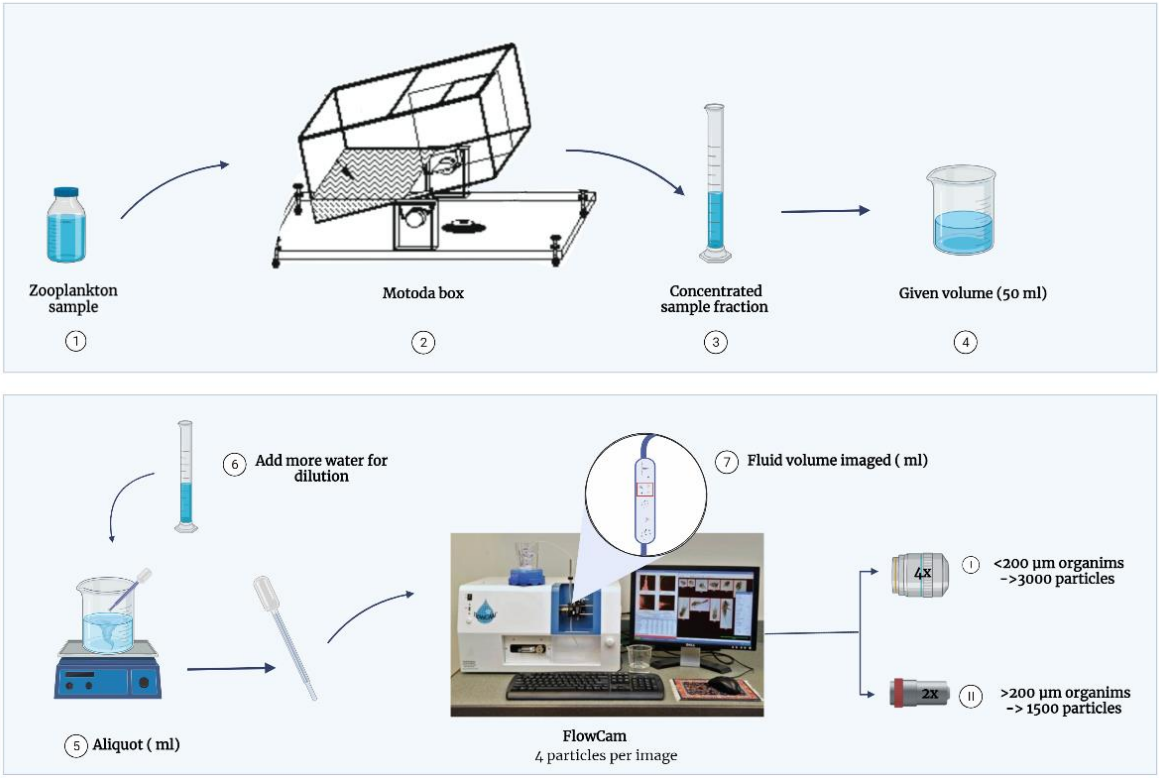


Figure 2.4. Protocol steps outline for processing a zooplankton sample in FlowCAM.

Figure 2.4 illustrates the FlowCAM analysis protocol: The zooplankton sample (1) is first fractionated using the Motoda splitter (2). The resulting fraction is then concentrated (3) and deposited in a container to which 50 ml of water is added (4). Subsequently, this continuously agitated size fraction on a mixer (5) is subjected to analysis using the FlowCAM in auto-image mode. During this process, the focus is confirmed, and a blank is completed. If more than 4 particles per image exceed the cell's field of view, additional water must be added to the aliquot (6) until the dilution is suitable for the FlowCAM (7).

For the size fraction <200 µm, a flow cell with a 4X magnification and a 300 µm field of view (FOV) was utilized, with particle analysis extended until 3000 counted particles (I). In the case of the size fraction between 200 and 500 µm, a flow cell with a 2X magnification and an 800 µm FOV was employed, with analysis conducted until 1500 counted particles (II).

The digitalized images were processed using the VisualSpeadsheet and ZOOPROCESS software (Gorsky et al., 2010a) thereby converting each photo into vignettes corresponding to individual particles. These vignettes were subsequently downloaded into EcoTaxa, a platform designed for the taxonomic classification of images (Picheral et al.,2023), utilizing the integrated automatic classification through a learning set (Figure 2.5). The final step involved manual validation of the classification, during which duplicates and bubbles were removed.

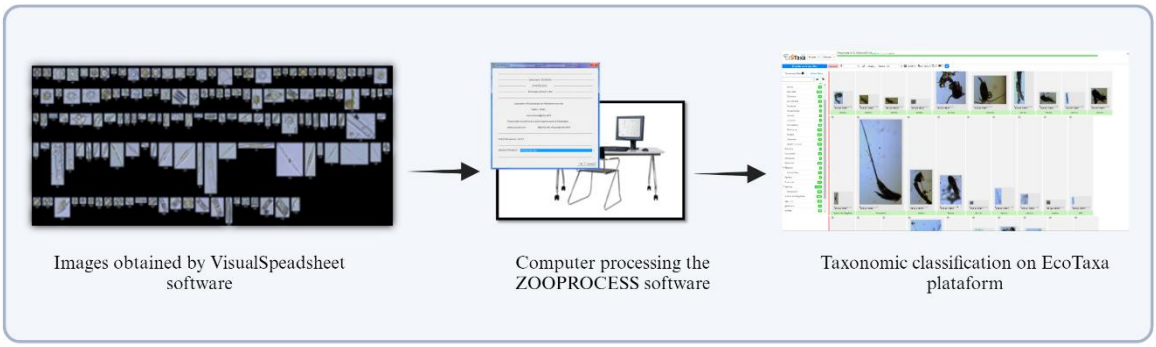


Figure 2.5. Schematic illustration of the methodology employed for zooplankton sample analysis, involving Visual Spead sheet and ZOOPROCESS software, followed by taxonomic classification using the EcoTaxa platform.

2.3.1.3. ZOOSCAN processing

The ZOOSCAN represents an advanced imaging system integrating an automated recognition algorithm. This system includes an adapter scanner with a sealed glass interface for accommodating liquid samples, linked to a computer endowed with the ZOOPROCESS software (García-Comas et al., 2011; Nowaczyk et al., 2011; Donoso et al., 2017; Carlotti et al., 2018; Feliú et al., 2020).

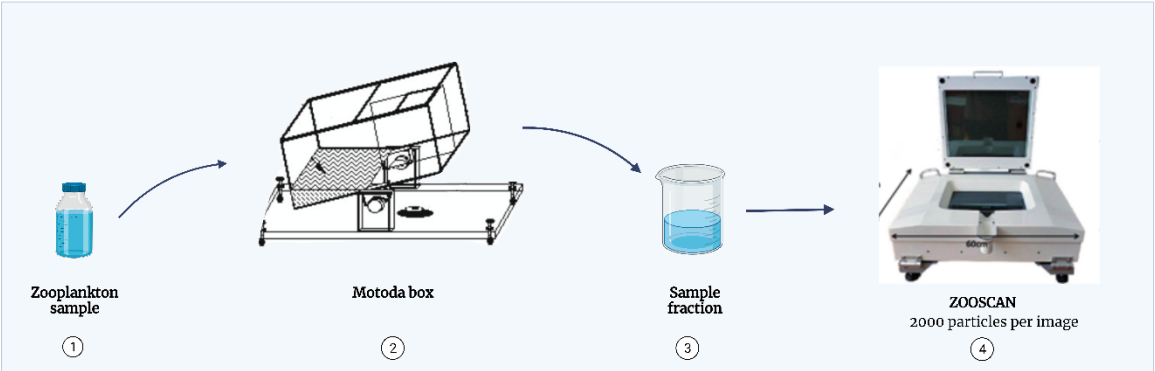


Figure 2.6. Protocol steps outline for processing a zooplankton sample in ZOOSCAN.

Figure 2.6 illustrates the ZOOSCAN analysis protocol: The zooplankton sample (1) is initially divided using the Motoda splitter (2). The resulting size fractions are then meticulously arranged in the scanning cell (3), ensuring careful manual separation of the zooplankton organisms to avoid overlapping entities and aiming for a count of approximately 2000 particles (4).

In the case of ZOOSCAN analysis, we divided the samples into two size fractions: <1000 µm and >1000 µm; as in the case of the Manta net (MERITE-HIPPOCAMPE) and Bongo net

(MOOSE-GE 19). For the remaining nets, fractions > 500 µm were considered. This method follows the established protocol set forth by Gorsky et al. (2010). This approach is essential to ensure that larger zooplanktonic organisms are adequately represented, as they might be significantly under-sampled if analyzed together with smaller ones.

Following the scanning process, each individual image underwent analysis using ZOOPROCESS, an embedded feature within the ImageJ image analysis software (Rasband, 2005). Specifically, objects with an equivalent spherical diameter (ESD) exceeding 300 µm were exclusively targeted for identification and subsequent analysis, consistent with the approach delineated by Gorsky et al. (2010).

2.3.1.4. Automatic classification of plankton groups

For both the FlowCAM and ZOOSCAN techniques, distinct biological components and particles were differentiated:

For the FlowCAM, a learning dataset was created in Ecotaxa, enabling us to achieve a comprehensive taxonomic identification. For instance, in the case of copepods, we were able to identify certain species and genera. However, for the sake of more effective comparison and alignment with the data acquired by ZOOSCAN, we ultimately grouped and categorized them into broader taxonomic categories. This approach encompassed various organisms, including eukaryotic microalgae, prokaryotic cyanobacteria, larger zooplanktonic groups, and inert detrital matter, including marine snow and aggregates.

In the case of ZOOSCAN analysis, we refined the classification using a learning set validated by Feliú (2020). This learning set, supplemented by manual corrections, facilitated the taxonomic classification of significant zooplankton groups, as well as inert detrital components such as marine snow and aggregates.

Finally, a number of taxonomically classified zooplankton categories were identified in terms of their abundances, including: nauplii, copepods, crustaceans (grouping such as euphausiids, mysids, and other less abundant crustaceans), appendicularians, chaetognaths, gelatinous organisms (grouping such as hydromedusas, salps, siphonophores, cnidarians, and other less abundant gelatinous organisms), alongside a diverse collection of other zooplankton taxa (including molluscs, polychaetes, and less prevalent protozoans), grouped as "miscellaneous". This approach enabled the identification of predominant zooplankton groups within distinct size fractions (Table 2.1).

Table 2.1. Summary outlining the prevailing zooplankton categories within the various size fractions, along with details regarding the examples of organisms and the conducted image analysis.

Size fractions	Zooplankton categories	Examples of organisms	Type of analysis
< 200 µm	Nauplii		Flowcam
	Small copepods	*Oithona* sp., *Oncaea* sp., *Euterpina* sp., *Microsetella* sp.	
	Small miscellaneous	Pteropoda, Copepods egg, Polychaeta larvae	
200-500 µm	Small copepods	*Oithona* sp., *Oncaea* sp., *Euterpina* sp.	FlowCam/ ZOOSCAN
	Large copepods	Calanidae, Corycaeidae	
500-1000 µm	Large copepods	Calanidae, Corycaeidae	ZOOSCAN
	Crustaceans	Ostracods, Amphipods, Zoea larvae	
>1000 µm	Gelatinous	Salps, Cnidaria, Hidromedusae,Doliolida	ZOOSCAN
	Appendicularians		
	Chaetognatha		
	Crustaceans	Mysidacea, Amphipods, Zoea larvae	

2.3.1.5. Biometry and size structure

Zooplankton images obtained from FlowCAM and ZOOSCAN are then subjected to automated processing using ZOOPROCESS, which performs tasks such as classification, enumeration, and size measurements (Figure 2.7) (Grosjean et al., 2004;Benfield et al., 2007; Bell and Hopcroft, 2008; Gorsky et al., 2010; Vandromme et al., 2012). As highlighted by Vandromme et al. (2012), this software carries out two fundamental functions: (1) it segments the original image into distinct valid targets by identifying regions with pixel gray levels falling below a threshold of 243 (8-bit grayscale, where black = 0 and white = 255), and (2) it quantifies 46 variables for characterizing objects, encompassing attributes like gray levels, fractal dimension, shape, and size (Gorsky et al., 2010, Vandromme et al., 2012). For our analyses, the object area, object ESD, major axis, minor axis, and the identity of the observed organism were considered. The identity was validated by a learning set (using ImageJ or Ecotaxa, as corresponds), followed by manual correction of the organisms in each category.

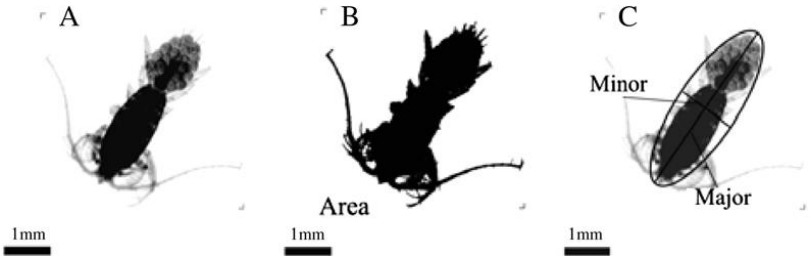


Figure 2.7. Scheme of the image analysis process conducted using ZOOPROCESS. (A), Raw image of a copepod female with eggs, (B), same object in black and white with a threshold of 243 for the computation of the area and (C), computation of minor and major axes of the best fitting ellipse. Figurure from Vandromme et al. (2012).

With the zooplankton organisms, with the object area obtained by the translation of pixel data into a quantitative area in μm^2, we derive the individual body weight from the relationship established by Lehette and Hernández-León (2009). Then a ratio carbon / dry weight was computed and the body weight was expressed as µg C ind $^{-1}$, using a relationship given by Gorsky et al. (1988), this estimation will be explained in detail in the following section 2.3.3. Finally, the zooplankton biomass expressed as mg C m^{-3}, was calculated by summing the individual products of the mean body weight of each zooplankton group and its corresponding abundance. In addition, the object ESD allowed us to estimate the biovolume.

Another crucial aspect is the determination of the size structure using the FlowCAM /ZOOSCAN combination, derived from the size fractions obtained through sieving. To prevent the overlap of organisms between the 200-500 µm size fraction analyzed by FlowCAM and the 200-1000 µm size fraction analyzed by ZOOSCAN, a merged methodology was adopted. Through meticulous examination of the dataset, corresponding to the size of each organism analyzed, and adhering to the criteria outlined by Feliú (2020), it was established that the most effective approach involved FlowCAM computing the ESD size-classes below 300 µm, while ZOOSCAN handled the ESD size-classes above 300 µm. This hybrid strategy allows for the comprehensive determination of the complete size spectrum.

2.3.2. Data analysis of plankton abundance and community structure

2.3.2.1. Community descriptors with FlowCAM and ZOOSCAN data

The analysis of zooplankton abundance (Ind/m^3 and percentage) and biomass (mg DW/m^3 and percentage) was carried out based on size fractions and ESD size-classes using data obtained from FlowCAM and Zooscan. This comprehensive analysis spanned

zooplanktonic sampling stations from both the MERITE-HIPPOCAMPE and MOOSE-GE 2019 cruises.

2.3.2.2. Community descriptors and diversity index

During both cruises, zooplankton taxa composition was also established through microscopy identification performed by specialists (Nouha Makhlouf for HIPPOCAMPE and Loic Guilloux for MOOSE-GE 19) allowing a more precise description of the zooplankton community.

For the MOOSE-GE 19 expedition, the abundance of the various taxa identified by microscopy was considered to observe spatial variations in the zooplankton community. This assessment involved calculating several diversity and richness indices, including the Shannon diversity index (H'), Pielou evenness (J'), species richness (Margalef, d), Brillouin diversity index (H), Fisher (α), Lambda diversity index, and 1-Lambda. These calculations were carried out using PRIMER v7 software (Anderson et al., 2008).

For HIPPOCAMPE, we have not performed the same analysis, since a thorough analysis of the taxonomic data is still ongoing by Nouha Makhlouf. However, we will sometimes refer to Makhlouf's results for comparison with MOOSE-GE 19 data. The same observation is also valuable for the following paragraph on Rank frequency diagrams.

2.3.2.3. Rank frequency diagrams (RFD) and p1/p2 ratio

For the evaluation of changes in the zooplankton community structure, the Rank Frequency Diagrams (RFD; Frontier, 1976; Frontier et al., 2008) were utilized. These diagrams visually portray the abundance of taxa or species in descending order, reflecting the transition from more common to rarer, all presented logarithmically.

This procedure includes ranking taxa according to their abundance and computing the frequency of each species relative to the total sample abundance. Subsequently, this frequency is plotted logarithmically against species ranks on the x-axis. Modifications in the RFD shape offer insights into the community's condition, especially its maturity. Steeper slopes imply a youthfully dominated community with prominent high-ranked taxa, while a flatter slope characterizes a mature community with a balanced presence of higher-ranked species.

The RFDs were divided into two sections: the first included the top four taxa, and the second covered the subsequent ranks with an abundance above 0.5%. The p1/p2 ratio comes from comparing slopes obtained through linear regression of these segments. *p1* is slope of the linear regression for the upper portion of the RFD and *p2* is the slope of the lower portion of the RFD (Mouillot and Lepretre ,2000). A p1/p2 ratio below 1 indicates

high diversity and a convex RFD shape, while a ratio above 1 suggests low diversity and a concave RFD shape (Figure 2.8).

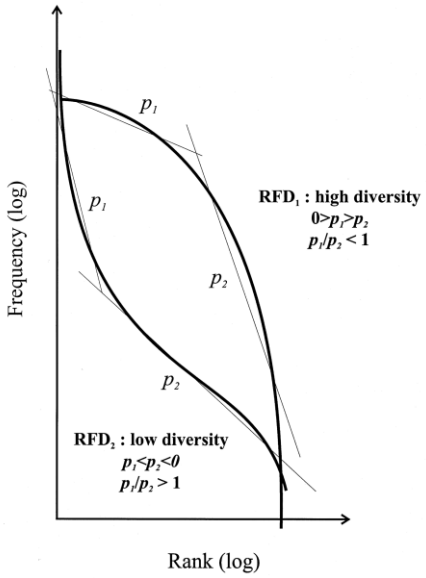


Figure 2.8. Two RFD with linear regressions for the first 4 ranks (p1 estimation) and the other ranks (p2 estimation). The first RDF (RDF1) shows a convex shape typical of a species community with high diversity (Frontier, 1976), p1/p2 is, therefore, lower than 1 whereas the second RDF (RDF2) shows a concave shape typical of a species community with low diversity (Frontier, 1976), p1/p2 is therefore higher than 1. All intermediate cases for the RFD shape can be observed in ecology. Figure from Mouillot and Lepretre (2000).

2.3.3. Data analysis of plankton group biomass and fluxes

2.3.3.1. Dry Weight Measurement

For the MERITE-HIPPOCAMPE cruise, in the laboratory, dry-weight biomasses (of half samples after Motoda splitting) were measured after drying samples on pre-weighted GF/F filters (60°C, 24h) and then re-weighted with a microbalance (Mettler, precision 0.1mg) according to the protocol established by Lovegrove (1966). From these overall results, the values obtained through image analysis tools (FlowCAM /ZOOSCAN) have been correlated, resulting in the derivation of the percentages corresponding to different categories of dry biomass (see Chapter 3).

For MOOSE-GE 19, the biomass Biovolume were estimated from the biovolume directly from the FlowCAM /ZOOSCAN treatment.

2.3.3.2. Biomass equations from zooplankton particle biometry and conversion factors

The contributions of zooplankton, detritus, and microphytoplankton components to the total weighted biomass were estimated by using the **area–weight relationships** from (Lehette and Hernández-León, 2009) for zooplankton (1), and **the biovolume-weight relationships** from (Alldredge, 1998) for detritus and microphytoplankton (2). Zooplankton biomass was converted to carbon assuming the carbon/dry-weight ratios given by Gosky et al., (1988) for Mediterranean zooplankton taxa:

(1) Body weight (µgDW) =a *(Area /1000000)^b

With Area in (μm^2)

(2) Detritus particle weight (µgDW) =c *(Biovolume)^d

With Biovolume in (mm^3)

where a and b, respectively, correspond to the intercept and slope values of the relationships specific to individual taxa as defined by Lehette and Hernández-León, (2009) and c and d, respectively, to microphytoplankton or detritus categories defined by Alldredge (1998).

2.3.3.3. Estimation of metabolic rates and fluxes

The zooplankton carbon demand (ZCD, in mg C m^{-3} d^{-1}) was computed for each zooplankton group from their biomass and from estimates of their daily ration:

$$ZCD = ration \times B_{zoo}$$

where B_{zoo} is the biomass of the zooplankton group considered (in mgC m^{-3}).

The ration (d^{-1}) is defined as the amount of food consumed per unit of biomass per day, and it is calculated as follows:

$$ration = (g_z + r)/A$$

where g_z is the growth rate, r is the weight-specific respiration, and A is the assimilation efficiency.

g_z was calculated following Zhou et al. (2010) as a function of seawater temperature, food availability, and individual body weight:

$$g_z = 0.033(C_a / C_a + 205e^{-0.125T}) \, e^{0.09T} \, w^{0.06}$$

Where T is the seawater temperature (°C); w is the individual body weight (mg C) calculated using the area–weight relationships from Lehette and Hernández-León (2009) and C_a is the autotrophic carbon (mgC m^{-3}) representing food availability, and estimated from *Chla* assuming a C/*Chla* ratio of 50/1. Here, we consider that the food is phytoplankton, following Calbet et al. (1996).

Assimilation efficiency (*A*) was considered as constant and equal to 0.7, following Nival et al. (1975). Weight-specific respiration rates (*r)* were estimated using the multiple regression model by Ikeda (1985) , with carbon body weight and temperature as independent variables:

$$\ln(y) = a_0 + a_1 \ln(x_1) + a_2 x_2$$

where *y* represents the oxygen consumption (in µl O_2 ind^{-1} h^{-1}), a_0= 0.5254, a_1= 0.8354 and a_2= 0.0601 are constants (see Ikeda, 1985); x_1 is the carbon body mass and x_2 is the habitat temperature (°C). *y* in µl was transformed into µM dividing by 22.4 and then in carbon considering the molecular weight of carbon (12) and assuming a respiratory quotient (RQ) of 1 in a median range of the values used by Mayzaud et al. (2005) for various taxonomic groups of zooplankton: 1µl O_2 = 12/22.4 µg C.

Ammonium and phosphorus excretion (in µg N or P ind^{-1} h^{-1}) were also estimated using the multiple regression models by Ikeda (1985) but where *y* represents the ammonium or the phosphorus excretion and where the constants are: a_0= -2.1763, a_1= 0.8293 and a_2= 0.0648 for ammonium excretion and a_0= -3.6031, a_1= 0.8622 and a_2= 0.0438 for phosphate excretion.

2.4. Statistical analysis

For MERITE-HIPPOCAMPE cruise, a Principal Component Analysis (PCA) was conducted on various environmental parameters. These parameters encompassed temperature, density, salinity, and chlorophyll concentration derived from in situ fluorescence measurements.

To analyze the spatial patterns of zooplankton communities, a matrix associating taxonomic groups with sampling stations was established using biomass values. This matrix was subjected to square-root transformation to compute Bray-Curtis similarity distances, recommended for composition analysis. The resulting similarity matrix was

subsequently subjected to non-metric multidimensional scaling (NMDS) for ordination. These two analyses were performed using PRIMER v7 software (Anderson et al., 2008).

NMDS generally help us to represent the species communities present in several localities in a reduced number of dimensions. If two locations are close together, this means that the species composition is somewhat similar. If they are far apart, it means that the species composition is not similar. The stress value of NMDS reflects how well the ordination summarizes the observed distances among the samples. The value of 0.07 found for our analysis is in the range of ideal representation in reduced dimensions.

Significant differences in biomasses, including total, size fractions, and taxa groups, were assessed using Student's t-tests. The comparisons were conducted between samples collected from two vertical nets spanning the entire water column with mesh sizes of 60 and 200 μm. Additionally, comparisons were made between samples collected from the entire water column and those from the CML, both 60 μm nets. Prior to analysis, the data were examined for normality using the Kolmogorov-Smirnov test and for homogeneity of variance using a Fisher F-test. The Mann-Whitney U-test was employed to evaluate variations in zooplankton grazing pressure among different areas.

For the MOOSE-GE 19 expedition, a hierarchical clustering analysis was employed to investigate the spatial distribution patterns of key environmental variables, including temperature, salinity, dissolved oxygen, chlorophyll-a, and MLD, using data collected from depths ranging between 0 to 200 meters. Station similarities were quantified using Euclidean distance (for environmental data), and the clustering process was executed utilizing Ward's linkage method within the R software. The relationships between the zooplankton community and the environmental variables were studied using a co-inertia analysis (Dolédec and Chessel, 1994) which involved combining results from a factorial correspondence analysis (FCA) on zooplankton taxa abundances and a PCA on environmental variables. Before conducting the analyses, the data were log-transformed to approximate a normal distribution. The software used for these analyses was ADE-4 (Thioulouse et al., 1997).

3. The MERITE-HIPPOCAMPE campaign

3.1. Introduction about MERITE-HIPPOCAMPE program

3.1.1. Objectives of the campaign

The MERITE-HIPPOCAMPE oceanographic cruise took place during the spring season from April 13 to May 14 in 2019, aboard the French Research Vessel Antea, and covered a North-South transect through the Mediterranean sea, from the French coast (La Seyne-sur-Mer, Northwestern Mediterranean) to the Gulf of Gabès in Tunisia (Southeastern Mediterranean). The principal aim of the MERITE-HIPPOCAMPE campaign was to investigate the accumulation and transfer of various organic and metallic contaminants in plankton, in comparison with their contents in the atmosphere and in the sea. Within the planktonic communities, a special focus was to identify potential bioaccumulation within the different components of planktonic food webs, namely bacterioplankton, phytoplankton, zooplankton and.

However, considerable gaps persist in understanding the capacity of plankton, particularly smaller fractions like pico- and nano-plankton, to accumulate and transfer contaminants. Methodological hurdles include segregating plankton into distinct size groups, distinguishing among bacterio, phyto, and zoo-plankton, and isolating non-living particulate matter from plankton. Challenges also encompass obtaining sufficient material for precise chemical analyses within each fraction and accurately discerning trophic relationships amid detritus and trophic level blending within each size fraction (Tedetti et al., 2023).

In this context, the MERITE-HIPPOCAMPE cruise strategically formulated a comprehensive research plan, employing advanced methodologies and tools to elucidate these questions. The primary emphasis was placed on selecting the potentially most productive zone in the water column: the chlorophyll maximum depth (CMD), a layer known for its high concentrations of plankton biomass, mainly phytoplankton and zooplankton. Sampling consisted of collecting volumes of water, suspended particles and plankton in this layer. To study potential contaminant transfers within plankton, observation of the planktonic community was carried out on the basis of size fractionation, ranging from from pico- (0.2–2 μm), nano- (2–20 μm), micro- (20–200 μm), and meso-plankton (200–2000 μm). The outcomes of these efforts are exemplified by the array of specialized articles authored by several authors, presented in a dedicated special

issue in the Marine Pollution Bulletin journal (https://www.sciencedirect.com/journal/marine-pollution-bulletin/special-issue/10B0SXC3XR2), aligning with the overarching objectives of the cruise.

3.1.2. Design of the campaign

In regard to the strategy of the MERITE-HIPPOCAMPE cruise, Tedetti et al. (2023) outlined the following key points:

1) Investigating contrasting ecological zones in the Mediterranean Sea during the spring bloom period, including urbanized bays (subject to anthropogenic impacts), intense fishing coastal areas, and offshore regions of eutrophic to oligotrophic productivity.

2) Characterizing water column properties through physical and biogeochemical measurements, with a focus on the DCM.

3) Maintaining ultra-clean conditions for accurate water and plankton sample collection and treatment, enabling precise analyses of inorganic and organic contaminants.

4) Collecting plankton, suspended particles, and water samples from the DCM and surface/subsurface waters, considering their significance in pelagic trophic interactions. This choice was driven by a main constraint: to gather substantial plankton biomass from a consistent site for comprehensive contaminant concentration assessment across various size fractions.

5) Fractionating collected samples into various size categories through filtration or sieving to facilitate subsequent analyses (0.2 µm to >2000 µm).

6) Sharing size-fractioned samples for a range of analyses, encompassing contaminants (trace metals, organometals, metalloids, organic contaminants, radionuclides, microplastics), plankton characteristics (biomass, size structure, taxonomy, diversity, pigments), and biogeochemical parameters (nutrients, chlorophyll a, particulate matter, isotopic ratios, biochemical compounds).

7) Utilizing multiple methods (taxonomy, optical measurements, chemical analyses) to differentiate between contributions of living (plankton) and non-living (detrital) components in contaminant accumulation and transfers.

8) Collecting atmospheric wet deposition samples (rain) to assess their potential role as contaminant sources for marine water and plankton. Ground stations were set up for parallel measurements, northern part (Marseille, France) and southern part (Sfax, Tunisia).

9) Sampling small pelagic plankton-feeding fishes in Tunisian waters to establish bioaccumulation factors for higher trophic levels.

3.1.3. Importance to characterize biota and zooplankton

Zooplankton plays a pivotal role in ecosystem dynamics, biogeochemical cycles, and the carbon pump (Banse, 1995; Lomartire et al., 2021). Positioned as a pivotal link within the trophic web, zooplankton capture and transfer energy to higher trophic levels, encompassing larger predators (Atkinson, 1996; Carlotti and Poggiale, 2010; Bănaru et al., 2013;Tedetti et al., 2023).

In this context, accumulation processes of contaminants, occurring through both dissolved and trophic pathways, have been confirmed to be influenced by factors such as size or age, trophic level, and habitat (Chouvelon et al., 2019). Therefore, a comprehensive characterization is imperative to enhance our understanding of these intricate dynamics.

During the MERITE-HIPPOCAMPE project, various analyses were conducted on samples collected at the DCM (also quoted as CML below) using Hydro-bios net (60 µm), *i.e.* on the metazooplankton: (1) Detailed analysis of the taxonomic and size structure of the zooplankton and associated flows (Fierro-González et al., 2023), which will be presented in the following paragraph, (2) Analyses of the zooplankton size fractions in terms of $\delta^{13}C/\delta^{15}N$ isotope ratios and biochemical content (Tesán-Onrubia et al., 2023), and finally (3) a large number of contaminants measurements in the size fractions (see in the Special Issue in Marine Pollution Bulletin "Plankton and Contaminants in the Mediterranean Sea: Biological pump and interactions from regional to global approaches" with the papers by Carlotti et al., 2023; Chifflet et al., 2023; Guigue et al., 2023; Tesán-Onrubia et al., 2023

3.2. Zooplankton biomass, size structure, and associated metabolic fluxes with focus on its roles at the chlorophyll maximum layer during the plankton-contaminant MERITE-HIPPOCAMPE cruise. Fierro-González et al., 2023

3.2.1. Introduction

Organic and metallic contamination levels have been monitored at alarming levels in large marine vertebrates (fish, mammals) in many regions and for several decades (Bouquegneau et al., 2002; Van der Oost et al., 2003; Weijs et al., 2014; Khairy et al., 2021). However, it is only recently that measurements of contaminants have become available in the surrounding environment and in the prey of these organisms, and have proven to be necessary for understanding the processes of contaminant accumulation in bottom-up food webs (Weijs et al., 2014). Several recent studies have demonstrated that plankton can be a key pathway for the uptake and transfer of contaminants entering the marine environment, playing a potential ecological role as the biological pump of contaminants (Tiano et al., 2014; Strady et al., 2015, Chouvelon et al., 2019). Trophic transfer models of contaminants underline the need for a better evaluation of transfer processes, particularly by trophic interactions, with a prerequisite being the availability of consistent data on contaminant content in successive trophic levels (Alekseenko et al., 2018). However, such studies are most often limited to a segment of the planktonic food-web for methodological reasons; to accurately measure these contaminant levels, large sample volumes are required and must enable distinction between different planktonic trophic levels. Pumping and filtering devices have been widely developed for collecting very high amounts of small particles and planktonic organisms smaller than microplankton (phyto- and zoo-) based on size-fractionation (*e.g.* Wen et al., 2018). A recent integrated study in the Gulf of Lion dedicated to investigating sardine and anchovy contamination (COSTAS) has extended this size fraction approach to the meso- and macro-zooplankton categories of net-collected organisms (Tiano et al., 2014; Chouvelon et al., 2019), giving an adequate fractional resolution for tracing contaminants in the planktonic network.

It is therefore important to further develop approaches that collect large plankton biomass in the same water bodies and that sort these biomasses by size fractions across the whole planktonic size range. The aim of the MERMEX MERITE program was to improve and test different approaches of collection/size fractionation of plankton biomasses in coastal areas (Bay of Toulon, Bay of Marseille, Gulf of Gabès), before defining a global protocol to be used along a north-south transect in the Mediterranean Sea, from the French coast to the Tunisian coast, passing offshore of Corsica and Sardinia: the MERITE HIPPOCAMPE campaign (Tedetti et al., 2023). The campaign consisted of

sampling large volumes of water and seston including plankton for measuring a large spectrum of organic and metallic contaminants (see details of survey strategy in Tedetti et al., 2023). For the 10 stations investigated, the samples were collected in one common layer in the water column, the chlorophyll maximum layer (CML), assumed to be the layer with the highest concentrations of plankton (mainly phytoplankton, but supposed to be attractive for zooplankton). Sampling was done using pumping systems (McLane pumps) and a horizontal towed Hydro-Bios net with 60 µm mesh-size net allowing discrimination up to 5 size-fractions between 0.2 and 60 µm and 5 size-fractions between 60 µm and a few mm (see details of methodology in Tedetti et al., 2023).

The aim of the present paper is to characterize the zooplankton components (from 60 µm to a few mm) in the different fractions of the samples collected at the CML of each station for which the contaminant measurements were carried out. For each size-fraction, the contribution to the biomass of detritus, of phytoplankton, and among zooplankton of the major taxonomic groups has been quantified. Metabolic rates calculated from the size spectrum of each zooplanktonic size fraction enable estimation of trophic and excretion fluxes flowing through this size fraction. To assess whether the contribution of taxonomic groups to the zooplankton biomass in the CML reveals a particular niche or not, it is compared to similar analyses carried out on vertical features in the epipelagic zone (200m depth or bottom to surface).

3.2.2. Material and methods

3.2.2.1. Study area and sampling strategy

The MERITE-HIPPOCAMPE cruise was carried out between 13 April and 14 May 2019, during the spring bloom, along a north-south transect in the western Mediterranean Sea, from the French coast (Toulon, Marseille) to the Tunisian coast (Gulf of Gabès) aboard the French Research Vessel *Antea* (Figure 3.1). Ten stations were sampled during 2 legs. Five stations (St02, St04, St03, St10, and St11) from Toulon to Tunis during Leg 1 (second half of April), and five other stations (St15, St17, St19, St09, and St01) from Tunis to the south of the Gulf of Gabès and then on the return to Toulon-La Seyne, during Leg 2 (first half of May). For each station, the date of sampling, the geographical position, the station depth, and the depth of different samples (CTD and net tows explained below) are presented in Table 3.1.

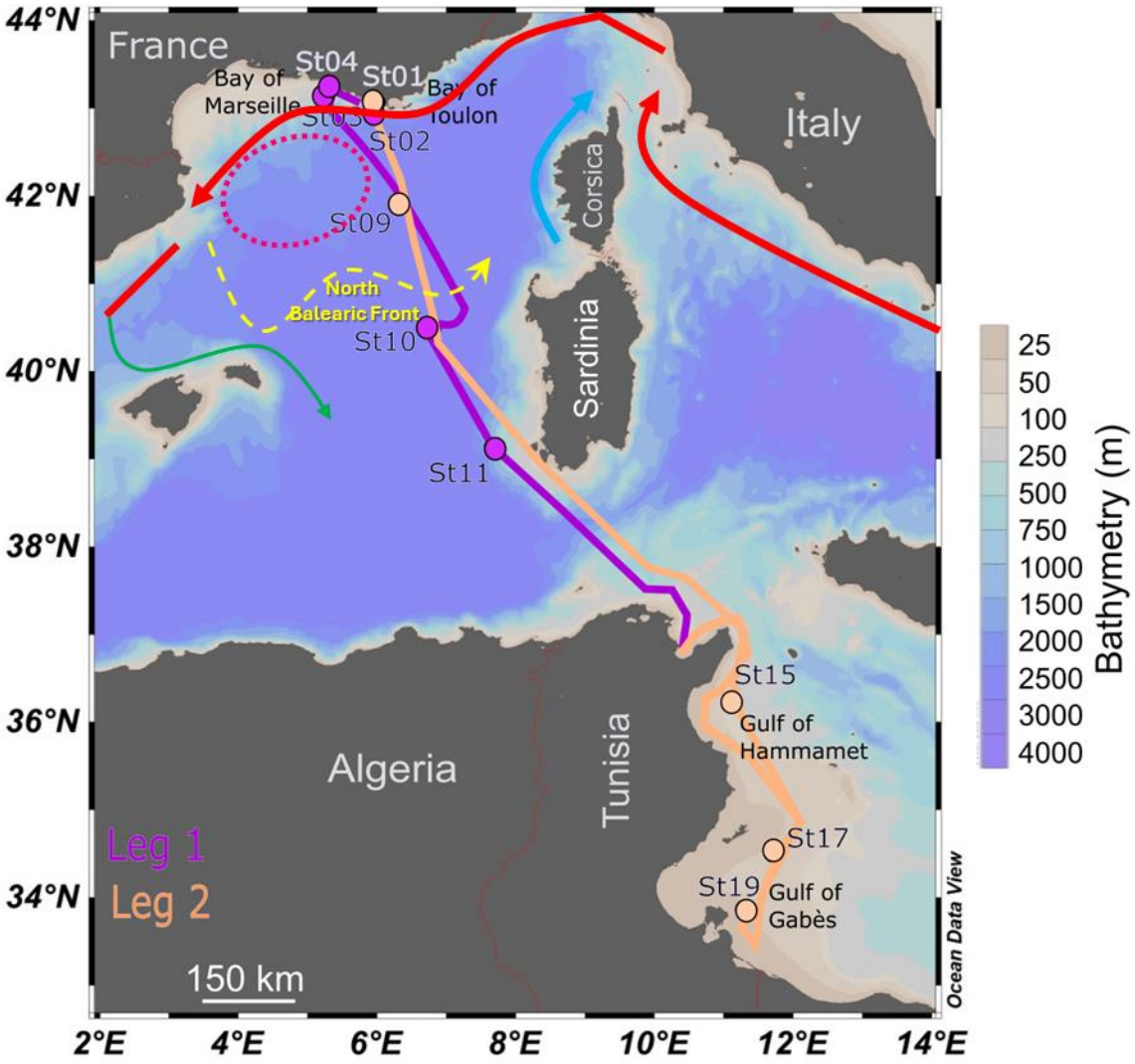


Figure 3.1. Map of sampled stations during the two legs of the MERITE-HIPPOCAMPE cruise (13 April-14 May 2019) on board the RV *Antea.* To indicate the Balearic Front on the map: The red arrows represent the northern current, the green arrow represents the Balearic current, the dashed yellow line represent the northern Balearic front, the light blue represent the West Corsica current, and the circle of dashed lines represents the area of deep convection in the center of the Gulf of Lion.

Table 3.1. Stations sampled during the MERITE-HIPPOCAMPE cruise: date, geographical position, bottom depths, maximum depths of CTD cast and of vertical triple net tow, and depth of horizontal Hydro-Bios net tow.

Station	Date	Latitude (N)	Longitude (E)	Bottom Depth (m)	Depth of CTD cast (m)	Depth Triple vertical net (m)	Depth Hydro-Bios net (m)
st01	11-05-2019	43°04.398	5°58.838	91	88	80	24
st02	15-04-2019	42°56.009	5°57.739	1770	250	210	31
st03	20-04-2019	43°08.823	5°14.199	95	100	85	55
st04	16-04-2019	43°14.876	5°19.001	58	50	48	35
st09	09-05-2019	41°54.661	6°20.163	2575	250	200	20
st10	24-04-2019	40°23.251	7°11.034	2791	250	180	40
st11	25-04-2019	39°08.193	7°40.382	1378	250	182	35
st15	30-04-2019	36°12.164	11°08.057	100	95	80	68
st17	02-05-2019	34°30.118	11°43.593	48	48	39	37
st19	03-05-2019	33°51.226	11°20.165	50	50	42	39

3.2.2.2. Environmental Data

At each station, an oceanographic carousel equipped with a CTD Seabird SBE 911plus to measure the hydrological variables (temperature, density and salinity) was deployed down to 250 m for open-sea stations or near the bottom for shallower stations (see Table 3.1). In addition, the CTD was coupled with several sensors including chlorophyll-a fluorescence (Chla; Aqua Tracka, Chelsea ctg).

3.2.2.3. Zooplankton sampling and sample processing

Zooplankton samples were obtained using three different types of nets for different strata in the water column (Table 3.2). A Multiple Plankton Sampler (Midi type, Hydro-Bios) with a square aperture surface of 0.25 m^2 towed at a constant speed of around 2 knots was used for sampling horizontally at the depth of the CML (see sampling depth for each station in Table 3.1), with five successive closing nets of 60 µm mesh-size, each of them filtering a water volume of around 50 to 80 m^3 (estimated by automatic detection with internal and external flowmeters, and according to plankton load before clogging), subsequently, the nets were accumulated to obtain enough matter for the different analyses. A Manta net was used for surface sampling, with a rectangular aperture of 0.7 × 0.4 m, and a 60 µm mesh-size net, towed at a constant speed of 2 knots for 10 minutes.

A steel frame with three circles (triple-net), each with a 60 cm diameter opening, was towed vertically at a constant speed of 0.7 m/s through the water column from 200 m

depth (or near the bottom) to the surface (see depth of vertical net lines for each station in Table 3.1). Three different mesh size nets - 60, 120 and 200 µm - were attached to the triple-net. The sample collected by the 120 µm net was not analyzed in this study, since the samples collected with the 60 and 200 µm nets provided a complete coverage of the zooplankton size spectrum. Moreover, the community observed within the 60 µm vertical net can be compared with the one collected at the DCM with the Hydrobios net.

Table 3.2. Scheme of treatments of the various size-fractions from the 3 nets used during the MERITE-HIPPOCAMPE cruise.

Net type	Net mesh-size (µm)	Purpose of sampling	Size fractions (µm)	Weight	Size fractions (µm)	Imagery treatment
Hydro-Bios	60	Contaminants Microplastics Plankton diversity	>2000	Dry weight	>2000	Zooscan
			1000-2000	Dry weight	1000-2000	Zooscan
			500-1000	Dry weight	500-1000	Zooscan
			200-500	Dry weight	200-500	FlowCam
			60-200	Dry weight	60-200	FlowCam
Triple Vertical	200	Plankton diversity	≥200	Dry weight	>1000	Zooscan
					200-1000	Zooscan
	60	Plankton diversity	≥60	Dry weight	>500	Zooscan
					200-500	FlowCam
					60-200	FlowCam
Manta	60	Microplastics Plankton diversity	>300	Dry weight	>1000	Zooscan
					300-1000	Zooscan
			60-300	Dry weight	200-300	FlowCam
					60-200	FlowCam

For further zooplankton analysis (biomass imagery, and microscopy), the samples from the different nets were fractionated using stainless-steel sieves of different mesh-sizes. The fractionation scheme slightly differed between nets due to different scientific objectives (Table 3.2). The samples from Hydro-Bios multinet were fractionated on board through a column of into five size fractions (60-200, 200-500, 500-1000, 1000-2000 and >2000 µm). These size-fractions were defined for studying the changes of contaminants with plankton size and therefore large volumes (between 300 and 2400 m^3) were filtered in order to get enough plankton in all fractions to measure contaminants (Tedetti et al., 2023). Around 10% of each of these fractions were kept for zooplankton diversity analysis (NB: however, at a few stations, not enough plankton material was recovered for the largest fractions, *i.e.* stations 04, 17 and 19). Then, they were split into two sub-samples:

one kept at -20 °C for further dry biomass weighing (mg DW m^{-3}), and the other one preserved in 4% borax-buffered formalin for imagery treatment. Manta net sample splitting prototocl was imposed for a comparison with a classical 300 µm mesh-size Manta net deployed in parallel (EU-MSFD protocols, results not presented in this paper). Thus, two fractions (below and above 300 µm) were considered for weighing, and then sub-fractionating was done for imagery analysis, allowing comparisons with Hydro-Bios samples. For the 60 µm mesh-size vertical net, only the lowest three size fractions common with those of Hydro-Bios were considered (because the plankton content was generally low). However, larger fractions were observed in the 200 µm mesh size net. Sub-samples of each fraction from the Manta net and vertical nets were preserved in a similar way as for Hydro-Bios samples and for similar analysis (see Table 3.2).

3.2.2.4. Zooplankton imagery treatment

Sample fractions below 500 µm were processed using a FlowCAM (see Table 3.2; Yokogawa Fluid Imaging Technologies Inc. Series VS-IV benchtop model (C. Sieracki et al., 1998). The other fractions were treated using a ZOOSCAN (Gorsky et al., 2010b). For both imagery sample treatments (FlowCam and Zooscan), the analyses were done following the protocol described by (Feliú et al., 2020). Distinct biological components and particles were differentiated: microalgae (eukaryotic microalgae and prokaryotic cyanobacteria) and non-living detritus material (marine snow, aggregates), and several living taxonomic groups of zooplankton: nauplii, copepods, crustaceans, appendicularians, gelatinous organisms, chaetognaths, and other diverse zooplankton groups (including molluscs, polychaetes, and rare protozoans) gathered in one group named 'miscellaneous' below. For each category, the abundance of organisms (ind m^{-3}) or particles (nb m^{-3}), and their area (mm^2) and biovolume (mm^3) were provided.

3.2.2.5. Biomass measurements and derived carbon demand, respiration, and excretion by zooplankton

In the laboratory, dry-weight biomasses were determined after drying samples on pre-weighed GF/F filters (60 °C, 24 h) and then re-weighed with a microbalance (Mettler, precision 0.1 mg) according to the protocol established by Lovegrove (1966). The contributions of zooplankton, detritus, and microalgae components to the total weighed biomass were estimated by using for zooplankton individuals the relationships from (Lehette and Hernández-León, 2009b) between body-area and body-weight, and for detritus and microalgae particles the biovolume-weight relationships from (Alldredge,

1998a). Zooplankton biomass was converted into carbon assuming the carbon/dry-weight ratios given by (Gorsky et al., 1988b) for Mediterranean zooplankton taxa.

The zooplankton carbon demand (ZCD, in mg C m^{-3} d^{-1}), respiration rates and ammonium and phosphorus excretion rates (both in µmol L^{-1} d^{-1}) were computed following the protocol described by (Feliú et al., 2020), and based on allometric relationships to individual body-weight. More details are presented in Chapter 2 ("Material and Methods").

3.2.2.6. Data analysis

A principal component analysis (PCA) was performed on the environmental parameters, including temperature, density, salinity, and chl*a* concentration (from in situ fluorescence measurements). For the spatial patterns of zooplankton communities, a taxonomic group–station matrix was created using the biomass values; this was square-root transformed to estimate Bray–Curtis similarity distances. The similarity matrix was then ordinated using non-metric multidimensional scaling (NMDS). These two analyses were performed using PRIMER v7 software (Anderson et al., 2008).

We tested for significant differences in biomasses (total, size fractions, and taxa groups) using Student's t-tests between samples of the two vertical nets of the whole water column with mesh-size of 60 and 200 µm, and between samples of the whole water column (COL-60) and from CML. Data were first verified for normality using the Kolmogrow-Smirnov test and for homogeneity of variance using a Fisher F-test. Mann Whitney U-test was used to compare the grazing pressure of zooplankton between areas.

Below, CML, SURF, COL refer to the three different strata sampled with nets, respectively, the chlorophyll maximum layer, the surface layer, and the integrated water column layer. COL-60 and COL-200 refer to the mesh-size nets of 60 and 200 µm used for the integrated water column tow.

3.2.3. Results

3.2.3.1. Spatial pattern of environmental variables

The first axis of the principal component analysis (PCA) on environmental variables (79.6% of variability) correlated with changes of temperature and salinity separating the stations located north (St01 to St09) and south (St10 to St19) of the Balearic front. Stations St10 and St11 have intermediate positions with their temperature and salinity in COL (both stations) and CML (St10 only) being close to those of the northern stations, whereas temperature and salinity are close to those of the southern stations for SURF and CML of St11. The second axis (15.6 %) is correlated with chlorophyll and differentiates

CML, SURF and COL values, more or less strong according to the stations, with the highest difference at St09 (Figure 3.2).

In general, the temperature and salinity profiles did not show strong stratification of the water column during the cruise (see detailed profiles of oceanographic and biological variables presented in Figure 3.4). Temperature values ranged from 14 to 17.8 °C at the surface (and very close values at CML), with the highest values recorded in the Gulf of Gabès.

In the southern basin, the coastal stations of Tunisia (St15, 17, and 19) and stations 10 and 11 presented salinity profiles below 38 (with the exception of St10, which had values higher than 38 below 79 m depth), whereas the northern stations were above 38 (with the exception of the first two meters of surface at St03). St09 presented the highest salinity in the northern basin and showed a strong contrast with St10, the nearest station in the southern basin. In general, the Chl-*a* vertical distribution presented a well-pronounced maximum at the CML, located near or above the bottom for most of the coastal stations (St19, 17, 15, and 03), or fluctuating in a more spread profile due to mixing (St01 and 04), St02 showing a typical Chl-*a* peak at mid-water depth. Among the offshore stations, St09 presented the highest values of Chl-*a* of the campaign, distributed in a broad surface mixed layer with a maximum value at 20 m, whereas St10 and St11 presented a CML at 40-45 m although more prominent at St10.

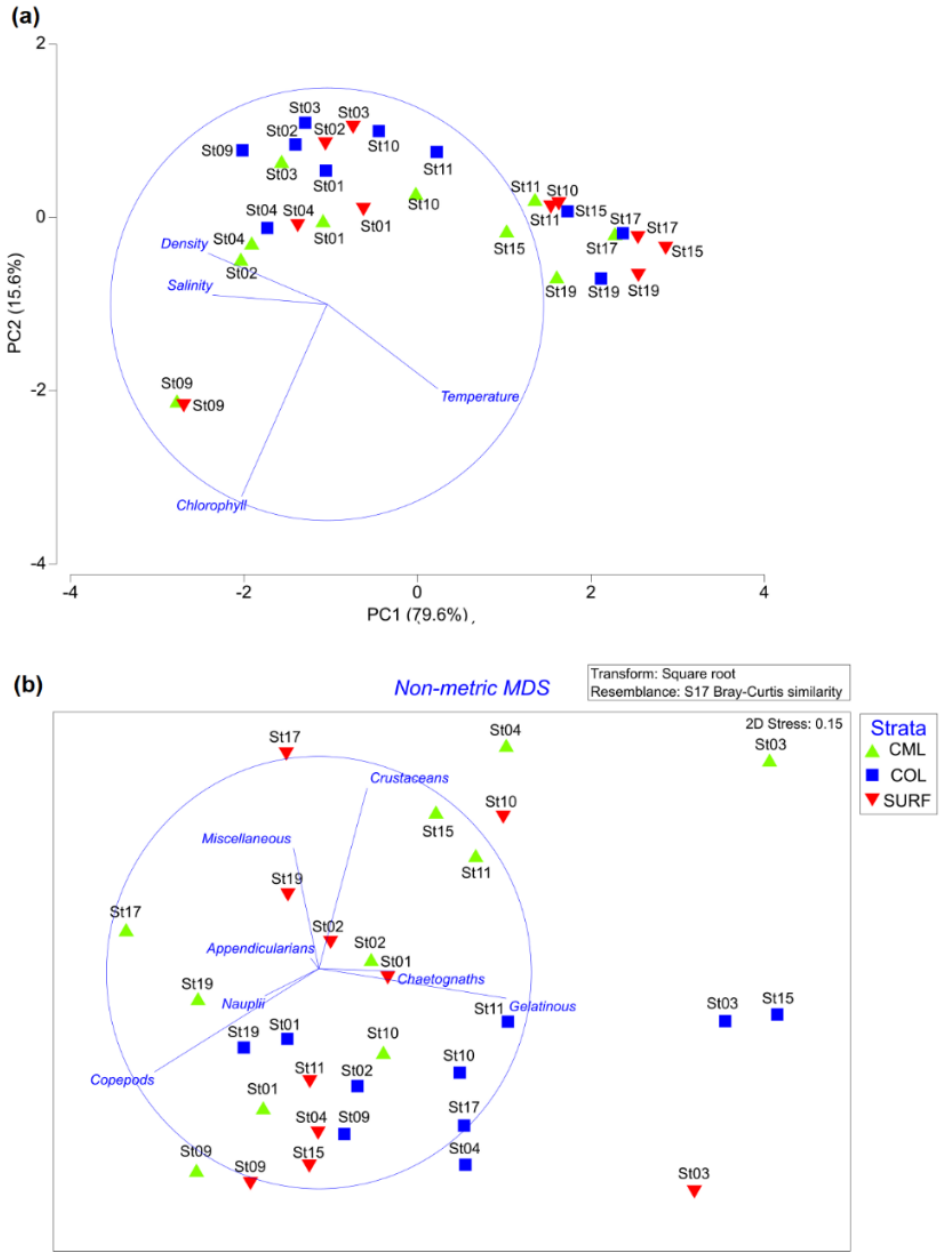


Figure 3.2. (a) Principal component analysis (PCA) ordination of four environmental indicators: temperature, salinity, density and chlorophyll, and (b) Nonmetric Multi-Dimensional Scaling (NDMS) on zooplankton taxa relative biomass, for all sampled stations of the MERITE-HIPPOCAMPE cruise. Blue squares: Integrated water column values (COL) from the bottom depth (or 200 m depth) to the surface. Green triangles: values at the chlorophyll maximum layer (CML). Red triangles: values at the surface layer (SURF).

3.2.3.2. Spatial patterns of plankton and detritus biomasses

NMDS analysis of the percentage of zooplankton taxa biomass reveals differences in compositions among strata for all stations. Some stations (St01, 02, 09, and 19) showed short distances between values of the three strata in the NMDS plot (Figure 3.2b) and this corresponded to only small differences, among these strata, in biomass composition with high dominance of the copepods (Figure 3.3a-d). Inversely, in the other stations (St03, 04, 10, 11, 15, and 17), wide differences between values of the three strata in the NMDS plot are related to the dominance of other taxonomic groups in one or two layers, *e.g*. importance of crustaceans (others than copepods) at the CML at St03, 04, 11 and 15, or in SURF at St10 and 17, or dominance of gelatinous (others than appendicularians) in COL at St15. From NMDS no clear regional patterns in zooplankton biomass composition appear, nor evident differences between coastal and off-shore stations, which would indicate for each station a local influence of hydrography and short-term meteorology on the biological biomass distribution.

The total sampled biomass was often higher at the CML than in COL-60 (St01, 02, 04, 09, 11, and 17), but in some cases, it was equivalent (St10, 15 and 17) or even lower (St03) and there was no significant difference between the mean values of the two strata (T-test; p=0.12). Both strata showed higher values at the coastal stations (St01, 04, 17 and 19) than at the oceanic stations (St02, 09, 10, 11). SURF showed total biomass generally much lower (Figure 3.3e-h) and significantly different than those recorded in COL or CML (paired t-test, p=0.035 and 0.020, respectively). Detritus was almost absent in SURF (Figure 3.3f) but represented a high proportion of the total sampled biomass in COL and CML, particularly in the shallowest southern (St17 and 19) and northern stations (St04 at the CML) (Figure 3.3e and 3g). Microalgae were collected at the CML of almost all stations but always with very low biomass compared to detritus and zooplankton, except at some coastal stations (St01, 04, 17, and 19). They were very low in most COL samples, except at St17 and were almost absent in SURF. The absolute values of zooplankton biomass showed neither a clear spatial pattern nor a significant difference (paired t-test, $p>0.1$) between the mean values of the three sampled strata (Figure 3.3e-h).

The comparison between the two vertical nets, the 60 μm (COL-60) (Figure 3.3c and 3g) and the 200 μm (COL-200) (Figure 3.3d and 3h) mesh-size nets, showed firstly that detritus and microalgae were collected almost exclusively by COL-60. In general, zooplankton biomass was of the same order for COL-60 and COL-200 (paired T-test; p=0.16), but with some differences in percentages of taxa. Nauplii, copepods, crustaceans, and miscellaneous presented significant differences between the COL nets (paired t-test, $p < 0.05$), whereas no differences appeared for appendicularians, chaetognaths, and gelatinous organisms.

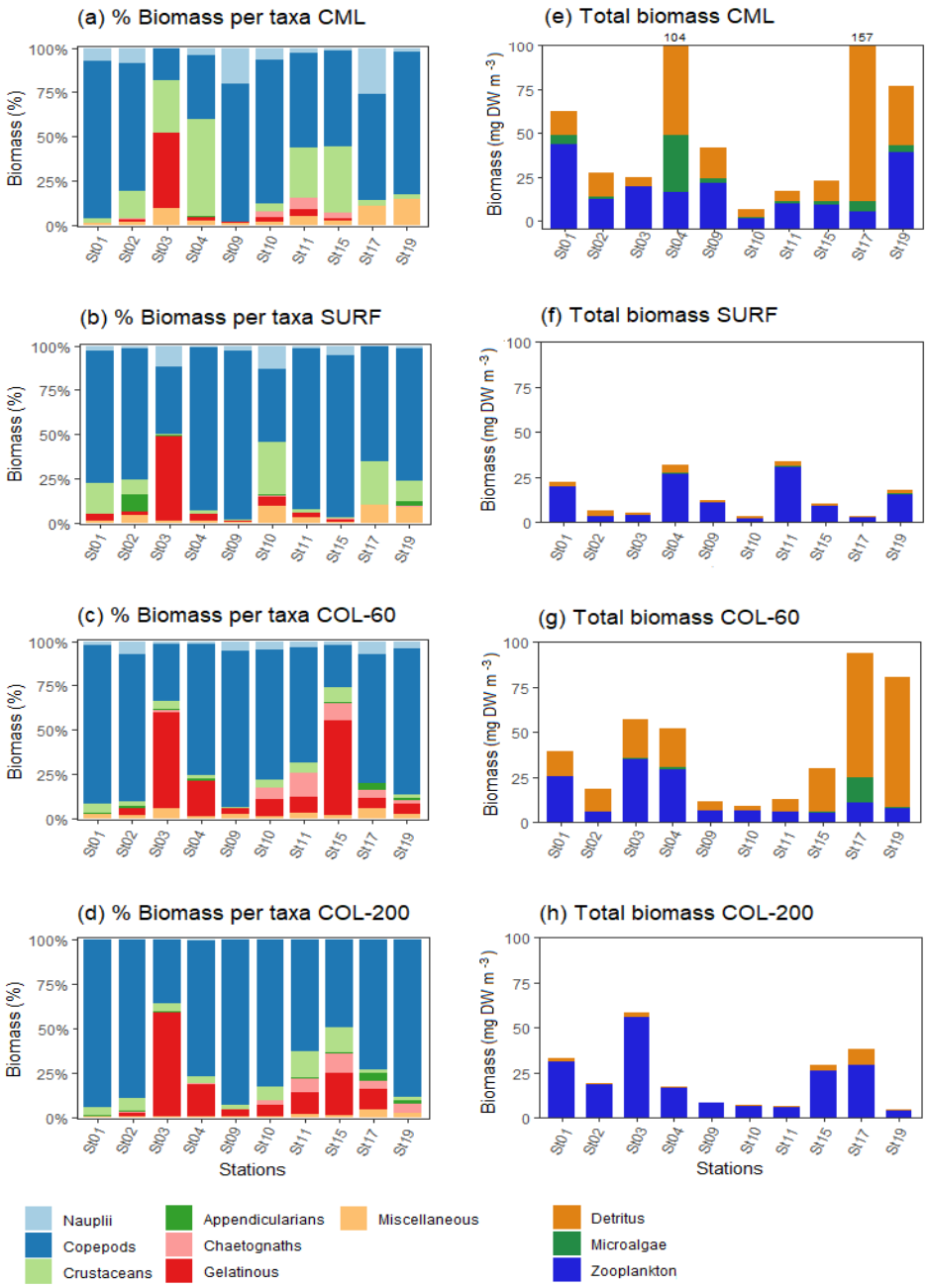


Figure 3.3. *Left column*: Cumulated percentages of zooplankton taxa biomasses sampled at each station in the different strata (a) at the Chlorophyll maximum layer (CML), with the 60 µm mesh-size Hydro-Bios nets, (b) at the surface layer (SURF) with the 60 µm mesh-size Manta net, and in the whole water column with a vertical tow (c) of the 60 µm (COL-60) and (d) of the 200 µm (COL-200) mesh-size nets. *Right column*: Total biomass concentration (mg DW m^{-3}) (e) at the Chlorophyll maximum layer (CML), (f) at the surface layer (SURF), and for the integrated water column with (g) net 60 µm (COL-60) and (h) net 200 µm (COL-200). The colored bars, blue, green and orange, represent the cumulated contributions to the total biomass concentrations by zooplankton, microalgae and detritus, respectively.

3.2.3.3. Zooplankton and detritus biomass in different layers at each station

St01 is a coastal station in the inner Bay of Toulon (Figure 3.4a). The water column presents a light thermocline at 10 m and a homogeneous salinity over the 80 m profile. The fluorescence profile presents values of around 0.3 mg Chl-*a* m^{-3} at the surface, a maximum of 0.59 mg Chl-*a* m^{-3} at around 20 m (CML), and then a regular decrease down to the bottom. CML presents high values of zooplankton biomass (45.8 mg DW m^{-3}), almost twice the COL averaged biomass over 80 m (25.2 mg DW m^{-3}) and SURF biomass (19.7 mg DW m^{-3}). For detritus, the CML biomass is comparable to the COL biomass, whereas SURF biomass is weak. Microalgae were found at the CML. Zooplankton biomass was dominated by copepods and nauplii in the three strata, respectively 96, 92, and 78% for CML, COL and SURF (Figure 3.3a-c), and SURF differed by relatively high biomass of crustaceans and gelatinous organisms.

St02 is offshore of Toulon Bay (Figure 3.4b). The water column presents almost homogenous temperature and salinity profiles. The fluorescence profile presents values around 0.2 mg Chl-*a* m^{-3} at the surface and a maximum value of 0.93 mg Chl-*a* m^{-3} at 32 m (CML). Microalgae were found at CML only.

For detritus, CML biomass is comparable to COL biomass (14.2 and 12.6 mg DW m^{-3}, respectively), whereas SURF biomass is weak (2.8 mg DW m^{-3}). The zooplankton biomass was twice as high at CML (10.4 mg DW m^{-3}) than in COL (5.5 mg DW m^{-3}) and three times higher than in SURF (3.5 mg DW m^{-3}). The contribution of zooplankton taxa differed between strata (Figure 3.3a-c) with the highest percentage of crustaceans in CML (15%), compared to SURF and COL (8 and 3% respectively), and also in the case of appendicularians only present in SURF (10%).

St03 is situated offshore of Marseille Bay, above the head of the Planier Canyon on the shelf break (Figure 3.4c). The water column presents a homogeneous temperature profile, whereas salinity has low values at the surface. The fluorescence profile ranged between 0.08 mg Chl-*a* m^{-3} in SURF and 0.39 m^{-3} at CML (52 m). Microalgae were almost absent. The highest zooplankton and detritus biomass values were registered in COL (average ~85 m, 35 and 22 mg DW m^{-3}, respectively), and the lowest values in SURF (4.1 and 0.8 mg DW m^{-3}). Zooplankton biomass shows a strong dominance of gelatinous organisms in all strata (42.5% in CML and 54.2% in COL) (Figure 3.3a-c). Crustaceans represent 30% of zooplankton biomass in CML but were low in COL (4.6%) and SURF (0.7%).

St04 is within the Bay of Marseille (Figure 3.4d). The water column presents a homogeneous temperature profile and a shallow halocline at 6 m. The fluorescence profile presents values of 0.6 mg Chl-*a* m^{-3} in SURF and a maximum of 0.83 mg Chl-*a* m^{-3} at CML (33 m). Higher biomass of detritus and microalgae were observed in the CML (50.5 and 30 mg DW m^{-3}, respectively) compared to SURF and COL. Inversely, zooplankton biomass

was higher in COL (29.1 mg DW m^{-3} over the 48 m of the water column) compared to SURF and CML (26.9 and 19.6 mg DW m^{-3}, respectively). The zooplankton biomass was different among strata, characterized by highest contribution of gelatinous organisms and copepods in COL (20.3 and 74%, respectively), whereas CML was dominated by crustaceans (55%), and SURF by copepods (93%) (Figure 3.3a-c).

St09 is an offshore station in the north of the North Balearic Thermal Front (Figure 3.4e). Both temperature and salinity profiles are homogeneous, although temperature displays a light thermocline at 22 m corresponding to the CML at the bottom of a surface mixed layer. The Chl-*a* profile shows high values (1.4 mg Chl-*a* m^{-3}) above the CML, and then sharply decreases down to 0.6 mg Chl-*a* m^{-3} at 39 m, and then to 0.1 mg Chl-*a* m^{-3} at 98 m. Very high biomass values of microalgae, detritus and zooplankton are recorded in the CML (respectively, 2.2, 16 and 25 mg DW m^{-3}). COL values (200-0 m averaged) for zooplankton and detritus biomass are more than twice as low as at CML. Although detritus and microalgae were negligible in SURF, SURF zooplankton was higher than the COL value. CML is characterized by high dominance of copepods and nauplii, with 78 and 20.3% respectively, whereas SURF is dominated by copepods with 96% (Figure 3.3a-c).

St10 is situated southwards of the Balearic Front (Figure 3.4f). The water column presents different strata with two thermoclines and haloclines respectively around 15 and 30 m, and a CML between 30 and 60 m (0.4 mg Chl-*a* m^{-3} at 42 m). Low biomasses of zooplankton, phytoplankton and detritus were found in all strata compared to other stations. COL presents higher zooplankton biomass (6.3 mg DW m^{-3}, on average over the upper 180 m) compared to CML (5.2 mg DW m^{-3}) and surface (2 mg DW m^{-3}). The detritus biomass at CML (4.2 mg DW m^{-3}) is twice as high as at SURF and COL. Microalgae were found only at the CML at a very low value. Zooplankton biomass composition appears different among strata (Figure 3.3a-c). CML and COL are quite similar, with copepods dominating the biomass (81 and 74% respectively). However, COL is differentiated by the contribution of gelatinous organisms and chaetognaths, with respectively 10 and 6% of the biomass. SURF is characterized by the dominance of copepods, crustaceans, and nauplii (41, 30 and 13%, respectively).

St11 is situated southwest of Sardinia (Figure 3.4g). The water column presents a deep thermocline and a halocline around 88 m, and a homogeneous fluorescence profile with values between 0.1 and 0.2 mg Chl-*a* m^{-3}, with the maximum situated at 35 m. Low biomass values of microalgae were collected, with the highest value in the CML (1 mg DW m^{-3}). SURF surprisingly presents high values of zooplankton biomass (30.2 mg DW m^{-3}), more than twice as high as CML (13.8 mg DW m^{-3}) and six times higher than COL (5.8 mg DW m^{-3} averaged value over 182 m). Detritus biomass shows its highest values in COL (7.1 mg DW m^{-3}) compared to CML (5. 4 mg DW m^{-3}), and low values at the SURF (2.6 mg DW m^{-3}). The zooplankton biomass presents high dominance of copepods at SURF (91%) but not at the CML (54%) due to a high proportion of crustaceans (28.3%,), whereas in COL

chaetognaths and gelatinous organisms were other major contributors (22.3%) (Figure 3.3a-c).

St15 is situated on the shelf of the Gulf of Hammamet on a 100 m depth sea floor (Figure 3.4h). The vertical profiles show steps of decreasing temperature values with depth, associated with similar steps of increasing salinity, probably corresponding to different layers. The fluorescence profile shows a peak between 59 and 67m, thus above the bottom boundary layer. Microalgae were found at the CML. The zooplankton biomass distribution is "classical", with the highest biomass accumulated at the CML (13.1 mg DW m^{-3}), twice the average value of COL (5.25 mg DW m^{-3}, over the 85 m). Detritus biomass was higher in COL than in the CML (24.4 and 13 mg DW m^{-3}, respectively) and even higher compared to SURF (0.97 mg DW m^{-3}). Contributions of zooplankton taxa to biomass presented strong differences between the three strata (Figure 3.3a-c). In CML, copepods and crustaceans dominate with 54 and 38% respectively, whereas only copepods almost dominate SURF strata with 91%. COL was characterized by the highest percentage of gelatinous organisms and chaetognaths, 54 and 9.2%, respectively.

St17 is situated in the north of the Gulf of Gabès (Figure 3.4i). The water column shows a light thermocline at 23 m and a homogeneous salinity profile. The fluorescence profile presents values of 0.02 mg Chl-*a* m^{-3} at the surface and a regular weak increase with depth down to the bottom. Microalgae are found at COL and CML. Comparable zooplankton biomasses are found in CML and COL (9.9 and 10.6 mg DW m^{-3}, respectively) whereas biomass is very weak in SURF. Very high detritus biomass cumulates in the CML (138.6 mg DW m^{-3}) in contrast with the lack of detritus in SURF (0.35 mg DW m^{-3}), whereas COL presented an intermediate value. The contribution of zooplankton taxa to biomass in the 3 strata slightly changed (Figure 3.3a-c), although copepods dominate in all three. Gelatinous organisms and chaetognaths are recorded with 6 and 5% for the COL but disappeared in SURF. The CML was characterized by a high presence of nauplii with 26% and miscellaneous at 11%.

St19 is the southern station in the Gulf of Gabès in shallow water (Figure 3.4j). A thermocline and a halocline occur around 30 m. The fluorescence profile presents values of 0.11 mg Chl-*a* m^{-3} at the surface, and regularly increases down to the bottom 0.54 mg Chl-*a* m^{-3}. Microalgae were found at the CML. The detritus biomass at the CML (31.4 mg DW m^{-3}) is much higher than in COL (2 mg DW m^{-3}) and SURF. CML zooplankton biomass (41.6 mg DW m^{-3}) was double the biomass measured in SURF (16 mg DW m^{-3}) and was much higher than in COL. Copepods dominated zooplankton in all strata (Figure 3.3a-c), whereas SURF differed by more crustaceans, CML by more miscellaneous, and COL by more gelatinous organisms.

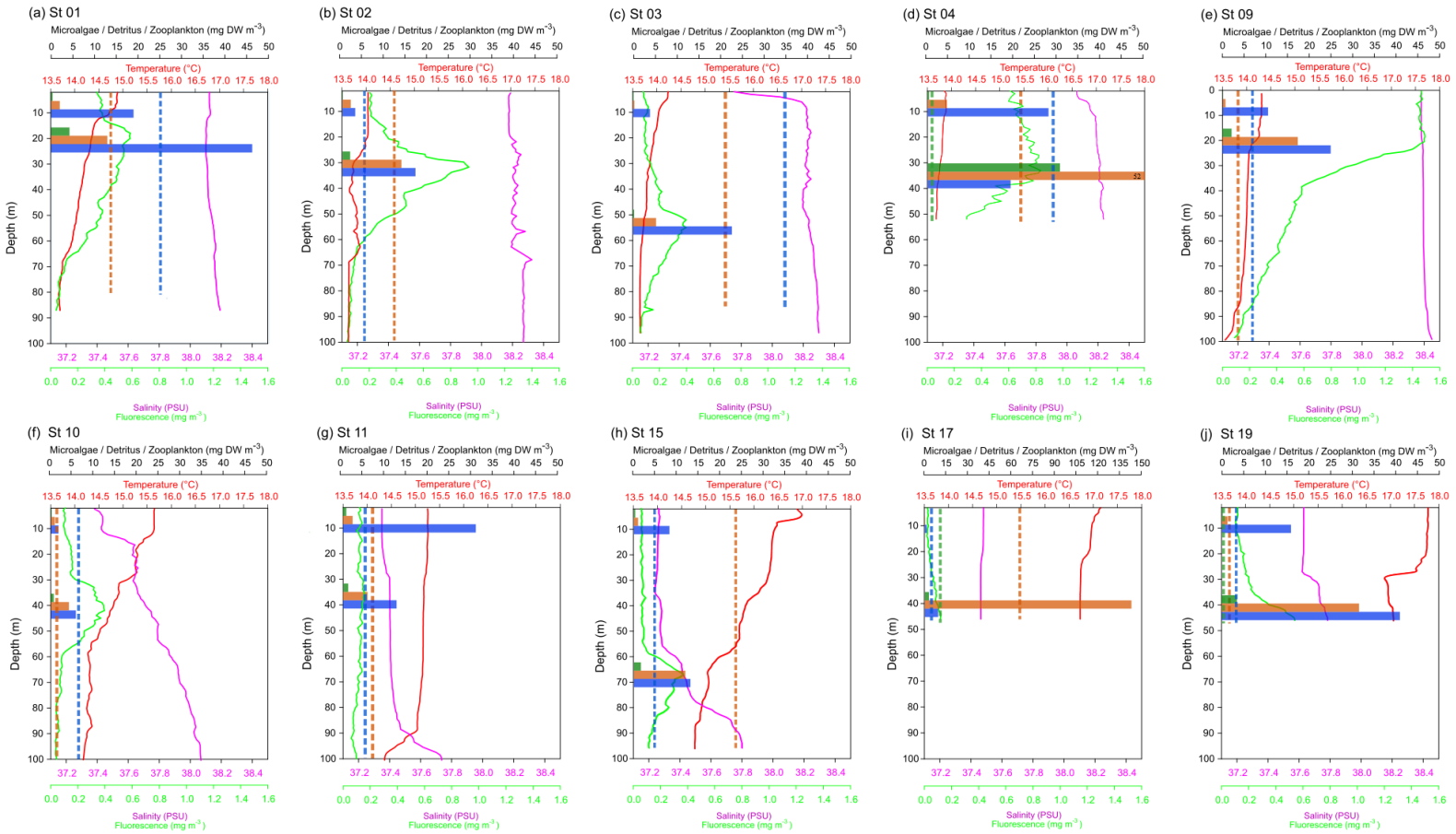


Figure 3.4. Vertical profiles of oceanographic variables (temperature, red line; salinity, pink line; and chlorophyll, green line) for all stations (a to j) during the MERITE-HIPPOCAMPE cruise. Biomass of microalgae (green bars), detritus (orange bars) and zooplankton blue bars) at the surface layer and at CML, and water column-averaged biomass (COL: bottom depth or 200 m deep to the surface) of microalgae (dotted green line), detritus (dotted orange line) and zooplankton (dotted blue line).

3.2.3.4. Zooplankton and detritus biomass in different size-fractions in the CML

Figure 3.5a shows the details of the distribution between sieved-size fractions of the biomass (see §3.2 and Table 3.2) collected with the Hydro-Bios net in the CML (Figure 3.3e). In general, detritus were concentrated in the lowest size fractions, and absent above 1000 µm, and similarly, microalgae (those retained in the Hydro-Bios net) accumulated in the smaller fractions, mostly in fraction 60-200 µm, plus in fraction 200-500 µm for St04 and 17. In contrast, zooplankton was distributed in all fractions with no clear pattern of dominance in a given size fraction among the stations. When detritus and microalgae biomasses were high in the first smaller fractions, zooplankton biomass was generally low in the largest fractions.

The percentages of zooplankton taxa biomasses (Figure 3.5b) were dominated by copepods and nauplii in the first smaller fractions, except at stations St17 and St19 where other plankton (miscellaneous) contributed substantially. At all stations, except St04, the fraction 200-500 µm was strongly dominated by copepods (more than 71%). At many stations, copepods still dominated the fraction 500-1000 µm (St01, 02, 03, 04, 09, 10, 19 more than 80%) and even the fraction 1000-2000 µm (St01, 02, 09, 10, 11). In the three largest fractions, crustaceans other than copepods could heavily dominate the biomass at some stations (St01, 02, 03, 09, 15 more than 52%), whereas at other stations, gelatinous organisms (St03, 10, 11, 19) and chaetognaths (St10, 11, 15) could make noticeable contributions. Appendicularians occur at some stations (St01, 04, 09) in the three smaller fractions, but with negligible biomass.

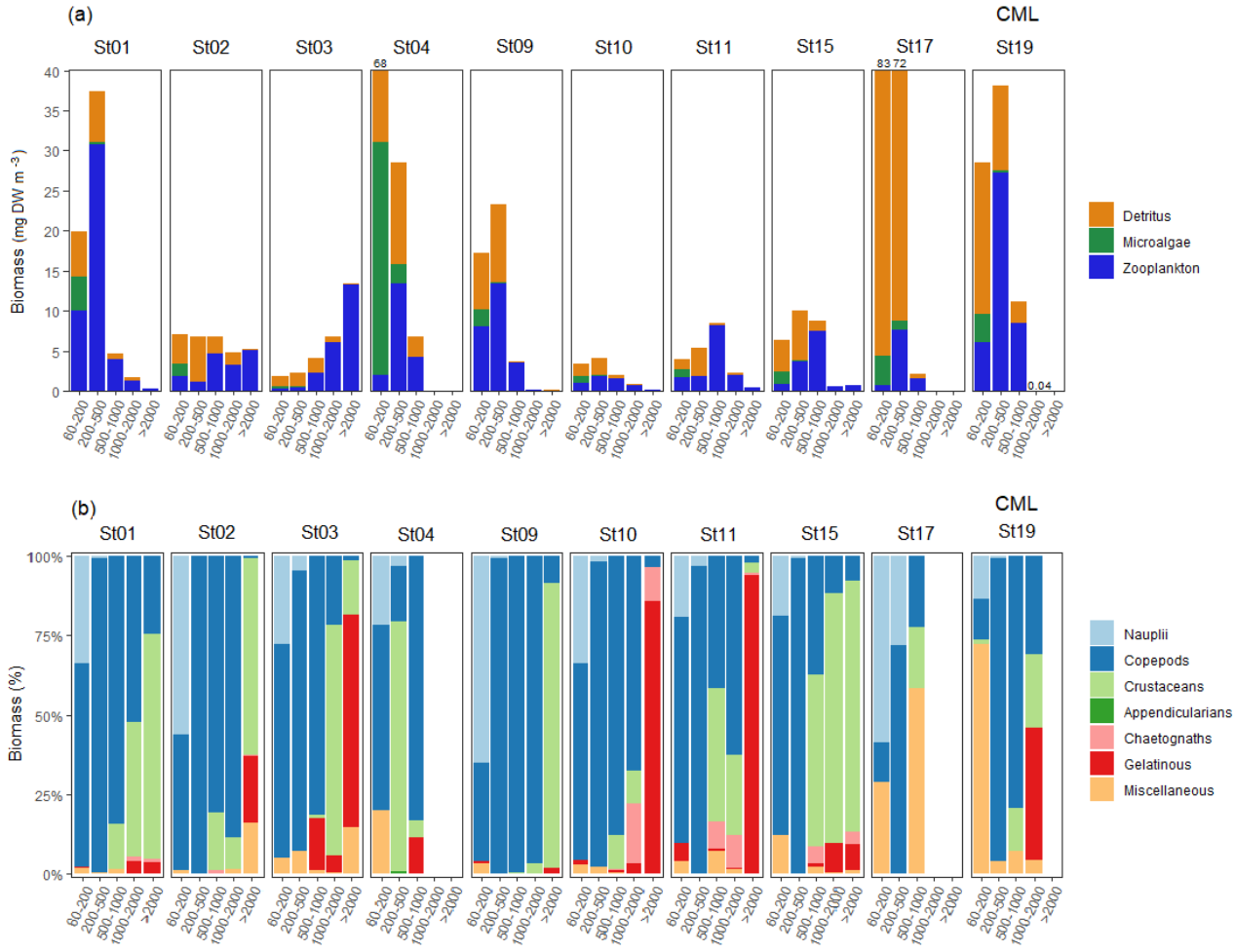


Figure 3.5. Plankton and detritus biomasses collected with the Hydro-Bios tow using 60 µm mesh-size net at Chlorophyll Maximum layer (CML) at the different stations during the MERITE-HIPPOCAMPE cruise. (a) Cumulated biomass concentrations (mg DW m^{-3}) of zooplankton (blue), microalgae (green), and detritus (orange), and (b) cumulated percentages of zooplankton taxa biomasses, in the five size fractions. Notes: (1) fraction 1000-2000 µm is missing for stations St04 and St17, and the fraction > 2000 µm is missing for stations St04, St17, and St19; (2) In the top panel for St04, 17, and 19 the numbers on the top of the bars the value reached by the cumulated biomass.

3.2.3.5. Comparisons of collected zooplankton and detritus biomasses in size fractions between CML and COL

At all stations, the contribution of the fraction 60-200 µm (Figure 3.6a) to the total zooplankton biomass in COL-60 was weak, *i.e.,* <9%, except <17% for St02, the biomass being distributed mostly in the fractions 200-500 µm and > 500 µm but rather unequally and without a regular pattern between stations. The distribution patterns of zooplankton among size classes were not always entirely similar between COL-60 and CML (Figure 3.6a and 5a), with the interesting exception of stations St03 and St15 where biomass concentrations increased with size-classes. It is noticeable that the contribution of the small fraction to the zooplankton biomass in CML was on average 2.5 times higher than in COL, and significantly different (Table 3.3).

In contrast to zooplankton distributions, detritus biomass in COL-60 (Figure 3.6a) was concentrated in the two first size-classes, mainly the first one (60-200 µm), and gave a very low contribution to the fraction >500 µm (see average values on Table 3.3). This pattern is different from that of CML (Figure 3.5a), where the contribution of the smaller fraction to biomasses was on average twice as low as in COL-60 (Table 3.2), whereas this contribution was much higher in the fractions above 200 µm. This shift in contributions of the detrital material in the successive size fractions was confirmed by significant differences between mean values (Table 3.3). In COL-60, when microalgae were collected, they were mostly present in the first class (Figure 3.6a), a characteristic common with samples in the CML.

Table 3.3. Summary of the biomass for plankton and detritus, and size fractions during the MERITE-HIPPOCAMPE cruise. Mean and SD estimated of total biomasses for detritus, microalgae and zooplankton and percentage for size fractions and zooplankton taxa at CML and COL. Comparison between mean values based on paired t-test on non-transformed and log-transformed data (with respectively symbols * and ** for significant differences, and (1) significant but without reaching necessary conditions.

	CML		COL		t-test on difference
	Mean	SD	Mean	SD	
Detritus (mg DW m^{-3})	29.69	42.26	20.23	20.52	
% 60-200	39.98	16.42	**69.52**	23.17	* **
% 200-500	**47.07**	13.08	26.29	21.10	*
% >500 (n=7)	**16.47**	14.46	4.18	3.37	**
Microalgae (mg DW m^{-3})	5.26	9.36	5.81	16.95	
% 60-200	90.29	5.12	90.51	11.62	
% 200-500	9.71	5.12	9.49	11.62	
% >500 (n=7)	-	-	-	-	
Zooplankton (mg DW m^{-3})	21.40	13.33	13.69	11.46	
% 60-200	**13.53**	8.48	5.78	4.99	* **
% 200-500	42.77	27.12	43.00	21.33	
% >500 (n=7)	54.22	31.58	51.22	23.50	
Nauplii (% total)	**8.07**	8.54	3.57	2.54	(1)
Copepods (% total)	62.19	22.46	69.22	23.13	
Crustaceans (% total)	**17.98**	18.80	3.57	2.54	**
Chaetognaths (% total)	1.35	2.19	**4.01**	4.65	**
Appendicularians (% total)	0.06	0.17	**0.97**	1.01	(1)
Gelatinous (% total)	5.49	13.09	**16.04**	20.79	**
Miscellaneous (% total)	4.86	4.88	2.62	1.76	
Nauplii (% 60-200)	34.84	18.57	46.33	14.42	
Copepods (% 60-200)	48.94	22.87	41.57	20.67	
Crustaceans (% 60-200)	0.14	0.44	0.01	0.03	
Chaetognaths (% 60-200)	-	-	-	-	
Appendicularians (% 60-200)	0.01	0.05	-	-	
Gelatinous (% 60-200)	0.74	1.68	0.86	2.39	
Miscellaneous (% 60-200)	15.33	22.03	11.23	11.44	
Nauplii (% 200-500)	4.37	8.50	2.22	2.25	
Copepods (% 200-500)	86.26	25.66	80.64	22.14	
Crustaceans%200_500	7.86	24.86	0.09	0.18	
Chaetognaths (% 200-500)	-	-	-	-	
Appendicularians (% 200-500)	0.08	0.25	**1.16**	1.19	(1)
Gelatinous (% 200-500)	0.00	0.00	13.62	22.66	
Miscellaneous (% 200-500)	1.43	2.44	2.26	2.74	
Nauplii (%>500 (n=7))	0.02	0.04	0.03	0.04	
Copepods (%>500 (n=7))	59.19	28.82	64.51	26.69	
Crustaceans (%>500 (n=7))	**26.26**	18.14	6.87	3.35	**
Chaetognaths (%>500 (n=7))	3.08	3.53	8.40	10.27	
Appendicularians (%>500 (n=7))	0.01	0.01	**0.66**	0.67	(1)
Gelatinous (%>500 (n=7))	8.51	15.79	17.40	23.83	
Miscellaneous (%>500 (n=7))	2.94	3.41	2.13	1.73	

In terms of taxonomic contributors to zooplankton biomass of COL-60 (Figure 3.6b), nauplii and miscellaneous counterbalanced, and sometimes dominated over small copepods in the smaller fraction (60-200 µm). The fraction 200-500 µm was most often strongly dominated by copepods and completed by gelatinous organisms, excepted at St15 where gelatinous organisms dominated. Large copepods generally dominate the biomass in larger fractions (> 500 µm), but some stations presented high contributions of gelatinous organisms and crustaceans (St03, 10, 11, 15, and 17). The contribution of crustaceans was high in CML both for the total biomass and for the fractions above 500 µm. Inversely, the contribution of gelatinous organisms (and chaetognaths at a few stations) was much higher in COL-60 than in CML. These trends were confirmed by significant differences between mean values (Table 3.3).

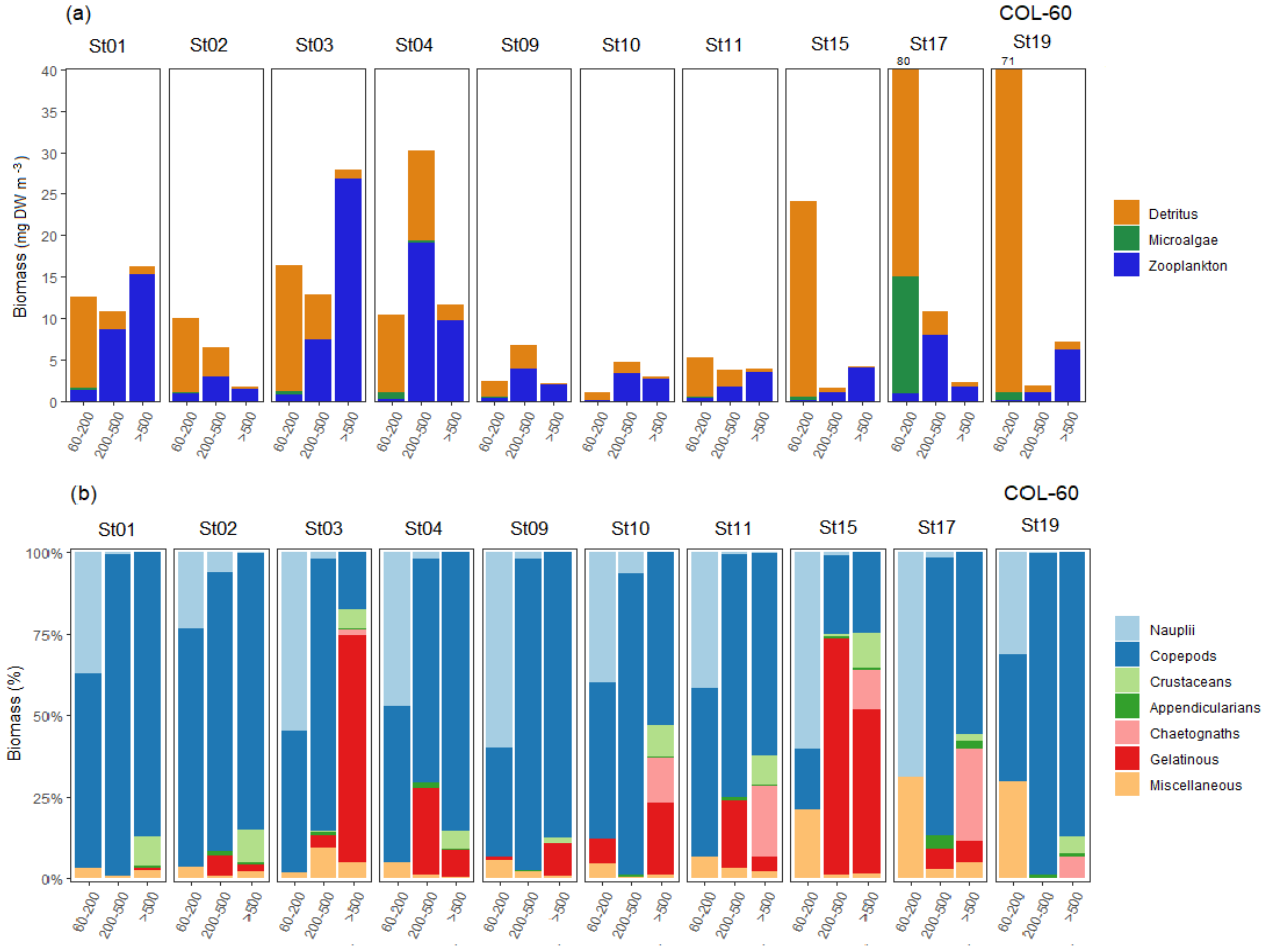


Figure 3.6. Plankton and detritus biomasses collected with the vertical net tow using 60 µm mesh-size net (COL-60) at the different stations during the MERITE-HIPPOCAMPE cruise: (a) Cumulated biomass concentrations (mg DW m^{-3}) of zooplankton (blue), microalgae (green) and detritus (orange), and (b) cumulated percentages of zooplankton taxa biomasses, in the three size fractions. Note: In the top panel for St17 and 19 the numbers on the top of the bars were the value reached by the cumulated biomass.

3.2.3.6. Estimated zooplankton carbon demand and nitrogenous and phosphorous excretion

The daily carbon demand of zooplankton ranged from 0.5 to 5 mg C m^{-3} d^{-1} in COL and from 0.6 to 6.9 mg C m^{-3} d^{-1} at the CML, with the highest values at St19 for both strata (Figure 3.7a,d). The mean values show no significant difference between the two strata (paired t-test; p=0.21). When excluding the contribution of carnivorous forms (chaetognaths), this ZCD represented 2.7 to 22.7% of the phytoplankton stock per day at the CML and between 3.1 and 25% in COL, with no significant difference between the mean values of the two strata (paired t-test; p=0.29). This grazing pressure showed no clear spatial trend at the CML, but in COL the values were on average significantly lower at the northern stations (St01 to St09; mean = 7.3 ± 3.3%) than at the southern stations (St10 to St19; mean = 19.6 ± 6.0%), in association with a parallel and significant decrease of the phytoplankton biomass from 27.4 ± 20.2 mg C m^{-3} in the north to 7.8 ± 6.1 mg C m^{-3} in the south (Mann-Whitney U-tests; p=0.036 and 0.0002, respectively).

The daily nitrogen and phosphorous excretion (Figure 7b,e and Figure 7 c,f, respectively) varied between 4 and 908 µg N m^{-3} and between 0.5 and 131 µg P m^{-3}, respectively, and were not significantly different between the DCM and COL (paired t-test; p>0.3). The zooplankton excretion represented a daily N and P recycling equivalent to 0.2 to 19% of the DIN stock and to 0 to 21% of the DIP stock. In both cases the highest values were found at the DCM of St01 in relation to the very high zooplankton biomass at this level (see Figure 3.4a).

The contribution of the different size fractions to the ZCD was highly variable between stations and strata (Figure 3.8). The contribution of the smaller fraction (<500 µm) to the ZCD is more often highly predominant or at least comparable to that of larger fractions (>500 µm), except at St19 for COL and at St03 in CML where most of the ZCD (>80%) was from the larger fraction (>500 µm). On average, the relative contribution of the size-fractions to the ZCD showed no significant difference between CML and COL (paired t-test; p>0.1).

Considering the whole size-fractions, copepods were the major contributors to the ZCD, except in the CML at St04 where other crustaceans made an equivalent contribution (46.9% vs 47.3% for copepods). Other crustaceans also made an important contribution to ZCD in the CML at St15 (34.5%) and St02 (25.4%), whereas miscellaneous zooplankton was numerous in the CML at St19 (21.9%) and gelatinous organisms in the COL at St03 (18.4%) and St15 (28.5%). On average, copepods contributed significantly more to the ZCD in COL than in CML, and the same trend was observed for gelatinous organisms and appendicularians, whereas nauplii contributed more to the ZCD in CML than in COL (paired t-test; p<0.05). Overall, the total ZCD, and the contribution of size fractions or of taxa to this ZCD showed no clear spatial pattern.

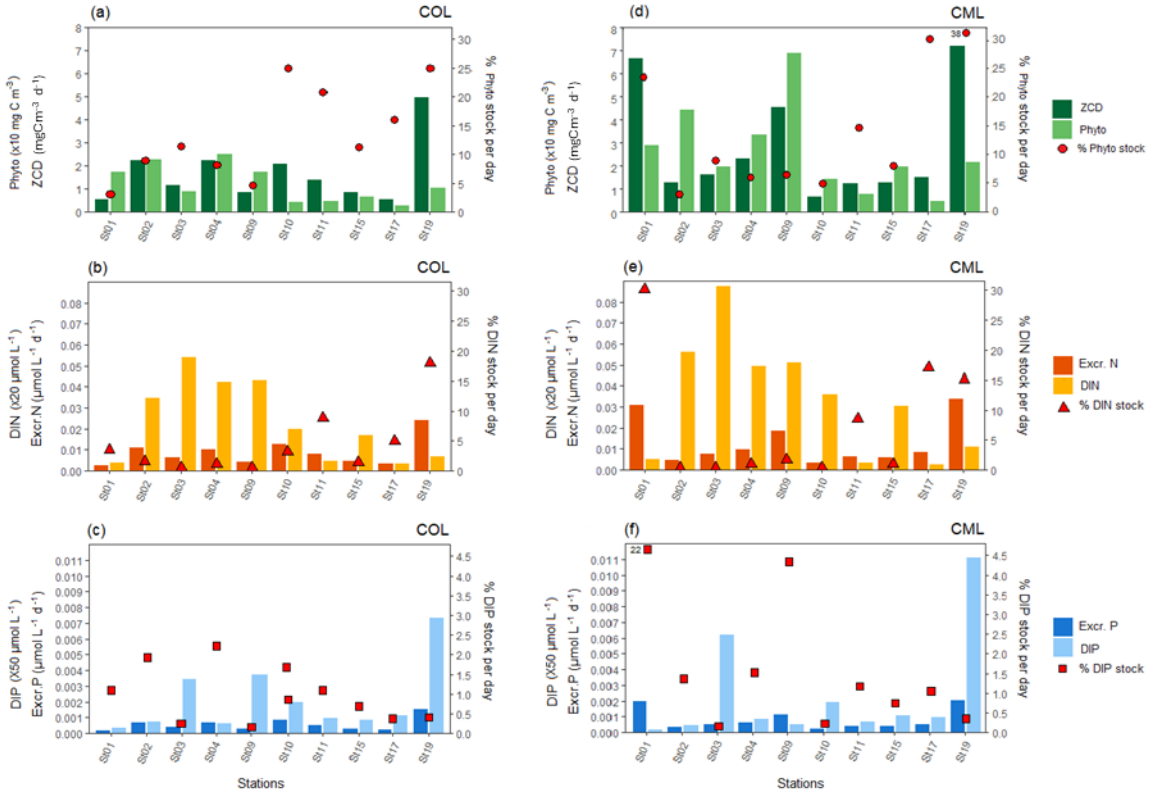


Figure 3.7. Zooplankton carbon demand and phytoplankton stock, and percentage on the ratio carbon demand / phytoplankton stocks (a, d), nitrogen excretion and DIN stock, and percentage on the ratio (b, e), phosphorous and DIP stock, and percentage on the ratio (c, f), respectively for COL (a, b, c) and CML (d, e, f). Note: In panel (f) the number for station 01 gives the value of %DIP stock out of scale.

The contributions of size-fractions or the taxa to N and P excretion rates were very similar to those of ZCD (*i.e.* similar to Figure 3.8). All values for ZCD and excretion rates are presented in the annexes material.

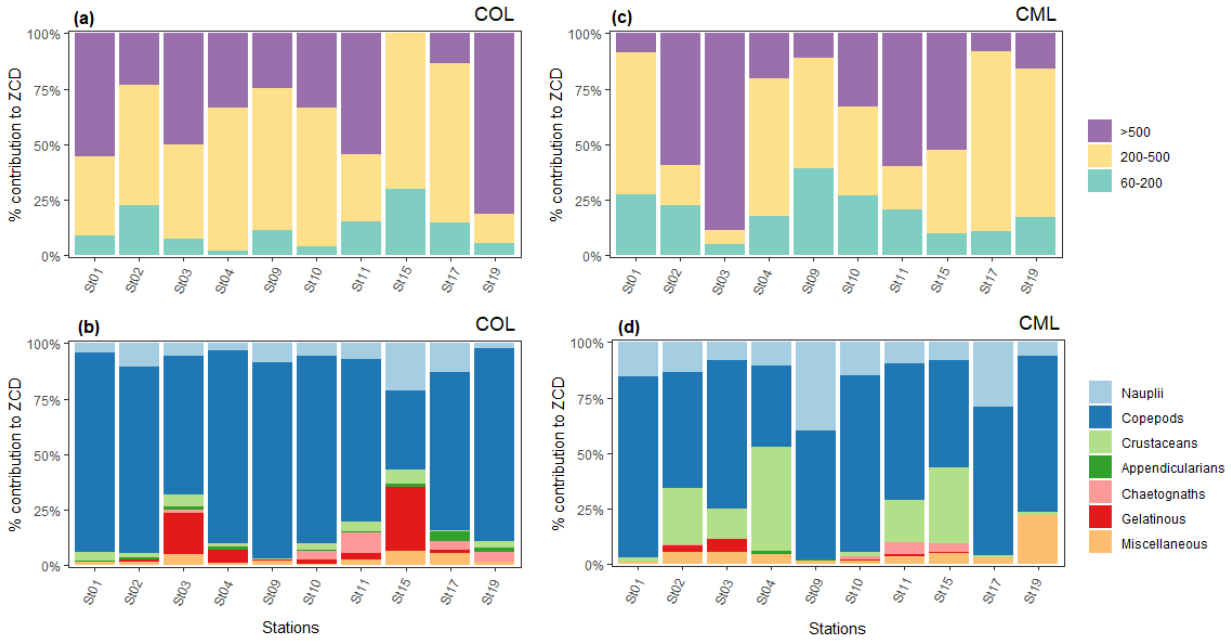


Figure 3.8. Contributions in cumulated percentages of size-fractions (a, c) and zooplankton taxa (b, d) to the zooplankton carbon demand in COL (a, b) and CML (c, d).

3.2.4. Discussion

3.2.4.1. Overview of the spatial patterns of environmental and biological variables during the MERITE-HIPPOCAMPE cruise

As the campaign took place over one month in the spring along a north-south transect with 10 stations sampled, either on the way out or on the way back, the environmental and biological characteristics of the stations did not enable a clear regional spatial pattern to be obtained, and local climatic and hydrodynamic conditions predominated over the spatial gradients. This means that the results obtained on the biotic compartment and ultimately in the contaminant studies must be interpreted in a mostly local context. Nevertheless, the present work contributes to broadening the characterization of plankton and detritus biomass distribution in the three different strata over several regions in the Mediterranean Sea.

We could highlight some global differences between the stations located north and south of the Balearic front, in terms of temperature and salinity values (see Figure 3.2), in phytoplankton biomass in both COL and CML (see Figure 3.7a and 7d), but only for COL in zooplankton carbon demand (see Figure 3.7a). These patterns are probably linked to a

late impact of the deep winter convection in the Gulf of Lion in 2019, a relatively convective and productive year (Margirier et al., 2020; Bosse et al., 2022), in the northern part of our transect (*i.e.* down to the Balearic front), whereas the generally low plankton productivity of the southern region can be increased by long-term mesoscale features isolated from the Atlantic current (Millot and Taupier-Letage, 2005b), such as at our stations 10 and 11 (Rwawi et al., 2023), or by the impact of Saharan dust (Riandey et al., 2005; Feliú et al., 2020; Guieu et al., 2020) such as at our stations 10, 11 and 19 (Tedetti et al., 2023).

Some differences between coastal (St01, 03, 04, 15, 17, and 19) and open sea stations (St02, 09, 10, and 11) in terms of detritus and zooplankton biomasses (see Figure 3.3g) could be linked in coastal stations to resuspension of sedimentary particulate matter induced by local wind-driven currents, and for zooplankton to limited deep vertical migration compared to open sea stations (since sampling was always performed during daylight, when most zooplankton are found in deeper water). However, the zooplankton biomass (total and in taxonomic contribution) does not show any specific gradient from north to south whatever the strata or the net considered (see Figure 3.1b and Figure 3.3). It is likely that the small number of sampled stations, especially in oceanic areas, as well as the long duration of our campaign do not allow identification of large north-south patterns that have nevertheless been widely documented for zooplankton in other studies (Mazzocchi et al., 2007; Siokou-Frangou et al., 2010; Saiz et al., 2014). Moreover, these studies have also mentioned that more local hydrodynamic or atmospheric conditions occur in addition to these large global patterns.

For each station, our study strategy enabled us to identify vertical gradients provided that recent local climatic and hydrodynamic conditions did not lead to excessive mixing (see Figure 3.4). Some stations (St01, 02, 03, 10, and 15) showed a rather typical stratification with clear vertical physical gradients and a deep maximum of chlorophyll, but this was not systematically reflected in the zooplankton biomasses. For various reasons, other stations did not show clear stratification. Station 04 had among the highest zooplankton biomass at the surface, probably related to a homogenization of the water column. Very shallow coastal stations in Tunisia showed accumulations of Chl*a* and zooplankton in a CML just above the bottom (St17 and St19). This phytoplankton biomass bulk above the bottom where zooplankton accumulates as well is a phenomenon also encountered in the Gulf of Lion (B. Espinasse et al., 2014). The Tunisian coastal stations (St15, 17, and 19) did not show higher zooplankton concentrations in the water column compared to the northern coastal stations (St01, 03, and 04). This may be more related to their high detritus load than to differences in community structure when compared to the northern coastal stations. This detritus load may be a consequence of mixing and retention due to the high tidal currents in the Gulf of Gabès (Béjaoui et al., 2019).

The oceanic offshore stations presented a quite different pattern for the reasons explained below. Station 09 is located in the usual area of the deep-convection (Margirier

et al, 2020). Although it was visited at the end of the survey (8-9 May), which was a little more than one month after the peak of the phytoplankton bloom observed at the end of March, it was the richest station in Chla, nitrate and silicate from the whole MERITE-HIPPOCAMPE cruise (Tedetti et al., 2023). Station 09 had a true mixed layer above the CML up to the surface, inducing higher Chla and zooplankton concentrations in CML and SURF, compared to COL (see Figure 3.4e). Although the stratification appeared quite moderate (almost homogeneous temperature and salinity), the high chlorophyll in the layer 0-25 m might be due to previous steps of stratification and to mesoscale structures in this area in this period (Rwawi et al., 2023). Similar high zooplankton concentrations present in the upper layer in the post-bloom phase in the deep-convection area have already been described by (Donoso et al., 2017a).

Station 02 is an oceanic station, situated in the broad periphery of the deep convection area (following Donoso et al., 2017), very close to the coast but also impacted by other different phenomena: intrusions of the northern current, hydrodynamic processes linked to the shelf break, and coastal impacts. This station sampled in the early phase of the cruise, under very bad weather conditions, presented a clear CML, despite a homogeneous physical structure. It is separated from the open ocean by the North Current and is not much affected by deep convection due to this natural barrier (Millot and Taupier-Letage, 2005b). Zooplankton sampling at stations 10 and 11 in the western oceanic waters of Sardinia was performed with a time lag of one day and occurred respectively 2 and 3 days after a dust event (22 April). The zooplankton biomass and taxonomic structure showed an interesting contrast between these two stations, particularly with differences in surface (Figure 3.3b and f; Figure 3.4f and g), which could be consistent with zooplankton quick response to dust effect in a few days (Feliú et al., 2020).

In contrast, differences in CML (Figure 3.3a and e; Figure 3.4f and g), not comparable to those observed at the surface, might be rather due to an additional specific 3D-mesoscale context of each station (Rwawi et al., 2023) impacting the vertical structure and differentiating the SURF and CML layers (see Figure 3.4 f and g), and the integrated values over the water column appeared buffered (Figure 3.3c and g; Figure 3.4f and g). For oceanic station 11, the water column seems very homogeneous down to 90 m, with a very low Chl-a maximum, and the low zooplankton biomass from the vertical net in the upper 200 m is due to the very low biomass below 90 m. The very high value for zooplankton at the surface may be due to enhanced productivity since a high density of copepodite stages was observed (Makhlouf, pers. comm.).

3.2.4.2. Biological specificities of the CML

Due to the sampling strategy centered on the CML layer for measurements of contaminant contents in plankton, our focus on zooplankton characterization in the CML appears to be unique compared to previous regional studies in the Mediterranean Sea.

Zooplankton net sampling is usually carried out by vertical net tows in the epipelagic zone (0-200 m) or just under the surface layer when studying the hyponeuston. These two types of sampling were also carried out during the MERITE-HIPPOCAMPE cruise to allow better characterization of the CML by comparisons with other strata.

At the scale of the basin, this comparison shows first of all an accumulation of detritus most often occurring at the CML, whereas SURF always presented the lowest detritus loads (see Figure 3.4). Sometimes the CML was also a layer of accumulated microphytoplankton, mostly chain-aggregated and/or linked to detritus *e.g*. station 04 (see Figure 3.4d). Among all stations, zooplankton biomass was on average higher at the CML than in COL and SURF (respectively 1.5 and 1.7 times higher), but the differences between the 3 strata were not statistically significant due to very high variability. According to the stratification and the intensity of the chlorophyll peak around the identified CML in each station profile, we can indeed distinguish 4 cases: (1) no accumulation of zooplankton at the CML when the peak is not well-formed (St04, 11, and 17), (2) accumulation of zooplankton at the CML when the peak is well-formed (St01, 02, 15, and 19) but also (3) no accumulation despite a well-formed peak (St03 and 10), and finally (4) the case of station 09 is a bit different with a high concentration of zooplankton at the CML but with a 0-25m layer quasi-uniformly rich in Chl-*a*.

Our observations were not dedicated to the fine characterization of vertical profiles of phytoplankton, marine snow, and zooplanktonic groups, as shown in recent studies such as those described by several authors (e.g. Möller et al., 2012, Lombard et al., 2019, Briseño-Avena et al., 2020) using combinations of video sensors and net hauls enabling correlation of the aggregation layers to detrital and planktonic particles. However, our observations can be analyzed in the light of patterns described in these articles. Accumulation of detritus (marine snow) and large phytoplankton the most often slightly below the CML has been already documented in many situations. Very often, accumulation of zooplankton occurred as well (Nowaczyk et al., 2011;Möller et al., 2012; Espinasse et al., 2014; Saiz et al., 2014; Briseño-Avena et al., 2020), but was quite variable between taxa as shown by video observations (Möller et al., 2012; Briseño-Avena et al., 2020). In particular the aggregation of nauplii, copepodites and small copepods at the CML was already described during the stratification period in the Mediterranean (Alcaraz, 1985, 1988; Alcaraz et al., 2007; Sabatés et al., 2007, 2008; Olivar et al., 2010; Nowaczyk et al., 2011; Saiz et al., 2014), showing that this chlorophyll-rich layer constitutes a favorable habitat for the reproduction of copepods, particularly in oligotrophic conditions, where the CML can be considered as an “oasis” to sustain secondary production (Saiz et al., 2014). The high biomass of crustaceans recorded in the CML (mainly euphausiids larvae) may be explained by an adaptation of their vertical migration to track the most favorable trophic conditions, as reported in several studies (Sameoto, 1986; Guglielmo et al., 2011; Zagami et al., 2011; Granata et al., 2020).

Inversely, gelatinous filter feeders (appendicularians, salps and doliolids) seem to avoid the CML, in agreement with many previous observations (Fenaux, 1968; Paffenhöfer et al., 1991; Briseño-Avena et al., 2020). In this layer, these filter-feeders might be disturbed by high accumulation of detritus and large algal cells leading to a decline in food quality (López-Urrutia et al., 2003) and/or to house clogging in the case of appendicularians (Feliú et al., 2020; Tiselius et al., 2003). The low abundance of chaetognaths and (presumably) of other gelatinous carnivorous organisms at the CML is rather surprising because we might have expected to high concentrations of these carnivorous organisms at a level where the stock of zooplankton prey would be more abundant. This could be related to day-night migration strategies, where these groups would be present in deeper waters during the day, thus avoiding larger predators (Granata et al., 2020). Their scarcity in our Hydro-Bios samples could be also linked to their active swimming out of the capture path of the net probably favored by a quicker net clogging compared to the vertical net (Sameoto et al., 2000).

Such aggregation of matter and plankton linked to the CML has relevant implications for the functioning and structuring of the pelagic food web in the Mediterranean (Saiz et al., 2014). In our study, the high biomass of zooplankton over a wide size spectrum (from nauplii to large crustaceans) and its intense metabolic activity shown by high ZCD and excretion values are signs of increased trophic fluxes at this level. High densities of larvae of small pelagic zooplanktivorous fish such as anchovy have been reported as well (Sabatés et al., 2007, 2008; Olivar et al., 2010), showing the importance of CML for the trophic transfer of matter and contaminants towards higher trophic levels.

3.2.4.3. Characterizing the biota in size fractions to interpret biogeochemical and contaminant fluxes

The first characteristic of our Hydro-Bios samples is the high proportion of detritus, mainly in the size-fractions below 500 µm at all stations. Thus, the interpretation of contaminant levels in these fractions must be done cautiously to take account of a potential bias linked to these detritus content which may have various (mineral or organic) origins. In this paper, we have not gone into a detailed description of the nature of the detritus particles. These detritus probably have different sources and compositions in the coastal zone (resuspension of inorganic and organic particles from the sediment in addition to pelagic production of detritus particles) and the offshore zone (pelagic detritus particles to which may be added particles from atmospheric inputs). As mentioned in section 4.2, patterns of vertical distributions of detrital particles which accumulate below the productive layer in the water column have already been well documented. This may have consequences for the biogeochemical cycles of contaminants and their accumulation/transfer processes in planktonic food webs in the Mediterranean Sea. Firstly, suspended particles (microphytoplankton and detrital particles) represent active surfaces for the adsorption and absorption of hydrophobic contaminants (Castro-

Jiménez et al., 2021). Secondly, these suspended particles are also the site of intense microbial activity (Alldredge and Silver, 1988; Dolan and Marrasé, 1995; Azam and Long, 2001; Calbet et al., 2002) which can certainly play a role in the accumulation and transfer of contaminants (Capo et al., 2020; Castro-Jiménez et al., 2021; da Fonseca et al., 2022; Chifflet et al., 2023), some components of which, such as ciliates, are known to be the preferred prey of mesozooplankton (Saiz and Calbet, 2011). And thirdly, a large part of these particles will sink (depending of their size and shape) and will export matter and contaminants into deeper layers (Bouloubassi et al., 2006; Romero et al., 2015; Bacosa et al., 2020) potentially integrated in the mesopelagic food-web (Romero et al., 2018). In the case of our MERITE-HIPPOCAMPE cruise, the fractions below 500 µm were much more impacted by detritus and microalgae at St04 and ST 17 (>90%) than at St01 and 09 (~50%), which clearly induced differences in biochemical compositions (see fig 3 in Tesán-onrubia et al., 2023) and contaminant levels (see Figures 4 and 5 in Guigue et al., 2023; see Table 3.S4 in Chifflet et al., 2023).

The second characteristic concerns the trophic types of the dominant zooplanktonic species within the two smallest fractions (60-200 and 200-500 µm) which modulate the associated impacts on estimate fluxes. In MERITE-HIPPOCAMPE, these fractions, dominated herbivorous and omnivorous zooplankton types (small copepods and nauplii, or small pteropods), showed isotope ratios $\delta^{13}C/\delta^{15}N$ confirming a trophic level around 2 (Tesán-Onrubia et al., 2023b), relatively higher trophic fluxes (our Figure 3.5 and 7) and substantial contaminant contents (see Figures 4 and 5 in Guigue et al., 2023; see Table 3.S4 in Chifflet et al., 2023), such as for stations St01, 04, 09, and 19. This key role of herbivorous zooplankton in contaminant transfer has been already demonstrated in high latitude ecosystems where a few species massively dominate (e.g. Foster et al., 2012).

The third characteristic concerns the large fractions. First, the sampling of these fractions in our study was certainly impacted by clogging with detritus and microphytoplankton, favoring net avoidance of large organisms. Inversely for stations with low biomasses of detritus and microphytoplankton, larger fractions presented higher proportion (e.g. St03). Moreover, it is also crucial to define the dominant trophic types in planktonic fractions > 500 µm. During MERITE-HIPPOCAMPE, these fractions were either marked by the presence of typical carnivores, mainly chaetognaths, hydromedusae and siphonophores (St03, 10, 11, see Figure 3.5b), or the presence of large crustaceans dominated by euphausiids and decapods (St01, 02, 09 and 15). Increased proportions of carnivorous zooplankton in largest size fractions compared to smallest fractions (<500 µm) highly dominated by herbivorous / omnivorous organisms, were already reported in the Gulf of Lion (B. Espinasse et al., 2014) and in the Bay of Marseille (Tiano et al., 2014a). It is noticeable that ZCD and excretion rates calculated for St03, 10 and 11 were the lowest, linked to the lower weight specific-rates of the larger organisms. This increased proportion of carnivorous forms in the two largest fractions agree with the trophic level (TL) derived from isotopic analyses on the same fractions (Tesán-Onrubia et al., 2023): mean TL around 2.5, with highest values also found at St10 and 11 (TL of 3.6

and 2.8, respectively), suggesting a high proportion of secondary consumers. It is interesting to note that aliphatic hydrocarbons (AH) levels at these stations suggested a potential biomagnification process in the planktonic food chain (see fig 4 in Guigue et al., 2023).

Taxonomic determination by very large groups would merit being further refined, especially for copepods whose trophic characteristics vary from pure herbivory to carnivory (Kouwenberg, 1994; Espinasse et al., 2014), and gelatinous plankton, which covers very different trophic groups, from large herbivorous filter feeders (salps, doliolids) to carnivores (jellyfish, siphonophores, ctenophores).

3.2.5. Conclusion

The choice of sampling in the CML for this study regarding the role of plankton as a contaminant pump was guided by the aims of (1) collecting a high biomass of plankton from the same location to measure levels of a wide range of contaminants, and over a broad spectrum of planktonic size fractions, and (2) being located in an important layer for pelagic trophic interactions in both the coastal and off-shore areas. The present paper has characterized the nature of the particles and zooplankton collected by the nets at depth and demonstrated the similarities and differences of this planktonic community to that of the water column.

The different distribution patterns of planktonic biomass encountered among the different stations during the MERITE-HIPPOCAMPE campaign should make it possible to compare contrasted situations of the accumulation or not of contaminants in the planktonic food web according to the pattern of these distributions.

By looking at the different size fractions of zooplankton that reflect different trophic levels (Tesán-Onrubia et al., 2023b), we have shed new light on the processes of accumulation (or not) of contaminants, particularly in relation to studies where the zooplankton is either taken as a whole (Battuello et al., 2016), with the whole of the zooplankton caught by a mesh size net of 300 µm) or based on particular taxa but requiring their selective collection (Ndah et al., 2022). The method described in this paper, which characterizes successive fine size classes, provides an additional dimension for understanding the functioning of planktonic food webs in contaminant accumulation processes.

3.3. General conclusion on the role of zooplankton for MERITE-HIPPOCAMPE purposes

In pelagic food webs, body size exerts a fundamental influence on a variety of ecological factors including production rates, energy needs, mortality rates, and predator-prey interactions (Cohen et al., 1993; Ljungström et al., 2020). Moreover, the changes in taxonomic composition between zooplankton size fractions modify as well the rates of these different processes (Carlotti et al., 2008; Hunt et al., 2017). As a result, the adoption of a size-based approach has become essential to analyze the structure and functionality of the planktonic compartment, with special emphasis on the smallest, often underestimated fractions.

During the MERITE-HIPPOCAMPE campaign, our results revealed differences in zooplankton distributions in different stations across the Mediterranean Sea (North-South gradient). The present analysis characterizing the composition of zooplanktonic taxonomic groups in each of the biomass size fractions, as well as the contribution of microalgae and detritus to these size fractions, represents crucial information for interpreting the levels of various contaminants in these size fractions, and ultimately for understanding potential biomagnification processes. (see journal Marine Pollution Bulletin, IF : 5.8, https://www.sciencedirect.com/journal/marine-pollution-bulletin/special-issue/10B0SXC3XR2). This collaborative effort is being undertaken in the context of exploring contaminant accumulation within the planktonic food web.

3.3.1. Additional information provided for the study of the biochemistry and isotope ratios of zooplankton size fractions

Tesán-Onrubia et al. (2023a) conducted a comprehensive analysis of the spatial variations in biochemical composition and isotope ratios within size-fractionated plankton across the Mediterranean Sea. Comparing these results with the biomass proportions of detritus, algae, and zooplankton (Figure 3.9), and of the main zooplankton groups (Figure 3.10) within the same size-classes (from our study) help in their analyses. Stations were grouped into the northern (St01, St02, St03, and St04), central (St09, St10, and St11), and southern (St15, St17, and St19) regions. Besides, such a comparison complements our understanding of the trophic dynamics, inferred from Tesán-Onrubia's Bayesian model (Figure 3.11).

Tesán-Onrubia et al (2023a)' study revealed higher concentrations of proteins, lipids, and isotopes in zooplankton in comparison to phytoplankton. It's worth noting that zooplankton, irrespective of their size, exhibit a no susceptibility to contaminant accumulation due to their strong affinity for proteins and lipids.

Furthermore, the isotopic compositions exhibited spatial variations, signifying distinct carbon sources among plankton size fractions, particularly in coastal and offshore areas. These variations play a crucial role in influencing contaminant exposure levels. Coastal regions displayed elevated trophic levels alongside lower zooplankton biomass, resulting in intensified predation rates. Within the zooplankton community, the 200–500 µm size-fraction, predominantly comprising copepods (Figure 3.10), demonstrated the highest energy content in terms of carbon, underscoring their critical role as a primary food resource for numerous planktivorous fish species. The lower protein and lipid contents in the largest fraction (>2000µm) may be attributed to the higher proportion of gelatinous organisms, which constitute approximately 40% of the biomass on average.

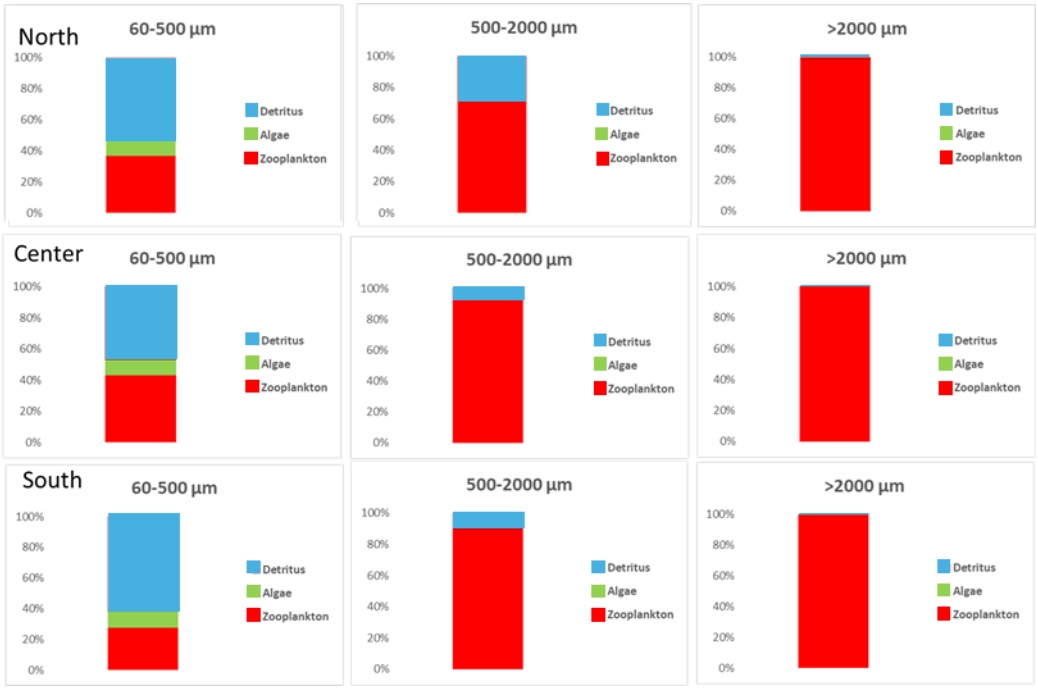


Figure 3.9. Biomass percentage distribution of detritus (Blue), algae (Green), and zooplankton (Red) across the northern (St01, St02, St03, and St04), central (St09, St10, and St11), and southern (St15, St17, and St19) regions, categorized by different size-fractions.

In the trophodynamic model by Tesán-Onrubia et al., (2023a) (Figure 3.11C), the substantial consumption of picoparticles by the 60-500 µm fraction may raise questions, given that metazooplankton in this size range is primarily dominated by small copepods (Figure 3.11B), which predominantly feed on nanoplankton. However, the substantial presence of detritus and algae in this fraction (>50% in average; Figure 3.11A) suggests the potential significance of heterotrophic protozoans (ciliates and flagellates) associated with this detritus, and known to be avid consumers of picoplankton (Fenchel, 1980). Moreover; the higher proportion of these detrital particles in the south and north coastal stations compared to the deep central station may suggest regional disparity in the consumption of picoparticles by the smaller zooplankton size-fraction Figure 3.10.

The extensive consumption of nanoparticles by the 500-2000µm fraction, and to a lesser extent by the 60-500 fraction, aligns with the high percentage of copepods in these size fractions for the southern, central, and northern regions (averaging 65% and 85%, respectively). Additionally, the heightened consumption of microparticles by the >2000µm fraction (Figure 3.11C), predominantly dominated by omnivorous (large crustacea), or carnivorous (gelatinous, likely siphonophores and jellyfish) zooplankton (Figure 3.11B), suggests that these microparticles are primarily of heterotrophic origin, likely originating from small metazoans and large protozoans.



Figure 3.10. Biomass percentage distribution of taxonomic groups within zooplankton across northern, central, and southern stations, categorized by different size fractions.

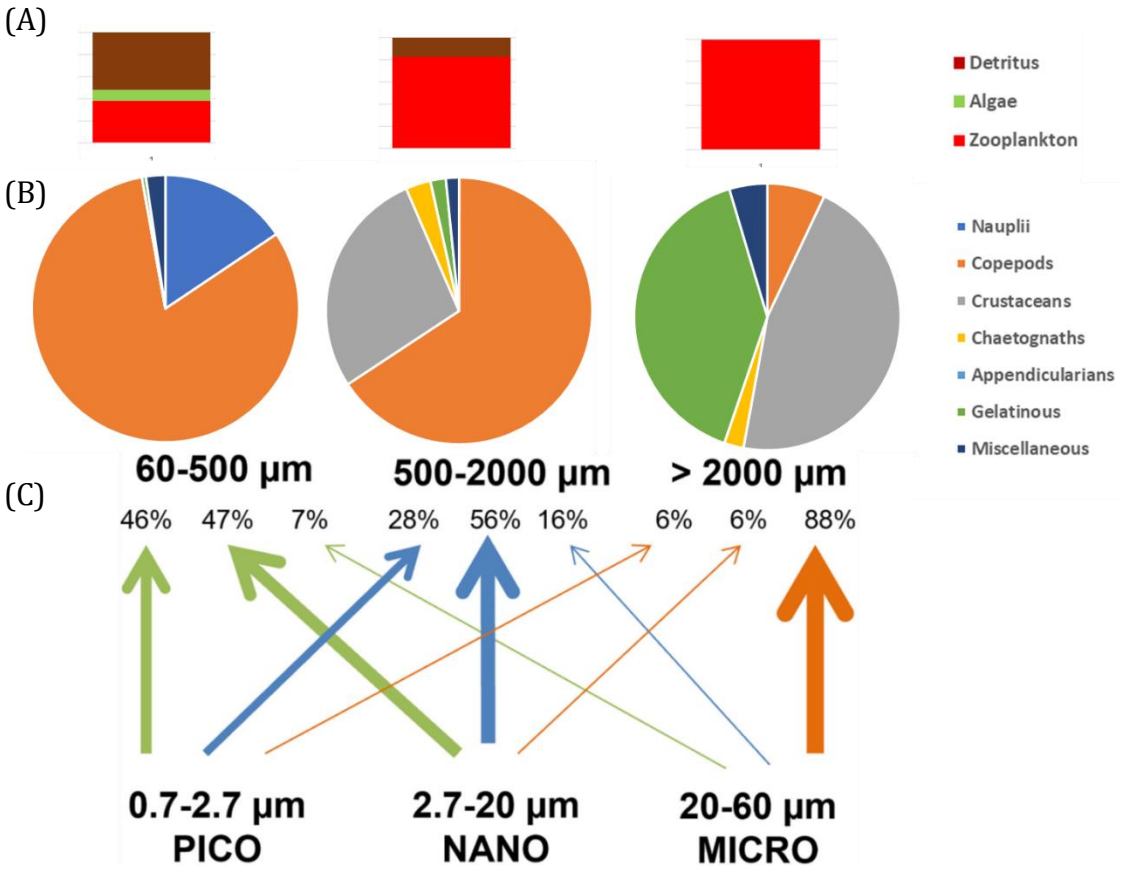


Figure 3.11. Comparison of mean biomass percentages of (A) detritus, algae, and zooplankton and of (B) zooplankton groups within different zooplankton size-fractions (mean values from Figure 3.9 and 3.10) with (C) trophic transfer of pico, nano and micro particles to the same zooplankton size-fractions (from Tesán-Onrubia et al., 2023a). The arrows' thickness indicates the respective contributions, with percentages noted nearby.

3.3.2. Major inputs of Zooplankton analyses for contaminants

Zooplankton plays a vital role in the transfer of trace metals to higher trophic levels and is fundamental for basic studies on metals in marine environments (Tedetti et al., 2023). The results obtained by Guigue et al. (2023) involved the analysis of hydrocarbon, Aliphatic hydrocarbons (HA) and polycyclic aromatic hydrocarbons (PAH), levels in water and size-fractionated plankton from the western Mediterranean as part of the MERITE-HIPOCAMPPE expedition. Their findings revealed that zooplankton, primarily composed of copepods, exhibited remarkably low lipid content, a characteristic consistent with the oligotrophic conditions in the Mediterranean waters, along with poor seasonality of food supply for plankton. Anthropogenic PAHs were identified in water

samples from all stations, though their presence in plankton communities was overshadowed by predominant biogenic indicators (Hydrocarbons terrestrial or marine). Pristane (aliphatic hydrocarbon) emerges as a component in the category of low molecular weight compounds (<n-C22), consistent with the abundance of zooplankton, especially the dominance of copepods. The notably high pristane levels observed in the 200–500 and 500–1000 µm fractions at Station 11 correlated with a significant presence of zooplankton observed in our study.

In the context of Tesán-Onrubia et al. (2023b)'s research on mercury (Hg), the heightened concentration of methylmercury (MMHg) in larger size fractions at offshore stations could potentially be attributed to a reduced proportion in detritus reported by our study (Figure 3.10).

To above results agree with the study by Chifflet et al. (2023) who conducted an assessment of metal and metalloid transfer within planktonic food webs spanning from bacteria to zooplankton. The results unveiled divergent concentrations of these elements in coastal and offshore regions, influenced by a combination of atmospheric deposition and local anthropogenic influences. Notably, disparities emerged between the southern coastal zone and the latter two zones (northern coastal zone and the offshore zone). While δ^{65}Cu exhibited a robust correlation with *Prochlorococcus* sp. and picoeukaryotes in the offshore zone, an inverse relationship was observed between δ^{65}Cu and copepods in the southern coastal area. These divergences in community structure in the southern coastal zone could be the result of biogeochemical interactions with Cu.

In the northern coastal zone, the biomagnification of essential elements was predominantly governed by copepod activities. This finding is in concordance with the substantial contribution of copepods to metabolic fluxes, encompassing ingestion and excretion, in this particular area (refer to Figure in the annex for details).

In a complementary study, Carlotti et al. (2023) investigated the presence of microplastics (MPs) in the maximum chlorophyll layer along the north-south transect in the Mediterranean Sea, directly comparing them with zooplankton concentrations to characterize a potential impact of microplastics loading on the prey available to planktivorous fish. They observed a high concentration of MPs, primarily entrapped in aggregates near the CML, with an average concentration of 42.9 ± 45.4 MPs per cubic meter, of which 96 ± 4% were in the form of fibers. The ratios between mesozooplankton and MPs, as well as between detritus and MPs, in the maximum chlorophyll layer, were 223 ± 315 and 2544 ± 2268, respectively.

4. Zooplankton structure and functioning during MOOSE-GE 2019 campaign

4.1. Introduction

The Mediterranean Ocean Observing System for the Environment (MOOSE) constitutes a sustained, comprehensive program established to facilitate the continuous monitoring of water masses, thermohaline circulation, and material fluxes within the North Western Mediterranean Sea (NWMS), encompassing the Ligurian and Provençal sub-basins, as well as the shelf break area of the Gulf of Lions (Coppola and Testor, 2019). Its overarching objective is the identification and characterization of environmental in relation to climate change and anthropogenic influences. The Liguro-Provençal sub-basin serves as a notable example of the occurrence of deep-water convection within the Mediterranean. This complex process is driven by a synergy of intense winter atmospheric phenomena, notably the Mistral and Tramontane winds, in conjunction with oceanic preconditioning, as pointed by Margirier et al. (2020) and Seyfried et al. (2019) (Figure 4.1, Top panel). Their fundamental role in the vertical redistribution of heat, carbon dioxide, biogeochemical elements, and marine productivity is paramount. In 2019, it was recorded that the depth reached by the deep convection was approximately 500 meters (Figure 4.1, bottom panel). For a more detailed explanation, please consult Chapter 1, § 1.1.3.

The MOOSE observation program integrates both Eulerian observatories and autonomous mobile platforms to enhance long-term monitoring across the entire North-Western basin of the Mediterranean (Figure 4.2). The integrated observation system comprises (1) mooring sites with high-frequency temporal monitoring of water's physical variables (temperature, salinity, and currents) through five deep anchoring lines (located at DYFAMED, LION, MOLA, Planier, and Antares sites), (2) monthly assessment of hydrological structure encompassing physical, chemical, and biological parameters across the entire water column at three designated sites (DYFAMED, MOLA, and Antares), as well as glider transects enabling measurements of temperature, salinity, oxygen, and chlorophyll fluorescence, among others; and (3) an annual large-scale field campaign known as 'MOOSE grande échelle' (MOOSE-GE), conducted every summer. This integrated approach ensures comprehensive insight into the complex dynamics and environmental changes within the North-Western Mediterranean basin.

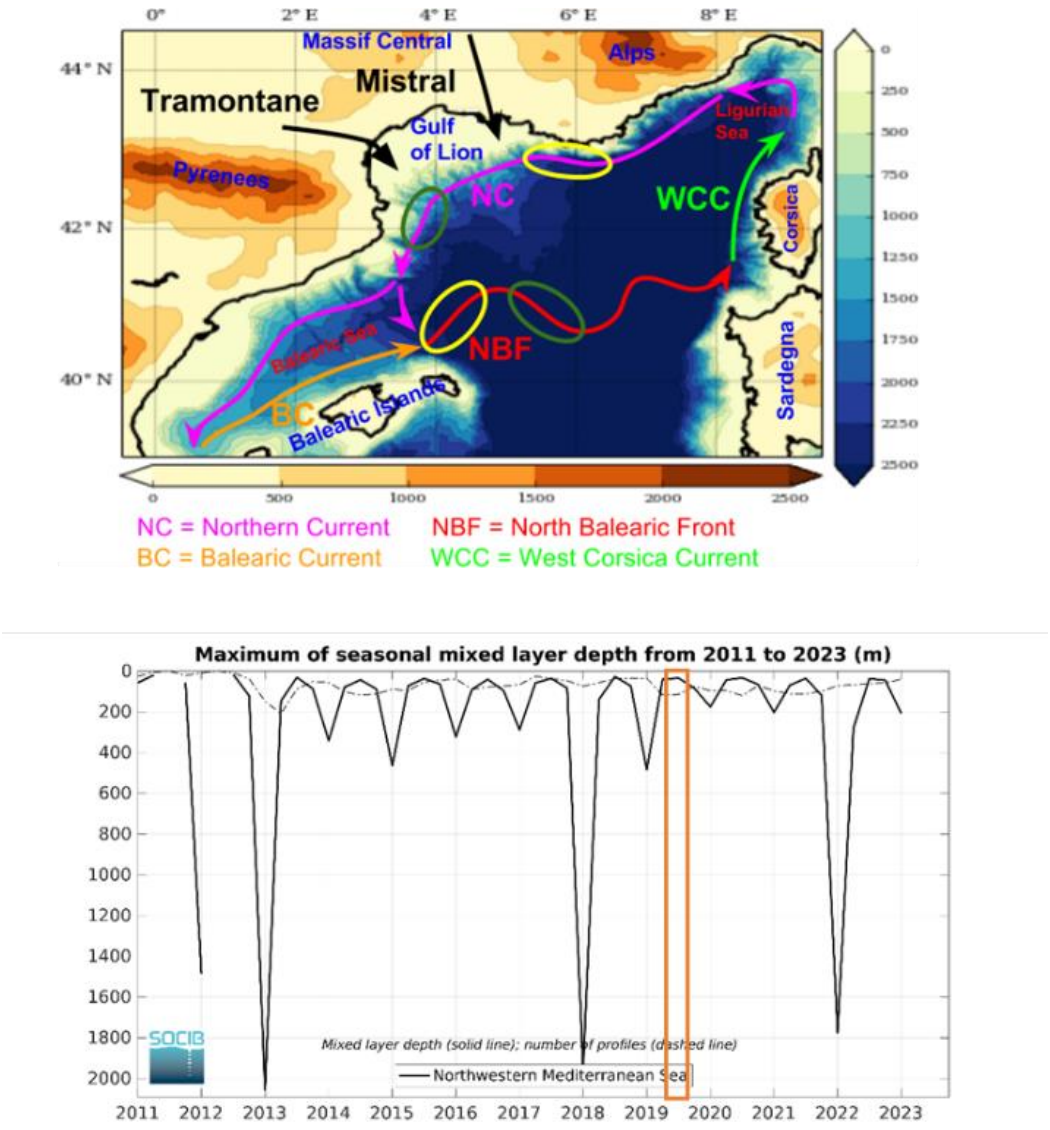


Figure 4.1. Deep convection in the in the northwestern Mediterranean Sea: Top panel, Schematic representation of the surface oceanic circulation (Figure from Seyfried et al., 2019). Colored area: orography in brown and bathymetry in blue. The directions of the prevailing mistral and tramontane winds are indicated with black arrows. Up-front and down-front wind zones are indicated with yellow and green ellipses, respectively. Bottom panel, Timeseries from 2011 to the last available season of the maxima of the mixed layer depth. The MLD values averaged over the sub-regional seasonal distributions from Juza and Tintoré (2023) for Provor Buoys. The orange frame delineates the period of MOOSE-GE 2019.

In the present chapter, we undertake a comprehensive analysis of the zooplankton community structure and distribution within the NWMS during the MOOSE-GE 2019 cruise (June 06 to July 01, 2019), with a particular focus on its interaction with environmental variables. The study encompassed the NWMS basin, with a central emphasis on the Provençal and Ligurian sub-basins and was geographically delineated to the south by a line connecting the Balearic Islands and Sardinia, and to the north by the Ligurian Coast and the Gulf of Lions shelf break. Notably, we integrated comparative insights drawn from Donoso (2017) research during MOOSE-GE 2014 (4th to 22nd July 2014) and Feliú (2020) study during MOOSE-GE 2017 (August 31st to 23rd September 2017), as well as with the HIPPOCAMPE cruise (Chapter 3 of this thesis) conducted during the spring of 2019, to enrich our analytical framework.

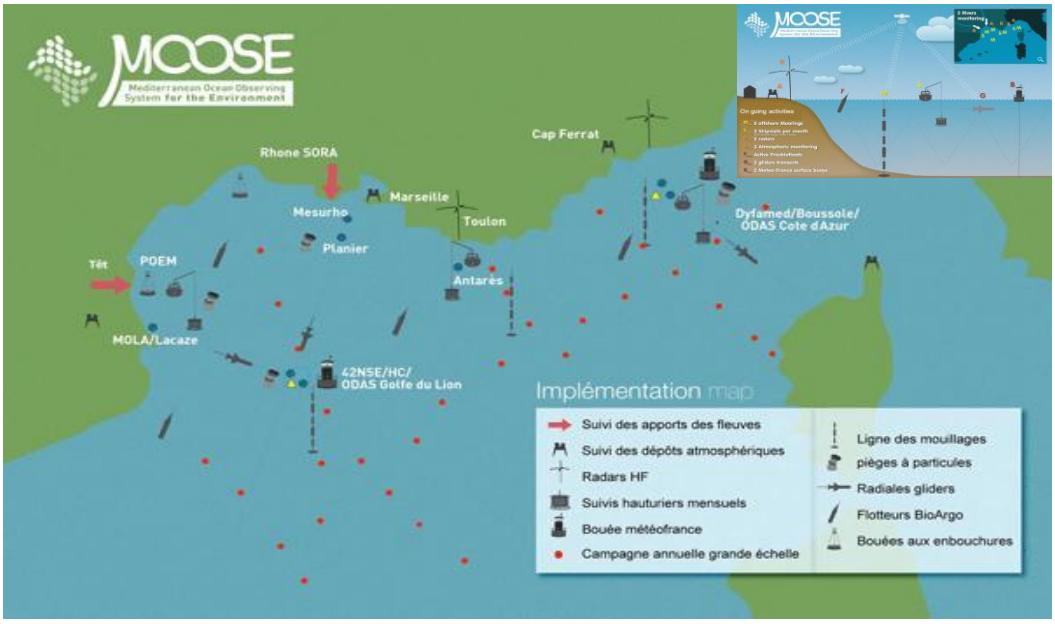


Figure 4.2. The MOOSE observation system with its diverse monitoring tools. Extracted from http://www.moose-network.fr/?p=579 Coppola et al., 2019)

4.2. Materials and Methods

The MOOSE-GE cruise was conducted onboard the RV Thalassa from June 06 to July 01, 2019 and the track consisted of 118 stations (Figure 4.3). The transect, divided into Leg 1 and Leg 2, encompassed the North-Western Mediterranean Sea (NWMS) basin, with a focus on the Ligurian Sea (LS), Gulf of Lion Shelf Break (GLSB), Central Provencal Basin (CPB), and Southern Provencal Basin (SPB).

At each station vertical profiles of physical variables were recorded using CTD-Rosette cast (temperature, salinity, dissolved oxygen, and fluorescence). The mixed-layer depth (MLD) was estimated using a 0.5 ºC difference criterion from a reference temperature of 10 m (de Boyer Montégut et al., 2004). Other data available from Niskin Rosette are the nutrient profiles: nitrites and nitrates (NO_2 + NO_3), and phosphates (PO_4) used for fluxes estimations.

Zooplankton sampling was conducted at 18 out of the 118 stations, with 200-0 m vertically tows using a Bongo net with a 120 µm mesh size (60 cm mouth diameter and constant speed of 1 ms^{-1}) equipped with filtering cod ends. The volume of the samples was estimated using the ring diameter and the length of the towed cable. After the net was retrieved onto the deck, the samples were promptly preserved in a 4% borax-buffered formalin solution.

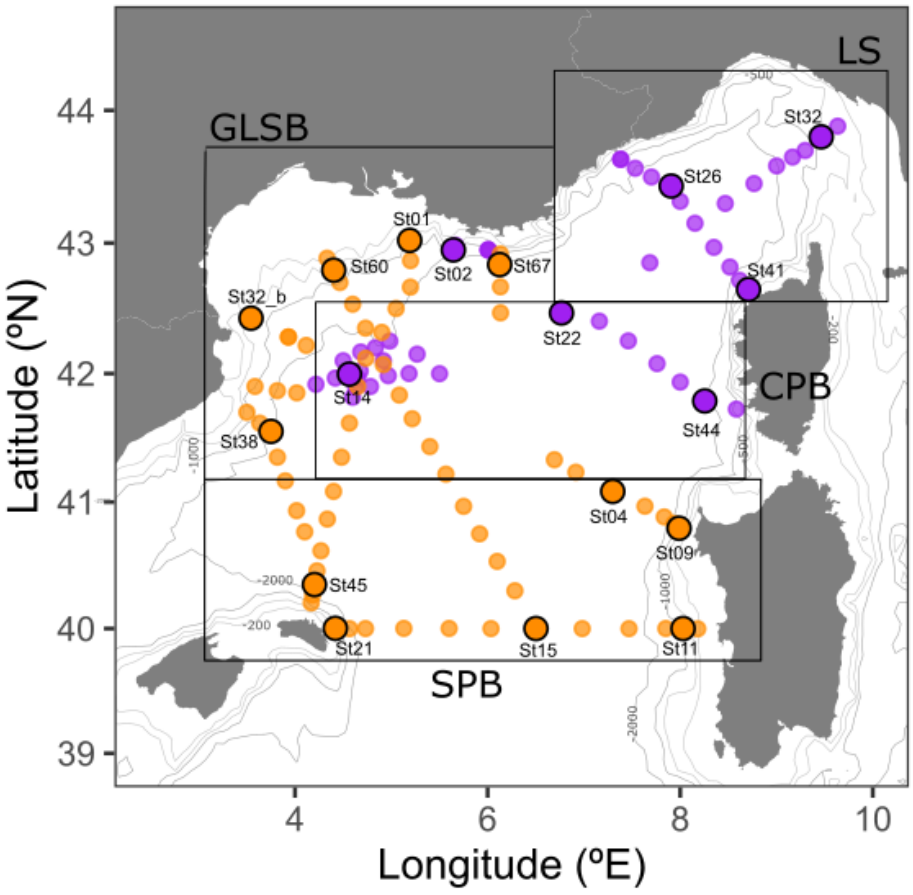


Figure 4.3. Map of the stations sampled during MOOSE-GE 2019. Purple and orange circles correspond to the station track during Leg1 and Leg2, respectively. Zooplankton stations: dots surrounded with a black circle. Rectangles define different areas. GLSB=Gulf of Lions Shelf break, LS=Ligurian Sea, CPB=Central Provencal Basin, SPB= Southern, Provencal Basin.

In the laboratory, samples were analyzed using combined tools with FlowCAM and ZOOSCAN image analyzers. For this, the initial sample was divided into four distinct size fractions: two smaller fractions for the FlowCAM analysis, <200 µm and 200 µm – 500 µm, and two large fractions for the ZOOSCAN analysis, specifically 200 µm – 1000 µm and >1000 µm.

To obtain a complete size spectrum and avoid overlap of organisms between the 200-500 µm fraction analyzed by FlowCAM and the 200-1000 µm fraction analyzed by ZOOSCAN, a combined approach was employed. Through careful analysis of the data and following the criteria established by Feliú (2020), it was determined that the optimal combination involved FlowCAM calculating the ESD size-classes below 300 µm, while ZOOSCAN calculated the ESD size-classes above 300 µm (Figure 4.4). Using this combination of data, the full final size spectrum was accurately determined. The abundance, biomass, and metabolic rates were estimated for each ESD size-classes, using the same approach as for the MERITE-HIPPOCAMPE data (see Chapter 3).

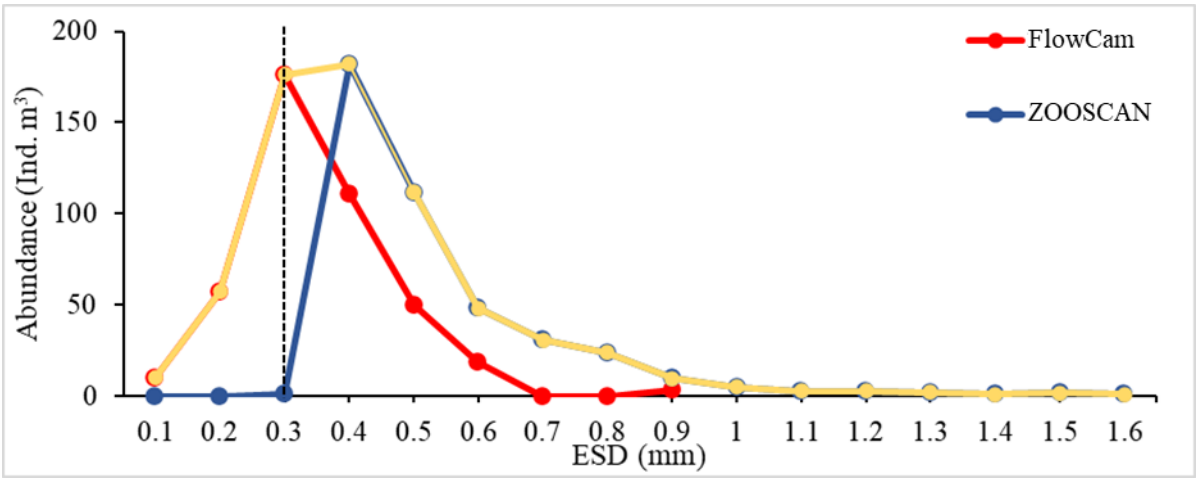


Figure 4.4. Size spectrum of St15 as an example, obtained by FlowCAM (represented in red) and ZOOSCAN (represented in blue) independently and the combination of FlowCAM < 300 µm of ESD and ZOOSCAN >300 µm of ESD (represented in yellow).

On the other hand, taxonomic abundances of zooplankton taxa groups were estimated through direct observation of subsamples under a microscope, allowing for a more detailed taxonomic composition assessment (by Loïc Guilloux).

Spatial variations in the zooplankton community were assessed using several complementary diversity indices: The Shannon diversity index (H') evaluates species diversity within a community, taking into account both the relative abundance of each species and the total number of species present. Pielou evenness (J') is a measure that helps in the interpretation of H' by standardizing it by the natural logarithm of the total

number of species. It ranges between 0 and 1, with values tending towards 1 when the different species have similar abundances. Species richness (Margalef, d) represents the total number of species present in a sample pondered by the natural logarithm of the total number of individuals. The Brillouin diversity index (H) evaluates the biological diversity of a community, considering both species richness and relative abundance. Fisher (α) is a statistical measure used in species diversity analysis. Lambda diversity index and 1-Lambda are used to assess biological diversity in a sample. Lambda represents the rate of change in species number relative to sample size, while 1-Lambda is the fraction of species present in a sample relative to the total possible species in the study area. All these estimations were applied to the data aquiied by microscopy and computed using PRIMER v7 software (Anderson et al., 2008).

The relationships between the zooplankton community and the environmental variables were studied using a co-inertia analysis (Dolédec and Chessel, 1994) that crossed the results of a factorial correspondence analysis (FCA) on the zooplankton taxa abundances and a principal component analysis (PCA) on the environmental variables. Prior to the analyses, the data were log-transformed to tend towards the normality of the distributions. These analyses were performed using ADE-4 software (Thioulouse et al., 1997).

For more comprehensive information on laboratory procedures, data analysis, and community parameter estimations, please refer to Chapter 2, the "Material and Methods" section.

4.3. Results

4.3.1. Spatial patterns in the environment

The dendrogram with the three clusters and the position of the stations corresponding to these clusters are shown in Figure 4.5. The Figure 4.6 presents the boxplots for the average values within the upper 200 m of the water column of temperature, salinity, dissolved oxygen, fluorescence, and depth of the mixed layer.

Cluster blue grouped 45 stations, mainly peripheric of the study area, mostly in the SPB and some coastal stations in the GLSB, LS, and CPB characterized by high temperature and dissolved oxygen, low salinity and fluorescence, and a shallow MLD around 11m.

The cluster red grouped 37 stations mostly in the GLSB, LS, and CPB, characterized by the lowest temperature and dissolved oxygen values, high salinity, fluorescence, and the deepest MLD (see Figure 4.6). They correspond roughly to the area of the winter deep water formation.

Cluster green grouped 36 stations mostly distributed among CPB, LS, and GLSB areas and was characterized by intermediate mean values for all variables, compared to the blue and red clusters.

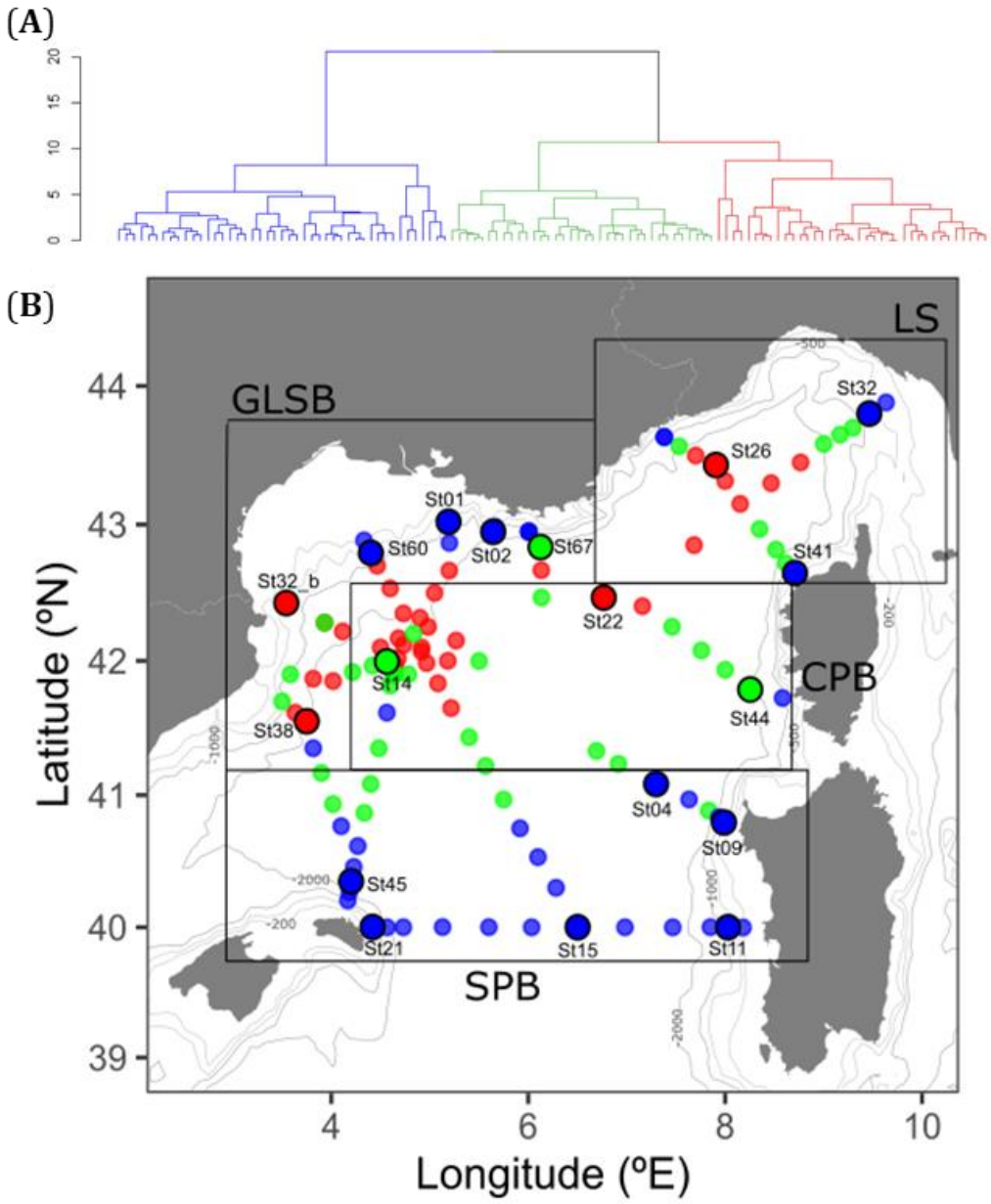


Figure 4.5. (A) Hierarchical clustering of environmental variables (temperature, salinity, dissolved oxygen, fluorescence, and mixed layer depth = MLD) within the upper 200 m of the water column with color frames for the 3 clusters obtained. (B) Map of the stations identified by clustering with the corresponding color code, dots surrounded by a black circle denotes the zooplankton net sampling stations.

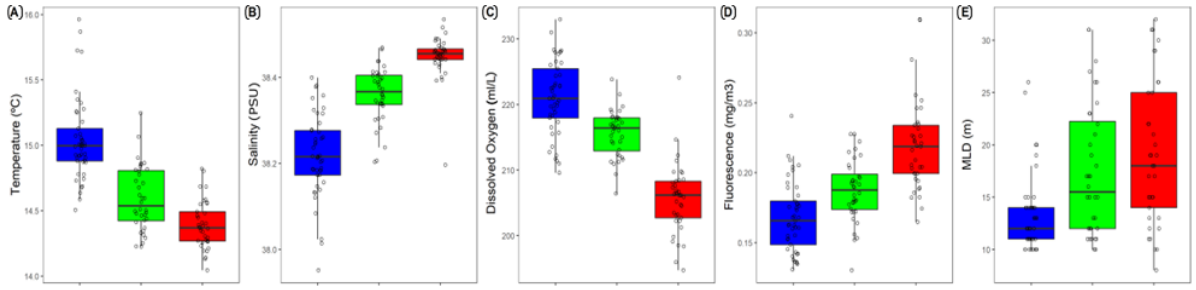


Figure 4.6. Boxplots for the average values within the upper 200 m of the water column of temperature (A), salinity (B), dissolved oxygen (C), fluorescence (D), and depth of the mixed layer (E), for the three clusters during the MOOSE-GE 2019 cruise. The horizontal bar indicates the median, the box indicates lower and upper quartiles (25% and 75%), and the whiskers indicate maximum and minimum values inside a range of 1.5 times the interquartile range, respectively. Black circles indicate the dispersion of the data.

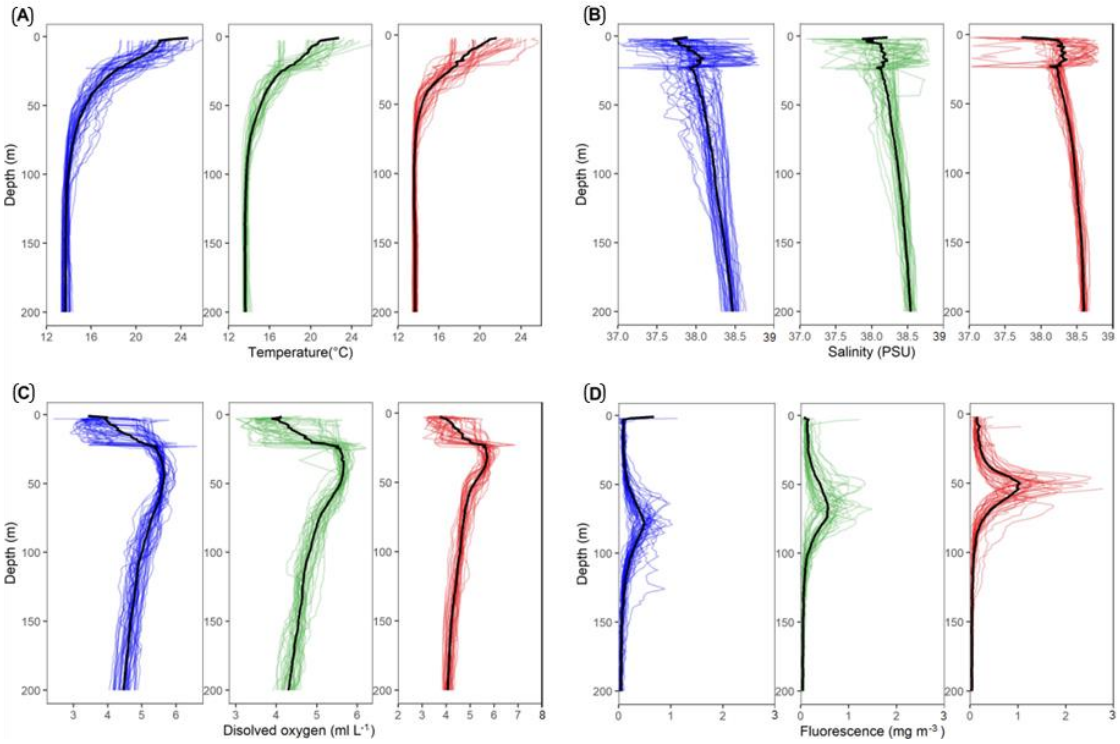


Figure 4.7. Vertical distribution profiles of temperature (A), salinity (B), dissolved oxygen (C), and fluorescence (D) grouped by clusters (see color symbols in Figure 4.5). The black line corresponds to the median value for each cluster.

The vertical profiles showed that, for the temperature, the blue cluster has a more pronounced cline, with the highest surface temperatures (Figure 4.7). For salinity and oxygen, in general, the values among the three clusters showed a similar pattern, but the blue recorded a greater range of surface salinity variability. The chlorophyll maximum was observed shallower and was well pronounced in cluster red, around 50-60m (most of the central stations of the deep convection zone) while it deepened in the blue cluster (most of the peripheral stations).

4.3.2. Spatial patterns of zooplankton from imagery treatment

The GLSB region, located in the north, exhibited the highest total zooplankton abundance and biomass compared to other areas (2614±1196 Ind/m^3 and 6752±1398 µgDW/m^3, respectively), but st26 of the LS region showed the highest values (4878 Ind/m^3 and 12682 µgDW/m^3; Figures 4.8 A and B and 4.9 A and C). Additionally, both the north and the coastal areas of the Balearic Islands (at SPB) displayed high biomass values (St21 with 10822 µgDW/m^3 and St45 with 7625µgDW/m^3).

In general, copepods dominate the total abundance, indeed almost exclusively at CPB and stations St 38 of GLSB and St 26 and St 41 of LS (Figure 4.9 A, B). Nonetheless, in the SPB region, the combination of diverse organisms, appendicularians, and non-copepod crustaceans can reach up to 25% of the total abundance in St 15.

In terms of biomass, of particular interest is the observation in the SPB region, where biomasses of chaetognaths and other gelatinous (*i.e*. excluding appendicularians and chaetognaths) played a significant role in this area. On the other hand, it is observed in the SPB region, that miscellaneous and gelatinous biomass represents approximately 25 to 40% of the total biomass. Note also the very high contribution of gelatinous at St 32 in the LS.

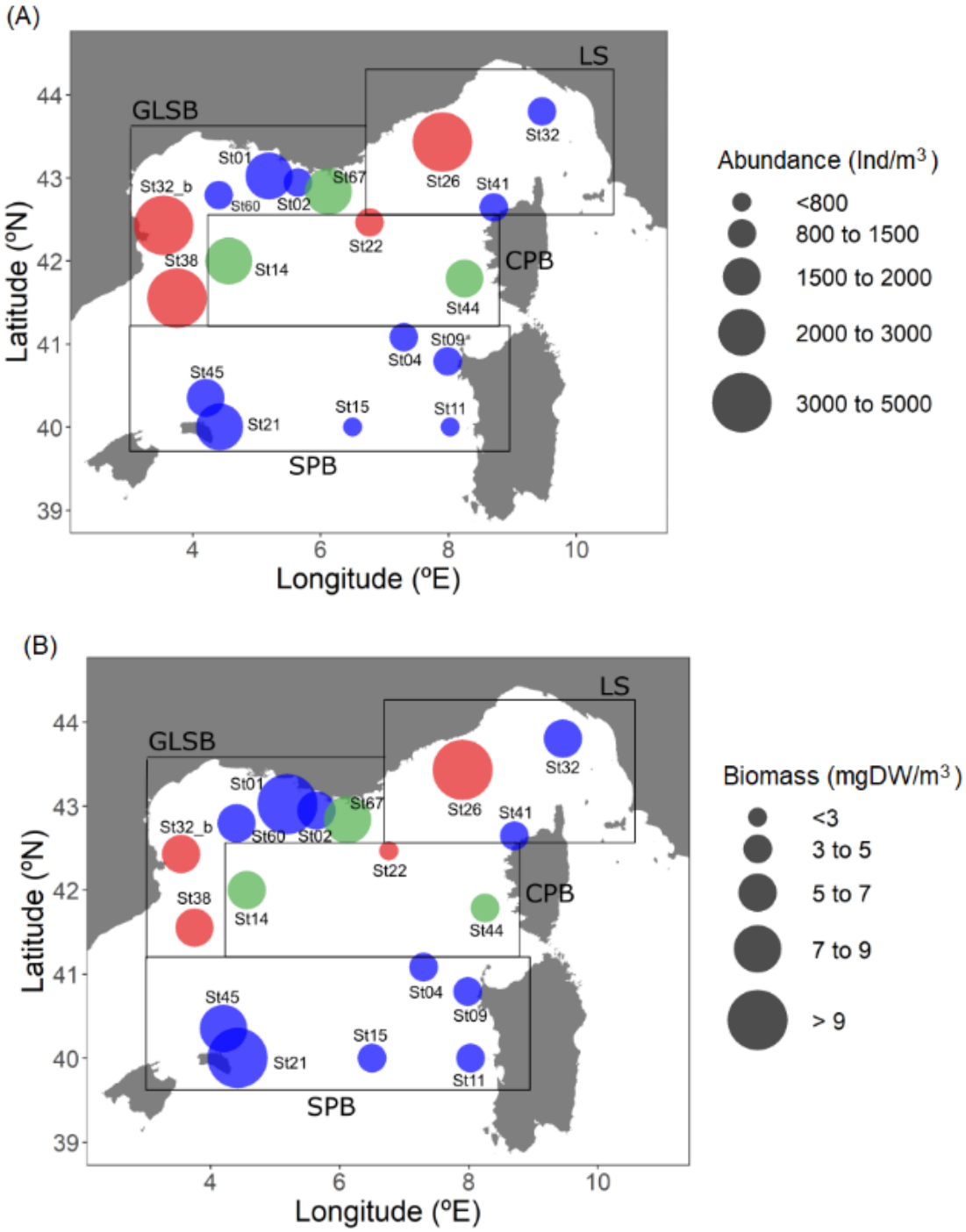


Figure 4.8. Spatial distributions of zooplankton variables during MOOSE-GE 2019. Abundance (A), biomass (B), from FlowCAM and ZOOSCAN treatment. Colors refer to the clusters defined in Figure 4.5.

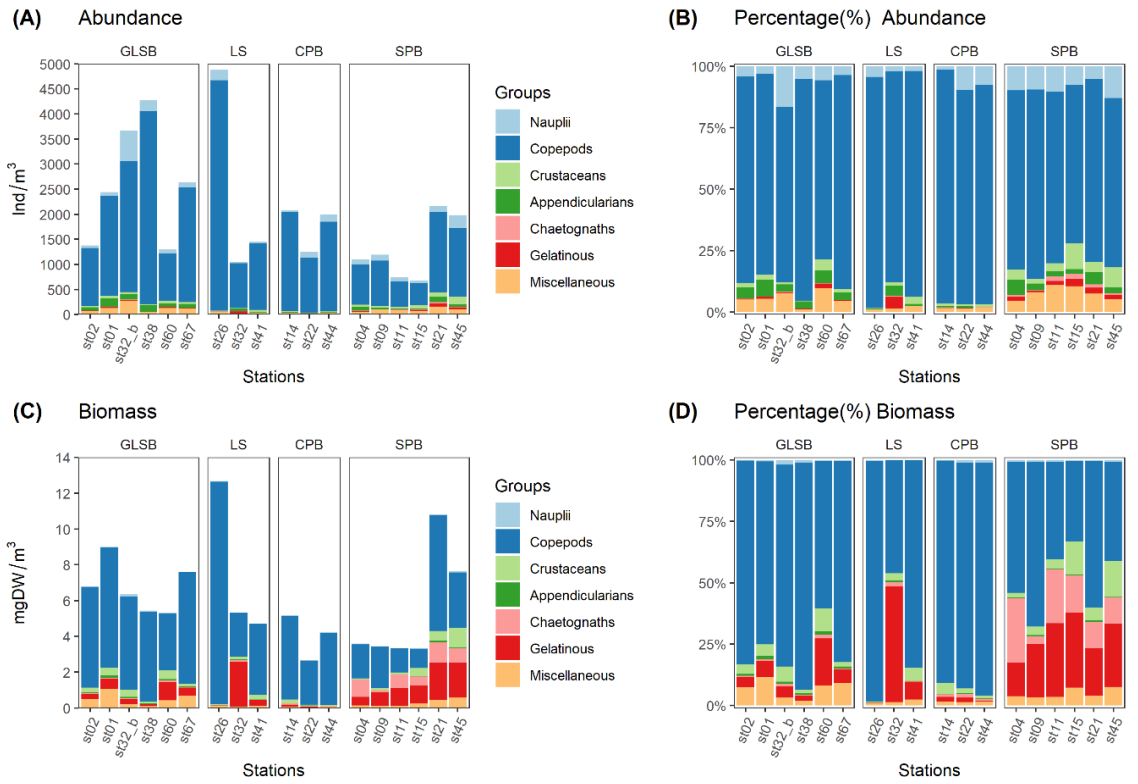


Figure 4.9. Zooplankton abundance (A, Ind/m3; B, percentage) and biomass (C, mg DW/m3; D, percentage) cumulated by taxa groups, estimated from FlowCam and ZOOSCAN for the different stations sampled during MOOSE-GE 2019 ordinated by regions.

In terms of abundance, the 300-500µm size class shows the highest percentage value, while the >2000 size-class have the lowest one. The size-classes <200 shows considerable abundances only at specific stations associated with coastal areas (St32_b, St 44) and in the SPB (Figure 4.10, A and B). In biomass, although the size-class 300-500 µm shows important values dominating in the St38, it is the 500-1000 µm size-class that displays the highest biomass values. In the SPB region, the >2000 µm shows higher biomass levels compared to other areas (Figure 4.10, C and D; Figure 4.11).

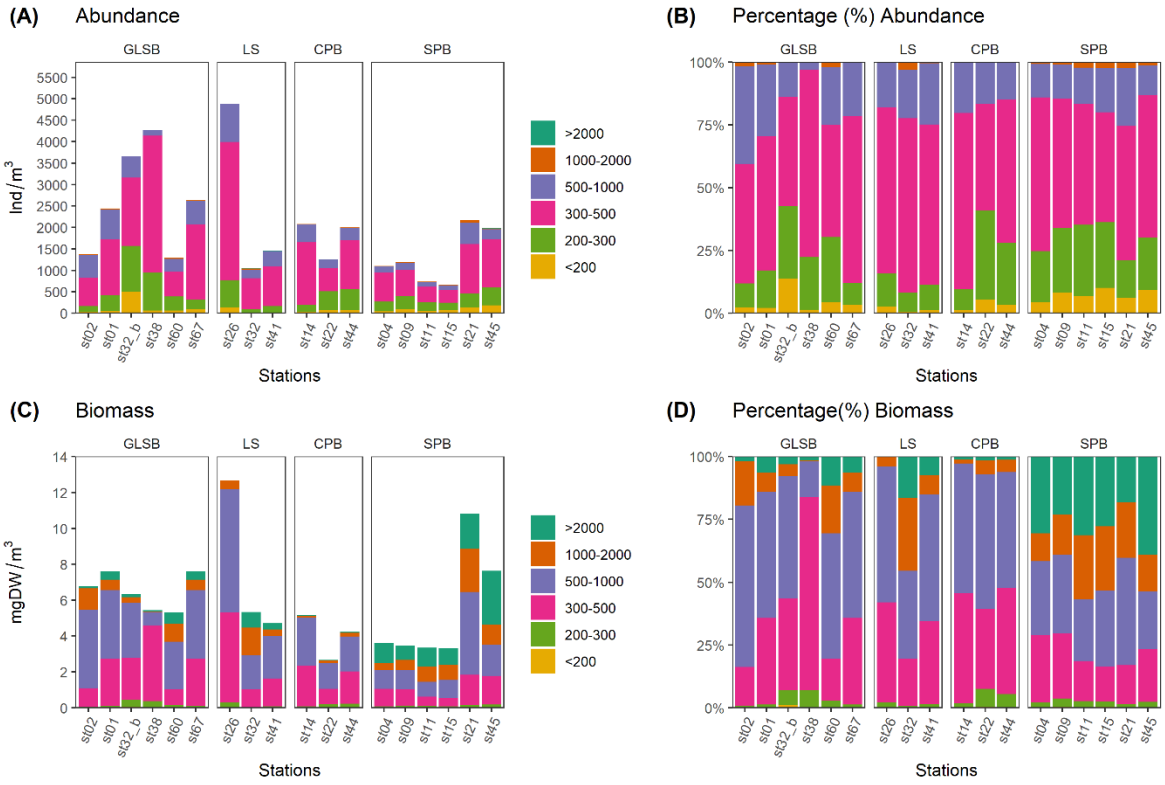


Figure 4.10. Zooplankton abundance (A, Ind/m^3; B, percentage) and biomass (C, mg DW/m^3; D, percentage) cumulated by ESD size-classes, estimated from FlowCam and ZOOSCAN for the different stations sampled during MOOSE-GE 2019 ordinated by regions.

The taxonomic composition of ESD size-classes in biomass (Figure 4.11) revealed that the <200 µm class was primarily characterized by the prevalence of nauplii and miscellaneous taxa. Additionally, gelatinous was in certain stations (*e.g.* St 15 and 45 in SPB). In the size-classes between 200 and 500 µm, copepods were highly dominant in all regions. In the 500 to 1000 µm class, copepods were also dominant but other taxonomic groups such as gelatinous organisms, crustaceans, miscellaneous, and appendicularians were important. This pattern becomes more pronounced in the 1000 to 2000 µm, where gelatinous organisms dominate in many stations, clearly in the SPB region. In the size-classes upper than 2000 µm, the dominance of gelatinous organisms is observed in the LS region and a portion of the GLSB region. However, appendicularians appear to be more prevalent in the CPB region and in some stations of the SPB region.

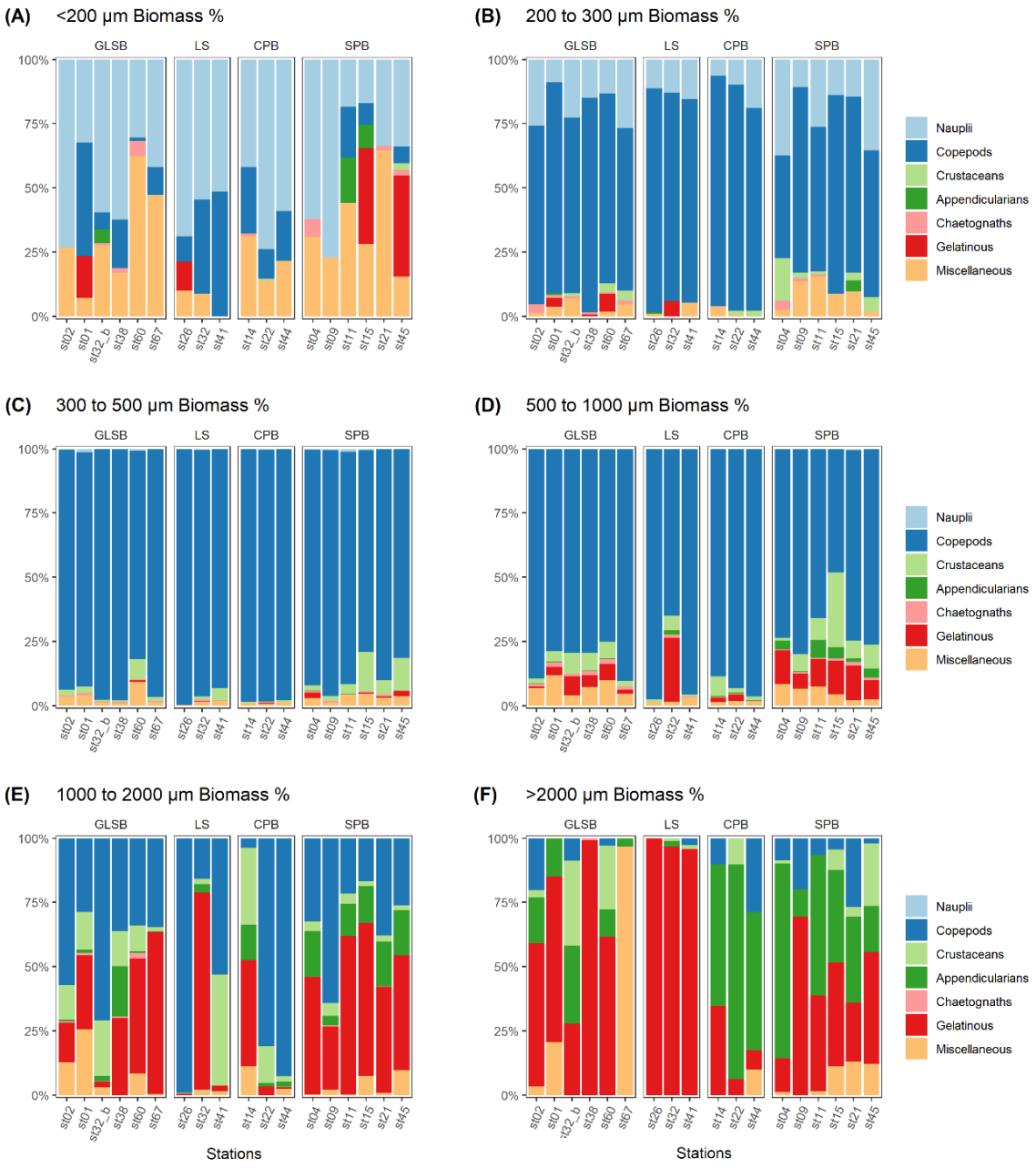


Figure 4.11. Zooplankton biomass percentage cumulated by taxa groups for each ESD size-classes estimated from FlowCam and ZOOSCAN for the different stations sampled during MOOSE-GE 2019 ordinated by regions.

4.3.3. Spatial patterns of zooplankton from microscopy analysis

The comparison between abundances estimated from microscope counting and FlowCam + ZOOSCAN present a positive relationship (R^2 =0.666) and was significant (p= <0.001) (Figure 4.12).

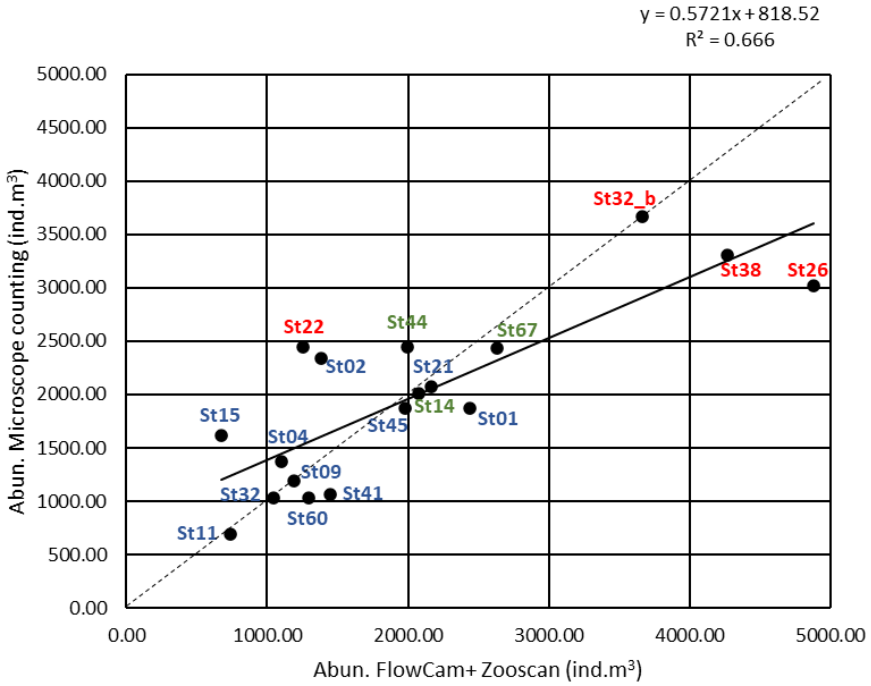


Figure 4.12. Comparison between abundances estimated from microscope counting and FlowCAM + ZOOSCAN. The black line represents the linear regression and the dashed line represents the identity line where y = x and the colors of the stations (red, green, and blue) correspond to the cluster classification given in Figure 4.5.

4.3.3.1. Zooplankton taxonomic composition and diversity from microscope counting

Based on microscopic counting, 102 zooplankton taxa were identified including 61 copepods (including nauplii) 31 other holoplanktonic taxa and 10 meroplanktonic taxa (Table 4.1).

Table 4.1. Percentages of abundances of all the taxa found during MOOSE-GE 2019 (microscopic treatment by Loïc Guilloux), along with the abbreviated names used in the multivariate analysis.

Taxa	Symbol	%
Copepoda		
Order Calanoida		
Acartia spp.	Ac	0.22
Acartia clausi	Acl	0.14
Aetideidae	Ae	0.01
Aetideus armatus	Aear	0.00
Calanidae	Cal	0.99
Calanus helgolandicus	Cahel	0.00
Calocalanus spp.	Calo	2.43
Candacia spp.	Can	0.03
Candacia armata	Canar	0.00
Candacia simplex	Cansi	0.00
Candacia varicans	Canva	0.00
Centropages typicus	Centy	5.20
Centropages violaceus	Cenvi	0.01
Chiridius spp.	Chi	< 0.01
Clausocalanus spp.	Clau	5.55
Clausocalanus/Paracalanus/Pseudocalanus	Cl/Pr/Pse	26.21
Eucalanus hyalinus	Eucah	0.01
Euchaeta spp.	Euch	0.07
Euchirella rostrata	Euro	< 0.01
Haloptilus acutifrons	Haa	< 0.01
Haloptilus longicornis	Hal	0.09
Heterorhabdus spp.	Het	0.04
Lucicutia spp.	Luc	0.06
Mecynocera clausi	Mecl	0.06
Mesocalanus tenuicornis	Meste	0.02
Mesocalanus/Neocalanus	Mes/Neo	0.05
Nannocalanus minor	Nam	0.08
Neocalanus spp.	Neo	< 0.01
Neocalanus gracilis	Neog	< 0.01
Paracalanus spp.	Par	0.26
Paraeuchaeta hebes	Pah	< 0.01
Pontellidae	Pon	0.01
Pontella mediterranea	Ponme	< 0.01
Pleuromamma spp.	Ple	0.27
Pleuromamma gracilis	Pleg	0.03
Subeucalanus monachus	Sumo	< 0.01
Temora spp.	Tem	0.01
Temora stylifera	Temst	0.22
Order Cyclopoida		
Agetus spp.	Age	0.03
Agetus flaccus	Agef	0.01
Copilia mediterranea	Copm	< 0.01
Copilia spp.	Cop	0.01
Corycaeus clausi	Corc	0.01
Corycaeus spp.	Cor	0.03
Corycaeidae	Cory	0.54
Ditrichocorycaeus spp.	Dit	0.01
Ditrichocorycaeus anglicus	Dita	0.07
Onychocorycaeus spp.	Ony	0.01
Onychocorycaeus ovalis	Onyo	0.03
Urocorycaeus furcifer	Urof	0.06
Farranula spp.	Far	0.15
Oithona spp.	Oit	18.57
Oncaeidae	Onc	8.66
Sapphirina spp.	Sap	< 0.01
Vettoria granulosa	Vetg	0.02
Vettoria spp.	Vet	0.01
Order Harpacticoida		
Clytemnestrinae	Cly	0.02
Euterpina acutifrons	Euta	0.06
Microsetella spp.	Mic	1.97
Order Mormoniloida		
Mormonillidae	Mor	0.13
Nauplii	Nau	9.41
Holoplankton		
Class Apendicularia		
Fritillariidae	Fri	5.88
Oikopleuridae	Oik	3.06
Other Appendicularia	App	1.60
Superorder Cladocera		
Evadne spp.	Ev	0.67
Penilia spp.	Pe	0.54
Pseudevadne spp.	Pse	0.32
Order Amphipoda		
Hyperiidae	Hyp	< 0.01
Platyscelus serratulus like	Pla	< 0.01
Phrosinidae	Phr	< 0.01
Phronima	Phro	< 0.01
Order Pteropoda		
Clio spp.	Cli	0.03
Creseis spp.	Cres	0.38
Creseis acicula	Crea	0.41
Creseis conica	Crec	< 0.01
Creseis virgula	Crev	0.08
Desmopterus spp.	Des	< 0.01
Limacina bulimoides	Lib	0.23
Limacina inflata	Lii	1.26
Limacina lesueurii	Lil	0.01
Limacina trochiformis	Lit	0.01
Order Isopoda		
Isopoda	Iso	0.01
Order Holoplanktonic taxa		
Cnidaria	Cni	0.24
Doliolida	Dol	0.21
Chaetognatha	Chae	0.40
Euphausiacea	Eup	0.25
Ostracoda	Ost	0.86
Salpidae	Salp	0.18
Siphonophora	Siph	0.03
Abylidae	Aby	< 0.01
Diphyidae	Dip	0.11
Eudoxoides spiralis	Eus	0.01
Solmundella spp.	Sol	< 0.01
Meroplanktonic		
Order Decapoda		
Anomura spp.	An	< 0.01
Brachyura spp.	Bra	< 0.01
Other Meroplankton taxa		
Bivalvia	Biv	0.46
Branchiostoma spp.	Bran	< 0.01
Cirripedia	Cir	0.02
Cymbulia peronii	Cym	< 0.01
Echinopluteus larva	Ech	0.01
Ophiopluteus larva	Oph	0.04
Teleostei	Tel	0.02
Pelagia noctiluca	Pel	< 0.01
Polychaeta	Pol	0.83
Oxygyrus spp.	Oxy	0.01
Phoronida	Pho	0.01
Pterotrachea spp.	Pte	< 0.01

Copepods, including nauplii and copepodites, were the most abundant group, constituting together 82.2% of the total abundance. Among copepods, Calanoida represented the dominant taxa (42.4%), followed by Cyclopoida (28.2%), Harpacticoida (2.1%), and Mormonilloida (0.13%).

Non-copepod holoplanktonic species that contributed to the overall abundance included Appendicularia (10.5%), Pteropoda (2.4%), Cladocera (1.5%), Ostracoda (2.3%), Isopoda (0.01%), and Amphipoda (0.01%).

Other meroplankton species accounted for 1.4% of the total abundance.

The diversity indices demonstrate consistent patterns. Stations located near the coast and in the southern regions (SPB) exhibited higher species diversity. Conversely, stations in the central zones of the GLSB and LS regions showed lower values (Table 4.2). The SPB and GLSB regions showed higher taxonomic richness and Shannon index values, indicating a greater diversity of species and lower dominance of a few species in these areas. Conversely, both LS and CPB showed very low values (Figure 4.15 C and D).

Table 4.2. Values of diversity indices for all stations of the MOOSE-GE 2019 based on microscopic counts: Total individuals (N), total number of species (S), Species richness Margalef (d), Pielou's evenness (J'), and diversity indices of Brillouin, Fisher, Shannon, Lambda, and 1-Lambda.

Region	Leg	Station	N	S	d	J'	Brillouin	Fisher	Shannon (H')	Lambda	1-Lambda'
GLSB	1	St02	2152	49	6.26	0.66	2.53	8.93	2.57	0.12	0.88
	2	St01	1731	35	4.56	0.72	2.50	6.21	2.54	0.12	0.89
	2	St32_b	3296	40	4.82	0.63	2.29	6.41	2.31	0.16	0.84
	2	St38	3076	29	3.49	0.49	1.63	4.43	1.65	0.26	0.74
	2	St60	934	47	6.73	0.70	2.63	10.43	2.71	0.10	0.90
	2	St67	2080	37	4.71	0.56	2.00	6.39	2.03	0.21	0.79
LS	1	St26	2800	28	3.40	0.52	1.71	4.33	1.73	0.28	0.72
	1	St32	861	38	5.48	0.60	2.14	8.14	2.20	0.19	0.81
	1	St41	985	33	4.64	0.61	2.09	6.58	2.15	0.20	0.81
CPB	1	St14	1968	31	3.96	0.49	1.65	5.22	1.67	0.34	0.66
	1	St22	2148	29	3.65	0.54	1.80	4.74	1.83	0.25	0.75
	1	St44	2011	28	3.55	0.64	2.12	4.60	2.15	0.16	0.84
SPB	2	St04	1248	34	4.63	0.60	2.06	6.45	2.11	0.18	0.82
	2	St09	1040	51	7.20	0.61	2.32	11.24	2.38	0.15	0.86
	2	St11	591	33	5.01	0.73	2.44	7.54	2.54	0.12	0.88
	2	St15	1475	58	7.81	0.73	2.90	12.04	2.97	0.08	0.92
	2	St21	1900	45	5.83	0.73	2.73	8.27	2.78	0.09	0.91
	2	St45	1562	48	6.39	0.65	2.45	9.37	2.50	0.15	0.85

4.3.3.2. Rank frequency diagrams and Adult/copepodite ratio

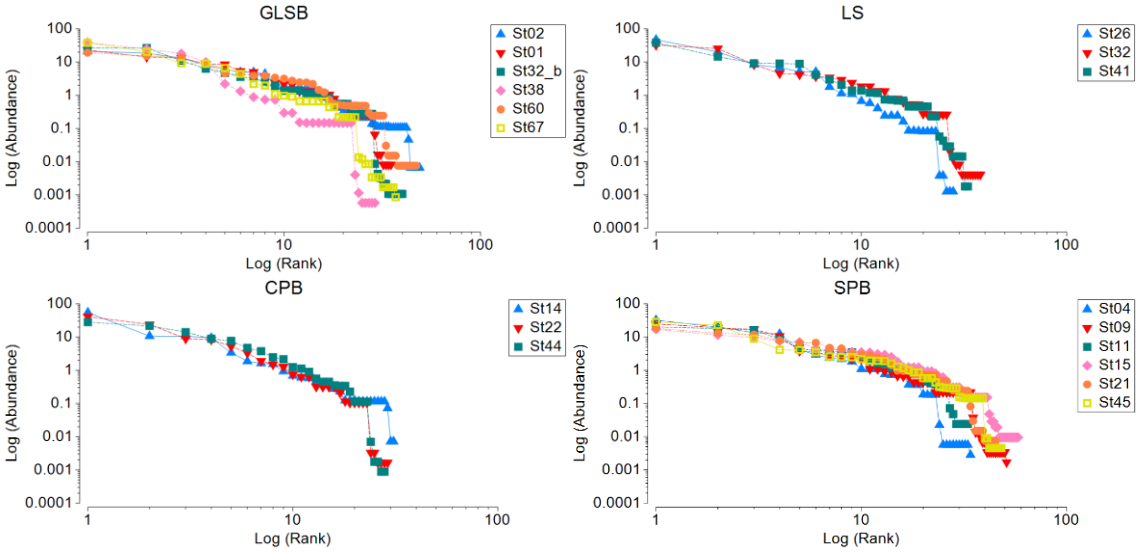


Figure 4.13. Rank frequency diagrams grouped by regions.

The rank frequency distribution (RFD, Figure 4.13) analysis revealed distinct patterns among the different regions. In general, stations located in the GLSB showed concave-shaped RFDs with an observable change in the third rank. In contrast, stations in the LS region showed rectilinear RFDs characterized by a dominance of taxa in the first rank. Similar observations were made in the CPB region, where rectilinear RFDs and taxonomic dominance of the first rank were prominent. In particular, SPB stations show a noticeable shift from the fourth rank onward.

A characterization of RFDs is given by the p1/p2 ratio with low values (below 1) indicating mature community having high diversity and a convex RFD shape (see § 2.3.2.3). On the other hand, the ratio adults/copepodites (computed for the whole copepod species or genera) gives a rough picture of the demographic structure of the copepod community; with a high ratio corresponding to a more mature community. Consistently we roughly observed a negative relationship between both ratios (Figure 4.1.4) showing the rather good link between the taxonomic diversity of the zooplankton and maturity of the copepod community.

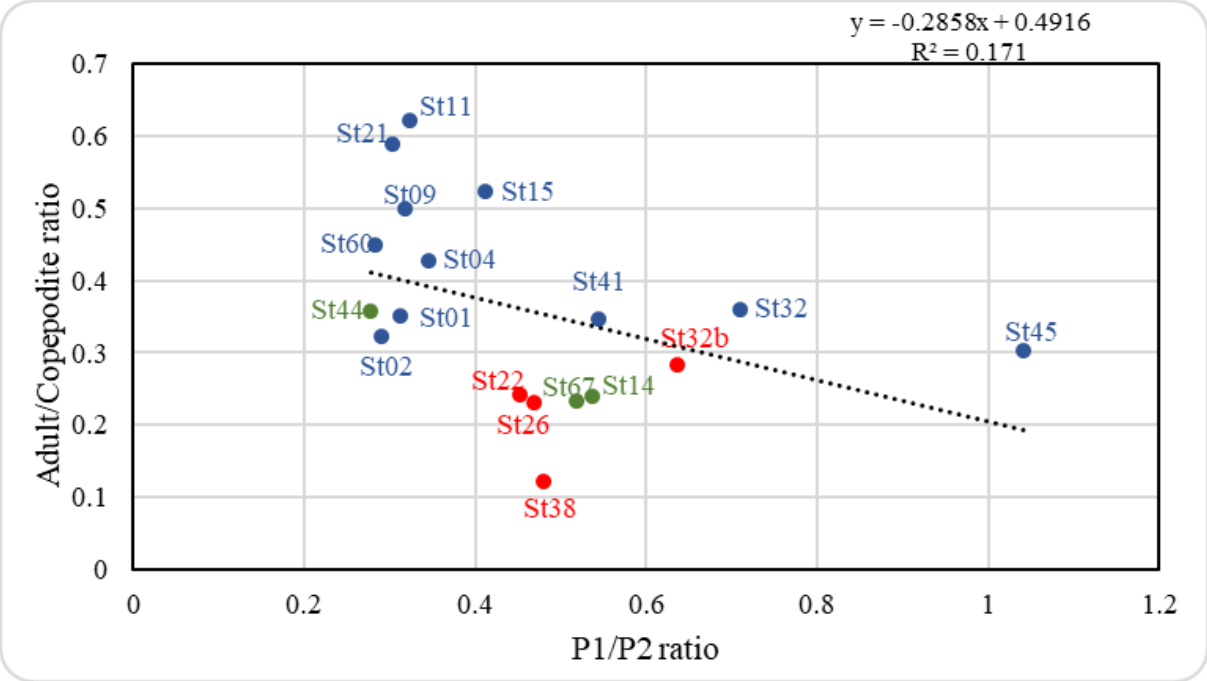


Figure 4.14. Linear regression between Adults/Copepodites ratio and p1/p2 ratio. Colors of the stations (red, green, and blue) correspond to the cluster classification given in Figure 4.5.

Across all surveyed stations, Station 45 in the SPB region displayed the highest p1/p2 ratio, yet its adult/copepodite ratio remained within the typical range observed across most stations (Figure 4.14 and 4.15). Notably, this station exhibited a Shannon index consistent with the overall average of all stations. Conversely, the remaining stations demonstrated p1/p2 ratios below 1 and an average adult/copepodite ratio 0.3 on average, indicating a high level of maturity in the summer community.

Conversely, the GLSB region displayed the lowest adult/copepodite ratios (Figure 4.15), which corresponded to the lowest observed Shannon index values. The SPB and GLSB regions showed higher taxonomic richness and SPB presented the higher Shannon index values, indicating a greater diversity of species and lower dominance of a few species. Conversely, both LS and CPB showed very low values.

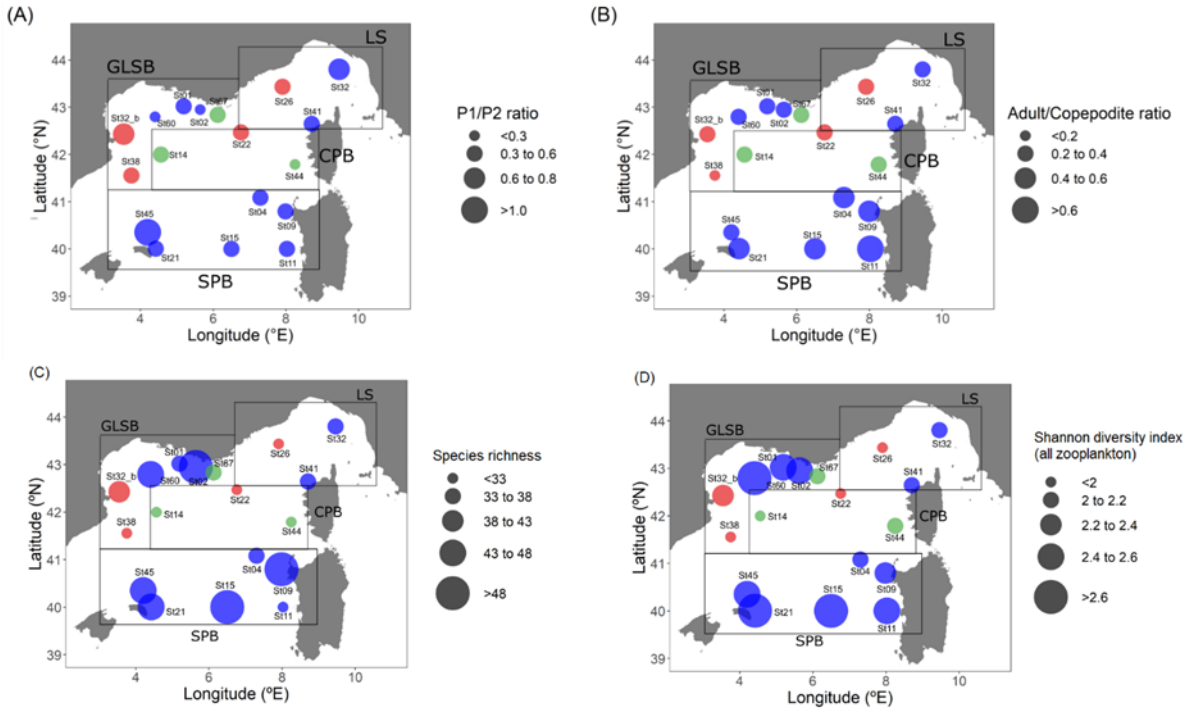


Figure 4.15. Spatial distributions of (A) P1/P2 ratio and (B) Adult/Copepodite ratio; (C) Species richness and (D) Shannon diversity index from microscopic treatment from microscopic treatment. Colors of the stations (red, green, and blue) correspond to the cluster classification given in Figure 4.5.

4.3.3.3. Multivariate analysis on zooplankton community

The first factorial plane of the co-inertia analysis explained 89.8% of the total variance, with the first axis contributing 58.43%. In the environmental system (Figure 4.16, A and C), Axis 1 revealed a distinct opposition between stations characterized by elevated temperature, dissolved oxygen, and surface shallow (blue cluster) and stations with higher salinity and fluorescence levels (red cluster). Axis 2 mostly shows a geographical opposition between northern coastal stations (st01, 02, and 32b) and Southern/coastal stations (St11, 09, and 26) characterized by higher salinity and temperature. In the zooplankton system (Figure 4.16, B and D), the distribution of the stations follows roughly the same pattern as in the Environment system with several taxa (*Euchirella rostrata*, Phrosinidae, *Creseis conica*, *Limacina lesueurii*, *Copilia* spp., Hyperiidae) highly correlated on Axis 1 with the stations of the blue cluster and other taxa (*Mesocalanus tenuicornis*, *Candacia varicans*, *Vettoria granulosa*, *Corycaeus clausi*, *Corycaeus* spp., Aetideidae) correlated with stations of the red cluster. Some taxa (*Platyscelus serratulus*, *Aetideus armata*, *Acartia clausi*) are well correlated with southern coastal stations, and others (*Subeucalanus monachus*, *Eudoxoides spiralis*, *Solmundella* spp., *Anomura* spp.) with norther coastal stations. The good correlations found between the coordinates of the

stations of the two systems highlight the good link between zooplankton community structure and environmental variables both in terms of environmental clusters (Axes 1; Figure 4.15 E) and North-south opposition of coastal stations (Axes 2; Figure 4.15 F).

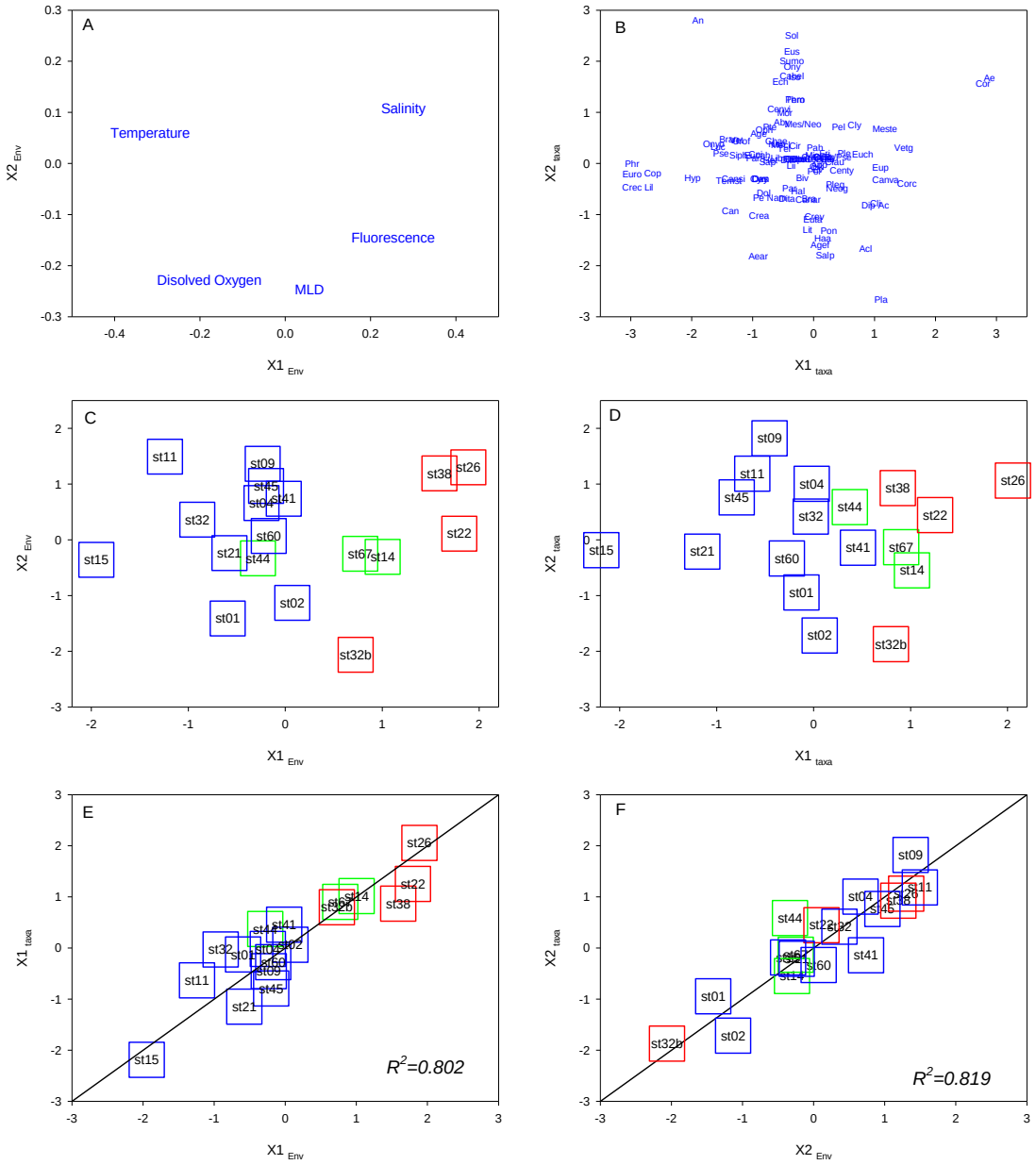


Figure 4.16. Co-inertia analysis. Ordination on the plans (1, 2) of the environmental variables (A) and the abundance of the zooplankton taxa identified in the microscope (B) and of the stations in the "Environment system" (C) and in the "Zooplankton system" and plots of the stations on the first (C) and second (D) axes of the two systems. The line represents the equality between the coordinates of the two systems. Colored squares identify the different clusters given in Figure 4.5.

Examining, within the three clusters, the taxa classified as rare (*i.e*. characterized by low overall abundance and occurrence and relating them to Axis 1 of the coinertia analysis (X1 taxa), certain taxa are exclusively present in the blue cluster and exhibit a negative correlation (i.e. negative coordinate) with X1 taxa (Table 4.3). Conversely, the taxa present in the red cluster show a positive correlation with X1 taxa. For the most abundant taxa present in all three clusters, it is observed that they all exhibit a positive correlation with X1 taxa. Furthermore, the highest abundances are distributed between the red and green clusters. This underscores the significance of not solely focusing on the most prevalent organisms but also recognizing the value of rare species in elucidating station-specific characteristics.

Table 4.3. Mean abundance of rare and abundant taxa per environmental cluster and their coordinates on the first axis (X1 tax) of the co-inertia analysis, bold characters indicate higher average values.

	Mean abundance per cluster (ind/m^3)			
	Blue	**Green**	**Red**	**X1 tax**
Rare taxa				
Euchirella rostrata	**0.01**	0.00	0.00	-2.98
Phrosinidae	**0.01**	0.00	0.00	-2.98
Creseis conica	**0.03**	0.00	0.00	-2.98
Limacina lesueurii	**0.21**	0.00	0.00	-2.98
Copilia spp.	**0.25**	0.00	0.00	-2.64
Corycaeus clausi	0.00	0.00	**0.75**	1.53
Corycaeus spp.	0.00	0.06	**2.83**	2.78
Aetideidae	0.00	0.00	**0.57**	2.88
Abundant taxa				
Fritillariidae	93.38	21.56	**243.78**	0.18
Oithona spp.	251.32	348.33	**680.21**	0.21
Clausocalanus/Paracalanus/Pseudocalanus	252.05	718.87	**1071.89**	0.31
Clausocalanus spp.	40.57	**319.95**	135.99	0.34
Centropages typicus	76.65	**185.39**	106.93	0.46

Analyzing the mean similarity and dissimilarity for clusters and regions (Table 4.4), it is observed that they share similar main contributors, which in general are taxa described as cosmopolitan. However, it is observed that the cluster shows higher values for similarity (Red) and dissimilarity (Blue-Red) compared to the regions. This finding agrees with previous results of the co-inertia analysis, suggesting that the distribution of taxa is more linked to environmental characteristics than to spatial distribution.

Table 4.4. Average similarity (within groups) and dissimilarity (between groups) and main contributing taxa to these average values for the environmental clusters (top) and the regions (bottoms), bold characters indicate higher average values.

ENVIRONMENTAL CLUSTERS

	Stations	Similarity	Main contributors	Cumulative abundances of taxa (%)
Blue	St01, St02, St04, St09, St11, St15, St21, St32, St41, St45, and St60	65.84	*Oithona, Cla/Para/Ps, Oncaeidae*	20.5
Green	St14, St44, and St67	72.2	*Cla/Para/Ps, Oithona, Clausocalanus*	11.8
Red	St22, St26, St32_b, and St38	**73.91**	*Oithona, Cla/Para/Ps, Oncaeidae*	22.8
		Dissimilarity		
Blue - Green		37.18	*Cla/Para/Ps, Clausocalanus, C. typicus*	
Blue -Red		**40.3**	*Cla/Para/Ps, Oithona, Fritillaridae*	
Green-Red		28.86	*Fritillaridae, Cla/Para/Ps, Oithona*	

REGIONS

	Stations	Similarity	Main contributors	Cumulative abundances of taxa (%)
GSLB	St02, St01, St32_b, St37, St60, and St67	64.81	*Cla/Para/Ps, Oithona, Oncaeidae*	22.4
CPB	St14, St22, and St44	**72.28**	*Cla/Para/Ps, Oithona, Clausocalanus*	12.4
LS	St26, St32, and St41	65.00	*Cla/Para/Ps, Oithona, Oncaeidae*	9.1
SPB	St04, St09, St11, St15, St21, and St45	68.7	*Oithona, Cla/Para/Ps, Oncaeidae*	11
		Dissimilarity		
GLSB - CPB		33.6	*Clausocalanus, Cla/Para/Ps, Oithona*	
GLSB-LS		35.29	*Cla/Para/Ps, Oithona, Fritillaridae*	
CPB-LS		27.66	*Cla/Para/Ps, Clausocalanus, Oithona*	
GLSB-SPB		38.46	*Cla/Para/Ps, C. typicus, Fritillaridae*	
CPB-SPB		**39.45**	*Cla/Para/Ps, Clausocalanus, C. typicus*	
LS-SPB		38.02	*Cla/Para/Ps, C. typicus, Fritillaridae*	

4.3.1. Fluxes through zooplankton

4.3.1.1. Carbon demand

The LS and SPB regions displayed a significant range of variation in zooplankton carbon demand (ZCD), spanning from 54.1 to 304.9 mg C m^{-2} d^{-1}. The lowest ZCD value was recorded at Station 15, while the highest was observed at Station 26 (Table 4.5 and Figure 4.17 and 4.18).

In average the LS region exhibited higher values of ZCD (164.9 ± xx mg C m^{-2} d^{-1}), followed by GLSB (161.7 ± xx mg C m^{-2} d^{-1}). These values then decreased further south to SPB (87.6± xx mg C m^{-2} d^{-1}). Interestingly, stations in this region that were closer to the Balearic Islands, particularly Mallorca (st 21 an 45), recorded higher values compared to stations near Sardinia (st4, 9 and 11), which would be due to the influence of the circulation in this area of the region.

The ZCD represents from 2.1% to 15.3% of the daily phytoplankton stock observed at SPB station 15 and LS station 26, respectively, and higher percentages were observed in the GLSB (6-11%) and LS (6-15%) regions than in CPB (3-7%) and SPB (2-10%).

Table 4.5. Phytoplankton stock in C, zooplankton stock in C, zooplankton carbon demand impact on phytoplankton stock per day, zooplankton carbon demand, zooplankton production and zooplankton P/B ratio by region during MOOSE-GE 2019. * Phytoplankton stock in C= Autotrophic carbon Ca = Chl*a* x 50 in mg C/m^2. Values computed from 0-200m.

Leg	Station	Phytoplankton stock (mg C/ m^2)	Zooplankton stock in C (mg C/m^2)	Zooplankton/Phytoplankton ratio (%)	Grazing impact (%)	ZCD (mg C/m^2 d^1)	Zooplankton production (mg C/m^2)	P/B (day^{-1})
1	st02	2017.9	615.8	30.0	7.6	153.1	26.3	0.043
2	st01	1836.9	791.0	42.1	11.0	202.2	32.0	0.040
2	st32_b	2460.0	576.8	23.0	6.9	170.5	30.2	0.052
2	st38	2348.4	508.1	21.5	7.0	165.2	27.0	0.053
2	st60	1729.2	417.0	22.4	5.8	101.3	15.8	0.038
2	st67	1973.0	683.0	34.1	9.0	177.8	26.8	0.039
1	st26	1993.8	1213.7	60.9	15.3	304.9	44.5	0.037
1	st32	1402.4	321.4	18.3	5.5	78.4	10.5	0.033
1	st41	1797.0	422.8	23.1	6.2	111.5	17.1	0.040
1	st14	1795.2	482.8	26.5	6.8	123.2	16.5	0.034
1	st22	2031.4	249.6	12.1	3.1	63.6	9.3	0.037
1	st44	1597.5	403.5	25.1	6.8	109.8	15.2	0.038
2	st04	1453.6	284.5	14.0	3.8	65.6	9.2	0.032
2	st09	1657.8	270.6	14.8	2.1	36.2	7.7	0.028
2	st11	1308.0	227.9	11.5	3.5	54.6	8.1	0.036
2	st15	1376.9	224.9	12.0	3.5	54.1	8.3	0.037
2	st21	1732.7	843.4	41.1	10.3	192.9	31.1	0.037
2	st45	1624.4	549.4	27.4	6.9	122.0	18.9	0.034

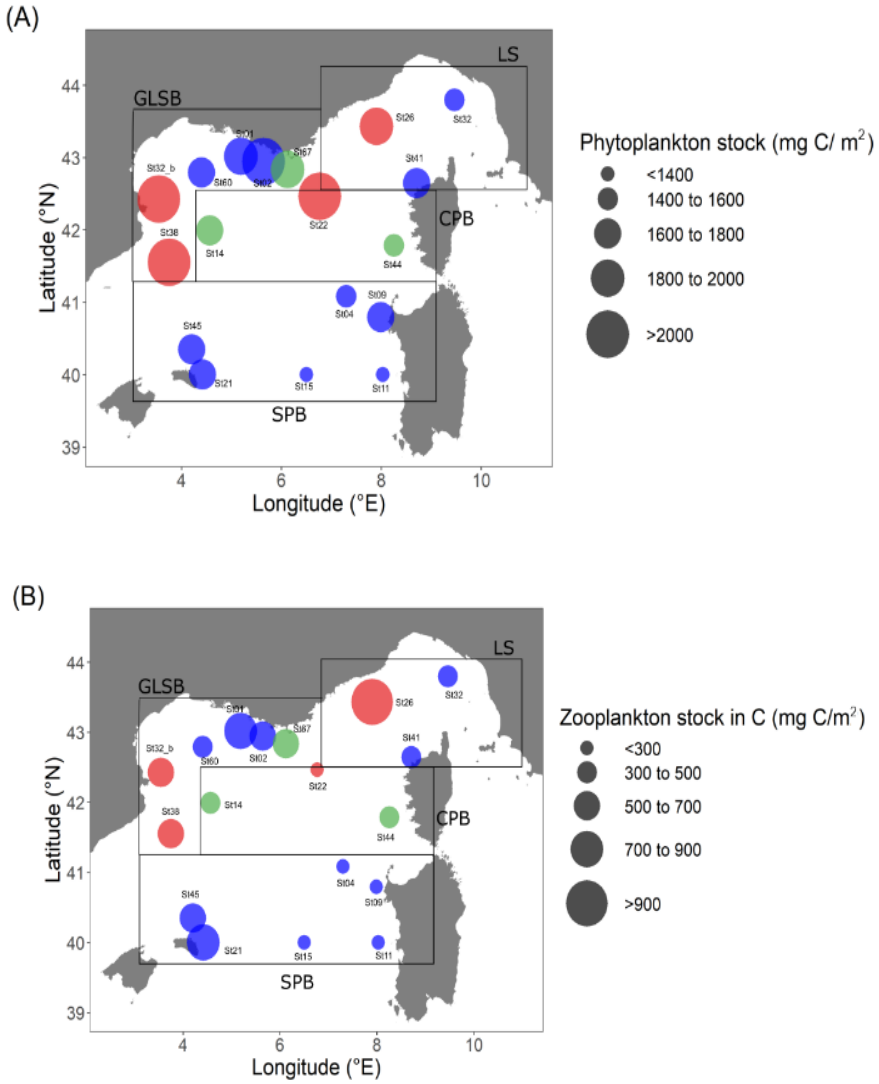


Figure 4.17. Spatial distributions of Phytoplankton stock (A; in mg C/m^2) and Zooplankton stock (B; in mg C/m^2).

Coastal stations, especially in the GLSB, exhibit the highest phytoplankton stocks (Figure 4.17). Interestingly, the zooplankton pattern was roughly similar to those of phytoplankton across various stations in this region, despite phytoplankton values being nearly double those of zooplankton. This suggests that high phytoplankton values may contribute to elevated zooplankton values in these stations. However, exceptions are observed in stations near the west coast (St 32_b and St 38), where the differences between the high phytoplankton values and the low zooplankton values could be physically influenced by the interaction between the northern current and the Balearic current, or alternatively by the quality of the phytoplankton.

4.3.1.2. Nitrogen and phoshorous excretion

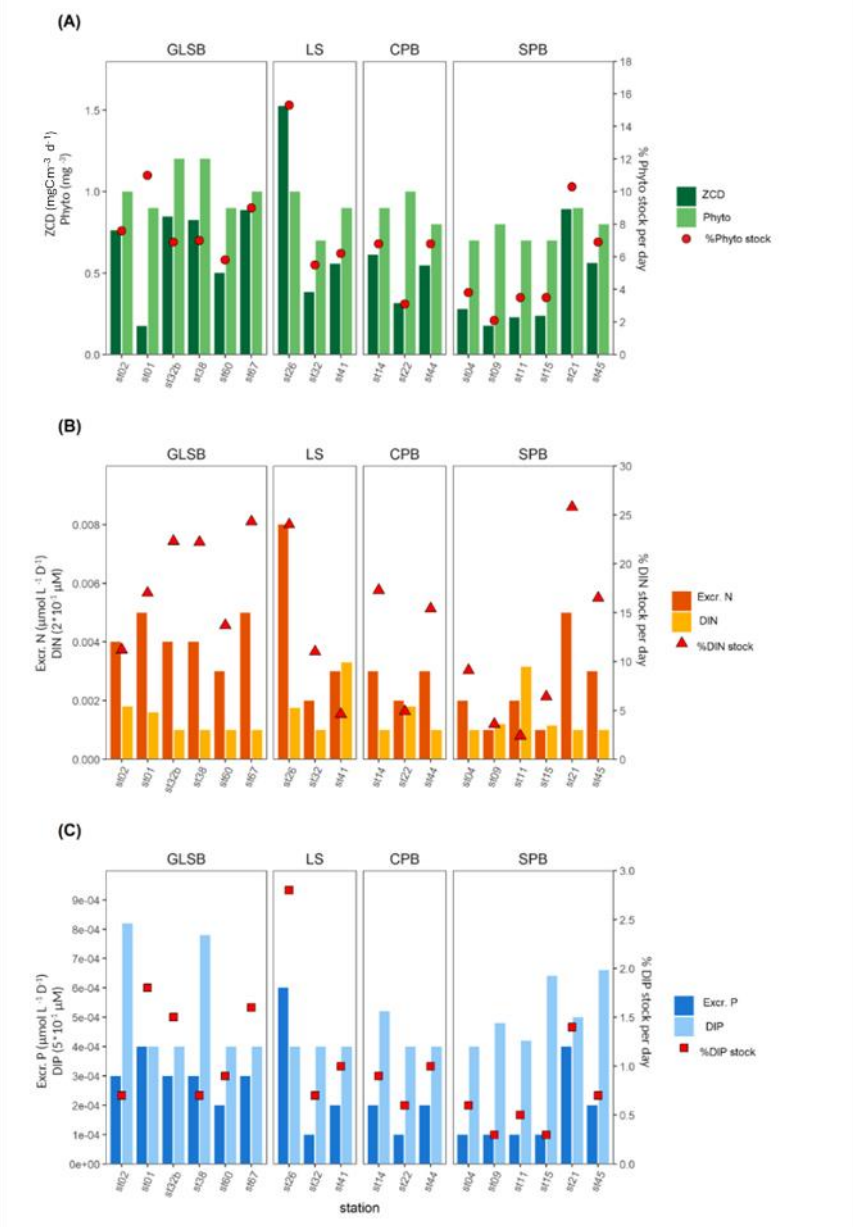


Figure 4.18. Grazing and metabolic rates of zooplankton during MOOSE-GE 2019. (A) Zooplankton carbon demand and phytoplankton stock, and ratio percentage, (B) nitrogen excretion and DIN stock, and ratio percentage, and (C) phosphorous excretion and DIP stock, and ratio percentage. Values of DIN and DIP stocks averaged above the nutricline.

The zooplankton excretion represented a daily N and P recycling equivalent to 2.4% to 26% of the dissolved inorganic nitrogen (DIN) stock at stations St11 and St21 situated within the SPB region. In contrast, at stations St09 and St15 (both within SPB, each at 0.3% of DIN), as well as the notably higher value at St26 (located at LS), the contribution to dissolved inorganic phosphorus (DIP) stocks was lower, ranging from 0.3% to 2.8%. Of note, both GLSB and LS regions, characterized by elevated excretion rates, also exhibited high levels of zooplankton abundance and biomass. This discrepancy in the contribution of zooplankton excretion to DIN and DIP stocks can be attributed to variations in the N/P ratio between excretion and the existing nutrient stocks.

Table 4.6. Zooplankton nitrogen and phosphorous excretion rates estimated, contribution of the N and P recycling and nutrients concentrations in the upper layer above the nutricline for the different stations sampled by region during MOOSE-GE 2019.

Region	Leg	Station	Nitrogen Excretion (µgN m^{-3} d^{-1})	%DIN stock day^{-1}	NO_3- [µmol /L]	Phosphorous Excretion (µgP m^{-3} d^{-1})	%DIP stock day^{-1}	PO_4^{3-} [µmol /L]
GLSB	1	st02	56.2	11.2	0.04	8.2	0.7	0.04
	2	st01	76.3	17.0	0.032	11.0	1.8	0.02
	2	st32_b	62.4	22.3	0.02	8.8	1.5	0.02
	2	st38	62.2	22.2	0.02	8.6	0.7	0.039
	2	st60	38.4	13.7	0.02	5.6	0.9	0.02
	2	st67	68.1	24.3	0.02	9.8	1.6	0.02
LS	1	st26	117.4	24.0	0.035	17.1	2.8	0.02
	1	st32	30.9	11.0	0.02	4.5	0.7	0.02
	1	st41	42.5	4.6	0.066	6.1	1.0	0.02
CPB	1	st14	48.5	17.3	0.02	7.0	0.9	0.026
	1	st22	24.5	4.9	0.036	3.5	0.6	0.02
	1	st44	43.1	15.4	0.02	6.1	1.0	0.02
SPB	2	st04	25.5	9.1	0.02	3.7	0.6	0.02
	2	st09	11.9	3.6	0.024	2.0	0.3	0.024
	2	st11	21.0	2.4	0.063	3.0	0.5	0.021
	2	st15	20.6	6.4	0.023	3.0	0.3	0.032
	2	st21	72.2	25.8	0.02	10.6	1.4	0.025
	2	st45	46.3	16.5	0.02	6.8	0.7	0.03

4.4. Discussion

4.4.1. Environmental context

During the MOOSE-GE 2019 campaign, sampling stations were grouped into three clusters based on temperature, salinity, dissolved oxygen, fluorescence, and mixed layer depth (MLD). While visually discerning a direct correlation between cluster distribution and specific regions was challenging, our observations suggest a closer association with the influence of deep convection (Millot and Taupier-Letage, 2005a). Stations within the red cluster (highest salinity, fluorescence, and MLD at greater depths) were mostly

located in the area influenced by winter deep water formation in the Gulf of Lyon. The blue cluster (highest temperature and oxygen) predominantly occupied coastal areas across all regions studied in this cruise, with a notable concentration in the SPB region. While stations within the green cluster (intermediate values between the other two clusters) were more dispersed throughout space, with their distribution interspersed between the red and blue clusters (Figure 4.5).

4.4.2. Zooplankton abundance, biomass, community structure, and diversity during the MOOSE-GE 2019 cruise

4.4.2.1. Imaging techniques and microscope

Abundance values obtained through imaging techniques (ZOOSCAN and FlowCam particle counts combined) in MOOSE-GE 19 matched well with the counts from traditional microscopy (by Loic Guilloux, Figure 4.12). Nevertheless, some stations (st38, 26, 15, 22 and 02) display differences in estimating abundance between the imaging and microscopy methods. It's important to mention that these discrepancies fall within an acceptable range, as indicated by previous studies (Feliú, 2020). These discrepancies in abundance could potentially be attributed to (1) the inclusion of small organisms <300 µm, effectively captured by FlowCAM, yet challenging to accurately quantify using traditional microscopy methods, and (2) when the microscope count yields a higher abundance, it could be attributed to an underestimation resulting from the number of sample splits required to obtain an adequate concentration for analysis. This scenario can occur, for example, when samples contain a high abundance of phytoplankton, necessitating higher dilution for cleaner microscopic observation. Similar is for imaging tools, especially the FlowCAM, which follows a protocol that regulates the saturation in the equipment cell during counting (aiming to obtain approximately 4 particles per photograph). Therefore, the aliquot must be adequately diluted to meet the requirements. Consequently, this dilution step may result in a reduced zooplankton count compared to the microscope count results.

4.4.2.2. Spatial patterns of Abundance and Biomass

On a spatial scale, the Gulf of Lion Shelf Break and Ligurian Sea demonstrate notably elevated zooplankton abundance and biomass, contrasting with the relatively diminished values recorded in the Southern Provencal Basin and Central Provencal Basin (Figure 4.9). Additionally, a distinct pattern emerges regarding contribution of main taxonomic groups to zooplankton abundance and biomass, with a discernible north-to-south gradient

depicting declining percentages of copepods in the SPB, as also noted in the HIPPOCAMPE study for spring-time. The observed spatial pattern can be attributed to the notable abundance of small copepods (belonging to <500 ESD size-class, Figure 4.10). Moreover, in terms of biomass, the presence of crustaceans, gelatinous organisms, and miscellaneous taxa (especially pteropods) plays a crucial role in driving higher biomass levels in LS and GLSB regions.

In contrast, CPB shows a prevalence of copepods in terms of biomass. Although the total biomass values among the stations in this region show no significant differences, st14 stands out, displaying higher biomass values in smaller ESD size classes compared to other stations in the same region (Figure 4.10). Within the SPB, the overall low abundance and biomass can be attributed to the importance of large organisms (>1000 µm; Figure 4.11), primarily consisting of gelatinous organisms, miscellaneous, and appendicularians.

Appendicularians have been found in the larger fractions, although most organisms are typically described as having trunks measuring more than 300 µm (Aravena and Palma, 2002). However, their presence in this large fraction could be due to their tendency to coil up, preventing them from being effectively "filtered" through the sieves during sample fractionation.

The comparison of our results with the data collected during MOOSE-GE 2017 using the same methodology (Table 4.7) shows that in early summer (MOOSE-GE 2019), there is a twice higher zooplankton abundance, compared to the late summer of the previous year (MOOSE 2017), whereas biomass remain relatively consistent between the two expeditions. This may indicate a shift in size structure, with late summer displaying a dominance of larger animals compared to early summer. This is consistent with the classical seasonal pattern of community dynamics: (i) early summer characterized by an abundance of small organisms following the spring bloom, along with a peak in reproduction and recruitment within populations, and (ii) late summer with an increase in larger organisms associated with cohort development and mortality processes. This trend is even more evident in GLSB and LW potentially more influenced by the sequence of deep convection followed by the spring bloom, while in CPB and SPB both abundance and biomass are in the same range between the two periods.

In the case of the GLSB, topography exerts a significant influence. This aspect was already highlighted in the MOOSE-17 study by Feliú (2020), who proposed that the higher zooplankton concentrations above the GLSB are the result of higher productivity in the region, influenced by upwelling and ebb processes interacting with the North Mediterranean Current, especially along the submarine canyons of the continental margin (Durrieu De Madron et al., 2011). This provides a possible explanation for the high levels of zooplankton abundance and biomass observed in this area (Sabatés and Olivar, 1996).

Similarly, the discrepancies observed in MOOSE-GE 19, compared to MOOSE-GE 17, can be attributed to the dynamics of deep convection during the cruise. This natural preconditioning is further affected by the random component derived from mesoscale variability (Margirier et al., 2020).

Table 4.7 Comparison of mean (± standard deviation) values of zooplankton abundance, biomass and taxonomic diversity between MOOSE-GE 2019 and MOOSE-GE 2017 cruises. Data of MOOSE-GE 2017 from Feliú (2020).

	MOOSE-GE 19	**MOOSE-GE 17**
	June 06 - July 01, 2019	Aug 31- Sept 23, 2017
	Early summer	Late summer
	Bongo net 120 µm	Bongo net 120 µm
	Zooscan + FlowCam	Zooscan + FlowCam
Abundance (Ind.m^3)	2039 ± 608	1091 ± 580
Biomass (mgDW/m^3)	6 ±1.6	5.2 ±2.6
Shannon index (H´)	2.2 ± 0.3	2.4 ± 0.2
p1/p2	0.5 ± 0.2	0.7 ± 0.3
Abundance (Ind.m^3)		
GLSB	2613.8 ± 1195.9	1374
LS	2458.1 ± 2105.2	1061
CPB	1775.2 ± 454.4	997
SPB	1308.8 ± 628.5	915
Biomass (mgDW/m^3)		
GLSB	6.7 ± 1.4	4
LS	7.5 ± 4.4	5
CPB	4.0 ± 1.2	4
SPB	5.4 ± 3.1	5
Shannon index (H´)		
GLSB	2.3 ± 0.4	2.6 ± 0.1
LS	1.6 ± 0.9	2.2 ± 0.3
CPB	2 ± 0.3	2.2 ± 0.1
SPB	2.5 ± 0.3	2.5 ± 0.1
p1/p2		
GLSB	0.4 ± 0.1	0.5 ± 0.2
LS	0.6 ± 0.1	0.9 ± 0.4
CPB	0.4 ± 0.1	1.1 ± 0.1
SPB	0.5 ± 0.3	0.5 ± 0.2

4.4.2.3. Community structure and diversity

In terms of taxonomic richness, the SPB and GLSB regions show higher values compared to the CPB and the LS. This trend is also evident in the distribution of the Shannon diversity index, indicating greater diversity in the former regions. Several studies have emphasized the impact of various factors, including local wind-driven currents, depth, location, topography, oceanographic patterns, and spatial-temporal variability, on shaping the community structure (Kvile et al., 2014; Saiz et al., 2014a). Low diversity in LS, also reported during MOOSE-GE 2017 (Feliu, 2020) may be linked to heterogeneous hydrodynamic structure with a divergence zone in the central area favoring phytoplankton production and large-omnivorous copepods (*e.g*. Pleurommama sp., *Eucalanus* spp., *Calanus* spp.) and decreasing diversity (Pinca and Dallot, 1997).

During MOOSE-GE 19, the dominance of copepods (82%), as observed in our study, is a prominent feature of the mesozooplankton community structure in the Mediterranean Sea (Siokou-Frangou et al., 2010a). This pattern is consistent with previous large-scale observations conducted in the same region (Donoso et al., 2017; Feliú, 2020). Small copepods are the dominant group in all regions. Specifically, in the Provencal Basin, *Paracalanus/Clausocalanus/Pseudocalanus* spp. and *Oithona* spp. were notably present, as reported by Nowaczyk et al. (2011). Similarly, in the Ligurian Sea, *Paracalanus/Clausocalanus/Pseudocalanus* spp., *Oithona* spp., and Oncaeidae were prominent taxa.

Among the non-copepod groups, Fritillariidae and Oikopleuridae (Appendicularians) were found to be the most abundant, along with *Limacina inflata* (Pteropoda). These taxonomic orders align with those previously reported for MOOSE-GE 17 (Feliu, 2020).

In the Provencal Basin, there was a notable abundance of gelatinous organisms, appendicularians, and chaetognaths, particularly in the ESD size-class above 1000 µm. Similarly, in the Ligurian Sea, specifically at St32, gelatinous organisms were prominent (mostly larval stages of hydromedusae, doliolides, and salps). The presence of the carnivorous organisms, such as chaetognaths and hydomedusae, may play a role in shaping the abundance patterns in these areas through predation dynamics (Yebra et al., 2020).

The patterns of taxa distribution within the environmental clusters can be explained by two key factors: (1) the prevalence of dominant species and their corresponding abundances, and (2) the occurrence of rare species with low abundances that exhibit presence/absence patterns within the clusters. These findings indicate that beyond the specific regions studied, the distribution and composition of taxa could be primarily shaped by water-mass characteristics rather than by geographical differences. We observed a strong correspondence between habitats (defined by environmental

clustering) and zooplankton communities (classified through coinertia analysis), indicated by a good alignment. Notably, the community associated with the red cluster, which represents regions influenced by deep convection, exhibited a higher contribution from CPB stations, indicating a robust and persistent community structure. This suggests a memory effect, where the zooplankton community in summer retains characteristics established during the spring after the occurrence of convection events.

Indeed, the copepod community in MOOSE-GE 19 exhibits high maturity and diversity during the summer season (Figure 4.14 and 4.15 D). The higher p1/p2 ratio during the spring bloom period suggests a greater level of development of populations and lower diversity within the community. These findings align with the HIPPOCAMPE study for the same year in spring by Makhlouf (pers. Comm. 2023).

4.4.2.4. Contribution of zooplankton to carbon, nitrogenous and phosphorous fluxes

The Mediterranean Sea is generally classified as an oligotrophic ecosystem; however, it exhibits notable spatial trophic gradients, such as north-south and west-east gradients (Moutin et al., 2012), and temporal variations in trophic conditions, such as during the Winter-Spring transition and Spring bloom periods (D'Ortenzio and Ribera d'Alcalà, 2009; Lavigne et al., 2015; Donoso et al., 2017; Mayot et al., 2017). Indeed, the MOOSE-GE 19 cruise took place at end of spring-early summer, long after the phytoplankton bloom. During this period, the daily impact of zooplankton grazing did not exhibit a distinct pattern among regions but accounted for 2 to 15% of the phytoplankton stock. These values are similar to those recorded during MOOSE-GE 2017 (4 to 18%; Feliu, 2020). Donoso (2017) reported that the grazing pressure exerted by copepods on phytoplankton exhibited a significant increase from winter (8%) to spring (46%), followed by a decrease in summer (9%). Therefore, our values would fall within the transitional period between spring and early summer.

In the larger fractions (>500 µm), the taxonomic composition was primarily characterized by the presence of carnivorous organisms, including large crustaceans, gelatinous organisms and chaetognaths. In contrast, the smaller fractions (<500 µm) were predominantly occupied by herbivorous/omnivorous organisms, such as small copepods, nauplii, and miscellaneous taxa (*e.g*., pteropods), suggesting a high proportion of primary consumers, mainly herbivorous.

Similar findings have been previously reported in the Gulf of Lion (Boris Espinasse et al., 2014), in the Bay of Marseille (Tiano et al., 2014b), and along a north-south transect in the western basin during the Hippocampe Cruise (Fierro-González et al., 2023).

Regarding nitrogen and phosphorus excretion by zooplankton, it is worth noting that studies examining metabolic rates are relatively scarce, with a predominant focus on the western Mediterranean Sea (Alcaraz, 1988; Calbet et al., 1996; Gaudy et al., 2003), as emphasized by Siokou-Frangou et al. (2010). Hence, conducting a direct comparison between MOOSE-GE 19 and previously published studies may present challenges due to the limited availability of data in this specific area.

Gaudy et al. (2003) reported on nitrogen and phosphorus excretion rates in the Gulf of Lions using a silk net with a mesh size of 80 µm, focusing specifically on the larval stages of copepods. They found that excreted nitrogen accounted for 31% and phosphorus for 16% of primary production requirements during spring, and 10% and 27% during winter. However, it should be noted that these values do not match the rates reported for the water column during MOOSE-GE 19, which showed an average of 19% for nitrogen and 1.2% for phosphorus during the summer. Similarly, in the HIPPOCAMPE study using a 60 µm vertical net, nitrogen, and phosphorus excretion rates were 1.7% and 1.35%, respectively, in spring.

These results provide evidence that the utilization of imaging tools serves as a reliable proxy for approaching metabolic flux estimations.

4.5. Conclusion

Our study, conducted in early summer 2019, provides comprehensive insights into the status of the zooplankton community, enabling comparisons with other marine ecosystems or with previous years in the same region. Through the utilization of state-of-the-art imaging techniques and meticulous microscope counting, we systematically collected data covering abundance, biomass, size distribution, community composition, and diversity of zooplankton. We complemented this with estimations of fluxes through the use of allometric relationships applied to the zooplankton size distribution and habitat characteristics (temperature and Chl*a*). These comprehensive methods were subsequently integrated with a suite of environmental variables, providing a robust framework for a nuanced understanding of the zooplankton ecosystem.

Our results highlight that environmental patterns were primarily influenced by the deep convection. The deep convection area (DCA) area exhibits characteristics of colder, saltier, oxygen-depleted waters, coupled with heightened levels of chlorophyll and a deeper MLD, characteristics of the deep convection phenomenon and demonstrated how these features contributed to the differentiation among stations (red, green, and blue clusters). Furthermore, we discerned a clear north-south gradient in both zooplankton abundance and biomass. Noteworthy is the observation of increased zooplankton stocks in the GLSB and the LS, that may be linked to underlying topographical features, the mesoscale structures and the North Balearic front. Copepods were the predominant group in the zooplankton community, although the community displayed differing taxonomic compositions across ESD size-classes. The smaller fractions were mainly composed of nauplii, miscellaneous taxa, and small copepods, while the larger fractions were characterized by the presence of gelatinous organisms, crustaceans, miscellaneous organisms, and appendicularians. Additionally, trophic conditions played a crucial role, with an overall mature community observed in early summer, indicating a pre-spring bloom scenario in the months leading up to the zooplankton sampling. This study showed that the zooplankton community composition was more related to water mass characteristics than to regional localization. This highlights the quick responses of zooplankton communities to environmental changes and the importance of “moving” habitats already pointed out in the Gulf of Lion by Espinasse et al (2014).

Our findings also highlight the dynamic trophic conditions in the Mediterranean Sea. The impact of zooplankton carbon demand on phytoplankton stock ranged from 2-15% during the early summer of 2019, indicating a good scenario for sustaining the zooplankton community. However, the lack of data on zooplankton metabolic rates in this region presents a challenge for direct comparisons at a spatio-temporal level. This emphasizes the need for further research to fully understand the complex trophic dynamics of the Mediterranean Sea.

5. General discussion and perspectives

5.1. General discussion on the Mediterranean zooplankton characteristics across the Western Mediterranean Sea

This study has focused on the detailed examination of zooplankton communities during two expeditions conducted in 2019 in the Mediterranean Sea (Figure 5.1). The primary objective was to analyze the structural variability of mesozooplankton in the western basin and part of the Tunisian margin. Our approach has resulted in a comprehensive assessment of several biological variables, including abundance, biomass, diversity, size distribution, and associated fluxes. Below, we try to synthesize this information about the abundance and community structure, and functional importance of zooplankton across the Western Mediterranean Sea in comparison with previous studies.

5.1.1. Patterns of abundance and community structure of zooplankton across the Western Mediterranean Sea

Our results reveal a consistent pattern in zooplankton distribution from north to south. The influence of seasonal deep convection on zooplankton communities is noticeable in the North-Western Mediterranean Sea, with significant effects observed in spring (MERITE-HIPPOCAMPE) and extending into early summer (MOOSE-GE 19 campaign). This indicates discernible variations for these two contrasted seasons. This influence is evident across various zooplankton measures, including abundance (from 7282 ± 2297 to 2039 ± 608 Ind/m^3 on average), biomass (from 16 ± 13 to 6 ±1.6 mg C/m^3 on average), as well as community composition and structure. Zooplankton abundance and diversity indices across various regions of the Western, Southern, and Tunisian margins in the Mediterranean Sea reveal a broad spectrum of variation (table 5.1). During the MERITE-HIPPOCAMPE cruise in spring we observed a predominant spatial trend in abundance of epipelagic zooplankton, with higher values found in the Gulf of Lions shelf break compared to the Provencal Basin. These higher values in the North are likely influenced

by topographical effects on vertical water movement, interacting with the Northern Mediterranean Current along the underwater canyons of the continental margin (Durrieu de Madron et al., 2011, Feliú 2020). A similar pattern was noted a few months later during the summer expedition of MOOSE-GE 19, where the highest zooplankton values in the water column were recorded in the same region, though marginally lower than those observed in spring. Remarkably, the values recorded during the MOOSE-GE 19 are comparable to those reported in PEACETIME 2017 and MOOSE-GE 17, despite being conducted in different years but within the same season. After the bloom period, distinct regional patterns in abundance become evident. These patterns align with findings from other studies, which also demonstrate a decrease in zooplankton stocks from north to south and from west to east (Dolan et al., 2002; Siokou-Frangou et al., 2010, Donoso, 2017; Feliú, 2020).

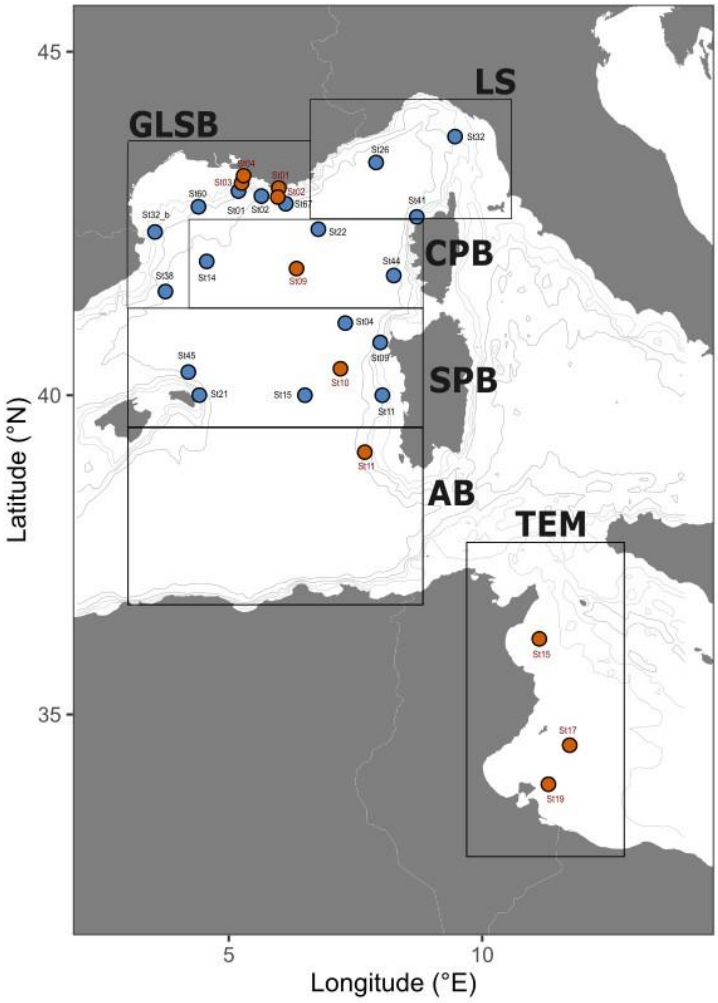


Figure 5.1. Map showing the sampling stations of the MERITE-HIPPOCAMPE cruise (red) and the MOOSE-GE 19 expedition (blue). The black rectangles defined different areas: LS= Ligurian Sea, GLSB= Gulf of Lion Shelf Break, CPB= Central Provencal Basin, SPB= Southern Provencal Basin, APB= Algero-Provencal Basin, and TEM= Tunisian Eastern Margin.

In this regard, we conducted a supplementary investigation to assess the progressive stages of community maturity, characterized as juvenile in spring and maturing in summer, as evidenced by the p1/p2 ratio values obtained for both seasons. This aligns with the framework established by Frontier (1976) and implies a post-bloom scenario with a zooplankton response. This analysis of the p1/p2 ratio provides valuable insights into the community's structure, suggesting an almost immediate post-bloom scenario for the MERITE-HIPPOCAMPE (Spring) and more prolonged and spatially extended post-bloom conditions for the MOOSE-GE 19 campaign (early Summer).

This aligns with the observed strong relationship between environmental factors and the structure of zooplankton communities during the MOOSE-GE 2019 expedition. These findings not only validate but also reinforce the outcomes of the MOOSE-GE 2017 campaign, as documented by Feliú (2020). In this context, zooplankton communities are characterized by a prevalence of "moving habitats", exhibiting temporal shifts in response to hydrodynamic processes and the variability of temperature and salinity (north-south gradient). This stands in contrast to more stable regional habitats. Unlike phytoplankton, zooplankton integrates environmental cues over extended periods, corresponding to considerable drift within regions, as noted by Qiu et al. (2010). Zooplankton also exhibits regional variations associated with local hydrodynamic conditions. For instance, there are high zooplankton stocks observed in the Gulf of Lions shelf break, likely due to topographical features, and in the Ligurian Sea, possibly linked to mesoscale structures. This alignment is consistent with the research conducted by Espinasse et al. (2014) in the Gulf of Lions, further emphasizing the correlation with ecoregions.

The comparison of our results with previous studies can also be made considering different regions of the NWMS (Table 5.1)

In the Provencal Basin the abundance values recorded during the summerwere similar to those reported during late spring in the Peacetime 2017 campaign. Additionally, our values observed for spring, especially for the 60 µm mesh size, were close to those presented by MOOSE-GE 14 during the summer using a 120 µm mesh size. However, when we compare the results from our two cruises, the values fall within the range of those reported in MOOSE-GE 17, taking into account the seasonal variations.

In the Algero Provencal Sea, where only one station was sampled during the MERITE-HIPPOCAMPE cruise, we relied on previous investigations in this area, such as Peacetime 2017 campaign, Nowaczyk et al. (2011) , and Siokou-Frangou et al. (2019). We observed substantial disparities in abundance values across these various studies. These discrepancies can be ascribed to a combination of factors, encompassing geographical positioning, sample quantity acquired, sampling seasons, and the specific methodologies employed for both sampling and analysis. The sampling includes considerations such as net mesh size, towing depth, and the utilization of microscopic or imaging techniques for

sample scrutiny. For instance, within the MERITE-HIPPOCAMPE expedition, it becomes apparent that mesh size plays a pivotal role in abundance estimation.

For the Tunisian eastern margin, we compared our results with studies conducted near the Sicily Channel (Nowaczyk et al., 2011a) and observed higher levels of abundance during the MERITE-HIPPOCAMPE cruise. This could be attributed to previous reports indicating that this area experiences high temperatures and a dominance of "large" phytoplankton organisms like microplankton (Ciavatta et al., 2019). For instance, in the Gulf of Gabès, unlike many parts of the eastern Mediterranean, there is no nutrient depletion in summer (Drira et al., 2010), and consistent nutrient supply throughout the year, influenced by various factors. Béjaoui et al. (2019) highlight the efficiency of remineralization and nitrogen fixation. In comparison to other Mediterranean regions, inorganic nitrogen deposition is relatively low, but phosphorus deposition falls within typical levels for the eastern Mediterranean Basin. Moreover, there is a significant atmospheric deposition of organic nitrogen and phosphorus.

Comparing diversity indices for the zooplankton community is not simple due to variations in methodologies across different studies. However, our results show a pattern emerges: areas closer to the coast tend to exhibit higher diversities compared to regions such as the Algero Provencal Basin. Overall, the rather high diversity during our study may correspond to seasonal patterns with highest values generally recorded in spring-summer (Ribera d'Alcala et al., 2004). This is especially evident when considering the low values recorded during winter or early spring in DEWEX 2017 (Donoso, 2017).

Table 5.1. Comparison of zooplankton abundance and Shannon index in different areas of the Mediterranean Sea. *Value originally in H' (log2) but transformed to H' (log ln) for comparision.

Region	Period	Net mesh size (µm)	Depth sampled (m)	Abundance (Ind.m^3)	Shannon index	Reference
NWMS - Provencal sea	April to May 2019 Spring	200	0-200	526 ± 13.8	1.9 ± 0.02 (2.8 ± 0.2*)	MERITE-HIPPOCAMPE Makhlouf Belkahia (pers. Comm. 2023)
NWMS - Provencal sea	April to May 2019 Spring	60	0-200	2915.4 ± 1674.4	-	MERITE-HIPPOCAMPE Makhlouf Belkahia (pers. Comm. 2023)
NWMS - Provencal sea	June to July 2019 Late summer	120	0-200	1464 ± 594	2.3 ± 0.43	MOOSE-GE 19
NWMS - Provencal sea	May to June 2017 Late Spring	100 -200	0-300	1638 ± 433	-	PEACETIME 2017 Feliú (2020)
NWMS - Provencal sea	july 2014 Summer	120	0-200	2676.5 ± 795.5	-	MOOSE-GE 14 Donoso (2017)
NWMS - Provencal sea	July 1999 Summer	200	0-300	338	-	Siokou et al. (2019)
NWMS - Provencal sea	Spring 2008	200	0-200	1731	-	Mazzocchi et al. (2014)
NWMS - Provencal sea	Aug to Sept 2017 Late summer	120	0-200	1004 ± 396	2.3 ± 0.2	MOOSE-GE 17 Feliú (2020)
NWMS - Ligurian Sea	June to July 2019 Late summer	120	0-200	2458.1 ± 2105.2	2.3 ± 0.3	MOOSE-GE 19
NWMS - Ligurian Sea	Aug to Sept 2017 Late summer	120	0-200	1061.4 ± 195.8	2.2 ± 0.3	MOOSE-GE 17 Feliú (2020)
NWMS - Ligurian Sea	july 2014 Summer	120	0-200	1141	-	MOOSE-GE 14 Donoso (2017)
NWMS - Provencal and Ligurian Seas	February 2013 Leg 1 Winter	120	0-250	608 (21 to 2548)	1.5 ± 0.5	DEWEX 2013 Donoso et al. (2017)
NWMS - Provencal and Ligurian Seas	April 2013 Leg2 spring	120	0-250	3668 (850 to 7205)	1.2 ± 0.4	DEWEX 2013 Donoso et al. (2017)
NWMS - Gulf of Lions	June to July 2019 Late summer	120	0-200	2613.8 ± 1195.9	2.3 ± 0.41	MOOSE-GE 19
NWMS - Gulf of Lions	April to May 2019 Spring	200	0-200	1443.5 ± 285.4	1.9 ± 0.05 (2.8 ± 0.5*)	MERITE-HIPPOCAMPE Makhlouf Belkahia (pers. Comm. 2023)
NWMS - Gulf of Lions	April to May 2019 Spring	60	0-200	7223.3 ± 3294.9	-	MERITE-HIPPOCAMPE Makhlouf Belkahia (pers. Comm. 2023)
NWMS - Gulf of Lions	Aug to Sept 2017 Late summer	120	0-200	1224.8 ± 995.1	2.56 ± 0.1	MOOSE-GE 17 Feliú (2020)
NWMS - Gulf of Lions	july 2014 Summer	120	0-200	2410	-	MOOSE-GE 14 Donoso (2017)
SWMS- Algero Provencal sea	April to May 2019 Spring	200	0-200	505.3	1.56 (2.256*)	MERITE-HIPPOCAMPE Makhlouf Belkahia (pers. Comm. 2023)
SWMS- Algero Provencal sea	April to May 2019 Spring	60	0-200	2520.4	-	MERITE-HIPPOCAMPE Makhlouf Belkahia (pers. Comm. 2023)
SWMS- Algero Provencal sea	May to June 2017 Late Spring	100 -200	0-300	1254 ± 191	-	PEACETIME 2017 Feliú (2020)
SWMS- Algero Provencal sea	July 1999 Summer	200	0-300	197	-	Siokou et al. (2019)
SWMS- Algero Provencal sea	June to July 2008 Summer	200	0-200	1561 ± 205	-	Nowaczyk et al.(2011)
Sicily Channel	June to July 2008 Summer	200	0-200	1407 ± 687	-	Nowaczyk et al.(2011)
Sicily Channel	Spring 2008	200	0-200	7065	-	Mazzocchi et al. (2014)
Tunisian Eastern Margin	April to May 2019 Spring	200	0-200	968.3 ± 547.9	2.7 ± 0.03 (3.9 ± 0.7*)	MERITE-HIPPOCAMPE Makhlouf Belkahia (pers. Comm. 2023)
Tunisian Eastern Margin	April to May 2019 Spring	60	0-200	3905.3 ± 2988.5	-	MERITE-HIPPOCAMPE Makhlouf Belkahia (pers. Comm. 2023)

5.1.2. Functional importance of zooplankton across the Western Mediterranean Sea in terms of biomasses and fluxes

Our results show that, for the western basin, there is a noticeable decline in zooplankton biomass from north-to-south gradient, which aligns with other studies (Table 5.2). Zooplankton biomass variations are correlated with primary production levels and food quality (Gaudy et al., 2003). High biomass values were noted along the Tunisian Eastern margin, which can be attributed to the elevated nutrient availability in this area, as previously explained. During the spring, a significant top-down influence of zooplankton on primary production was observed. This influence exhibited an increasing trend from the north to the south, with the Algero Provencal Sea and Tunisian Eastern Margin displaying the highest impacts (30% and 27.8%, respectively). These values generally exceeded the averages reported by other authors for the same season. In fact, our result shed light on the importance of small fractions, the smaller fraction (<500 μm) tends to make a highly predominant contribution to the grazing. Zooplankton prey preference plays a crucial role in regulating phytoplankton populations, exerting a strong top-down control on their abundance. On average, copepods (majority small) exhibited significantly higher contributions in abundance and biomass (refer Chapter 3 and 4).

In contrast, during summer, grazing impact values were very similar to those reported for MOOSE-GE 17 in the Ligurian Sea and the Gulf of Lion, but slightly lower for the Provencal Sea (refer to Table 5.2). The grazing impact remained relatively low throughout the survey. This stability could be attributed to a time lag between phytoplankton production and zooplankton development, potentially masking potential relationships between zooplankton size-structure and their impact on phytoplankton (Siokou-Frangou et al., 2010a). In summer, the regions of the Ligurian Sea and the Gulf of Lion exhibit high levels of biomass, mainly due to the abundant presence of crustaceans, gelatinous and diverse organisms, particularly pteropods. Furthermore, in general small copepods show a significant contribution on biomass, especially in the fractions between 200-500 μm. Additionally, the presence of nauplii and small miscellaneous organisms is noted in the smallest fraction (<200 μm).

Another key insight provided by our study pertains to how the MERITE-HIPPOCAMPE expedition offered a unique characterization of zooplankton in the CML (refer to Chapter 3). This direct assessment of biomass and grazing at this specific depth provided novel insights, distinguishing it from previous investigations in the Mediterranean Sea. Notable distinctions in zooplankton characteristics were observed in this layer, setting it apart from the broader water column. These distinctions encompassed the limited presence of gelatinous filter-feeding herbivores, potentially influenced by less favorable trophic conditions marked by a high detritus content. Moreover, there was a conspicuously high

biomass of crustaceans, primarily comprising euphausiid larvae, indicating an adaptation in their vertical migration patterns to optimize more favorable trophic conditions.

Table 5.2. Comparison of zooplankton biomass and grazing impact in different areas of the Mediterranean Sea.

Region	Period	Net mesh size (µm)	Depth sampled (m)	Biomass (mgDW/m^3)	Grazing impact (%)	Reference
NWMS - Provencal sea	April to May 2019 Spring	200	0-200	7.1 ±1.3	-	MERITE-HIPPOCAMPE Fierro-González et al. (2023)
NWMS - Provencal sea	April to May 2019 Spring	60	0-200	6.4 ±0.1	27 ± 31.04	MERITE-HIPPOCAMPE Fierro-González et al. (2023)
NWMS - Provencal sea	June to July 2019 Late summer	120	0-200	4.9 ± 2.7	5.2 ± 2.6	MOOSE-GE 19
NWMS - Provencal sea	May to June 2017 Late Spring	100 -200	0-300	5.5 ± 2.1	12.8 ± 4.6	PEACETIME 2017 Feliú (2020)
NWMS - Provencal sea	Spring 2008	200	0-200	13.15 ± 2.5	-	Mazzocchi et al. (2014)
NWMS - Provencal sea	Aug to Sept 2017 Late summer	120	0-200	4.3 ±0.6	9.4 ± 4.1	MOOSE-GE 17 Feliú (2020)
NWMS - Ligurian Sea	June to July 2019 Late summer	120	0-200	7.5 ± 4.4	9 ± 5.4	MOOSE-GE 19
NWMS - Ligurian Sea	Aug to Sept 2017 Late summer	120	0-200	4.7 ± 0.9	9.7 ± 3.5	MOOSE-GE 17 Feliú (2020)
NWMS - Provencal and Ligurian Seas	February 2013 Leg 1 Winter	120	0-250	12.3 (1.9 to 42.3)	7 ± 6	DEWEX 2013 Donoso et al. (2017)
NWMS - Provencal and Ligurian Seas	April 2013 Leg2 spring	120	0-250	64.5 (13.9 to 197.8)	42 ± 39	DEWEX 2013 Donoso et al. (2017)
NWMS - Gulf of Lions	June to July 2019 Late summer	120	0-200	6.7 ± 1.4	7.9 ± 1.8	MOOSE-GE 19
NWMS - Gulf of Lions	April to May 2019 Spring	200	0-200	30 ± 18.2	-	MERITE-HIPPOCAMPE Fierro-González et al. (2023)
NWMS - Gulf of Lions	April to May 2019 Spring	60	0-200	23.7 ± 12.8	8.8 ± 4.1	MERITE-HIPPOCAMPE Fierro-González et al. (2023)
NWMS - Gulf of Lions	Aug to Sept 2017 Late summer	120	0-200	6.9 ± 4.1	9.5 ± 5.6	MOOSE-GE 17 Feliú (2020)
NWMS - Gulf of Lions	January 1999	80-200	0-200	4.73 ± 2.53	3.6 to 83.1	Gaudy et al. (2003)
NWMS - Gulf of Lions	Mar to Apr 1998	80-200	0-200	9.56 ± 4.73	5.3 to 69	Gaudy et al. (2003)
SWMS- Algero Provencal sea	April to May 2019 Spring	200	0-200	5.9	-	MERITE-HIPPOCAMPE Fierro-González et al. (2023)
SWMS- Algero Provencal sea	April to May 2019 Spring	200	0-200	5.8	30.0	MERITE-HIPPOCAMPE Fierro-González et al. (2023)
SWMS- Algero Provencal sea	May to June 2017 Late Spring	100 -200	0-300	6.6 ± 0.6	17 ± 2.5	PEACETIME 2017 Feliú (2020)
SWMS- Algero Provencal sea	June to July 2008 Summer	200	0-200	5.4	-	Nowaczyk et al. (2011)
Sicily Channel	June to July 2008 Summer	200	0-200	6.6	-	Nowaczyk et al. (2011)
Sicily Channel	Spring 2008	200	0-200	2.2 ± 0.5	-	Mazzocchi et al. (2014)
Tunisian Eastern Margin	April to May 2019 Spring	200	0-200	20.1 ± 13.1	-	MERITE-HIPPOCAMPE Fierro-González et al. (2023)
Tunisian Eastern Margin	April to May 2019 Spring	60	0-200	6.5 ± 3.7	26.79 ± 18.3	MERITE-HIPPOCAMPE Fierro-González et al. (2023)

Armengol et al. (2019) emphasize the significance of comprehending the rate processes between producers and consumers, as well as understanding their biomass and community structure, in order to effectively model the ocean's carbon cycle. The correlation between zooplankton biomass and phytoplankton biomass, along with trophic transfer efficiency, offers valuable insights into ecosystem structure and functioning. Our findings indicate a generally strong relationship between food transfer at successive trophic levels (see Table 5.3), suggesting an effective overall transfer process. This suggests a well-aligned adaptation to the environment. Additionally, these environmental factors (Temperature, salinity, oxygen, fluorescence and MLD) also played a role in shaping species distribution and size structure within the community. Moreover, the type and size of available food resources likely influenced the presence of both smaller and larger species, as noted by Nowaczyk et al. (2011).

Table 5.3. Phytoplankton stock in C, zooplankton stock in C and Zooplankton/Phytoplankton ratio, in different areas of the Mediterranean Sea during MOOSE-GE 19 cruise. . LS= Ligurian Sea, GLSB= Gulf of Lion Shelf Break, CPB= Central Provencal Basin, and SPB= Southern Provencal Basin.

Region	Leg	Station	Phytoplankton stock (mg C/ m^2)	Zooplankton stock in C (mg C/m^2)	Zooplankton/Phytoplankton ratio (%)
GLSB	1	st02	2017.9	615.8	30.0
	2	st01	1836.9	791.0	42.1
	2	st32_b	2460.0	576.8	23.0
	2	st38	2348.4	508.1	21.5
	2	st60	1729.2	417.0	22.4
	2	st67	1973.0	683.0	34.1
LS	1	st26	1993.8	1213.7	60.9
	1	st32	1402.4	321.4	18.3
	1	st41	1797.0	422.8	23.1
CPB	1	st14	1795.2	482.8	26.5
	1	st22	2031.4	249.6	12.1
	1	st44	1597.5	403.5	25.1
SPB	2	st04	1453.6	284.5	14.0
	2	st09	1657.8	270.6	14.8
	2	st11	1308.0	227.9	11.5
	2	st15	1376.9	224.9	12.0
	2	st21	1732.7	843.4	41.1
	2	st45	1624.4	549.4	27.4

5.2. How our results on environment and zooplankton can characterize different regions in the western Mediterranean Sea?

5.2.1. Grouped data analyses of the two campaigns

A multivariate analysis on grouped dataset of the two campaigns is presented on Figure 5.2 with: on one hand a PCA on environmental variables including temperature, salinity, oxygen levels, chlorophyll concentration, and the depth of the mixing layer (MLD). And on the other hand, a NMDS on the relative abundances of zooplankton taxa, encompassing copepods, chaetognaths, appendicularians, other gelatinous – salps and hydrozoans -, other crustaceans – euphausiids, amphipods, ostracods, crustacean larvae -, other miscellaneous organisms – pteropods, echinoderms, other meroplanktonic larvae.

On the PCA of environmental variables, the first factorial plane explained 73% of the variance (of which 51% for the first axis). On this plane, the northern stations of both campaigns (MOOSE-GE 19 stations + stations H-1 to H-10) were rather grouped (in a same range of temperature and Chl-*a* content), with the exception of station H-9 of MERITE-HIPPOCAMPE due to a deep MLD (and then lower temperature and higher Chl-*a* values). Nevertheless, the PCA shows a rather compact cluster of the SPB (light blue squares), to which station M-44 (Coast of Corsica) and station M-32 (north of Corsica) and station M-41 (coastal Liguria) aggregate, representing an hydrodynamical continuum. Another cluster can be differentiated with stations in the Gulf of Lions (*lato sensu*) both on the shelf break (GLSB, green triangles) and in the near open sea (CPB blue triangle), either in or near the deep convection area, characterized by slightly lower temperature and higher Chl-*a*. Except station H-4 (bay of Marseille), the northern coastal stations of MERITE-HIPPOCAMPE (stations H-1, H-2 and H-3) also belong to this cluster.

In the NMDS of zooplankton, the northern stations (MOOSE-GE 19 stations + stations H-1 to H-10) were more spread out than in the PCA on environmental variables. It shows a clear singularization of the stations of LS and CPB (except station H-9 of MERITE-HIPPOCAMPE) as well as station 38 of MOOSE-GE 19 which are distinguished from the southern stations by a much higher contribution of copepods in the zooplankton community. All other northern stations are more balanced in terms of contributions of copepods and of miscellaneous organisms, but their distribution on the factorial plane depends on the contributions of other groups (chaetognaths gelatinous, appendicularians and crustacea).

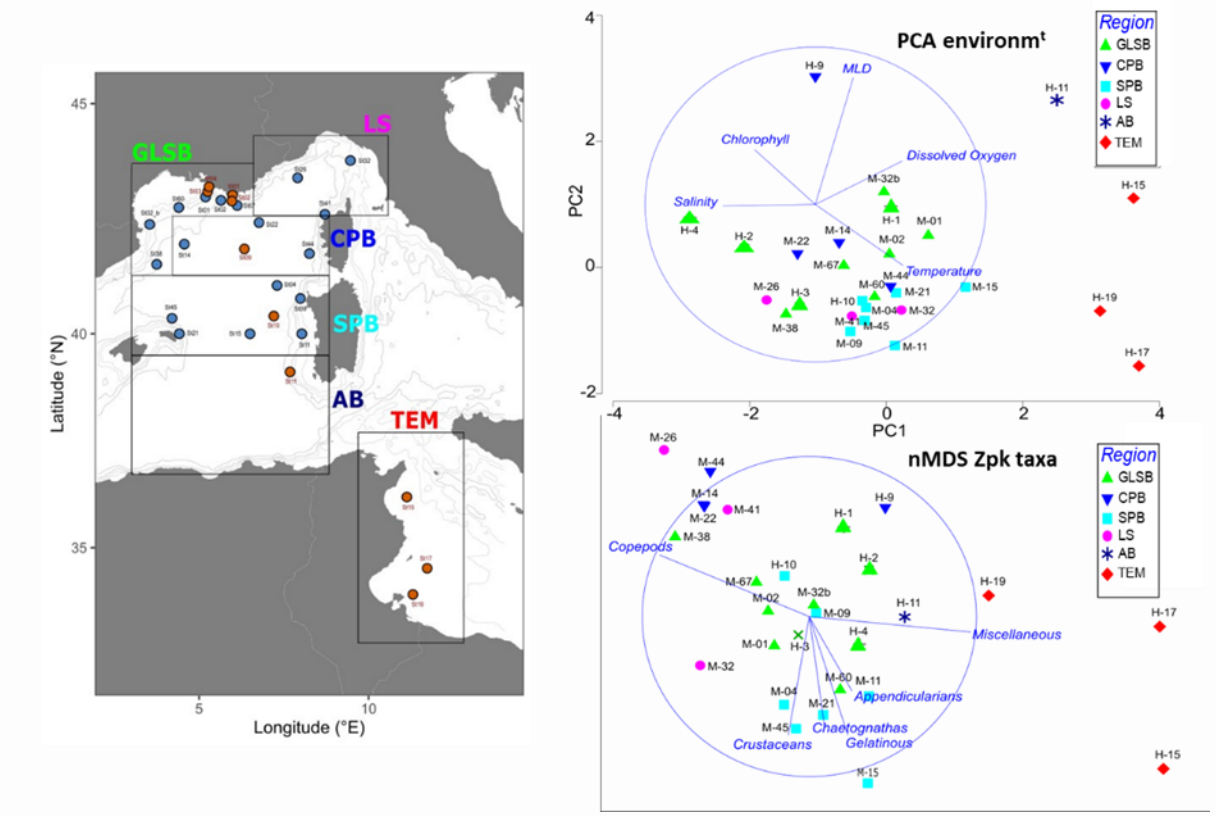


Figure 5.2. Joint analyses of environmental and zooplankton variables for Hippocame and MOOSE-GE 2019. Left panel: Map showing the sampling stations of the MERITE-HIPPOCAMPE (red) and the MOOSE-GE 19 (blue) campaigns. Meaning of acronyms for the regions: LS= Ligurian Sea in pink, GLSB= Gulf of Lion Shelf Break in green, CPB= Central Provencal Basin in blue, SPB= Southern Provencal Basin in ligthblue , AB= Algerian Basin in black, and TEM= Tunisian Eastern Margin in red. Right top panel: PCA on environmental variables. Right bottom panel: NMDS on the relative abundances of zooplankton groups.

In both analyses, the stations of the Tunisian margin (stations H-15, H-17 and H-19 of MERITE-HIPPOCAMPE, in red diamonds) formed a cluster distinguishable from all the other stations, and the sole station sampled in the Algerian basin (station H-11 of MERITE-HIPPOCAMPE) was rather close to this “southern” cluster characterized by lower salinity and higher chlorophyll, and lower contribution of copepods, mostly compensated by miscellaneous organisms.

5.2.2. How the results fit with proposed models of regionalization?

Our study does not allow to clearly discriminate between regions due to the lack of sampling points, especially in the South. However, when examining the proposed ecoregions from the literature, we could point out some adequacies with the spatial patterns highlighted in our analyses for environmental variables and zooplankton community (Figure 5.3).

Among the different regionalization models discussed by Ayata et al. (2018), we keep 3 of them for comparative discussion: 1) The model by Reygondeau et al. (2014) that used ecological niche modeling to project the potential distribution of a diverse range of marine species spanning various trophic levels. 2) The model proposed by Berline et al. (2014) based on hydrodynamic connectivity. 3) The model of Mayot et al. (2017), extending the one by D'Ortenzio and Ribera d'Alcalà (2009), based on seasonal changes in surface chlorophyll concentration and their interannual variability.

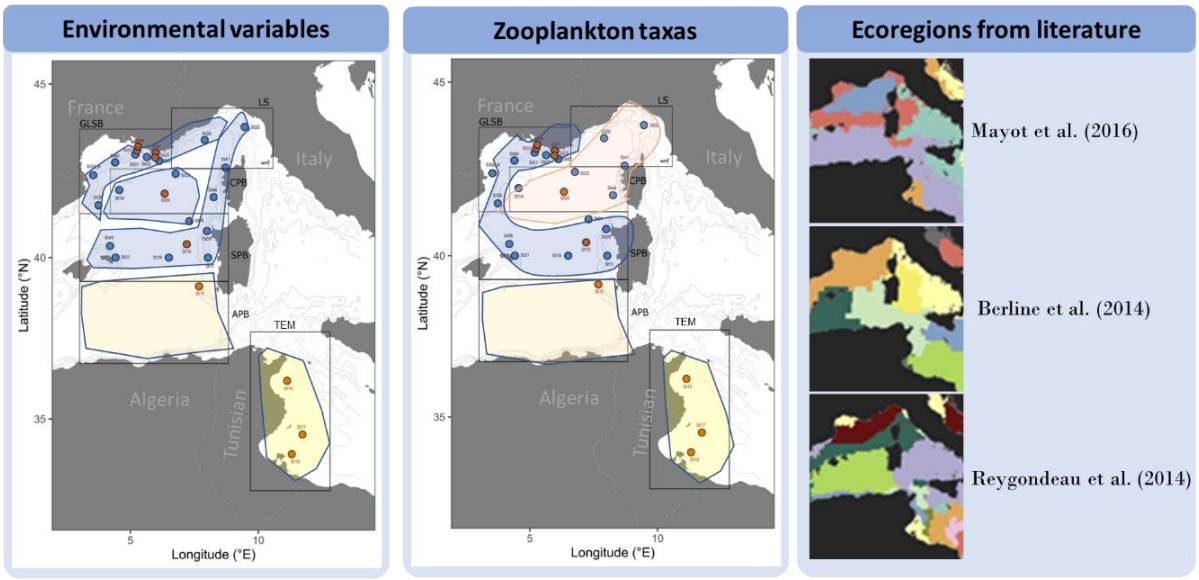


Figure 5.3. Tentative synthesis of our multivariate analysis of environmental variables (Left panel) and zooplankton taxas (Central panel), in regards with proposed ecoregions (Right panels) from Mayot et al., 2017 (top), Berline et al., 2014 (Middle), Reygondeau et al., 2014 (Bottom).

In our analyses, the pattern revealed by both approaches (environment and zooplankton) is a clear north-south separation at the level of the Balearic - South Sardinia line (around latitude 39°N) which corresponds to the southern rim of the extension of the Balearic front.

The three TEM stations and the AB station are relatively similar both in terms of zooplankton communities and of environmental variables, possibly owing to an effect of the circulation of Atlantic waters with a branch bifurcating northward before the Sicili-Tunisian channel, and another one going southwards along the Tunisian margin (see figure 1.2). From this point of view, this grouping is consistent with the proposed model by Berline et al. (2014). The innermost part of the region of the Gulf of Gabès appears distinct from the rest of the Tunisian margin in the 3 selected models. This trait does not emerge from our analyses perhaps due to the limited sampling (only 3 stations during MERITE-HIPPOCAMPE H-15, H-17, H-19). However, the analysis of climatic and anthropogenic pressures by Reygondeau et al. (2014) (Figure 1.12) presents the entire TEM as a homogeneously impacted region.

The identification of clusters was more challenging in the entire northern region, specifically north of the Balearic front (GLSB, PB, and LS), as illustrated by our classification results showing slight variations based on environmental or zooplankton criteria. Our two analyses reveal a deep-sea central zone in the Provencal basin that corresponds to the zone of influence of deep convection, however more spread towards the Ligurian Sea from zooplankton data analysis. This pattern agrees with the model of Mayot et al. (2017) (region in blue) but is also very close to those of Reygondeau et al. (2014) (region in brown) and Berline et al. (2014) (region in orange). Around this central zone, the environmental variables seem to firstly group the stations to the south and to the east in a region corresponding to the southern branch of the NWM Gyre, comprising the Balearic front and the Atlantic branch along Corsica. Secondly, another group of stations in the north and west stand out of the central region and seems to be under the common influence of the northern branch of the NWM gyre, starting from the Ligurian Sea, probably linked to the North Ligurian current, and continuing along the continental shelf of the Gulf of Lions, and down to the Catalan-Balearic area.

Concerning the zooplankton, the central zone, which corresponds to the deep convection area, is dominated by copepods, probably with an herbivorous diet, whereas the zone around corresponds to more mature communities with varied diets, and in particular carnivorous zooplankton groups (chaetognaths, hydrozoans).

5.3. Concluding remarks and perspectives

Our results demonstrate that the use of imaging tools in conjunction with classical taxonomy proves to be an invaluable approach to understanding and discerning patterns within the size structure of the zooplankton community.

On other hand, our study suggests that zooplankton, could be taken into account in finer regionalization analyses, even with a broad taxonomic resolution, but which would make it possible to define maturity indexes (*e.g*. p1/p2 ratio) for the zooplankton community as a criterion for distinguishing regions within the Mediterranean.

In addition to hydrological criteria and chlorophyll content, which are essential for defining fine regionalization, zooplankton footprints represent a more permanent marker of hydrodynamic phenomena, such as deep convection. Indeed, spatial variations in a zooplankton community are closely linked to physical phenomena that are themselves at the root of phytoplankton production, leading to an ecological succession of zooplanktonic trophic groups whose dynamics extend from one season to the next.

However, there are still many unanswered questions regarding ecoregionalization patterns. This would require optimized zooplankton observation strategies, sufficiently effective but feasible over time, to better discriminate regional zooplankton communities from north to south. Trans-Mediterranean sampling such as with a CPR (Continuous Plankton Recorder), which has already proved its worth in the North Atlantic, could be one solution, or drifting buoys instrumented with cameras or acoustics dedicated to zooplankton.

The results of the MERITE-HIPPOCAMPE programme (https://www.sciencedirect.com/journal/marine-pollution-bulletin/special-issue/10B0SXC3XR2) have demonstrated the role of zooplankton as a vector for contaminants in food webs emphasizing its importance and its specificities at the level of the CML, which have been little considered until now. Our proposal for a detailed regionalization, including zooplankton community (from the combination of imaging tools and classical taxonomic identification), would be all the more relevant given that the natural (*e.g*. climatic, river inputs, atmospheric deposition, etc.) and anthropogenic (*e.g*., industry, fisheries, tourism, etc.) pressures exerted on the Mediterranean Sea are also distributed very unevenly from one region to another (Reygondeau et al., 2014).

References

Adloff, F., Somot, S., Sevault, F., Jordà, G., Aznar, R., Déqué, M., Herrmann, M., Marcos, M., Dubois, C., Padorno, E., Alvarez-Fanjul, E., Gomis, D., 2015. Mediterranean Sea response to climate change in an ensemble of twenty first century scenarios. Clim. Dyn. 45, 2775–2802. https://doi.org/10.1007/s00382-015-2507-3

Anderson, M.J., Gorley, R.N. & Clarke, K.R., 2008. PERMANOVA+ for PRIMER: Guide to Software and Statistical Methods. PRIMER-E: Plymouth, UK.

Alcaraz, M., 1985. Vertical distribution of zooplankton biomass during summer stratification in the Western Mediterranean. In: Gibbs, P.E. (Ed.), Proceedings of the 19th European Marine Biology Symposium. Cambridge University Press, Cambridge, Plymouth, Devon, pp. 135–143.

Alcaraz, M., 1988. Summer zooplankton metabolism and its relations to primary production in the Western Mediterranean, edited by: Minas, J. H. and Nival, P., Océanographie pélagique méditerranéenne, Oceanol. Acta SP 9, 185–191.

Alcaraz, M., Calbet, A., 2003. Zooplankton Ecology., In Encyclopedia of Life Support Systems (EOLSS), Chapter: Marine Ecology, Publisher: UNESCO, 16 p.Alcaraz, M., Calbet, A., Estrada, M., Marrasé, C., Saiz, E., Trepat, I., 2007. Physical control of zooplankton communities in the Catalan Sea. Prog. Oceanogr., Ecological Functioning of the Iberian Seas: A synthesis of GLOBEC Research in Spain and Portugal 74, 294–312. https://doi.org/10.1016/j.pocean.2007.04.003

Alcaraz, M., Calbet, A., Estrada, M., Marras, C., Saiz, E., Trepat, I., 2007. Physical control902 of zooplankton communities in the Catalan Sea. Prog. Oceanogr. 74 (2–3), 294–312. https://doi.org/10.1016/j.pocean.2007.04.003.

Alekseenko, E., Thouvenin, B., Tronczyński, J., Carlotti, F., Garreau, P., Tixier, C., Baklouti, M., 2018. Modeling of PCB trophic transfer in the Gulf of Lions; 3D coupled model application. Mar. Pollut. Bull. 128, 140–155. https://doi.org/10.1016/j.marpolbul.2018.01.008

Almeda, R., Alcaraz, M., Calbet, A., Saiz, E., 2011. Metabolic rates and carbon budget of early developmental stages of the marine cyclopoid copepod *Oithona davisae*. Limnol. Oceanogr. 56, 403–414. https://doi.org/10.4319/lo.2011.56.1.0403

Álvarez, E., López-Urrutia, Á., Nogueira, E., 2012. Improvement of plankton biovolume estimates derived from image-based automatic sampling devices: application to FlowCAM. J. Plankton Res. 34, 454–469. https://doi.org/10.1093/plankt/fbs017

Alldredge, A.L., Silver, M.W., 1988. Characteristics, dynamics and significance of marine snow. Prog. Oceanogr. 20, 41–82. https://doi.org/10.1016/0079-6611(88)90053-5

Alldredge, A., 1998. The carbon, nitrogen and mass content of marine snow as a function of aggregate size. Deep Sea Res. Part Oceanogr. Res. Pap. 45, 529–541. https://doi.org/10.1016/S0967-0637(97)00048-4

Anderson, M.J., Gorley, R.N., Clarke, K.R., 2008. Guide to Software and Statistical Methods 218.

Adloff, F., Somot, S., Sevault, F., Jordà, G., Aznar, R., Déqué, M., Herrmann, M., Marcos, M., Dubois, C., Padorno, E., Alvarez-Fanjul, E., Gomis, D., 2015. Mediterranean Sea

response to climate change in an ensemble of twenty first century scenarios. Clim. Dyn. 45, 2775–2802. https://doi.org/10.1007/s00382-015-2507-3
Alcaraz, M., Calbet, A., Estrada, M., Marrasé, C., Saiz, E., Trepat, I., 2007. Physical control of zooplankton communities in the Catalan Sea. Prog. Oceanogr., Ecological Functioning of the Iberian Seas: A synthesis of GLOBEC Research in Spain and Portugal 74, 294–312. https://doi.org/10.1016/j.pocean.2007.04.003
Alekseenko, E., Thouvenin, B., Tronczyński, J., Carlotti, F., Garreau, P., Tixier, C., Baklouti, M., 2018. Modeling of PCB trophic transfer in the Gulf of Lions; 3D coupled model application. Mar. Pollut. Bull. 128, 140–155. https://doi.org/10.1016/j.marpolbul.2018.01.008
Alldredge, A., 1998a. The carbon, nitrogen and mass content of marine snow as a function of aggregate size. Deep Sea Res. Part Oceanogr. Res. Pap. 45, 529–541. https://doi.org/10.1016/S0967-0637(97)00048-4
Alldredge, A., 1998b. The carbon, nitrogen and mass content of marine snow as a function of aggregate size. Deep Sea Res. Part Oceanogr. Res. Pap. 45, 529–541. https://doi.org/10.1016/S0967-0637(97)00048-4
Alldredge, A.L., Silver, M.W., 1988. Characteristics, dynamics and significance of marine snow. Prog. Oceanogr. 20, 41–82. https://doi.org/10.1016/0079-6611(88)90053-5
Almeda, R., Alcaraz, M., Calbet, A., Saiz, E., 2011. Metabolic rates and carbon budget of early developmental stages of the marine cyclopoid copepod Oithona davisae. Limnol. Oceanogr. 56, 403–414. https://doi.org/10.4319/lo.2011.56.1.0403
Álvarez, E., López-Urrutia, Á., Nogueira, E., 2012. Improvement of plankton biovolume estimates derived from image-based automatic sampling devices: application to FlowCAM. J. Plankton Res. 34, 454–469. https://doi.org/10.1093/plankt/fbs017
Anderson, M.J., Gorley, R.N., Clarke, K.R., 2008. Guide to Software and Statistical Methods 218.
Aravena, G., Palma, S., 2002. Identificación taxonómica de las apendicularias capturadas en aguas epipelágicas de la zona norte de Chile (Tunicata, Appendicularia). Rev. Chil. Hist. Nat. 75, 307–325. https://doi.org/10.4067/S0716-078X2002000200005
Ariza, A., Garijo, J.C., Landeira, J., Bordes, F., Hernandez-Leon, S., 2015. Migrant biomass and respiratory carbon flux by zooplankton and micronekton in the subtropical northeast Atlantic Ocean (Canary Islands). Prog. Oceanogr. 134. https://doi.org/10.1016/j.pocean.2015.03.003
Armengol, L., Calbet, A., Franchy, G., Rodríguez-Santos, A., Hernández-León, S., 2019. Planktonic food web structure and trophic transfer efficiency along a productivity gradient in the tropical and subtropical Atlantic Ocean. Sci. Rep. 9, 2044. https://doi.org/10.1038/s41598-019-38507-9
Atkinson, A., 1996. Subantarctic copepods in an oceanic, low chlorophyll environment:ciliate predation, food selectivity and impact on prey populations. Mar. Ecol. Prog. Ser. 130, 85–96. https://doi.org/10.3354/meps130085
Aurelle, D., Thomas, S., Albert, C., Bally, M., Bondeau, A., Boudouresque, C., Cahill, A.E., Carlotti, F., Chenuil, A., Cramer, W., Davi, H., De Jode, A., Ereskovsky, A., Farnet, A., Fernandez, C., Gauquelin, T., Mirleau, P., Monnet, A., Prévosto, B., Rossi, V., Sartoretto, S., Van Wambeke, F., Fady, B., 2022. Biodiversity, climate change, and adaptation in the Mediterranean. Ecosphere 13, e3915. https://doi.org/10.1002/ecs2.3915

Ayata, S.-D., Irisson, J.-O., Aubert, A., Berline, L., Dutay, J.-C., Mayot, N., Nieblas, A.-E., D'Ortenzio, F., Palmiéri, J., Reygondeau, G., Rossi, V., Guieu, C., 2018. Regionalisation of the Mediterranean basin, a MERMEX synthesis. Prog. Oceanogr. 163, 7–20. https://doi.org/10.1016/j.pocean.2017.09.016

Azam, F., Long, R.A., 2001. Sea snow microcosms. Nature 414, 495–498. https://doi.org/10.1038/35107174

Bachiller, E., Irigoien, X., 2013. Allometric relations and consequences for feeding in small pelagic fish in the Bay of Biscay. ICES J. Mar. Sci. 70, 232–243. https://doi.org/10.1093/icesjms/fss171

Bacosa, H.P., Kamalanathan, M., Cullen, J., Shi, D., Xu, C., Schwehr, K.A., Hala, D., Wade, T.L., Knap, A.H., Santschi, P.H., Quigg, A., 2020. Marine Snow Aggregates are Enriched in Polycyclic Aromatic Hydrocarbons (PAHs) in Oil Contaminated Waters: Insights from a Mesocosm Study. J. Mar. Sci. Eng. 8, 781. https://doi.org/10.3390/jmse8100781

Balzan, M., El, A., Hassoun, A.E.R., Aroua, N., Baldy, V., Bou Dagher Kharrat, M., Branquinho, C., Dutay, J.-C., Bour, M., Médail, F., Mojtahid, M., Morán-Ordóñez, A., Roggero, P.P., Rossi, S., 2020. Climate and Environmental Change in the Mediterranean Basin - Current Situation and Risks for the Future Chapter 4 Ecosystems.

Bănaru, D., Mellon-Duval, C., Roos, D., Bigot, J.-L., Souplet, A., Jadaud, A., Beaubrun, P., Fromentin, J.-M., 2013. Trophic structure in the Gulf of Lions marine ecosystem (north-western Mediterranean Sea) and fishing impacts. J. Mar. Syst. 111–112, 45–68. https://doi.org/10.1016/j.jmarsys.2012.09.010

Battuello, M., Brizio, P., Mussat Sartor, R., Nurra, N., Pessani, D., Abete, M.C., Squadrone, S., 2016. Zooplankton from a North Western Mediterranean area as a model of metal transfer in a marine environment. Ecol. Indic. 66, 440–451. https://doi.org/10.1016/j.ecolind.2016.02.018

Béjaoui, B., Ben Ismail, S., Othmani, A., Ben Abdallah-Ben Hadj Hamida, O., Chevalier, C., Feki-Sahnoun, W., Harzallah, A., Ben Hadj Hamida, N., Bouaziz, R., Dahech, S., Diaz, F., Tounsi, K., Sammari, C., Pagano, M., Bel Hassen, M., 2019a. Synthesis review of the Gulf of Gabes (eastern Mediterranean Sea, Tunisia): Morphological, climatic, physical oceanographic, biogeochemical and fisheries features. Estuar. Coast. Shelf Sci. 219, 395–408. https://doi.org/10.1016/j.ecss.2019.01.006

Béjaoui, B., Ben Ismail, S., Othmani, A., Ben Abdallah-Ben Hadj Hamida, O., Chevalier, C., Feki-Sahnoun, W., Harzallah, A., Ben Hadj Hamida, N., Bouaziz, R., Dahech, S., Diaz, F., Tounsi, K., Sammari, C., Pagano, M., Bel Hassen, M., 2019b. Synthesis review of the Gulf of Gabes (eastern Mediterranean Sea, Tunisia): Morphological, climatic, physical oceanographic, biogeochemical and fisheries features. Estuar. Coast. Shelf Sci. 219, 395–408. https://doi.org/10.1016/j.ecss.2019.01.006

Bell, J.L., Hopcroft, R.R., 2008. Assessment of ZooImage as a tool for the classification of zooplankton. J. Plankton Res. 30, 1351–1367. https://doi.org/10.1093/plankt/fbn092

Benfield, M., Grosjean, P., Culverhouse, P., Irigolen, X., Sieracki, M., Lopez-Urrutia, A., Dam, H., Hu, Q., Davis, C., Hanson, A., Pilskaln, C., Riseman, E., Schulz, H., Utgoff, P., Gorsky, G., 2007. RAPID: Research on Automated Plankton Identification. Oceanography 20, 172–187. https://doi.org/10.5670/oceanog.2007.63

Berline, L., Rammou, A.-M., Doglioli, A., Molcard, A., Petrenko, A., 2014. A Connectivity-Based Eco-Regionalization Method of the Mediterranean Sea. PLOS ONE 9, e111978. https://doi.org/10.1371/journal.pone.0111978

Bhat, K.L., Sreepada, R.A., Ansari, Z.A., n.d. Biochemical composition of zooplankton from the northern Arabian Sea.

Bianchi, C.N., Morri, C., 2000. Marine Biodiversity of the Mediterranean Sea: Situation, Problems and Prospects for Future Research. Mar. Pollut. Bull. 40, 367–376. https://doi.org/10.1016/S0025-326X(00)00027-8

Bonnet, D., Richardson, A., Harris, R., Hirst, A., Beaugrand, G., Edwards, M., Ceballos, S., Diekman, R., López-Urrutia, A., Valdes, L., Carlotti, F., Molinero, J.C., Weikert, H., Greve, W., Lucic, D., Albaina, A., Yahia, N.D., Umani, S.F., Miranda, A., Santos, A. dos, Cook, K., Robinson, S., Fernandez de Puelles, M.L., 2005. An overview of Calanus helgolandicus ecology in European waters. Prog. Oceanogr. 65, 1–53. https://doi.org/10.1016/j.pocean.2005.02.002

Bouloubassi, I., Méjanelle, L., Pete, R., Fillaux, J., Lorre, A., Point, V., 2006. PAH transport by sinking particles in the open Mediterranean Sea: A 1 year sediment trap study. Mar. Pollut. Bull. 52, 560–571. https://doi.org/10.1016/j.marpolbul.2005.10.003

Bouquegneau, J.-M., Pillet, S., Das, K., Debacker, V., 2002. Heavy metals in marine mammals, in: Vos, J., O,ÄôShea, T., Fournier, M., Bossart, G., Bossart, G., Bossart, G. (Eds.), Toxicology of Marine Mammals, New Perspectives: Toxicology and the Environment. CRC Press. https://doi.org/10.1201/9780203165577.ch7

Briseño-Avena, C., Prairie, J.C., Franks, P.J.S., Jaffe, J.S., 2020. Comparing Vertical Distributions of Chl-a Fluorescence, Marine Snow, and Taxon-Specific Zooplankton in Relation to Density Using High-Resolution Optical Measurements. Front. Mar. Sci. 7, 602. https://doi.org/10.3389/fmars.2020.00602

Burrows, M., 2014. Geographical limits to species-range shifts are suggested by climate velocity. Nature. https://doi.org/10.1038/nature12976

Burrows, M.T., Schoeman, D.S., Buckley, L.B., Moore, P., Poloczanska, E.S., Brander, K.M., Brown, C., Bruno, J.F., Duarte, C.M., Halpern, B.S., Holding, J., Kappel, C.V., Kiessling, W., O'Connor, M.I., Pandolfi, J.M., Parmesan, C., Schwing, F.B., Sydeman, W.J., Richardson, A.J., 2011. The pace of shifting climate in marine and terrestrial ecosystems. Science 334, 652–655. https://doi.org/10.1126/science.1210288

Buskey, E., Hyatt, C., 2006. Use of the FlowCAM for semi-automated recognition and enumeration of red tide cells (Karenia brevis) in natural plankton samples. Harmful Algae 5, 685–692. https://doi.org/10.1016/j.hal.2006.02.003

Calbet, A., Alcaraz, M., Saiz, E., Estrada, M., Trepat, I., 1996. Planktonic herbivorous food webs in the catalan Sea (NW Mediterranean): temporal variability and comparison of indices of phyto-zooplankton coupling based on state variables and rate processes. J. Plankton Res. 18, 2329–2347. https://doi.org/10.1093/plankt/18.12.2329

Calbet, A., Broglio, E., Saiz, E., Alcaraz, M., 2002. Low grazing impact of mesozooplankton on the microbial communities of the Alboran Sea: a possible case of inhibitory effects by the toxic dinoflagellate Gymnodinium catenatum. Aquat. Microb. Ecol. 26, 235–246. https://doi.org/10.3354/ame026235

Calbet, A., Garrido, S., Saiz, E., Alcaraz, M., Duarte, C.M., 2001. Annual Zooplankton Succession in Coastal NW Mediterranean Waters: The Importance of the Smaller Size Fractions. J. Plankton Res. 23, 319–331. https://doi.org/10.1093/plankt/23.3.319

Capo, E., Bravo, A.G., Soerensen, A.L., Bertilsson, S., Pinhassi, J., Feng, C., Andersson, A.F., Buck, M., Björn, E., 2020. Marine snow as a habitat for microbial mercury

methylators in the Baltic Sea (preprint). Microbiology. https://doi.org/10.1101/2020.03.04.975987
Carlotti, F., Gérigny, O., Bienvenu, D., Ravel, C., Fierro-González, P., Guilloux, L., Makhlouf, N., Onrubia, J.T., Pagano, M., 2023. Microplastics in the maximum chlorophyll layer along a north-south transect in the Mediterranean Sea in comparison with zooplankton concentrations. Mar. Pollut. Bull. 196, 115614. https://doi.org/10.1016/j.marpolbul.2023.115614
Carlotti, F., Nival, S., 1991. Individual variability of development in laboratory-reared Temora stylifera copepodites: consequences for the population dynamics and interpretation in the scope of growth and development rules. J. Plankton Res. 13, 801–813. https://doi.org/10.1093/plankt/13.4.801
Carlotti, F., Poggiale, J.C., 2010. Towards methodological approaches to implement the zooplankton component in "end to end" food-web models. Prog. Oceanogr., Special Issue: Parameterisation of Trophic Interactions in Ecosystem Modelling 84, 20–38. https://doi.org/10.1016/j.pocean.2009.09.003
Carlotti, F., Thibault-Botha, D., Nowaczyk, A., Lefèvre, D., 2008. Zooplankton community structure, biomass and role in carbon fluxes during the second half of a phytoplankton bloom in the eastern sector of the Kerguelen Shelf (January–February 2005). Deep Sea Res. Part II Top. Stud. Oceanogr., KEOPS: Kerguelen Ocean and Plateau compared Study 55, 720–733. https://doi.org/10.1016/j.dsr2.2007.12.010
Castro-Jiménez, J., Bănaru, D., Chen, C.-T., Jiménez, B., Muñoz-Arnanz, J., Deviller, G., Sempéré, R., 2021. Persistent Organic Pollutants Burden, Trophic Magnification and Risk in a Pelagic Food Web from Coastal NW Mediterranean Sea. Environ. Sci. Technol. 55, 9557–9568. https://doi.org/10.1021/acs.est.1c00904
Chen, C.-T., Bănaru, D., Carlotti, F., Faucheux, M., Harmelin-Vivien, M., 2019. Seasonal variation in biochemical and energy content of size-fractionated zooplankton in the Bay of Marseille (North-Western Mediterranean Sea). J. Mar. Syst. 199, 103223. https://doi.org/10.1016/j.jmarsys.2019.103223
Chen, C.-T., Carlotti, F., Harmelin-Vivien, M., Guilloux, L., Bănaru, D., 2021. Temporal variation in prey selection by adult European sardine (*Sardina pilchardus*) in the NW Mediterranean Sea. Prog. Oceanogr. 196, 102617. https://doi.org/10.1016/j.pocean.2021.102617
Chifflet, S., Briant, N., Tesán-Onrubia, J.A., Zaaboub, N., Amri, S., Radakovitch, O., Bănaru, D., Tedetti, M., 2023. Distribution and accumulation of metals and metalloids in planktonic food webs of the Mediterranean Sea (MERITE-HIPPOCAMPE campaign). Mar. Pollut. Bull. 186, 114384. https://doi.org/10.1016/j.marpolbul.2022.114384
Chouvelon, T., Strady, E., Harmelin-Vivien, M., Radakovitch, O., Brach-Papa, C., Crochet, S., Knoery, J., Rozuel, E., Thomas, B., Tronczynski, J., Chiffoleau, J.-F., 2019. Patterns of trace metal bioaccumulation and trophic transfer in a phytoplankton-zooplankton-small pelagic fish marine food web. Mar. Pollut. Bull. 146, 1013–1030. https://doi.org/10.1016/j.marpolbul.2019.07.047
Christaki, U., Gaudy, R., Kerambrun, P., 1998. A study of the effects of migratory zooplankton on microbial populations in surface waters of the N.W. Mediterranean. J. Exp. Mar. Biol. Ecol. 225, 173–183. https://doi.org/10.1016/S0022-0981(97)00219-0
Ciavatta, S., Kay, S., Brewin, R.J.W., Cox, R., Di Cicco, A., Nencioli, F., Polimene, L., Sammartino, M., Santoleri, R., Skákala, J., Tsapakis, M., 2019. Ecoregions in the

Mediterranean Sea Through the Reanalysis of Phytoplankton Functional Types and Carbon Fluxes. J. Geophys. Res. Oceans 124, 6737–6759. https://doi.org/10.1029/2019JC015128

Cohen, J.E., Pimm, S.L., Yodzis, P., Saldaña, J., 1993. Body Sizes of Animal Predators and Animal Prey in Food Webs. J. Anim. Ecol. 62, 67–78. https://doi.org/10.2307/5483

Colin, S.P., Dam, H.G., 2007. Comparison of the functional and numerical responses of resistant versus non-resistant populations of the copepod Acartia hudsonica fed the toxic dinoflagellate Alexandrium tamarense. Harmful Algae 6, 875–882. https://doi.org/10.1016/j.hal.2007.05.003

Coll, M., Piroddi, C., Steenbeek, J., Kaschner, K., Lasram, F.B.R., Aguzzi, J., Ballesteros, E., Bianchi, C.N., Corbera, J., Dailianis, T., Danovaro, R., Estrada, M., Froglia, C., Galil, B.S., Gasol, J.M., Gertwagen, R., Gil, J., Guilhaumon, F., Kesner-Reyes, K., Kitsos, M.-S., Koukouras, A., Lampadariou, N., Laxamana, E., Cuadra, C.M.L.-F. de la, Lotze, H.K., Martin, D., Mouillot, D., Oro, D., Raicevich, S., Rius-Barile, J., Saiz-Salinas, J.I., Vicente, C.S., Somot, S., Templado, J., Turon, X., Vafidis, D., Villanueva, R., Voultsiadou, E., 2010. The Biodiversity of the Mediterranean Sea: Estimates, Patterns, and Threats. PLOS ONE 5, e11842. https://doi.org/10.1371/journal.pone.0011842

Cramp, A., Collins, M.B., Wakefield, S.J., 1987. Sedimentation in the Zakynthos Channel — A conduit link to the Hellenic Trench, eastern Mediterranean. Mar. Geol. 76, 71–87. https://doi.org/10.1016/0025-3227(87)90018-1

Criado-Aldeanueva, F., Soto-Navarro, F.J., García-Lafuente, J., 2012. Seasonal and interannual variability of surface heat and freshwater fluxes in the Mediterranean Sea: budgets and exchange through the Strait of Gibraltar. Int. J. Climatol. 32, 286–302. https://doi.org/10.1002/joc.2268

Crise, A., Allen, J.I., Baretta, J., Crispi, G., Mosetti, R., Solidoro, C., 1999. The Mediterranean pelagic ecosystem response to physical forcing. Prog. Oceanogr. 44, 219–243. https://doi.org/10.1016/S0079-6611(99)00027-0

da Fonseca, E.M., Gaylarde, C., Baptista Neto, J.A., Camacho Chab, J.C., Ortega-Morales, O., 2022. Microbial Interactions with Particulate and Floating Pollutants in the Oceans: A Review. Micro 2, 257–276. https://doi.org/10.3390/micro2020017

Dam, H.G., 2013. Evolutionary adaptation of marine zooplankton to global change. Annu. Rev. Mar. Sci. 5, 349–370. https://doi.org/10.1146/annurev-marine-121211-172229

de Boyer Montégut, C., Madec, G., Fischer, A.S., Lazar, A., Iudicone, D., 2004. Mixed layer depth over the global ocean: An examination of profile data and a profile-based climatology. J. Geophys. Res. Oceans 109. https://doi.org/10.1029/2004JC002378

Derbel, H., Châari, M., Neifar, L., 2012. Digenean species diversity in teleost fishes from the Gulf of Gabes, Tunisia (Western Mediterranean). Parasite J. Société Fr. Parasitol. 19, 129–135. https://doi.org/10.1051/parasite/2012192129

Dolan, J.R., Claustre, H., Carlotti, F., Plounevez, S., Moutin, T., 2002. Microzooplankton diversity: relationships of tintinnid ciliates with resources, competitors and predators from the Atlantic Coast of Morocco to the Eastern Mediterranean. Deep Sea Res. Part Oceanogr. Res. Pap. 49, 1217–1232. https://doi.org/10.1016/S0967-0637(02)00021-3

Dolan, J.R., Marrasé, C., 1995. Planktonic ciliate distribution relative to a deep chlorophyll maximum: Catalan Sea, N.W. Mediterranean, June 1993. Deep Sea Res. Part Oceanogr. Res. Pap. 42, 1965–1987. https://doi.org/10.1016/0967-0637(95)00092-5

Dolédec, S., Chessel, D., 1994. Coinertia analysis — An alternative method for studying species environment relationships. Freshw. Biol. 31.

Donoso, K., Carlotti, F., Pagano, M., Hunt, B.P.V., Escribano, R., Berline, L., 2017a. Zooplankton community response to the winter 2013 deep convection process in the NWMediterranean Sea: ZOOPLANKTON AND WINTER DEEP CONVECTION. J. Geophys. Res. Oceans 122, 2319–2338. https://doi.org/10.1002/2016JC012176

Donoso, K., Carlotti, F., Pagano, M., Hunt, B.P.V., Escribano, R., Berline, L., 2017b. Zooplankton community response to the winter 2013 deep convection process in the NWMediterranean Sea: ZOOPLANKTON AND WINTER DEEP CONVECTION. J. Geophys. Res. Oceans 122, 2319–2338. https://doi.org/10.1002/2016JC012176

D'Ortenzio, F., Ribera d'Alcalà, M., 2009. On the trophic regimes of the Mediterranean Sea: a satellite analysis. Biogeosciences 6, 139–148. https://doi.org/10.5194/bg-6-139-2009

Drira, Z., Hamza, A., Bel Hassen, M., Ayadi, H., Bouain, A., Aleya, L., 2010. Coupling of phytoplankton community structure to nutrients, ciliates and copepods in the Gulf of Gabès (south Ionian Sea, Tunisia). J. Mar. Biol. Assoc. U. K. 90, 1203–1215. https://doi.org/10.1017/S0025315409990774

Durrieu De Madron, X., Guieu, C., Sempéré, R., Conan, P., Cossa, D., D'Ortenzio, F., Estournel, C., Gazeau, F., Rabouille, C., Stemmann, L., Bonnet, S., Diaz, F., Koubbi, P., Radakovitch, O., Babin, M., Baklouti, M., Bancon-Montigny, C., Belviso, S., Bensoussan, N., Bonsang, B., Bouloubassi, I., Brunet, C., Cadiou, J.-F., Carlotti, F., Chami, M., Charmasson, S., Charrière, B., Dachs, J., Doxaran, D., Dutay, J.-C., Elbaz-Poulichet, F., Eléaume, M., Eyrolles, F., Fernandez, C., Fowler, S., Francour, P., Gaertner, J.C., Galzin, R., Gasparini, S., Ghiglione, J.-F., Gonzalez, J.-L., Goyet, C., Guidi, L., Guizien, K., Heimbürger, L.-E., Jacquet, S.H.M., Jeffrey, W.H., Joux, F., Le Hir, P., Leblanc, K., Lefèvre, D., Lejeusne, C., Lemé, R., Loÿe-Pilot, M.-D., Mallet, M., Méjanelle, L., Mélin, F., Mellon, C., Mérigot, B., Merle, P.-L., Migon, C., Miller, W.L., Mortier, L., Mostajir, B., Mousseau, L., Moutin, T., Para, J., Pérez, T., Petrenko, A., Poggiale, J.-C., Prieur, L., Pujo-Pay, M., Pulido-Villena, Raimbault, P., Rees, A.P., Ridame, C., Rontani, J.-F., Ruiz Pino, D., Sicre, M.A., Taillandier, V., Tamburini, C., Tanaka, T., Taupier-Letage, I., Tedetti, M., Testor, P., Thébault, H., Thouvenin, B., Touratier, F., Tronczynski, J., Ulses, C., Van Wambeke, F., Vantrepotte, V., Vaz, S., Verney, R., 2011. Marine ecosystems' responses to climatic and anthropogenic forcings in the Mediterranean. Prog. Oceanogr. 91, 97–166. https://doi.org/10.1016/j.pocean.2011.02.003

Durrieu de Madron, X., Guieu, C., Sempéré, R., Conan, P., Cossa, D., D'Ortenzio, F., Estournel, C., Gazeau, F., Rabouille, C., Stemmann, L., Bonnet, S., Diaz, F., Koubbi, P., Radakovitch, O., Babin, M., Baklouti, M., Montigny, C., Belviso, S., Bensoussan, N., Verney, R., 2011. Marine ecosystems' responses to climatic and anthropogenic forcings in the Mediterranean. Prog. Oceanogr. 91, 97–166. https://doi.org/10.1016/j.pocean.2011.02.003

El-Geziry, T.M., Bryden, I.G., 2010. The circulation pattern in the Mediterranean Sea: issues for modeller consideration. J. Oper. Oceanogr. 3, 39–46. https://doi.org/10.1080/1755876X.2010.11020116

Enajjar, S., Saïdi, B., Bradai, M., 2015. The Gulf of Gabès (Central Mediterranean Sea): a nursery area for sharks and batoids (Chondrichthyes: Elasmobranchs). Cah. Biol. Mar. 56, 143–150.

Espinasse, Boris, Carlotti, F., Zhou, M., Devenon, J.L., 2014. Defining zooplankton habitats in the Gulf of Lion (NW Mediterranean Sea) using size structure and environmental conditions. Mar. Ecol. Prog. Ser. 506, 31–46. https://doi.org/10.3354/meps10803

Espinasse, B., Harmelin-Vivien, M., Tiano, M., Guilloux, L., Carlotti, F., 2014. Patterns of variations in C and N stable isotope ratios in size-fractionated zooplankton in the Gulf of Lion, NW Mediterranean Sea. J. Plankton Res. 36, 1204–1215. https://doi.org/10.1093/plankt/fbu043

Feliú, G., Pagano, M., Hidalgo, P., Carlotti, F., 2020. Structure and function of epipelagic mesozooplankton and their response to dust deposition events during the spring PEACETIME cruise in the Mediterranean Sea. Biogeosciences 17, 5417–5441. https://doi.org/10.5194/bg-17-5417-2020

Fenchel, T., 1980. Relation between particle size selection and clearance in suspension-feeding ciliates. Limnol. Oceanogr. 25, 733–738. https://doi.org/10.4319/lo.1980.25.4.0733

Fernández de Puelles, M.L., Alemany, F., Jansá, J., 2007. Zooplankton time-series in the Balearic Sea (Western Mediterranean): Variability during the decade 1994–2003. Prog. Oceanogr., Ecological Functioning of the Iberian Seas: A synthesis of GLOBEC Research in Spain and Portugal 74, 329–354. https://doi.org/10.1016/j.pocean.2007.04.009

Fierro-González, P., Pagano, M., Guilloux, L., Makhlouf, N., Tedetti, M., Carlotti, F., 2023. Zooplankton biomass, size structure, and associated metabolic fluxes with focus on its roles at the chlorophyll maximum layer during the plankton-contaminant MERITE-HIPPOCAMPE cruise. Mar. Pollut. Bull. 193, 115056. https://doi.org/10.1016/j.marpolbul.2023.115056

Foster, K.L., Stern, G.A., Pazerniuk, M.A., Hickie, B., Walkusz, W., Wang, F., Macdonald, R.W., 2012. Mercury Biomagnification in Marine Zooplankton Food Webs in Hudson Bay. Environ. Sci. Technol. 46, 12952–12959. https://doi.org/10.1021/es303434p

FRONTIER, S., 1976. UTILISATION DES DIAGRAMMES RANG-FREQUENCE DANS L'ANALYSE DES ECOSYSTEMES. Util. DIAGRAMMES RANG-Freq. DANS Anal. Ecosyst.

Gauchery, T., Rovere, M., Pellegrini, C., Asioli, A., Tesi, T., Cattaneo, A., Trincardi, F., 2021. Post-LGM multi-proxy sedimentary record of bottom-current variability and downslope sedimentary processes in a contourite drift of the Gela Basin (Strait of Sicily). Mar. Geol. 439, 106564. https://doi.org/10.1016/j.margeo.2021.106564

Gaudy, R., Youssara, F., Diaz, F., Raimbault, P., 2003. Biomass, metabolism and nutrition of zooplankton in the Gulf of Lions (NW Mediterranean). Oceanol. Acta 26, 357–372. https://doi.org/10.1016/S0399-1784(03)00016-1

Gluchowska, M., Kwasniewski, S., Prominska, A., Olszewska, A., Goszczko, I., Falk-Petersen, S., Hop, H., Weslawski, J.M., 2016. Zooplankton in Svalbard fjords on the Atlantic–Arctic boundary. Polar Biol. 39, 1785–1802. https://doi.org/10.1007/s00300-016-1991-1

Gorsky, G., Dallot, S., Sardou, J., Fenaux, R., Carré, C., Palazzoli, I., 1988a. C and N composition of some northwestern Mediterranean zooplankton and micronekton species. J. Exp. Mar. Biol. Ecol. 124, 133–144. https://doi.org/10.1016/0022-0981(88)90116-5

Gorsky, G., Dallot, S., Sardou, J., Fenaux, R., Carré, C., Palazzoli, I., 1988b. C and N composition of some northwestern Mediterranean zooplankton and micronekton species. J. Exp. Mar. Biol. Ecol. 124, 133–144. https://doi.org/10.1016/0022-0981(88)90116-5

Gorsky, G., Ohman, M.D., Picheral, M., Gasparini, S., Stemmann, L., Romagnan, J.-B., Cawood, A., Pesant, S., Garcia-Comas, C., Prejger, F., 2010a. Digital zooplankton image analysis using the ZooScan integrated system. J. Plankton Res. 32, 285–303. https://doi.org/10.1093/plankt/fbp124

Gorsky, G., Ohman, M.D., Picheral, M., Gasparini, S., Stemmann, L., Romagnan, J.-B., Cawood, A., Pesant, S., Garcia-Comas, C., Prejger, F., 2010b. Digital zooplankton image analysis using the ZooScan integrated system. J. Plankton Res. 32, 285–303. https://doi.org/10.1093/plankt/fbp124

Granata, A., Bergamasco, A., Battaglia, P., Milisenda, G., Pansera, M., Bonanzinga, V., Arena, G., Andaloro, F., Giacobbe, S., Greco, S., Guglielmo, R., Spanò, N., Zagami, G., Guglielmo, L., 2020. Vertical distribution and diel migration of zooplankton and micronekton in Polcevera submarine canyon of the Ligurian mesopelagic zone (NW Mediterranean Sea). Prog. Oceanogr. 183, 102298. https://doi.org/10.1016/j.pocean.2020.102298

Grosjean, P., Picheral, M., Warembourg, C., Gorsky, G., 2004. Enumeration, measurement, and identification of net zooplankton samples using the ZOOSCAN digital imaging system. ICES J. Mar. Sci. 61, 518–525. https://doi.org/10.1016/j.icesjms.2004.03.012

Guglielmo, L., Minutoli, R., Bergamasco, A., Granata, A., Zagami, G., Antezana, T., 2011. Short-term changes in zooplankton community in Paso Ancho basin (Strait of Magellan): functional trophic structure and diel vertical migration. Polar Biol. 34, 1301–1317. https://doi.org/10.1007/s00300-011-1031-0

Guieu, C., D'Ortenzio, F., Dulac, F., Taillandier, V., Doglioli, A., Petrenko, A., Barrillon, S., Mallet, M., Nabat, P., Desboeufs, K., 2020. Process studies at the air-sea interface after atmospheric deposition in the Mediterranean Sea: objectives and strategy of the PEACETIME oceanographic campaign (May–June 2017) (preprint). Biogeochemistry: Open Ocean. https://doi.org/10.5194/bg-2020-44

Guigue, C., Tesán-Onrubia, J.A., Guyomarc'h, L., Bănaru, D., Carlotti, F., Pagano, M., Chifflet, S., Malengros, D., Chouba, L., Tronczynski, J., Tedetti, M., 2023a. Hydrocarbons in size-fractionated plankton of the Mediterranean Sea (MERITE-HIPPOCAMPE campaign). Mar. Pollut. Bull. 194, 115386. https://doi.org/10.1016/j.marpolbul.2023.115386

Guigue, C., Tesán-Onrubia, J.A., Guyomarc'h, L., Bănaru, D., Carlotti, F., Pagano, M., Chifflet, S., Malengros, D., Chouba, L., Tronczynski, J., Tedetti, M., 2023b. Hydrocarbons in size-fractionated plankton of the Mediterranean Sea (MERITE-HIPPOCAMPE campaign). Mar. Pollut. Bull. 194, 115386. https://doi.org/10.1016/j.marpolbul.2023.115386

Guiot, J., Cramer, W., 2016. Climate change: The 2015 Paris Agreement thresholds and Mediterranean basin ecosystems. Science 354, 465–468. https://doi.org/10.1126/science.aah5015

Halsband-Lenk, C., Carlotti, F., Greve, W., 2004. Life-history strategies of calanoid congeners under two different climate regimes: a comparison. ICES J. Mar. Sci. 61, 709–720. https://doi.org/10.1016/j.icesjms.2004.03.020

Halsband-Lenk, C., Hirche, H.-J., Carlotti, F., 2002. Temperature impact on reproduction and development of congener copepod populations. J. Exp. Mar. Biol. Ecol. 271, 121–153. https://doi.org/10.1016/S0022-0981(02)00025-4

Halsband-Lenk, C., Nival, S., Carlotti, F., Hirche, H.-J., 2001. Seasonal Cycles of Egg Production of Two Planktonic Copepods, Centropages typicus and Temora

stylifera, in the North-western Mediterranean Sea. J. Plankton Res. 23, 597–609. https://doi.org/10.1093/plankt/23.6.597
Hunt, B.P.V., Carlotti, F., Donoso, K., Pagano, M., D'Ortenzio, F., Taillandier, V., Conan, P., 2017. Trophic pathways of phytoplankton size classes through the zooplankton food web over the spring transition period in the north-west Mediterranean Sea. J. Geophys. Res. Oceans 122, 6309–6324. https://doi.org/10.1002/2016JC012658
Ikeda, T., 1985. Metabolic rates of epipelagic marine zooplankton as a function of body mass and temperature. Mar. Biol. 85, 1–11. https://doi.org/10.1007/BF00396409
Isbell, F., Craven, D., Connolly, J., Loreau, M., Schmid, B., Beierkuhnlein, C., Bezemer, T.M., Bonin, C., Bruelheide, H., de Luca, E., Ebeling, A., Griffin, J.N., Guo, Q., Hautier, Y., Hector, A., Jentsch, A., Kreyling, J., Lanta, V., Manning, P., Meyer, S.T., Mori, A.S., Naeem, S., Niklaus, P.A., Polley, H.W., Reich, P.B., Roscher, C., Seabloom, E.W., Smith, M.D., Thakur, M.P., Tilman, D., Tracy, B.F., van der Putten, W.H., van Ruijven, J., Weigelt, A., Weisser, W.W., Wilsey, B., Eisenhauer, N., 2015. Biodiversity increases the resistance of ecosystem productivity to climate extremes. Nature 526, 574–577. https://doi.org/10.1038/nature15374
Kessouri, F., Ulses, C., Estournel, C., Marsaleix, P., Severin, T., Pujo-Pay, M., Caparros, J., Raimbault, P., Pasqueron de Fommervault, O., D'Ortenzio, F., Taillandier, V., Testor, P., Conan, P., 2017. Nitrogen and Phosphorus Budgets in the Northwestern Mediterranean Deep Convection Region. J. Geophys. Res. Oceans 122, 9429–9454. https://doi.org/10.1002/2016JC012665
Khairy, M., Brault, E., Dickhut, R., Harding, K.C., Harkonen, T., Karlsson, O., Lehnert, K., Teilmann, J., Lohmann, R., 2021. Bioaccumulation of PCBs, OCPs and PBDEs in Marine Mammals From West Antarctica. Front. Mar. Sci. 8, 768715. https://doi.org/10.3389/fmars.2021.768715
Kim, Y., Lee, Jang Han, Kang, J.J., Lee, Jae Hyung, Lee, H.W., Kang, C.K., Lee, S.H., 2019. River discharge effects on the contribution of small-sized phytoplankton to the total biochemical composition of POM in the Gwangyang Bay, Korea. Estuar. Coast. Shelf Sci. 226, 106293. https://doi.org/10.1016/j.ecss.2019.106293
Kiørboe, T., Saiz, E., Tiselius, P., Andersen, K.H., 2018. Adaptive feeding behavior and functional responses in zooplankton. Limnol. Oceanogr. 63, 308–321. https://doi.org/10.1002/lno.10632
Kouwenberg, J.H.M., 1994. Copepod Distribution in Relation to Seasonal Hydrographics and Spatial Structure in the North-western Mediterranean (Golfe du Lion). Estuar. Coast. Shelf Sci. 38, 69–90. https://doi.org/10.1006/ecss.1994.1005
Kvile, K.Ø., Taranto, G.H., Pitcher, T.J., Morato, T., 2014. A global assessment of seamount ecosystems knowledge using an ecosystem evaluation framework. Biol. Conserv. 173, 108–120. https://doi.org/10.1016/j.biocon.2013.10.002
Lavigne, H., D'Ortenzio, F., Ribera D'Alcalà, M., Claustre, H., Sauzède, R., Gacic, M., 2015. On the vertical distribution of the chlorophyll <i>a</i> concentration in the Mediterranean Sea: a basin-scale and seasonal approach. Biogeosciences 12, 5021–5039. https://doi.org/10.5194/bg-12-5021-2015
Lazzari, P., Solidoro, C., Salon, S., Bolzon, G., 2016. Spatial variability of phosphate and nitrate in the Mediterranean Sea: A modeling approach. Deep Sea Res. Part Oceanogr. Res. Pap. 108, 39–52. https://doi.org/10.1016/j.dsr.2015.12.006
Le Bourg, B., Cornet-Barthaux, V., Pagano, M., Blanchot, J., 2015. FlowCAM as a tool for studying small (80–1000 μm) metazooplankton communities. J. Plankton Res. 37, 666–670. https://doi.org/10.1093/plankt/fbv025

Lehette, P., Hernández-León, S., 2009a. Zooplankton biomass estimation from digitized images: a comparison between subtropical and Antarctic organisms: Zooplankton biomass by digital images. Limnol. Oceanogr. Methods 7, 304–308. https://doi.org/10.4319/lom.2009.7.304

Lehette, P., Hernández-León, S., 2009b. Zooplankton biomass estimation from digitized images: a comparison between subtropical and Antarctic organisms: Zooplankton biomass by digital images. Limnol. Oceanogr. Methods 7, 304–308. https://doi.org/10.4319/lom.2009.7.304

Lejeusne, C., Chevaldonné, P., Pergent-Martini, C., Boudouresque, C.F., Pérez, T., 2010. Climate change effects on a miniature ocean: the highly diverse, highly impacted Mediterranean Sea. Trends Ecol. Evol. 25, 250–260. https://doi.org/10.1016/j.tree.2009.10.009

Letelier, R.M., Karl, D.M., Abbott, M.R., Bidigare, R.R., 2004. Light driven seasonal patterns of chlorophyll and nitrate in the lower euphotic zone of the North Pacific Subtropical Gyre. Limnol. Oceanogr. 49, 508–519. https://doi.org/10.4319/lo.2004.49.2.0508

Li, J., Lin, X., Chen, A., Peterson, T., Ma, K., Bertzky, M., Ciais, P., Kapos, V., Peng, C., Poulter, B., 2013. Global Priority Conservation Areas in the Face of 21st Century Climate Change. PLOS ONE 8, e54839. https://doi.org/10.1371/journal.pone.0054839

Lipizer, M., Berto, D., Cermelj, B., Fafandjel, M., Formalewicz, M., Hatzianestis, I., Ilijanić, N., Kaberi, H., Kralj, M., Matijevic, S., Molina Jack, M.E., Parinos, C., Tronczynski, J., Giani, M., 2022. Trace metals and polycyclic aromatic hydrocarbons in the Eastern Mediterranean sediments: Concentration ranges as a tool for quality control of large data collections. Mar. Pollut. Bull. 185, 114181. https://doi.org/10.1016/j.marpolbul.2022.114181

Ljungström, G., Claireaux, M., Fiksen, Ø., Jørgensen, C., 2020. Body size adaptions under climate change: zooplankton community more important than temperature or food abundance in model of a zooplanktivorous fish. Mar. Ecol. Prog. Ser. 636, 1–18. https://doi.org/10.3354/meps13241

López-Urrutia, Á., Irigoien, X., Acuña, J., Harris, R., 2003. In situ feeding physiology and grazing impact of the appendicularian community in temperate waters. Mar. Ecol. Prog. Ser. 252, 125–141. https://doi.org/10.3354/meps252125

Margirier, F., Testor, P., Heslop, E., Mallil, K., Bosse, A., Houpert, L., Mortier, L., Bouin, M.-N., Coppola, L., D'Ortenzio, F., Durrieu de Madron, X., Mourre, B., Prieur, L., Raimbault, P., Taillandier, V., 2020. Abrupt warming and salinification of intermediate waters interplays with decline of deep convection in the Northwestern Mediterranean Sea. Sci. Rep. 10, 20923. https://doi.org/10.1038/s41598-020-77859-5

Marshall, J., Schott, F., 1999. Open-ocean convection: Observations, theory, and models. Rev. Geophys. 37, 1–64. https://doi.org/10.1029/98RG02739

Mayot, N., D'Ortenzio, F., Uitz, J., Gentili, B., Ras, J., Vellucci, V., Golbol, M., Antoine, D., Claustre, H., 2017. Influence of the Phytoplankton Community Structure on the Spring and Annual Primary Production in the Northwestern Mediterranean Sea. J. Geophys. Res. Oceans 122, 9918–9936. https://doi.org/10.1002/2016JC012668

Mayzaud, P., Boutoute, M., Gasparini, S., Mousseau, L., Lefevre, D., 2005. Respiration in marine zooplankton—the other side of the coin: CO2 production. Limnol. Oceanogr. 50, 291–298. https://doi.org/10.4319/lo.2005.50.1.0291

Mazzocchi, M.G., Christou, E.D., Capua, I.D., Fernández de Puelles, M., Fonda-Umani, S., Molinero, J.C., Nival, P., Siokou-Frangou, I., 2007. Temporal variability of

Centropages typicus in the Mediterranean Sea over seasonal-to-decadal scales. Prog. Oceanogr. 72, 214–232. https://doi.org/10.1016/j.pocean.2007.01.004
Mazzocchi, M.G., Nervegna, D., D'Elia, G., Di Capua, I., Aguzzi, L., Boldrin, A., 2003. Spring mesozooplankton communities in the epipelagic Ionian Sea in relation to the Eastern Mediterranean Transient. J. Geophys. Res. Oceans 108. https://doi.org/10.1029/2002JC001640
Mazzocchi, M.G., Siokou, I., Tirelli, V., Bandelj, V., Fernandez de Puelles, M.L., Ak Örek, Y., de Olazabal, A., Gubanova, A., Kress, N., Protopapa, M., Solidoro, C., Taglialatela, S., Terbiyik Kurt, T., 2014. Regional and seasonal characteristics of epipelagic mesozooplankton in the Mediterranean Sea based on an artificial neural network analysis. J. Mar. Syst. 135, 64–80. https://doi.org/10.1016/j.jmarsys.2013.04.009
MEDOC GROUP, 1970. Observation of Formation of Deep Water in the Mediterranean Sea, 1969. Nature 227, 1037–1040. https://doi.org/10.1038/2271037a0
Micheli, F., Halpern, B.S., Walbridge, S., Ciriaco, S., Ferretti, F., Fraschetti, S., Lewison, R., Nykjaer, L., Rosenberg, A.A., 2013. Cumulative Human Impacts on Mediterranean and Black Sea Marine Ecosystems: Assessing Current Pressures and Opportunities. PLOS ONE 8, e79889. https://doi.org/10.1371/journal.pone.0079889
Mignot, A., Claustre, H., Uitz, J., Poteau, A., D'Ortenzio, F., Xing, X., 2014. Understanding the seasonal dynamics of phytoplankton biomass and the deep chlorophyll maximum in oligotrophic environments: A Bio-Argo float investigation. Glob. Biogeochem. Cycles 28, 856–876. https://doi.org/10.1002/2013GB004781
Millot, C., 1999. Circulation in the Western Mediterranean Sea. J. Mar. Syst. 20, 423–442. https://doi.org/10.1016/S0924-7963(98)00078-5
Millot, C., Taupier-Letage, I., 2005a. Circulation in the Mediterranean Sea, in: Saliot, A. (Ed.), The Mediterranean Sea, Handbook of Environmental Chemistry. Springer, pp. 29–66. https://doi.org/10.1007/b107143
Millot, C., Taupier-Letage, I., 2005b. Circulation in the Mediterranean Sea, in: Saliot, A. (Ed.), The Mediterranean Sea, Handbook of Environmental Chemistry. Springer Berlin Heidelberg, Berlin, Heidelberg, pp. 29–66. https://doi.org/10.1007/b107143
Møller, E., Thor, P., Nielsen, T., 2003. Production of DOC by Calanus finmarchicus, C. glacialis and C. hyperboreus through sloppy feeding and leakage from fecal pellets. Mar. Ecol. Prog. Ser. 262, 185–191. https://doi.org/10.3354/meps262185
Möller, K., St John, M., Temming, A., Floeter, J., Sell, A., Herrmann, J., Möllmann, C., 2012. Marine snow, zooplankton and thin layers: indications of a trophic link from small-scale sampling with the Video Plankton Recorder. Mar. Ecol. Prog. Ser. 468, 57–69. https://doi.org/10.3354/meps09984
Moriarty, R., Buitenhuis, E.T., Le Quéré, C., Gosselin, M.-P., 2013. Distribution of known macrozooplankton abundance and biomass in the global ocean. Earth Syst. Sci. Data 5, 241–257. https://doi.org/10.5194/essd-5-241-2013
Mouillot, D., Lepretre, A., 2000. Introduction of Relative Abundance Distribution (RAD) Indices, Estimated from the Rank-Frequency Diagrams (RFD), to Assess Changes in Community Diversity. Environ. Monit. Assess. 63, 279–295. https://doi.org/10.1023/A:1006297211561
Moutin, T., Van Wambeke, F., Prieur, L., 2012. Introduction to the Biogeochemistry from the Oligotrophic to the Ultraoligotrophic Mediterranean (BOUM) experiment. Biogeosciences 9, 3817–3825. https://doi.org/10.5194/bg-9-3817-2012
Ndah, A.B., Meunier, C.L., Kirstein, I.V., Göbel, J., Rönn, L., Boersma, M., 2022. A systematic study of zooplankton-based indices of marine ecological change and water quality:

Application to the European marine strategy framework Directive (MSFD). Ecol. Indic. 135, 108587. https://doi.org/10.1016/j.ecolind.2022.108587
Nival, P., Nival, S., Thiriot, A., 1975. Influence des conditions hivernales sur les productions phyto-et zooplanctoniques en Méditerranée Nord-Occidentale. V. Biomasse et production zooplanctonique — relations phyto-zooplancton. Mar. Biol. 31, 249–270. https://doi.org/10.1007/BF00387153
Nowaczyk, A., Carlotti, F., Thibault-Botha, D., Pagano, M., 2011a. Distribution of epipelagic metazooplankton across the Mediterranean Sea during the summer BOUM cruise. Biogeosciences 8, 2159–2177. https://doi.org/10.5194/bg-8-2159-2011
Nowaczyk, A., Carlotti, F., Thibault-Botha, D., Pagano, M., 2011b. Distribution of epipelagic metazooplankton across the Mediterranean Sea during the summer BOUM cruise. Biogeosciences 8, 2159–2177. https://doi.org/10.5194/bg-8-2159-2011
Olivar, M.P., Emelianov, M., Villate, F., Uriarte, I., Maynou, F., Álvarez, I., Morote, E., 2010. The role of oceanographic conditions and plankton availability in larval fish assemblages off the Catalan coast (NW Mediterranean): Larval fish assemblages off the Catalan coast. Fish. Oceanogr. 19, 209–229. https://doi.org/10.1111/j.1365-2419.2010.00538.x
Paffenhöfer, G.-A., Stewart, T.B., Youngbluth, M.J., Bailey, T.G., 1991. High-resolution vertical profiles of pelagic tunicates. J. Plankton Res. 13, 971–981. https://doi.org/10.1093/plankt/13.5.971
Pecl, G.T., Araújo, M.B., Bell, J.D., Blanchard, J., Bonebrake, T.C., Chen, I.-C., Clark, T.D., Colwell, R.K., Danielsen, F., Evengård, B., Falconi, L., Ferrier, S., Frusher, S., Garcia, R.A., Griffis, R.B., Hobday, A.J., Janion-Scheepers, C., Jarzyna, M.A., Jennings, S., Lenoir, J., Linnetved, H.I., Martin, V.Y., McCormack, P.C., McDonald, J., Mitchell, N.J., Mustonen, T., Pandolfi, J.M., Pettorelli, N., Popova, E., Robinson, S.A., Scheffers, B.R., Shaw, J.D., Sorte, C.J.B., Strugnell, J.M., Sunday, J.M., Tuanmu, M.-N., Vergés, A., Villanueva, C., Wernberg, T., Wapstra, E., Williams, S.E., 2017. Biodiversity redistribution under climate change: Impacts on ecosystems and human well-being. Science 355, eaai9214. https://doi.org/10.1126/science.aai9214
Pinca, S., Dallot, S., 1997. Zooplankton community structure in the Western Mediterranean sea related to mesoscale hydrodynamics. Hydrobiologia 356, 127–142. https://doi.org/10.1023/A:1003151609682
Qiu, Z.F., Doglioli, A.M., Hu, Z.Y., Marsaleix, P., Carlotti, F., 2010. The influence of hydrodynamic processes on zooplankton transport and distributions in the North Western Mediterranean: Estimates from a Lagrangian model. Ecol. Model. 221, 2816–2827. https://doi.org/10.1016/j.ecolmodel.2010.07.025
Ramfos, A., Isari, S., Somarakis, S., Georgopoulos, D., Koutsikopoulos, C., Fragopoulu, N., 2006. Mesozooplankton community structure in offshore and coastal waters of the Ionian Sea (eastern Mediterranean) during mixed and stratified conditions. Mar. Biol. 150, 29–44. https://doi.org/10.1007/s00227-006-0326-0
Reusch, T.B.H., Boyd, P.W., 2013. Experimental Evolution Meets Marine Phytoplankton. Evolution 67, 1849–1859. https://doi.org/10.1111/evo.12035
Riandey, V., Champalbert, G., Carlotti, F., Taupier-Letage, I., Thibault-Botha, D., 2005. Zooplankton distribution related to the hydrodynamic features in the Algerian Basin (western Mediterranean Sea) in summer 1997. Deep Sea Res. Part Oceanogr. Res. Pap. 52, 2029–2048. https://doi.org/10.1016/j.dsr.2005.06.004
Ribera d'Alcala, M., Conversano, F., Corato, F., Licandro, P., 2004. Seasonal patterns in plankton communities in a pluriannual time series at a coastal Mediterranean site (Gulf of Naples): an attempt to discern recurrences and trends. Carbon 68, 65–83.

Romero, I.C., Schwing, P.T., Brooks, G.R., Larson, R.A., Hastings, D.W., Ellis, G., Goddard, E.A., Hollander, D.J., 2015. Hydrocarbons in Deep-Sea Sediments following the 2010 Deepwater Horizon Blowout in the Northeast Gulf of Mexico. PLOS ONE 10, e0128371. https://doi.org/10.1371/journal.pone.0128371

Romero, I.C., Sutton, T., Carr, B., Quintana-Rizzo, E., Ross, S.W., Hollander, D.J., Torres, J.J., 2018. Decadal Assessment of Polycyclic Aromatic Hydrocarbons in Mesopelagic Fishes from the Gulf of Mexico Reveals Exposure to Oil-Derived Sources. Environ. Sci. Technol. 52, 10985–10996. https://doi.org/10.1021/acs.est.8b02243

Saba, G., Steinberg, D., Bronk, D., 2009. Effects of diet on release of dissolved organic and inorganic nutrients by the copepod Acartia tonsa. Mar. Ecol.-Prog. Ser. - MAR ECOL-PROGR SER 386, 147–161. https://doi.org/10.3354/meps08070

Sabatés, A., Olivar, M.P., 1996. Variation of larval fish distributions associated with variability in the location of a shelf-slope front. Mar. Ecol. Prog. Ser. 135, 11–20.

Sabatés, A., Salat, J., Palomera, I., Emelianov, M., Fernández De Puelles, M.L., Olivar, M.P., 2007. Advection of anchovy (Engraulis encrasicolus) larvae along the Catalan continental slope (NW Mediterranean). Fish. Oceanogr. 16, 130–141. https://doi.org/10.1111/j.1365-2419.2006.00416.x

Sabatés, A., Zaragoza, N., Grau, C., Salat, J., 2008. Vertical distribution of early developmental stages in two coexisting clupeoid species, Sardinella aurita and Engraulis encrasicolus. Mar. Ecol. Prog. Ser. 364, 169–180. https://doi.org/10.3354/meps07461

Saiz, E., Calbet, A., 2011. Copepod feeding in the ocean: scaling patterns, composition of their diet and the bias of estimates due to microzooplankton grazing during incubations. Hydrobiologia 666, 181–196. https://doi.org/10.1007/s10750-010-0421-6

Saiz, E., Calbet, A., Irigoien, X., Alcaraz, M., 1999. Copepod egg production in the western Mediterranean:response to food availability in oligotrophic environments. Mar. Ecol. Prog. Ser. 187, 179–189. https://doi.org/10.3354/meps187179

Saiz, E., Sabatés, A., Gili, J.-M., 2014a. The Zooplankton, in: Goffredo, S., Dubinsky, Z. (Eds.), The Mediterranean Sea. Springer Netherlands, Dordrecht, pp. 183–211. https://doi.org/10.1007/978-94-007-6704-1_11

Saiz, E., Sabatés, A., Gili, J.-M., 2014b. The Zooplankton, in: Goffredo, S., Dubinsky, Z. (Eds.), The Mediterranean Sea. Springer Netherlands, Dordrecht, pp. 183–211. https://doi.org/10.1007/978-94-007-6704-1_11

Sameoto, D., Wiebe, P., Runge, J., Postel, L., Dunn, J., Miller, C., Coombs, S., 2000. Collecting zooplankton, in: ICES Zooplankton Methodology Manual. Elsevier, pp. 55–81. https://doi.org/10.1016/B978-012327645-2/50004-9

Sameoto, D.D., 1986. Influence of the biological and physical environment on the vertical distribution of mesozooplankton and micronekton in the eastern tropical Pacific. Mar. Biol. 93, 263–279. https://doi.org/10.1007/BF00508264

Schroeder, K., Ribotti, A., Borghini, M., Sorgente, R., Perilli, A., Gasparini, G.P., 2008. An extensive western Mediterranean deep water renewal between 2004 and 2006. Geophys. Res. Lett. 35. https://doi.org/10.1029/2008GL035146

See, J.H., Campbell, L., Richardson, T.L., Pinckney, J.L., Shen, R., Guinasso, N.L., Jr., 2005. Combining New Technologies for Determination of Phytoplankton Community Structure in the Northern Gulf of Mexico 1. J. Phycol. 41, 305–310. https://doi.org/10.1111/j.1529-8817.2005.04132.x

Severin, T., Conan, P., Durrieu de Madron, X., Houpert, L., Oliver, M., Oriol, L., Caparros, J., Ghiglione, J.-F., Pujo-Pay, M., 2014. Impact of open-ocean convection on nutrients,

phytoplankton biomass and activity. Deep Sea Res. Part Oceanogr. Res. Pap. 94. https://doi.org/10.1016/j.dsr.2014.07.015
Seyfried, L., Estournel, C., Marsaleix, P., Richard, E., 2019. Dynamics of the North Balearic Front during an autumn tramontane and mistral storm: air–sea coupling processes and stratification budget diagnostic. Ocean Sci. 15, 179–198. https://doi.org/10.5194/os-15-179-2019
Sheldon, R.W., Prakash, A., Sutcliffe Jr., W.H., 1972. The Size Distribution of Particles in the Ocean1. Limnol. Oceanogr. 17, 327–340. https://doi.org/10.4319/lo.1972.17.3.0327
Sieburth, J.McN., Smetacek, V., Lenz, J., 1978. Pelagic ecosystem structure: Heterotrophic compartments of the plankton and their relationship to plankton size fractions 1. Limnol. Oceanogr. 23, 1256–1263. https://doi.org/10.4319/lo.1978.23.6.1256
Sieracki, C., Sieracki, M., Yentsch, C., 1998. An imaging-in-flow system for automated analysis of marine microplankton. Mar. Ecol. Prog. Ser. 168, 285–296. https://doi.org/10.3354/meps168285
Sieracki, C.K., Sieracki, M.E., Yentsch, C.S., 1998. An imaging-in-flow system for automated analysis of marine microplankton. Mar. Ecol. Prog. Ser. 168, 285–296. https://doi.org/10.3354/meps168285
Siokou, I., Zervoudaki, S., Velaoras, D., Theocharis, A., Christou, E.D., Protopapa, M., Pantazi, M., 2019. Mesozooplankton vertical patterns along an east-west transect in the oligotrophic Mediterranean sea during early summer. Deep Sea Res. Part II Top. Stud. Oceanogr., Revisiting the Eastern Mediterranean: Recent knowledge on the physical, biogeochemical and ecosystemic states and trends (Volume I) 164, 170–189. https://doi.org/10.1016/j.dsr2.2019.02.006
Siokou-Frangou, I., Christaki, U., Mazzocchi, M.G., Montresor, M., Ribera d'Alcalá, M., Vaqué, D., Zingone, A., 2010a. Plankton in the open Mediterranean Sea: a review. Biogeosciences 7, 1543–1586. https://doi.org/10.5194/bg-7-1543-2010
Siokou-Frangou, I., Christaki, U., Mazzocchi, M.G., Montresor, M., Ribera d'Alcalá, M., Vaqué, D., Zingone, A., 2010b. Plankton in the open Mediterranean Sea: a review. Biogeosciences 7, 1543–1586. https://doi.org/10.5194/bg-7-1543-2010
Siokou-Frangou, I., Christaki, U., Mazzocchi, M.G., Montresor, M., Ribera d'Alcala, M., Vaqué, D., Zingone, A., 2009. Plankton in the open Mediterranean Sea: A review. Biogeosciences Discuss. 7. https://doi.org/10.5194/bgd-6-11187-2009
Skovgaard, A., Saiz, E., 2006. Seasonal occurrence and role of protistan parasites in coastal marine zooplankton. Mar. Ecol. Prog. Ser. 327, 37–49. https://doi.org/10.3354/meps327037
Steinberg, D.K., Landry, M.R., 2017. Zooplankton and the Ocean Carbon Cycle. Annu. Rev. Mar. Sci. 9, 413–444. https://doi.org/10.1146/annurev-marine-010814-015924
Svensen, C., Seuthe, L., Vasilyeva, Y., Pasternak, A., Hansen, E., 2011. Zooplankton distribution across Fram Strait in autumn: Are small copepods and protozooplankton important? Prog. Oceanogr. 91, 534–544. https://doi.org/10.1016/j.pocean.2011.08.001
Svetlichny, L., Hubareva, E., Erkan, F., Gucu, A.C., 2000. Physiological and behavioral aspects of Calanus euxinus females (Copepoda: Calanoida) during vertical migration across temperature and oxygen gradients. Mar. Biol. 137, 963–971. https://doi.org/10.1007/s002270000405
Tedetti, M., Tronczynski, J., Carlotti, F., Pagano, M., Ismail, S.B., Sammari, C., Hassen, M.B., Desboeufs, K., Poindron, C., Chifflet, S., Zouari, A.B., Abdennadher, M., Amri, S., Bănaru, D., Abdallah, L.B., Bhairy, N., Boudriga, I., Bourin, A., Brach-Papa, C., Briant,

N., Cabrol, L., Chevalier, C., Chouba, L., Coudray, S., Yahia, M.N.D., de Garidel-Thoron, T., Dufour, A., Dutay, J.-C., Espinasse, B., Fierro-González, P., Fornier, M., Garcia, N., Giner, F., Guigue, C., Guilloux, L., Hamza, A., Heimbürger-Boavida, L.-E., Jacquet, S., Knoery, J., Lajnef, R., Belkahia, N.M., Malengros, D., Martinot, P.L., Bosse, A., Mazur, J.-C., Meddeb, M., Misson, B., Pringault, O., Quéméneur, M., Radakovitch, O., Raimbault, P., Ravel, C., Rossi, V., Rwawi, C., Hlaili, A.S., Tesán-Onrubia, J.A., Thomas, B., Thyssen, M., Zaaboub, N., Garnier, C., 2023. Contamination of planktonic food webs in the Mediterranean Sea: Setting the frame for the MERITE-HIPPOCAMPE oceanographic cruise (spring 2019). Mar. Pollut. Bull. 189, 114765. https://doi.org/10.1016/j.marpolbul.2023.114765

Tesán-Onrubia, J.A., Tedetti, M., Carlotti, F., Tenaille, M., Guilloux, L., Pagano, M., Lebreton, B., Guillou, G., Fierro-González, P., Guigue, C., Chifflet, S., Garcia, T., Boudriga, I., Belhassen, M., Zouari, A.B., Bănaru, D., 2023a. Spatial variations of biochemical content and stable isotope ratios of size-fractionated plankton in the Mediterranean Sea (MERITE-HIPPOCAMPE campaign). Mar. Pollut. Bull. 189, 114787. https://doi.org/10.1016/j.marpolbul.2023.114787

Tesán-Onrubia, J.A., Tedetti, M., Carlotti, F., Tenaille, M., Guilloux, L., Pagano, M., Lebreton, B., Guillou, G., Fierro-González, P., Guigue, C., Chifflet, S., Garcia, T., Boudriga, I., Belhassen, M., Zouari, A.B., Bănaru, D., 2023b. Spatial variations of biochemical content and stable isotope ratios of size-fractionated plankton in the Mediterranean Sea (MERITE-HIPPOCAMPE campaign). Mar. Pollut. Bull. 189, 114787. https://doi.org/10.1016/j.marpolbul.2023.114787

Thioulouse, J., Chessel, D., Dolédec, S., Olivier, J.-M., 1997. ADE-4 a Multivariate Analysis and Graphical Display Software. Stat. Comput. 7. https://doi.org/10.1023/A:1018513530268

Tiano, M., Tronczyński, J., Harmelin-Vivien, M., Tixier, C., Carlotti, F., 2014a. PCB concentrations in plankton size classes, a temporal study in Marseille Bay, Western Mediterranean Sea. Mar. Pollut. Bull. 89, 331–339. https://doi.org/10.1016/j.marpolbul.2014.09.040

Tiano, M., Tronczyński, J., Harmelin-Vivien, M., Tixier, C., Carlotti, F., 2014b. PCB concentrations in plankton size classes, a temporal study in Marseille Bay, Western Mediterranean Sea. Mar. Pollut. Bull. 89, 331–339. https://doi.org/10.1016/j.marpolbul.2014.09.040

Tiselius, P., Petersen, J., Nielsen, T., Maar, M., Møller, E., Satapoomin, S., Tönnesson, K., Zervoudaki, T., Christou, E., Giannakourou, A., Sell, A., Vargas, C., 2003. Functional response of Oikopleura dioica to house clogging due to exposure to algae of different sizes. Mar. Biol. 142, 253–261. https://doi.org/10.1007/s00227-002-0961-z

Turner, J.T., 2015. Zooplankton fecal pellets, marine snow, phytodetritus and the ocean's biological pump. Prog. Oceanogr. 130, 205–248. https://doi.org/10.1016/j.pocean.2014.08.005

Ulses, C., Estournel, C., Fourrier, M., Coppola, L., Kessouri, F., Lefèvre, D., Marsaleix, P., 2021. Oxygen budget of the north-western Mediterranean deep- convection region. Biogeosciences 18, 937–960. https://doi.org/10.5194/bg-18-937-2021

van der Oost, R., Beyer, J., Vermeulen, N.P.E., 2003. Fish bioaccumulation and biomarkers in environmental risk assessment: a review. Environ. Toxicol. Pharmacol. 13, 57–149. https://doi.org/10.1016/S1382-6689(02)00126-6

Vandromme, P., Stemmann, L., Garcìa-Comas, C., Berline, L., Sun, X., Gorsky, G., 2012. Assessing biases in computing size spectra of automatically classified zooplankton

from imaging systems: A case study with the ZooScan integrated system. Methods Oceanogr. 1–2, 3–21. https://doi.org/10.1016/j.mio.2012.06.001

Weijs, L., Hickie, B., Blust, R., Covaci, A., 2014. Overview of the Current State-of-the-Art for Bioaccumulation Models in Marine Mammals. Toxics 2, 226–246. https://doi.org/10.3390/toxics2020226

Weikert, H., Trinkaus, S., 1990. Vertical mesozooplankton abundance and distribution in the deep Eastern Mediterranean Sea SE of Crete. J. Plankton Res. 12, 601–628. https://doi.org/10.1093/plankt/12.3.601

Yebra, L., Espejo, E., Putzeys, S., Giráldez, A., Gómez-Jakobsen, F., León, P., Salles, S., Torres, P., Mercado, J.M., 2020. Zooplankton Biomass Depletion Event Reveals the Importance of Small Pelagic Fish Top-Down Control in the Western Mediterranean Coastal Waters. Front. Mar. Sci. 7, 608690. https://doi.org/10.3389/fmars.2020.608690

Zagami, G., Antezana, T., Ferrari, I., Granata, A., Sitran, R., Minutoli, R., Guglielmo, L., 2011. Species diversity, spatial distribution, and assemblages of zooplankton within the Strait of Magellan in austral summer. Polar Biol. 34, 1319–1333. https://doi.org/10.1007/s00300-011-0962-9

Zarauz, L., Irigoien, X., Fernandes, J.A., 2009. Changes in plankton size structure and composition, during the generation of a phytoplankton bloom, in the central Cantabrian sea. J. Plankton Res. 31, 193–207. https://doi.org/10.1093/plankt/fbn107

Zhou, M., Carlotti, F., Zhu, Y., 2010. A size-spectrum zooplankton closure model for ecosystem modelling. J. Plankton Res. 32, 1147–1165. https://doi.org/10.1093/plankt/fbq054

Zervoudaki, S., Christou, E.D., Nielsen, T.G., Siokou-Frangou, I., Assimakopoulou, G., Giannakourou, A., Maar, M., Pagou, K., Krasakopoulou, E., Christaki, U., Moraitou-Apostolopoulou, M., 2007. The importance of small-sized copepods in a frontal area of the Aegean Sea. J. Plankton Res. 29, 317–338. https://doi.org/10.1093/plankt/fbm018

ANNEXES

Annexes for Chapter 2

Annex 2.1. Script to calculate MLD in Matlab using function ra_mld.m based on de Boyer Montégut et al, (2004)

```
n=50;  #only for plot, shows the first X meters. if you want to show   the whole
       profile just put 100 or 1000
```

CHANGE DEPENDING ON EXPERIMENT 1m 5m or 10m

```
N=5;  # to start calculating the MLD from X meters.
       #if 1, start evaluating from the surface
       # if you put 5 start to evaluate from 5 m ...10 for 10m... etc.
 for i=1:118;  # goes through each one of the excel slides
    data=xlsread("ctd_original_1.xlsx",i,"A:G");  # select the columns with information
    zpos=find(data(:,1)>=N); zpos=min(zpos);  # this is to start from the depth selected above... N=1.. N
=5.. 10 etc
```

CHANGE 0.5 o 1 degC

```
    [mld]=ra_mld(data(zpos:end,3),data(zpos:end,2),data(zpos:end,1),1); #  function calculating MLD,
last value is criterion 0.5 o 1 degC

 mld=floor(mld);  # as the function calculates with all parameters,  delivers a result with a decimal
place,   but since excel is with integers then it is rounded to the nearest integer.
   # number base, example 13.2343 =>> 13

    pos=find(mld<data(:,1)); pos=min(pos);
   # this is in case the function calculates the MLD at any depth.
   # that is not in the excel, then look for the nearest depth

    h=figure("visible","off"); #  just not to show graphs that you are doing ... on to show
```

Temperature graph with a mark where it found the MLD

```
    subplot 131
    plot(data(1:n,2),-data(1:n,1),"b","linewi",2);
    hold on
    text(data(pos,2),-mld,"\rightarrow mld","fontweight","bold","fontsize",14);
    xlabel("Temperature (degC)","fontweight","bold","fontsize",13)
```

Salinity graph with a mark where the MLD was founded

```
 subplot 132
plot(data(1:n,3),-data(1:n,1), “r “, "linewi" ,2);
 hold on
 text (data(pos,3),-mld,"\rightarrow mld","fontweight","bold","fontsize",14);
   xlabel( "Salinity (psu", «fontweight ", "bold ", "fontsize ",13);
```

Density graph with a mark where the MLD was founded

```
   dens=sw_dens(data(1:n,3),data(1:n,2),data(1:n,1));
   subplot 133
   plot(dens,-data(1:n,1), "g ", "linewi ",2);
   hold on
   text(dens(pos),-mld,"\rightarrow mld","fontweight","bold","fontsize",14);
   xlabel("Density (kg/m^3)","fontweight","bold","fontsize",13);

   filename = sprintf("slide-%d", i);   to name the created figures

   sup_title=sprintf("MLD" =  d m «,mld);
```

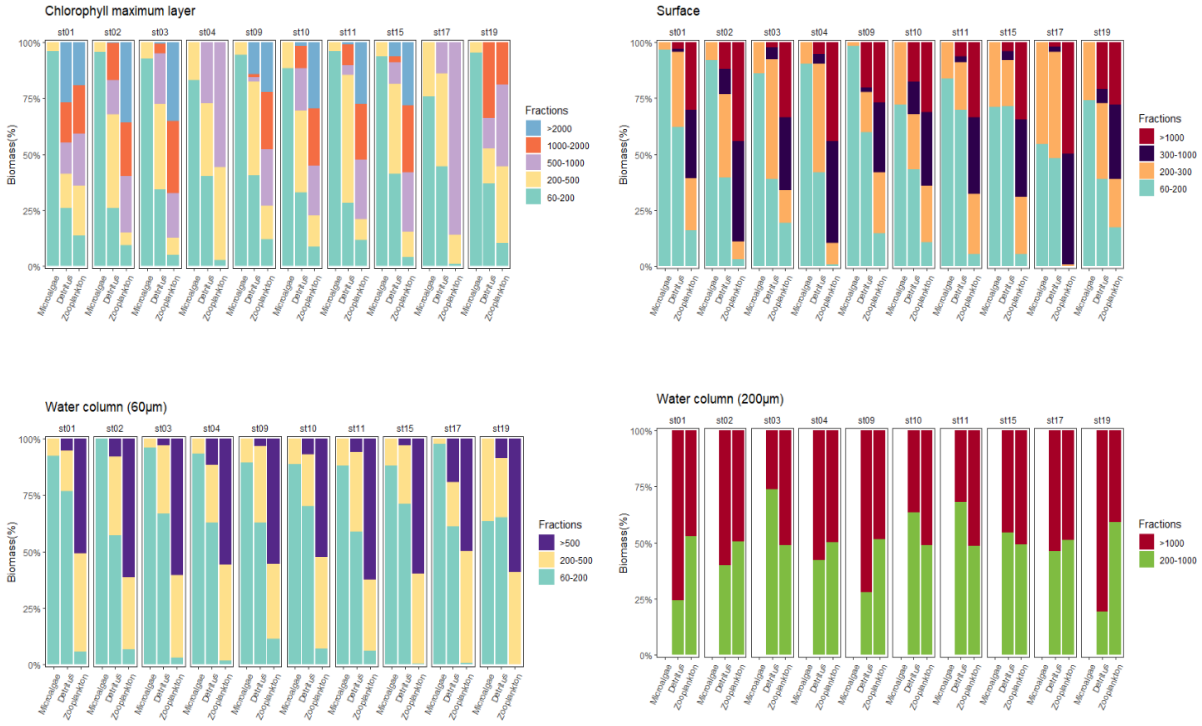
CHANGE DEPENDING ON THE EXPERIMENT 1m 5m o 10m

```
   saveas(h,["Figures5m_1degC/" filename], «png «); #saves the figures in a folder. Here I change it t
o Figures5m so that the other figures remain in another one. If you want to test with 10 m you chang
e Figures10m up there.

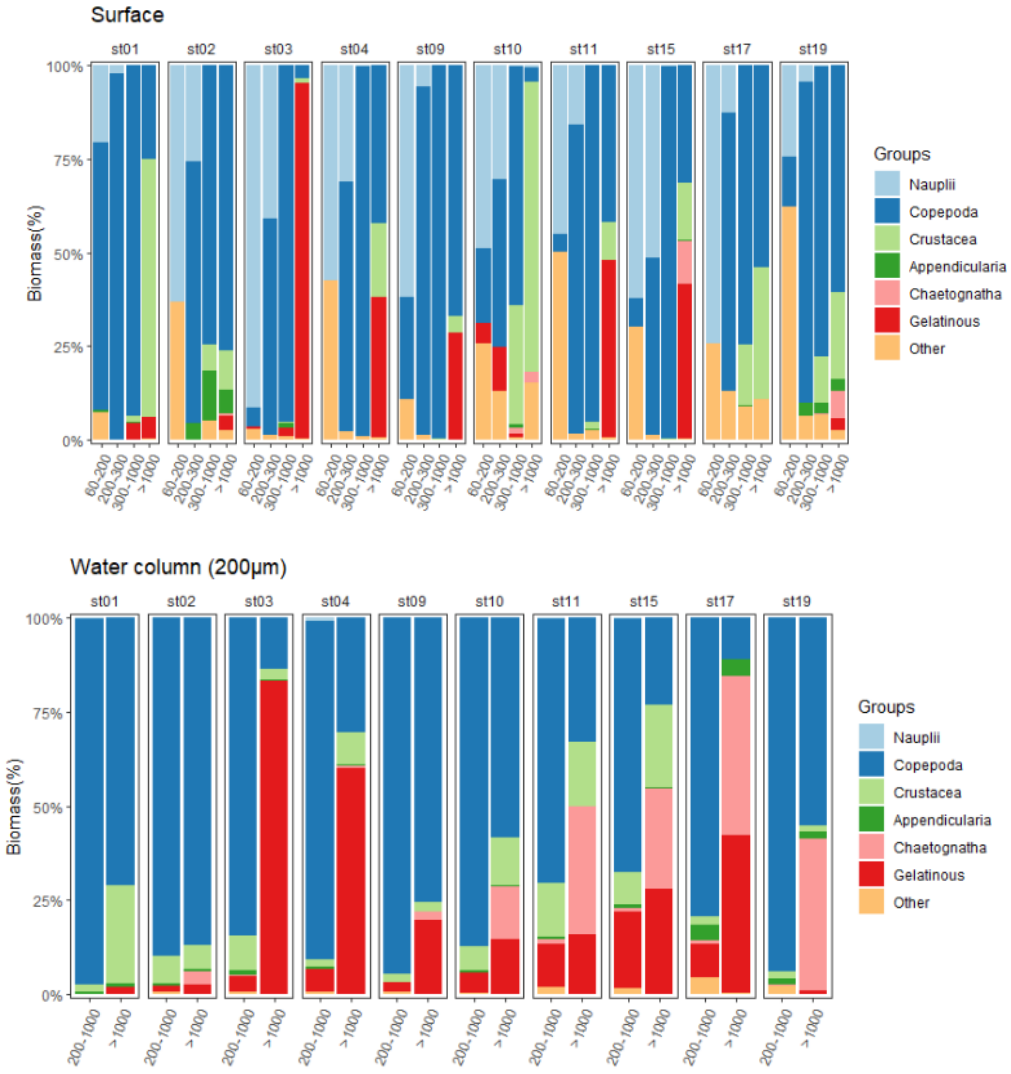
   MLD(:,i)=mld; # saves each value in order of excel slides... i.e. first value corresponds to
   slide 1, second value to slide 2, so on and so forth.
end
```

Annexes for Chapter 3

Annex 3.1. MERITE-HIPPOCAMPE cruise. Cumulative percentages of biomass across size fractions (Detritus, Microalgae, and Zooplankton) were calculated for the CML (using a 60 µm mesh-size net), Surface (using a 60 µm mesh-size net), and Water column (utilizing both 60 µm and 200 µm mesh-size nets).



Annex 3.2. MERITE-HIPPOCAMPE cruise. Cumulated percentages of zooplankton taxa biomasses, in different size fractions for Surface (mesh-size net 60 µm, 5 size-fractions considered) and Water column (mesh-size net 200 µm, 2 size-fractions considered)



Annex 3.3. MERITE-HIPPOCAMPE cruise. Daily zooplankton carbon demand (ZCD), the corresponding percentage of grazed phytoplankton, and contribution of size fractions and of taxa to the ZCD (in %) in the CML and in COL-60 for the different stations sampled.

	St01	St02	St03	St04	St09	St10	St11	St15	St17	St19
Chlorophyll Maximum Layer										
ZCD (mg C m^{-3} d^{-1})	6.48	1.24	0.91	2.20	4.33	0.60	1.12	1.33	1.43	6.88
% phytoplankton stock day^{-1}	22.3	2.8	4.7	6.6	6.3	4.3	14.5	6.8	34.6	31.9
% per Fraction										
60-200	27.2	22.6	4.7	17.6	39.4	27.1	20.8	9.8	10.8	17.2
200-500	64.0	18.1	6.8	62.1	49.5	39.7	19.3	37.4	81.1	66.7
500-1000	6.7	54.4	20.1	20.3	10.6	24.0	45.2	47.7	8.1	16.0
1000-2000	1.8	2.4	33.9	ND	0.4	8.8	14.1	2.2	ND	0.0
>2000	0.3	2.4	34.5	ND	0.1	0.4	0.6	2.8	ND	ND
% per Taxa										
Nauplii	15.2	13.6	8.1	10.7	39.6	15.0	9.5	7.9	29.3	6.1
Copepods	81.7	52.1	66.8	36.6	58.5	79.7	61.6	48.4	66.8	70.5
Crustaceans	2.0	25.4	13.7	46.9	0.1	1.9	18.8	34.5	0.7	1.5
Chaetognaths	0.1	0.5	0.0	0.0	0.0	1.3	5.8	3.8	0.0	0.0
Appendicularians	0.0	0.0	0.0	1.3	0.1	0.0	0.0	0.0	0.0	0.0
Gelatinous	0.1	3.2	6.1	0.1	0.1	0.4	0.9	0.5	0.0	0.0
Miscellaneous	0.9	5.3	5.4	4.5	1.6	1.7	3.4	4.8	3.2	21.9
Water Column										
ZCD (mg C m^{-3} d^{-1})	0.56	2.25	1.15	2.25	0.87	2.10	1.37	0.84	0.54	4.96
% phytoplankton stock day^{-1}	3.2	9.9	13.0	9.0	5.0	48.9	29.6	12.8	20.1	47.5
% per Fraction										
60-200	8.8	22.6	7.6	1.9	11.3	4.0	15.1	30.0	14.9	5.7
200-500	35.7	54.0	42.6	64.8	64.1	62.5	30.5	70.0	71.5	13.2
>500	55.5	23.3	49.9	33.3	24.7	33.5	54.3	0.0	13.6	81.1
% per Taxa										
Nauplii	4.0	10.3	5.7	3.1	8.6	5.6	7.1	21.1	13.1	2.3
Copepods	90.1	84.4	62.7	87.0	88.3	84.4	73.2	36.1	71.2	86.9
Crustaceans	3.8	2.0	5.3	1.5	0.4	3.3	4.3	6.0	0.2	3.1
Chaetognaths	0.0	0.0	1.7	0.1	0.0	3.8	9.3	0.0	3.7	4.5
Appendicularians	0.6	0.9	1.3	1.4	0.2	0.5	0.7	1.9	4.8	1.5
Gelatinous	0.1	1.1	18.4	6.1	0.6	1.7	2.9	28.5	1.6	0.0
Miscellaneous	1.4	1.3	4.9	0.9	1.9	0.8	2.5	6.5	5.4	1.7

Annex 3.4. MERITE-HIPPOCAMPE cruise.Zooplankton nitrogen excretion and percentage contribution of size fractions and of taxa to this excretion at the chlorophyll maximum layer (60µm Hydro-Bios sampling) and over the water column (60 µm-Vertical net sampling) of the different stations sampled.

	St01	St02	St03	St04	St09	St10	St11	St15	St17	St19
Chlorophyll Maximum Layer										
Nitrogen Excretion (µgN m^{-3} d^{-1})	416	72	55	130	246	44	83	89	120	447
%DIN stock day^{-1}	28.8	0.4	0.2	1.1	1.8	0.4	8.5	0.8	19.6	12.7
% per Fraction										
60-200	29.5	25.5	6.1	20.8	43.2	29.3	23.1	11.1	11.4	19.6
200-500	62.6	18.8	8.1	59.9	47.3	40.0	20.4	39.3	81.0	65.7
500-1000	6.1	52.1	22.0	19.4	9.1	22.6	42.2	45.3	7.6	14.6
1000-2000	1.5	2.0	32.2	ND	0.3	7.7	13.8	1.9	ND	0.0
>2000	0.2	1.6	31.6	ND	0.1	0.3	0.6	2.4	ND	ND
% per Taxa										
Nauplii	16.9	16.9	9.3	12.2	43.4	16.2	10.7	9.3	29.4	6.7
Copepods	80.2	56.1	69.5	39.2	54.4	78.8	62.2	49.5	66.7	67.3
Crustaceans	1.7	19.3	10.7	41.7	0.1	1.7	17.4	31.5	0.6	1.4
Chaetognaths	0.0	0.5	0.0	0.0	0.0	1.1	5.4	3.5	0.0	0.0
Appendicularians	0.0	0.0	0.0	1.3	0.1	0.0	0.0	0.0	0.0	0.0
Gelatinous	0.1	2.7	5.2	0.1	0.1	0.3	0.9	0.5	0.0	0.0
Miscellaneous	1.1	4.4	5.3	5.5	1.9	1.9	3.4	5.7	3.2	24.6
Water Column										
Nitrogen Excretion (µgN m^{-3} d^{-1})	38	153	88	144	62	179	115	68	47	339
%DIN stock day^{-1}	3.5	1.6	0.6	1.2	0.5	3.2	8.8	1.4	5.0	18.0
% per Fraction										
60-200	9.9	24.0	8.4	2.2	12.3	4.2	16.2	32.0	15.8	7.1
200-500	35.9	53.9	44.1	65.6	64.5	63.0	30.9	68.0	71.0	12.7
>500	54.1	22.1	47.5	32.2	23.2	32.8	52.9	0.0	13.3	80.2
% per Taxa										
Nauplii	4.6	11.1	6.3	3.5	9.3	5.8	7.7	22.3	13.8	2.9
Copepods	89.7	83.6	63.9	86.7	87.5	84.8	73.4	35.1	70.4	86.3
Crustaceans	3.6	1.8	5.0	1.5	0.4	3.2	4.2	5.7	0.2	2.9
Chaetognaths	0.0	0.0	1.6	0.1	0.0	3.4	8.6	0.0	3.5	4.1
Appendicularians	0.6	0.9	1.4	1.5	0.2	0.5	0.7	1.9	4.9	1.6
Gelatinous	0.1	1.1	17.1	5.9	0.5	1.6	2.9	27.9	1.6	0.0
Miscellaneous	1.5	1.4	4.6	1.0	2.1	0.8	2.5	7.1	5.6	2.2

Annex 3.5. MERITE-HIPPOCAMPE cruise. Zooplankton Phosphorous excretion and percentage contribution of size fractions and of taxa to this excretion at the chlorophyll maximum layer (60µm Hydro-Bios sampling) and over the water column (60 µm-Vertical net sampling) of the different stations.

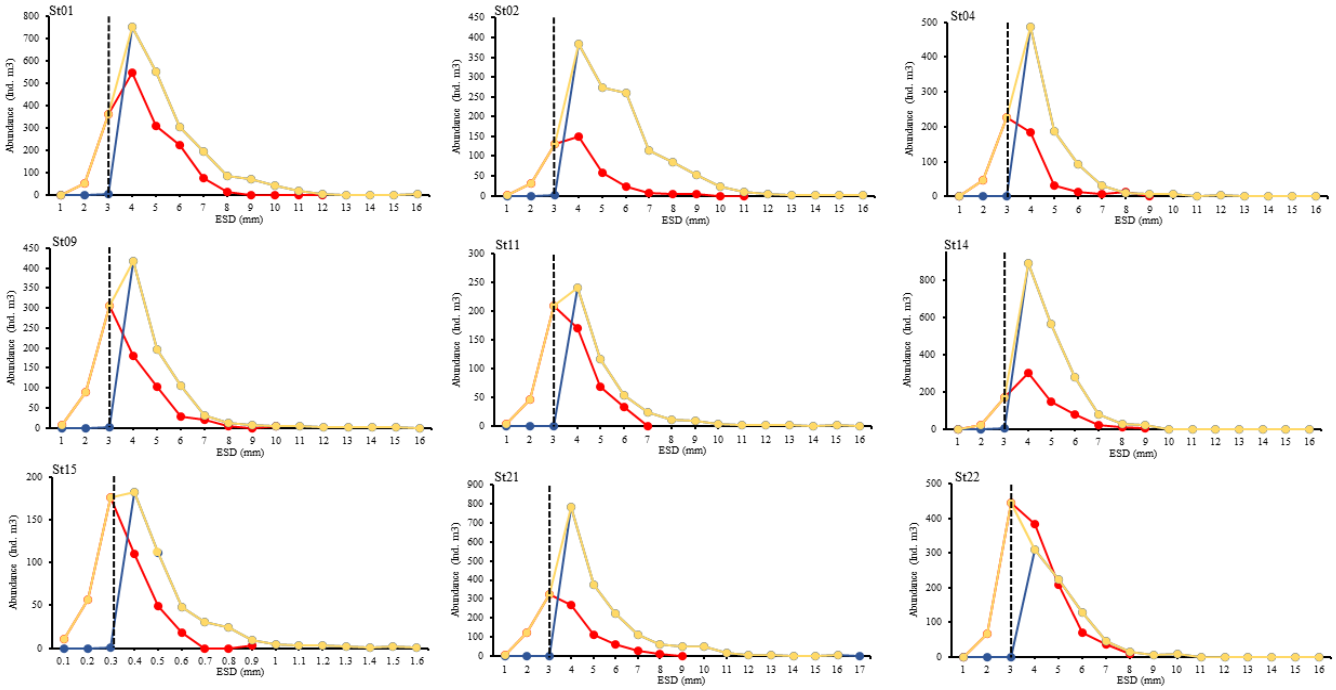
	St01	St02	St03	St04	St09	St10	St11	St15	St17	St19
Chlorophyll Maximum Layer										
Phosphorous Excretion (µgN m^{-3} d^{-1})	59.0	10.7	9.0	19.2	34.3	6.2	12.3	13.0	15.7	59.2
%DIP stock day^{-1}	20.7	1.3	0.1	1.7	4.3	0.2	1.2	0.6	1.2	0.3
% per Fraction										
60-200	27.7	23.4	4.9	18.3	40.6	27.1	20.5	9.9	10.4	17.6
200-500	63.8	18.4	7.0	61.6	48.9	39.9	19.2	37.8	81.3	66.7
500-1000	6.6	53.9	20.6	20.1	10.0	24.0	45.5	47.4	8.3	15.7
1000-2000	1.7	2.3	33.6	ND	0.3	8.7	14.2	2.1	ND	0.0
>2000	0.3	2.0	33.8	ND	0.1	0.4	0.6	2.7	ND	ND
% per Taxa										
Nauplii	15.5	14.7	8.1	11.0	40.9	14.9	9.3	8.0	29.2	6.2
Copepods	81.5	54.1	67.6	37.4	57.2	79.8	61.7	48.8	66.9	70.0
Crustaceans	1.9	22.7	13.0	45.5	0.1	1.9	19.0	34.0	0.7	1.5
Chaetognaths	0.1	0.5	0.0	0.0	0.0	1.3	5.9	3.8	0.0	0.0
Appendicularians	0.0	0.0	0.0	1.3	0.1	0.0	0.0	0.0	0.0	0.0
Gelatinous	0.1	3.0	5.9	0.1	0.1	0.4	0.9	0.5	0.0	0.0
Miscellaneous	0.9	4.9	5.3	4.7	1.7	1.7	3.3	4.8	3.2	22.3
Water Column										
Phosphorous Excretion (µgN m^{-3} d^{-1})	5.6	22.0	13.2	21.4	8.9	26.2	16.8	9.3	6.4	46.7
%DIP stock day^{-1}	1.1	1.9	0.2	2.2	0.2	0.9	1.1	0.7	0.4	0.4
% per Fraction										
60-200	8.9	22.8	7.3	1.9	11.2	3.8	14.4	29.2	14.0	5.6
200-500	35.8	54.1	42.4	65.0	64.2	62.2	30.4	70.8	72.1	13.1
>500	55.4	23.1	50.3	33.1	24.6	34.0	55.2	0.0	13.9	81.3
% per Taxa										
Nauplii	4.0	10.4	5.5	3.1	8.6	5.5	6.8	20.6	12.4	2.2
Copepods	90.1	84.3	62.6	87.0	88.3	84.2	73.2	36.4	72.0	87.1
Crustaceans	3.8	2.0	5.3	1.5	0.4	3.3	4.4	6.0	0.3	3.1
Chaetognaths	0.0	0.0	1.7	0.1	0.0	4.0	9.7	0.0	3.8	4.4
Appendicularians	0.6	0.9	1.3	1.4	0.2	0.5	0.7	1.9	4.8	1.5
Gelatinous	0.1	1.1	18.6	6.0	0.6	1.8	2.9	28.8	1.6	0.0
Miscellaneous	1.4	1.3	4.9	0.9	1.9	0.7	2.4	6.3	5.1	1.7

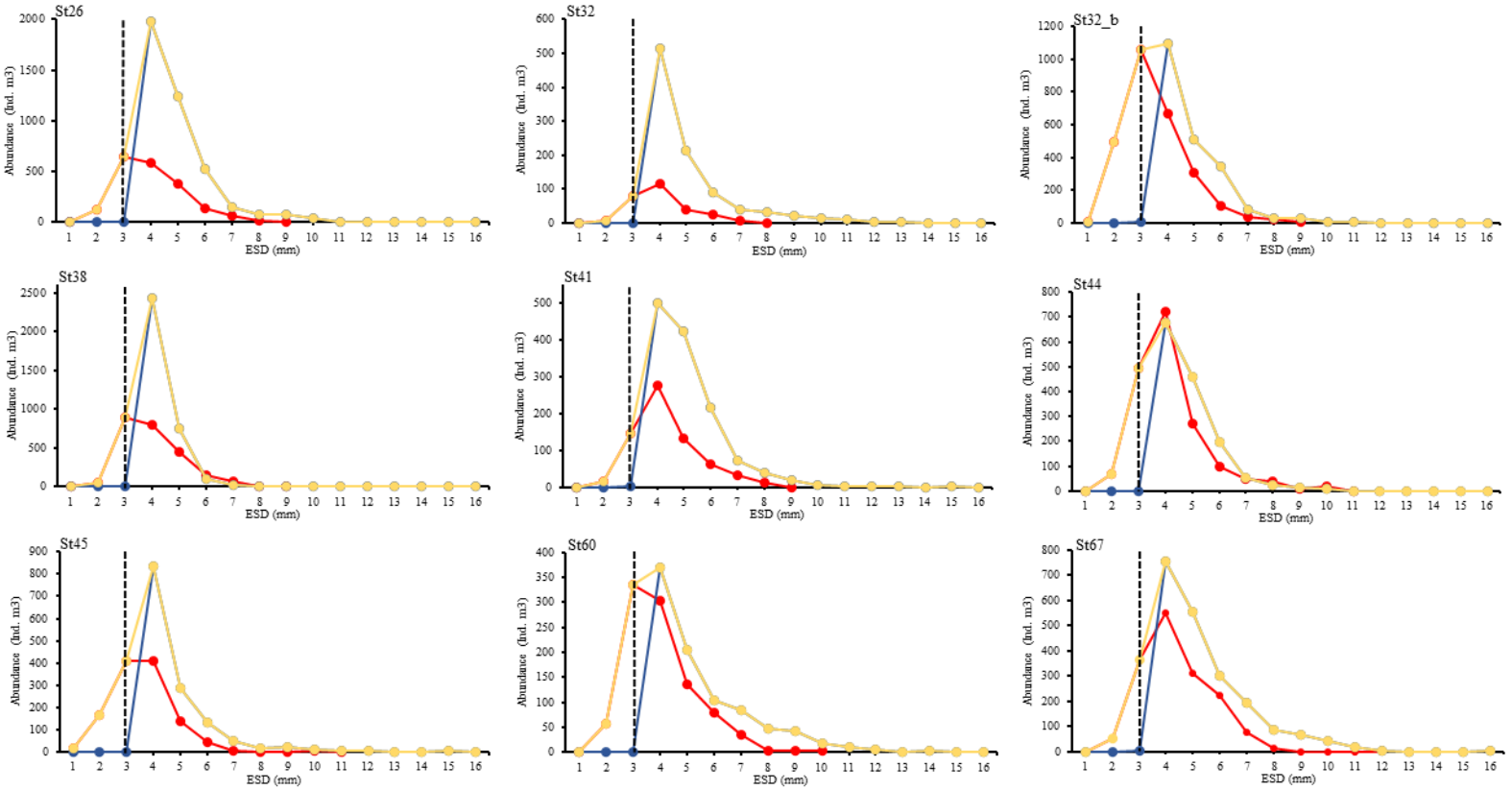
Annex 3.6. MERITE-HIPPOCAMPE cruise. Contributions in cumulated percentages of size-fractions and zooplankton taxa to the excretion rates in COL and CML.



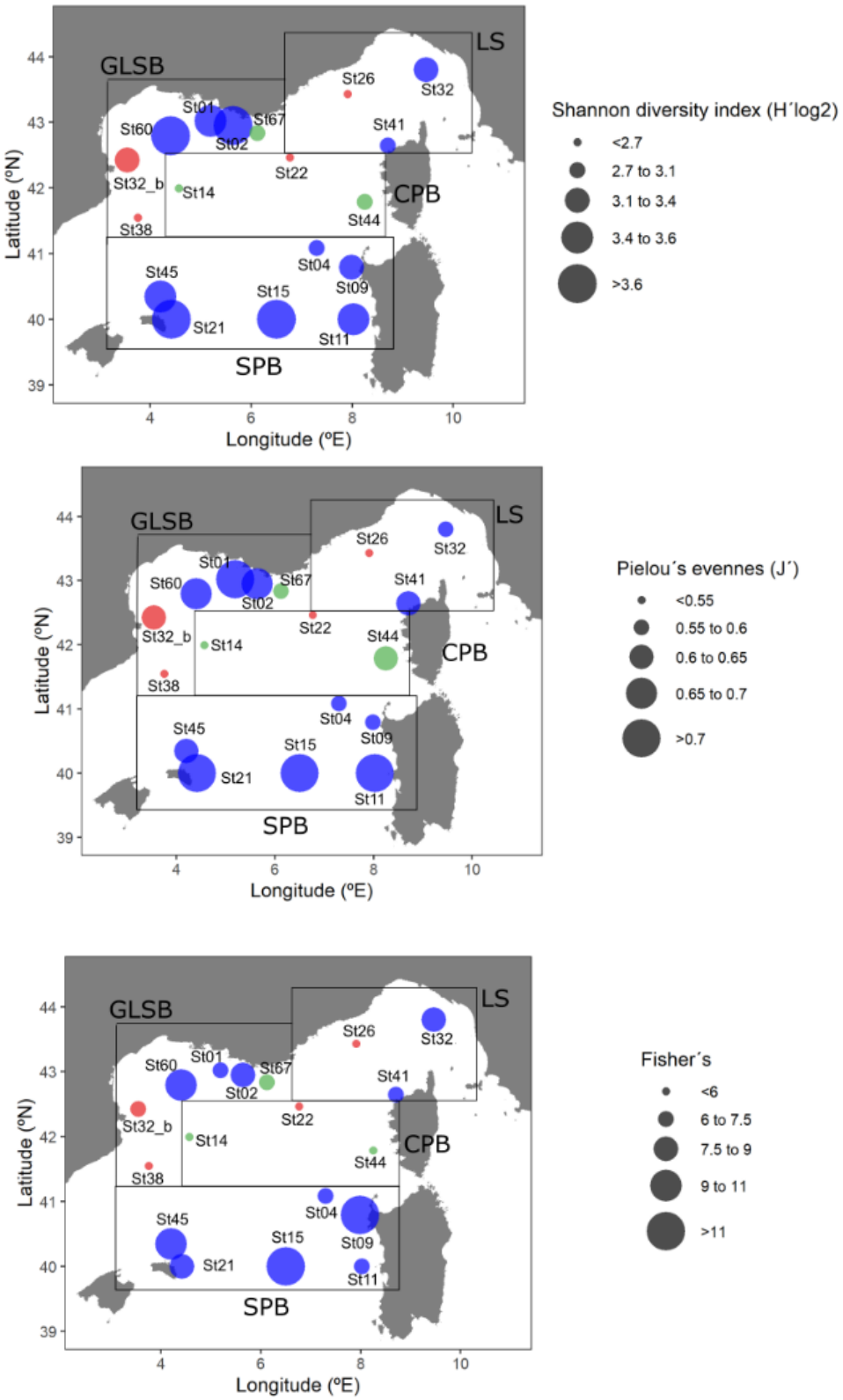
Annexes for Chapter 4

Annex 4.1. MOOSE-GE 19. Size class spectrum obtained by FlowCAM (represented in red) and ZOOSCAN (represented in blue) independently and the combination of FlowCAM < 300 µm of ESD and ZOOSCAN >300 µm of ESD (represented in yellow).

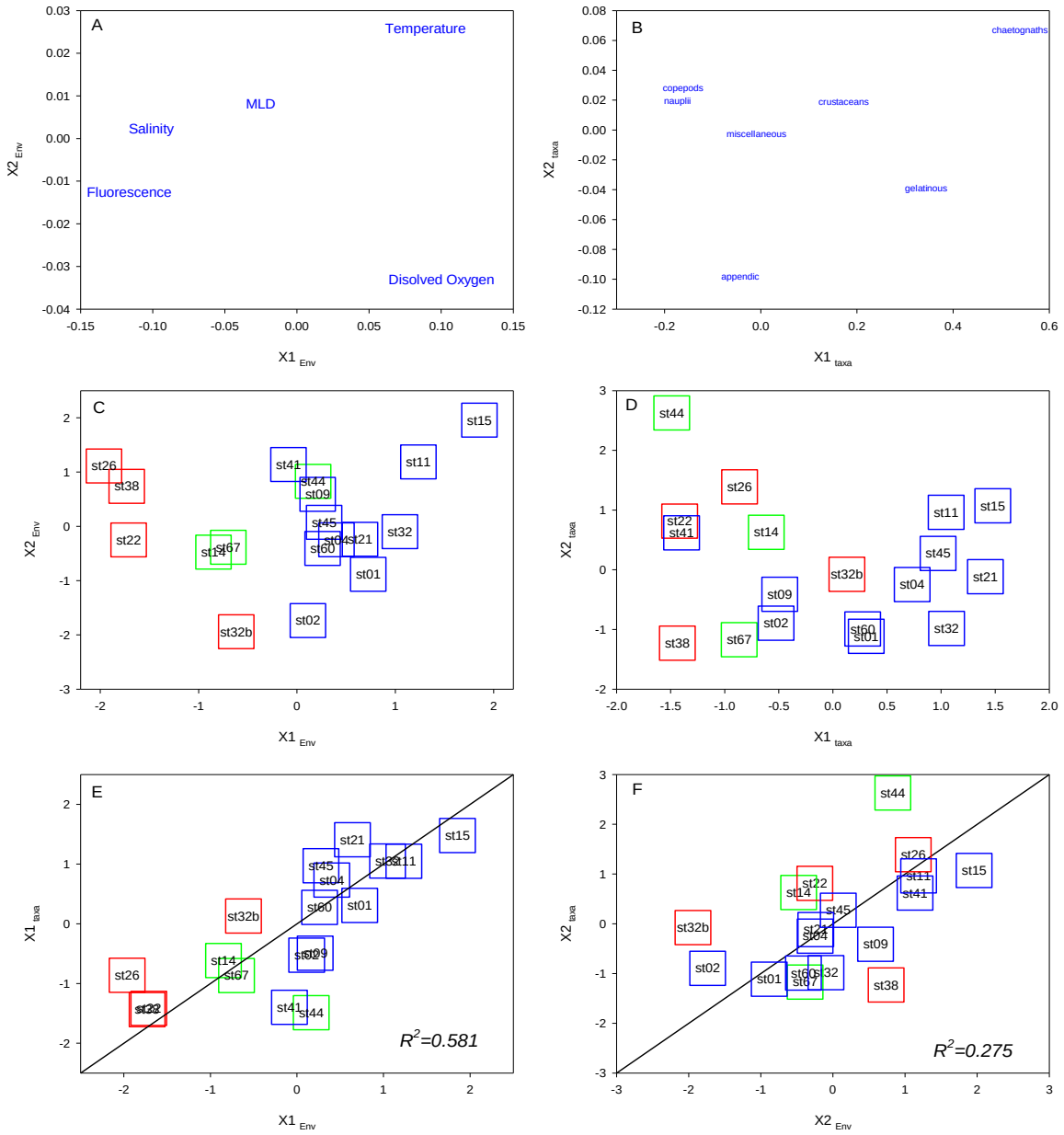



St26
St32
St32_b
St38
St41
St44
St45
St60
St67
Abundance (Ind. m3)
ESD (mm)

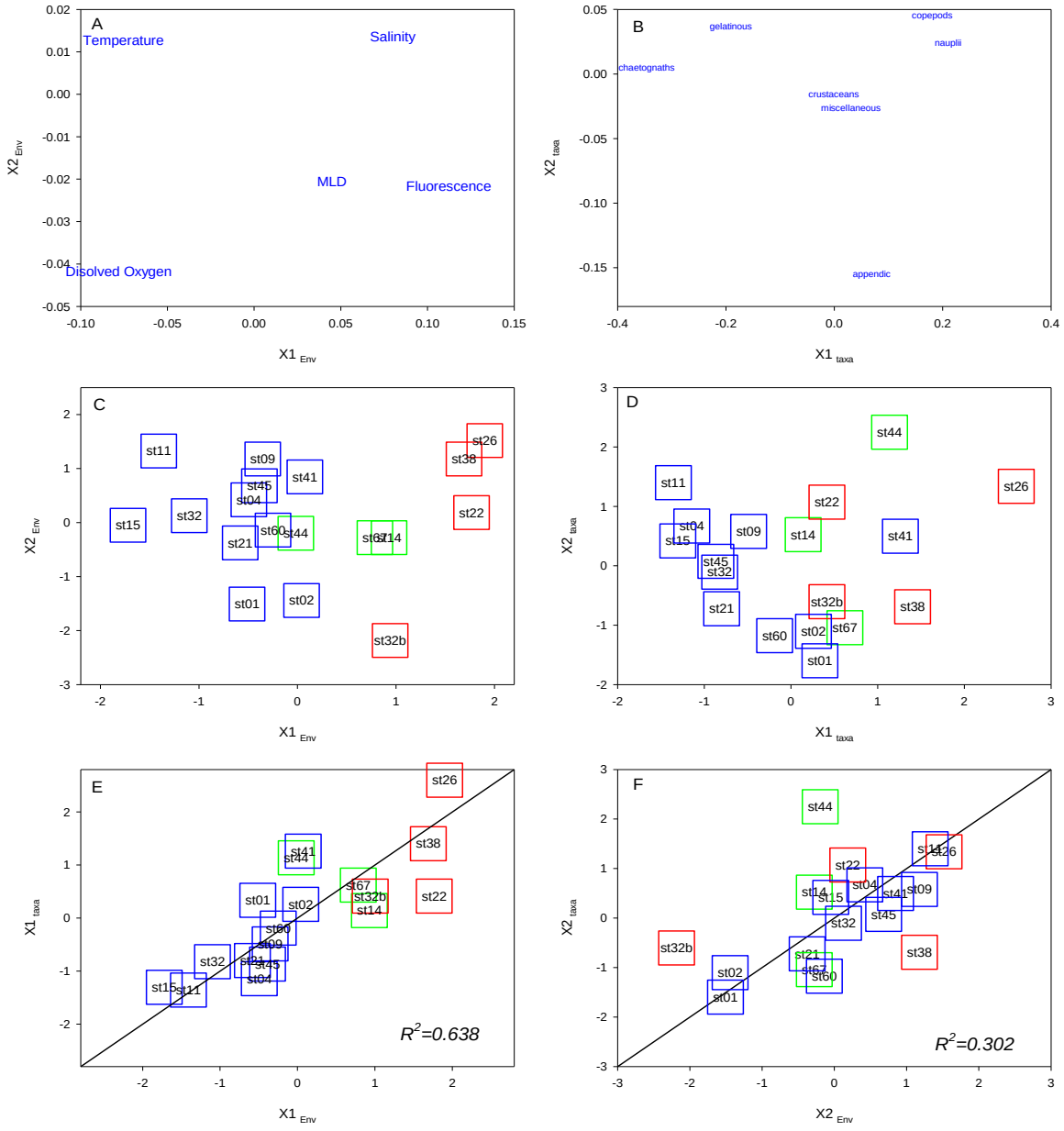
Annex 4.2. MOOSE-GE 19. Maps of various diversity index



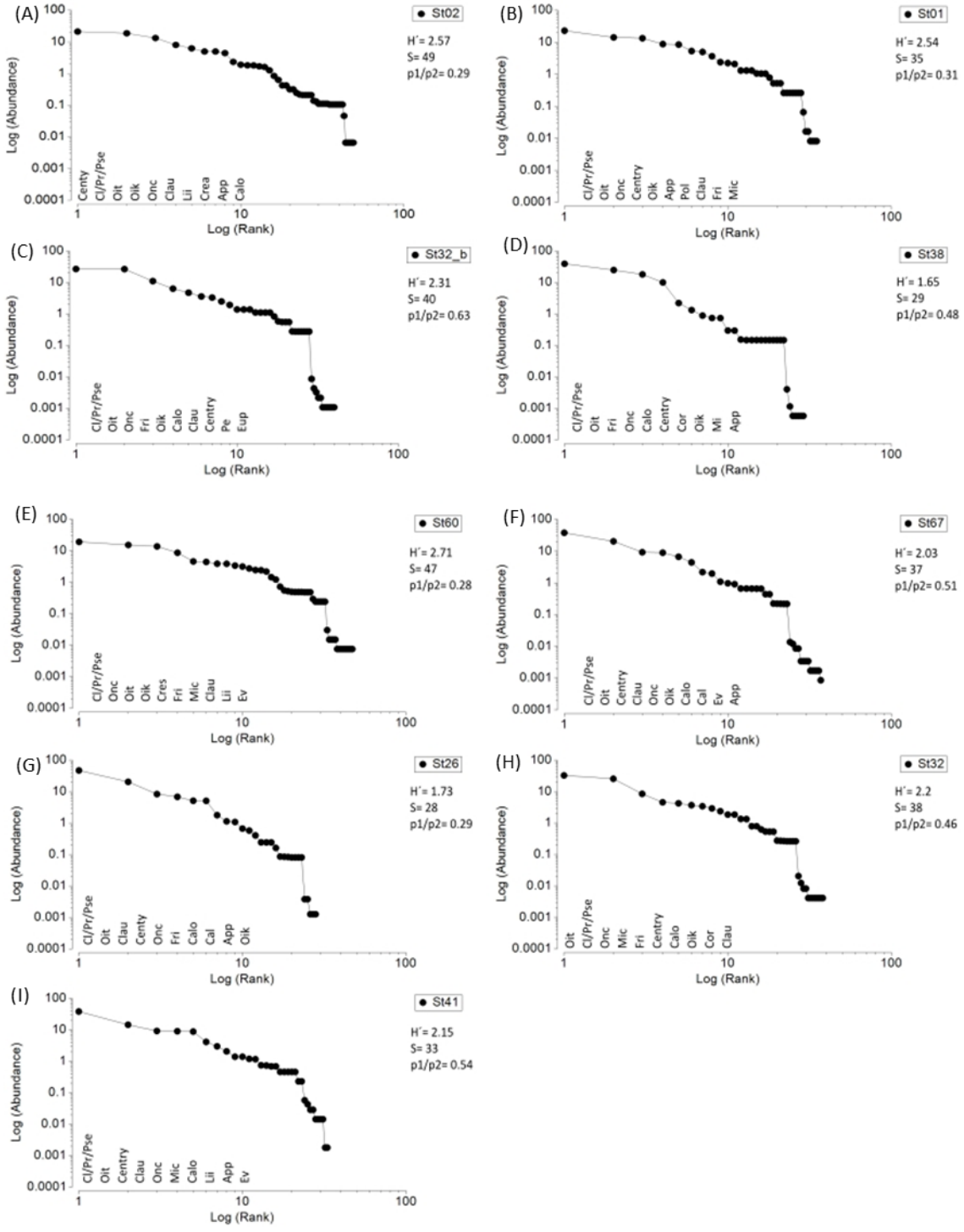
Annex 4.3. MOOSE-GE 19. Co-inertia analysis. Ordination on the plans (1, 2) of the environmental variables (A) and the abundance of the zooplankton taxa identified Imaging (Flowcam and Zooscan) (B) and of the stations in the "Environment system" (C) and in the "Zooplankton system" and plots of the stations on the first (C) and second (D) axes of the two systems. The line represents the equality between the coordinates on the two systems. Colored squares identify the different clusters.

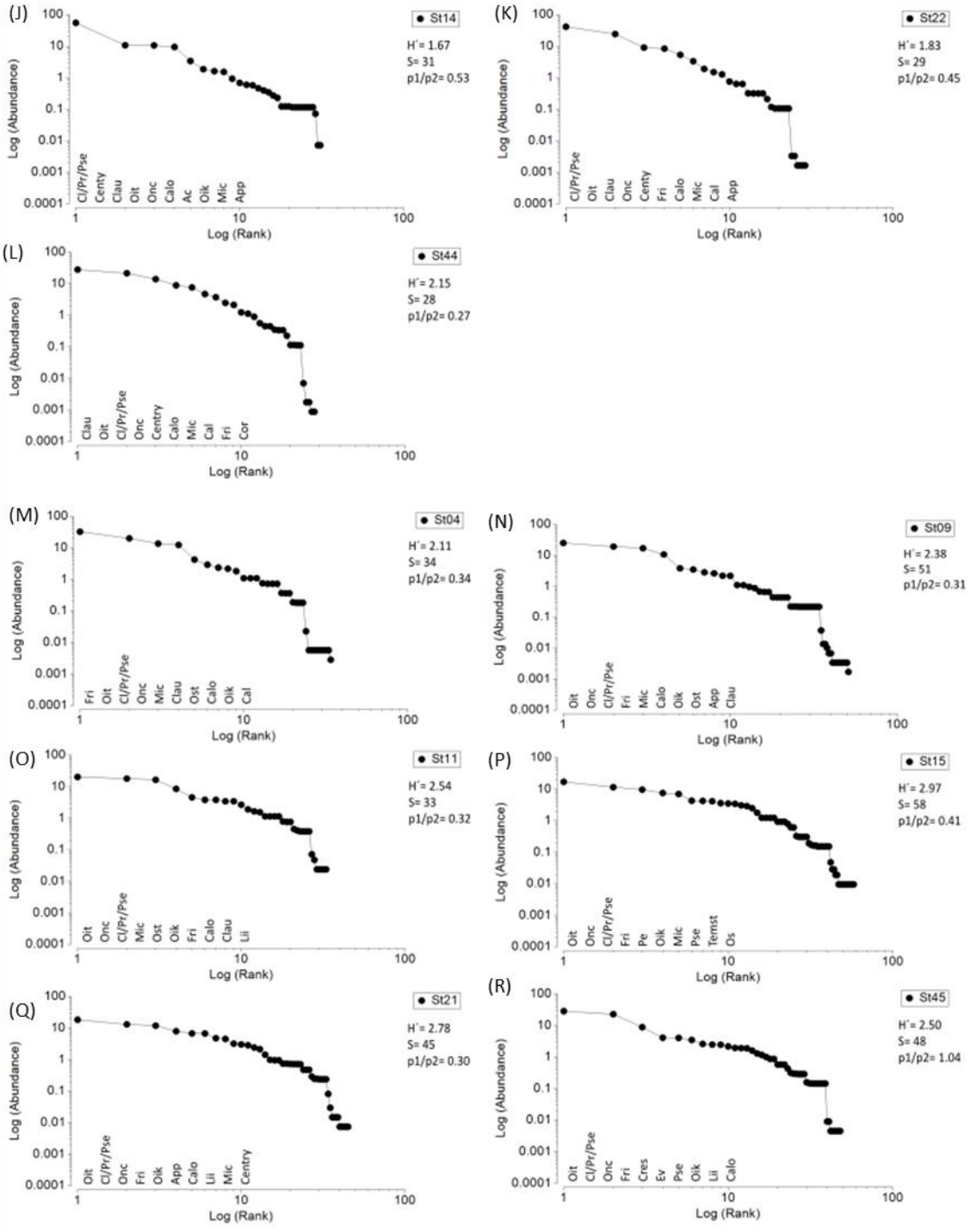


Annex 4.4. MOOSE-GE 19. Co-inertia analysis. Ordination on the plans (1, 2) of the environmental variables (A) and the biomass of the zooplankton taxa identified Imaging (Flowcam and Zooscan) (B) and of the stations in the “Environment system” (C) and in the “Zooplankton system” and plots of the stations on the first (C) and second (D) axes of the two systems. The line represents the equality between the coordinates on the two systems. Colored squares identify the different clusters.



Annex 4.5. MOOSE-GE 19. Rank frequency diagrams of the zooplankton community: A, B, C, D, E, and F correspond to GLSB region; G, H, and I correspond to LS region; J, K, and L correspond to CPB region; and M, N, O, P, Q, and R correspond to SPB region.




(J)
St14
H´= 1.67
S= 31
p1/p2= 0.53
Cl/Pr/Pse
Centy
Clau
Olt
Onc
Calo
Ac
Oik
Mic
App
(K)
St22
H´= 1.83
S= 29
p1/p2= 0.45
Cl/Pr/Pse
Olt
Clau
Onc
Centy
Fri
Calo
Mic
Cal
App
(L)
St44
H´= 2.15
S= 28
p1/p2= 0.27
Clau
Olt
Cl/Pr/Pse
Onc
Centry
Calo
Mic
Cal
Fri
Cor
(M)
St04
H´= 2.11
S= 34
p1/p2= 0.34
Fri
Olt
Cl/Pr/Pse
Onc
Mic
Clau
Ost
Calo
Oik
Cal
(N)
St09
H´= 2.38
S= 51
p1/p2= 0.31
Olt
Onc
Cl/Pr/Pse
Fri
Mic
Calo
Oik
Ost
App
Clau
(O)
St11
H´= 2.54
S= 33
p1/p2= 0.32
Olt
Onc
Cl/Pr/Pse
Mic
Ost
Oik
Fri
Calo
Clau
Lii
(P)
St15
H´= 2.97
S= 58
p1/p2= 0.41
Olt
Onc
Cl/Pr/Pse
Fri
Pe
Oik
Mic
Pse
Temst
Os
(Q)
St21
H´= 2.78
S= 45
p1/p2= 0.30
Olt
Cl/Pr/Pse
Onc
Fri
Oik
App
Calo
Lii
Mic
Centry
(R)
St45
H´= 2.50
S= 48
p1/p2= 1.04
Olt
Cl/Pr/Pse
Onc
Fri
Cres
Ev
Pse
Oik
Lii
Calo
Log (Abundance)
Log (Rank)

Annex : Publication

Marine Pollution Bulletin 193 (2023) 115056



Contents lists available at ScienceDirect

Marine Pollution Bulletin

journal homepage: www.elsevier.com/locate/marpolbul





Zooplankton biomass, size structure, and associated metabolic fluxes with focus on its roles at the chlorophyll maximum layer during the plankton-contaminant MERITE-HIPPOCAMPE cruise

Pamela Fierro-González [a], Marc Pagano [a], Loïc Guilloux [a], Nouha Makhlouf [a,b], Marc Tedetti [a], François Carlotti [a,*]

[a] Aix Marseille Univ, Université de Toulon, CNRS, IRD, MIO UM 110, 13288 Marseille, France
[b] Université de Carthage Faculté des Sciences de Bizerte, Zarzouna 7021, Tunisia

ARTICLE INFO

Keywords:
Zooplankton biomass
Zooplankton structure size and taxonomic groups
Metabolic fluxes
Vertical versus horizontal sampling
Mediterranean North-South transect

ABSTRACT

Recent studies have demonstrated that plankton can be a key pathway for the uptake and transfer of contaminants entering the marine environment up to top predators.

The plankton-contaminant MERITE-HIPPOCAMPE cruise was devoted to quantifying contaminants in water and the whole plankton size range (10 size fractions) at 10 stations along a north-south transect in the western Mediterranean Sea from the French to the Tunisian coasts through the Provençal and Algerian basins. Pumping and filtering devices and net sampling have been used for collecting very high amounts of small particles and planktonic organisms in the chlorophyll maximum layer (CML). The present paper characterizes the zooplankton components for which the contaminant measurements were carried out. At each station, a horizontal towed Hydro-Bios net with a 60 μm mesh-size net was used to discriminate 5 size-fractions from 60 μm to a few mm. For each size-fraction, one part of the sample was used for dry weight measurements and the other one for estimating the contribution to biomass of detritus, phytoplankton, and among zooplankton of the major taxonomic groups based on the imagery tools ZOOSCAN and FLOWCAM. In each zooplankton size fraction, metabolic rates were calculated from the size spectrum to estimate trophic and excretion fluxes flowing through this fraction. These observations were compared to a similar analysis of tows in the upper layer (vertical) and the surface layer (horizontal).

The total sampled biomass concentration at the CML was higher than in the water column (COL) and much higher than at the surface (SURF) in most of the stations, but in the CML and COL a substantial contribution was due to detritus mostly concentrated in the smallest size-fractions (60–200 μm and 200–500 μm). Absolute values of zooplankton biomass show neither a clear spatial pattern nor a significant difference between strata. The CML layer was dominated by copepods similarly to COL and SURF, but presented a higher contribution of nauplii and a near absence of appendicularians. At some stations, crustaceans and gelatinous plankton could be important contributors to CML. The zooplankton biomass composition of the two smallest fractions (<500 μm) was dominated by nauplii, small copepods and, occasionally, by small miscellaneous organisms (mostly pteropodes). In contrast, clear differences between stations appeared for the largest fractions (>500 μm) due to large crustaceans, gelatinous organisms, and chaetognaths. These changes in biomass composition according to size fractions suggest a progressive trophic shift from dominant herbivory in the smallest fractions to more contrasted trophic structure (including carnivory) in the largest fractions.

The daily carbon demand and the N and P excretion of zooplankton were on average higher at the CML but with no significant difference with COL. The zooplankton grazing represented 2.7 to 22.7 % of the phytoplankton stock per day, whereas its excretion represented a daily N and P recycling compared to dissolved inorganic nitrogen and phosphorus stocks ranging respectively from 0.2 to 19 % and from 0 to 21 %. This information should help in the interpretation of the content of various contaminants in zooplankton fractions.

* Corresponding author.
E-mail address: francois.carlotti@mio.osupytheas.fr (F. Carlotti).

https://doi.org/10.1016/j.marpolbul.2023.115056
Received 4 October 2022; Received in revised form 29 March 2023; Accepted 9 May 2023
0025-326X/© 2023 Elsevier Ltd. All rights reserved.

1. Introduction

Organic and metallic contamination levels have been monitored at alarming levels in large marine vertebrates (fish, mammals) in many regions and for several decades (Das et al., 2002; Van der Oost et al., 2003; Weijs et al., 2014; Khairy et al., 2021). However, it is only recently that measurements of contaminants have become available in the surrounding environment and in the prey of these organisms, and have proven to be necessary for understanding the processes of contaminant accumulation in bottom-up food webs (Weijs et al., 2014). Several recent studies have demonstrated that plankton can be a key pathway for the uptake and transfer of contaminants entering the marine environment, playing a potential ecological role as the biological pump of contaminants (Tiano et al., 2014; Strady et al., 2015; Chouvelon et al., 2019). Trophic transfer models of contaminants underline the need for a better evaluation of transfer processes, particularly by trophic interactions, with a prerequisite being the availability of consistent data on contaminant content in successive trophic levels (Alekseenko et al., 2018). However, such studies are most often limited to a segment of the planktonic food-web for methodological reasons; to accurately measure these contaminant levels, large sample volumes are required and must enable distinction between different planktonic trophic levels. Pumping and filtering devices have been widely developed for collecting very high amounts of small particles and planktonic organisms smaller than microplankton (phyto- and zoo-) based on size-fractionation (e.g. Wen et al., 2018). A recent integrated study in the Gulf of Lion dedicated to investigating sardine and anchovy contamination (COSTAS) has extended this size fraction approach to the meso- and macro-zooplankton categories of net-collected organisms (Tiano et al., 2014; Chouvelon et al., 2019), giving an adequate fractional resolution for tracing contaminants in the planktonic network.

It is therefore important to further develop approaches that collect large plankton biomass in the same water bodies and that sort these biomasses by size fractions across the whole planktonic size range. The aim of the MERMEX MERITE program was to improve and test different approaches of collection/size fractionation of plankton biomasses in coastal areas (Bay of Toulon, Bay of Marseille, Gulf of Gabès), before defining a global protocol to be used along a north-south transect in the Mediterranean Sea, from the French coast to the Tunisian coast, passing offshore of Corsica and Sardinia: the MERITE HIPPOCAMPE campaign (Tedetti et al., 2023). The campaign consisted of sampling large volumes of water and seston including plankton for measuring a large spectrum of organic and metallic contaminants (see details of survey strategy in Tedetti et al., 2023). For the 10 stations investigated, the samples were collected in one common layer in the water column, the chlorophyll maximum layer (CML), assumed to be the layer with the highest concentrations of plankton (mainly phytoplankton, but supposed to be attractive for zooplankton). Sampling was done using pumping systems (McLane pumps) and a horizontal towed Hydro-Bios net with 60 μm mesh-size net allowing discrimination up to 5 size-fractions between 0.2 and 60 μm and 5 size-fractions between 60 μm and a few mm (see details of methodology in Tedetti et al., 2023).

The aim of the present paper is to characterize the zooplankton components (from 60 μm to a few mm) in the different fractions of the samples collected at the CML of each station for which the contaminant measurements were carried out. For each size-fraction, the contribution to the biomass of detritus, of phytoplankton, and among zooplankton of the major taxonomic groups has been quantified. Metabolic rates calculated from the size spectrum of each zooplanktonic size fraction enable estimation of trophic and excretion fluxes flowing through this size fraction. To assess whether the contribution of taxonomic groups to the zooplankton biomass in the CML reveals a particular niche or not, it is compared to similar analyses carried out on vertical features in the epipelagic zone (200 m depth or bottom to surface).

2. Material and methods

2.1. Study area and sampling strategy

The MERITE-HIPPOCAMPE cruise was carried out between 13 April and 14 May 2019, during the spring bloom, along a north-south transect in the western Mediterranean Sea, from the French coast (Toulon, Marseille) to the Tunisian coast (Gulf of Gabès) aboard the French Research Vessel *Antea* (Fig. 1). Ten stations were sampled during 2 legs. Five stations (St02, St04, St03, St10, and St11) from Toulon to Tunis during Leg 1 (second half of April), and five other stations (St15, St17, St19, St09, and St01) from Tunis to the south of the Gulf of Gabès and then on the way back to Toulon - La Seyne, during Leg 2 (first half of May). For each station, the date of sampling, the geographical position, the station depth, and the depth of different samples (CTD and net tows explained below) are presented in Table 1.

2.2. Environmental data

At each station, an oceanographic carousel equipped with a CTD Seabird SBE 911plus to measure the hydrological variables (temperature, density and salinity) was deployed down to 250 m for open-sea stations or near the bottom for shallower stations (see Table 1). In addition, the CTD was coupled with several sensors including chlorophyll-a fluorescence (Chla; Aqua Tracka, Chelsea ctg).

2.3. Zooplankton sampling and sample processing

Zooplankton samples were obtained using three different types of nets for different strata in the water column (Table 2). A Multiple Plankton Sampler (Midi type, Hydro-Bios) with a square aperture surface of 0.25 m^2 towed at a constant speed of around 2 knots was used for sampling horizontally at the depth of the CML (see sampling depth for each station in Table 1), with five successive shut-off nets of 60 μm mesh-size, each of them filtering a water volume of around 50 to 80 m^3 (estimated by automatic detection with internal and external flowmeters, and according to plankton load before clogging). A Manta net was used for surface sampling, with a rectangular aperture of 0.7 × 0.4 m, and a 60 μm mesh-size net, towed at a constant speed of 2 knots for 10

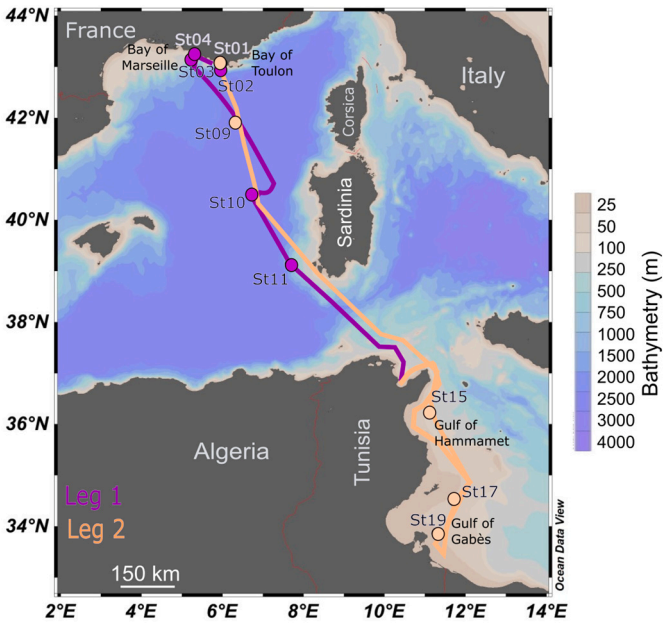


Fig. 1. Map of sampled stations during the two legs of the MERITE-HIPPOCAMPE cruise (13 April–14 May 2019) on board the RV *Antea*.

min.

A steel frame with three circles (triple-net), each with a 60 cm diameter opening, was towed vertically at a constant speed of 0.7 m/s through the water column from 200 m depth (or near the bottom) to the surface (see depth of vertical net lines for each station in Table 1). Three different mesh size nets - 60, 120 and 200 μm - were attached to the triple-net. The sample collected by the 120 μm net was not analyzed in this study, since the samples collected with the 60 and 200 μm nets provided a complete coverage of the zooplankton size spectrum. Moreover, the community observed within the 60 μm vertical net can be compared with the one collected at the DCM with the Hydrobios net.

For further zooplankton analysis (biomass imagery, and microscopy), the samples from the different nets were fractionated using stainless-steel sieves of different mesh-sizes. The fractionation scheme slightly differed between nets due to different scientific objectives (Table 2). The samples from Hydro-Bios were fractionated on board through a column of into five size fractions (60–200, 200–500, 500–1000, 1000–2000 and >2000 μm). These size-fractions were defined for studying contaminants and therefore large volumes (between 300 and 2400 m^3) were filtered in order to get enough plankton in all fractions to measure contaminants and other parameters (Tedetti et al., 2023). Around 10 % of each of these fractions were kept for zooplankton analysis (NB: however, at a few stations, not enough plankton material was recovered for the largest fractions, i.e. stations 04, 17 and 19). Then, they were split into two sub-samples: one kept at −20 °C for further dry biomass weighing (mg DW m^{-3}), and the other one preserved in 4 % borax-buffered formalin for imagery treatment. The protocol of fractions for Manta nets was imposed for a comparison with a classical 300 μm mesh-size Manta net deployed in parallel (EU-MSFD protocols, results not presented in this paper). Thus, two fractions (below and above 300 μm) were considered for weighing, and then sub-fractionating was done for imagery analysis, allowing comparisons with Hydro-Bios samples. For the 60 μm mesh-size vertical net, only the lowest three size fractions common with those of Hydro-Bios were considered (because the plankton content was generally low). However, larger fractions were observed in the 200 μm mesh size net. Sub-samples of each fraction from the Manta net and vertical nets were preserved in a similar way as for Hydro-Bios samples and for similar analysis (see Table 2).

2.4. Zooplankton imagery treatment

Sample fractions below 500 μm were processed using a FlowCAM (see Table 2; Yokogawa Fluid Imaging Technologies Inc. Series VS-IV benchtop model (Sieracki et al., 1998). The other fractions were treated using a ZOOSCAN (Gorsky et al., 2010). For both imagery sample treatments (FlowCam and Zooscan), the analyses were done following the protocol described by Feliú et al. (2020). Distinct biological components and particles were differentiated: microalgae (eukaryotic microalgae and prokaryotic cyanobacteria) and non-living detritus material (marine snow, aggregates), and several living taxonomic groups of zooplankton: nauplii, copepods, crustaceans, appendicularians, gelatinous organisms, chaetognaths, and other diverse zooplankton groups (including molluscs, polychaetes, and rare protozoans) gathered in one group named 'miscellaneous' below. For each category, the abundance of organisms (ind m^{-3}) or particles (nb m^{-3}), and their area (mm^2) and biovolume (mm^3) were provided.

2.5. Biomass measurements and derived carbon demand, respiration, and excretion by zooplankton

In the laboratory, dry-weight biomasses were determined after drying samples on pre-weighed GF/F filters (60 °C, 24 h) and then re-weighed with a microbalance (Mettler, precision 0.1 mg) according to the protocol established by Lovegrove (1966). The contributions of zooplankton, detritus, and microalgae components to the total weighed biomass were estimated by using for zooplankton individuals the relationships from Lehette and Hernández-León (2009) between body-area and body-weight, and for detritus and microalgae particles the biovolume-weight relationships from Alldredge (1998). Zooplankton biomass was converted into carbon assuming the carbon/dry-weight ratios given by Gorsky et al. (1988) for Mediterranean zooplankton taxa.

The zooplankton carbon demand (ZCD, in mg C m^{-3} d^{-1}), respiration rates and ammonium and phosphorus excretion rates (both in μmol L^{-1} d^{-1}) were computed following the protocol described by Feliú et al. (2020), and based on allometric relationships to individual body-weight.

2.6. Data analysis

A principal component analysis (PCA) was performed on the environmental parameters, including temperature, density, salinity, and chlorophyll concentration (from in situ fluorescence measurements). For the spatial patterns of zooplankton communities, a taxonomic group–station matrix was created using the biomass values; this was square-root transformed to estimate Bray–Curtis similarity distances. The similarity matrix was then ordinated using non-metric multidimensional scaling (NMDS). These two analyses were performed using PRIMER v7 software (Anderson et al., 2008).

We tested for significant differences in biomasses (total, size fractions, and taxa groups) using Student's *t*-tests between samples of the two vertical nets of the whole water column with mesh-size of 60 and 200 μm, and between samples of the whole water column (COL-60) and from CML. Data were first verified for normality using the Kolmogrow-Smirnov test and for homogeneity of variance using a Fisher F-test. Mann Whitney *U* test was used to compare the grazing pressure of zooplankton between areas.

Below, CML, SURF, COL refer to the three different strata sampled with nets, respectively, the chlorophyll maximum layer, the surface layer, and the integrated water column layer. COL-60 and COL-200 refer to the mesh-size nets of 60 and 200 μm used for the integrated water column tow.

Table 1
Stations sampled during the MERITE-HIPPOCAMPE cruise: date, geographical position, bottom depths, maximum depths of CTD cast and of vertical triple net tow, and depth of horizontal Hydro-Bios net tow.

Station	Date	Latitude (N)	Longitude (E)	Bottom depth (m)	Depth of CTD cast (m)	Depth Triple vertical net (m)	Depth Hydro-Bios net (m)
st01	11-05-2019	43°04.398	5°58.838	91	88	80	24
st02	15-04-2019	42°56.009	5°57.739	1770	250	210	31
st03	20-04-2019	43°08.823	5°14.199	95	100	85	55
st04	16-04-2019	43°14.876	5°19.001	58	50	48	35
st09	09-05-2019	41°54.661	6°20.163	2575	250	200	20
st10	24-04-2019	40°23.251	7°11.034	2791	250	180	40
st11	25-04-2019	39°08.193	7°40.382	1378	250	182	35
st15	30-04-2019	36°12.164	11°08.057	100	95	80	68
st17	02-05-2019	34°30.118	11°43.593	48	48	39	37
st19	03-05-2019	33°51.226	11°20.165	50	50	42	39

3. Results

3.1. Spatial pattern of environmental variables

The first axis of the principal component analysis (PCA) on environmental variables (79.6 % of variability) correlated with changes of temperature and salinity separating the stations located north (St01 to St09) and south (St10 to St19) of the Balearic front. Stations St10 and St11 have intermediate positions with their temperature and salinity in COL (both stations) and CML (St10 only) being close to those of the northern stations, whereas temperature and salinity are close to those of the southern stations for SURF and CML of St11. The second axis (15.6 %) is correlated with chlorophyll and differentiates CML, SURF and COL values, more or less strong according to the stations, with the highest difference at St09 (Fig. 2).

In general, the temperature and salinity profiles did not show strong stratification of the water column during the cruise (see detailed profiles of oceanographic and biological variables presented in Fig. 4). Temperature values ranged from 14 to 17.8 °C at the surface (and very close values at CML), with the highest values recorded in the Gulf of Gabès.

In the southern basin, the coastal stations of Tunisia (St15, 17, and 19) and stations 10 and 11 presented salinity profiles below 38 (with the exception of St10, which had values higher than 38 below 79 m depth), whereas the northern stations were above 38 (with the exception of the first two meters of surface at St03). St09 presented the highest salinity in the northern basin and showed a strong contrast with St10, the nearest station in the southern basin. In general, the Chla vertical distribution presented a well-pronounced maximum at the CML, located near or above the bottom for most of the coastal stations (St19, 17, 15, and 03), or fluctuating in a more spread profile due to mixing (St01 and 04), St02 showing a typical Chl*a* peak at mid-water depth. Among the offshore stations, St09 presented the highest values of the campaign, distributed in a broad surface mixed layer with a maximum value at 20 m, whereas St10 and St11 presented a CML at 40–45 m although more prominent at St10.

3.2. Spatial patterns of plankton and detritus biomasses

NMDS analysis of the percentage of zooplankton taxa biomass reveals differences in compositions among strata for all stations. Some stations (St01, 02, 09, and 19) showed short distances between values of the three strata in the NMDS plot (Fig. 2b) and this corresponded to only small differences, among these strata, in biomass composition with high dominance of the copepods (Fig. 3a–d). Inversely, in the other stations (St03, 04, 10, 11, 15, and 17), wide differences between values of the three strata in the NMDS plot are related to the dominance of other taxonomic groups in one or two layers, e.g. importance of crustaceans at the CML at St03, 04, 11 and 15, or in SURF at St10 and 17, or dominance of gelatinous in COL at St15. From NMDS no clear regional patterns in zooplankton biomass composition appear, nor evident differences between coastal and off-shore stations, which would indicate for each station a local influence of hydrography and short-term meteorology on the biological biomass distribution.

The total sampled biomass was often higher at the CML than in COL-60 (St01, 02, 04, 09, 11, and 17), but in some cases, it was equivalent (St10, 15 and 17) or even lower (St03) and there was no significant difference between the mean values of the two strata (*t*-test; $p = 0.12$). Both strata showed higher values at the coastal stations (St01, 04, 17 and 19) than at the oceanic stations (St02, 09, 10, 11). SURF showed total biomass generally much lower (Fig. 3e–h) and significantly different than those recorded in COL or CML (paired *t*-test, $p = 0.035$ and 0.020, respectively). Detritus was almost absent in SURF (Fig. 3f) but represented a high proportion of the total sampled biomass in COL and CML, particularly in the shallowest southern (St17 and 19) and northern stations (St04 at the CML) (Fig. 3e and g). Microalgae were collected at the CML of almost all stations but always with very low biomass compared to detritus and zooplankton, except at some coastal stations (St01, 04, 17, and 19). They were very low in most COL samples, except at St17 and were almost absent in SURF. The absolute values of zooplankton biomass show neither a clear spatial pattern nor a significant difference (paired *t*-test, $p > 0.1$) between the mean values of the three sampled strata (Fig. 3e–h).

The comparison between the two vertical nets, the 60 μm (COL-60) (Fig. 3c and g) and the 200 μm (COL-200) (Fig. 3d and h) mesh-size nets, shows firstly that detritus and microalgae were collected almost exclusively by COL-60. In general, zooplankton biomass was of the same order for COL-60 and COL-200 (paired *t*-test; $p = 0.16$), but with some differences in percentages of taxa. Nauplii, copepods, crustaceans, and miscellaneous presented significant differences between the COL nets (paired *t*-test, $p < 0.05$), whereas no differences appeared for appendicularians, chaetognaths, and gelatinous organisms.

3.3. Zooplankton and detritus biomass in different layers at each station

St01 is a coastal station in the inner Bay of Toulon (Fig. 4a). The water column presents a light thermocline at 10 m and a homogeneous salinity over the 80 m profile. The fluorescence profile presents values of around 0.3 mg Chl*a* m^{-3} at the surface, a maximum of 0.59 mg Chl*a* m^{-3} at around 20 m (CML), and then a regular decrease down to the bottom. CML presents high values of zooplankton biomass (45.8 mg DW m^{-3}), almost twice the COL averaged biomass over 80 m (25.2 mg DW m^{-3}) and SURF biomass (19.7 mg DW m^{-3}). For detritus, the CML biomass is comparable to the COL biomass, whereas SURF biomass is weak. Microalgae were found at the CML. Zooplankton biomass was dominated by copepods and nauplii in the three strata, respectively 96, 92, and 78 % for CML, COL and SURF (Fig. 3a–c), and SURF differed by relatively high biomass of crustaceans and gelatinous organisms.

St02 is offshore of Toulon Bay (Fig. 4b). The water column presents

Table 2
Scheme of treatments of the various size-fractions from the 3 nets used during the MERITE-HIPPOCAMPE cruise.

Net type	Mesh-size (μm)	Size fractions (μm)	Weight	Size fractions (μm)	Imagery treatment
Hydro-Bios	60	>2000	Dry weight	>2000	Zooscan
		1000–2000	Dry weight	1000–2000	Zooscan
		500–1000	Dry weight	500–1000	Zooscan
		200–500	Dry weight	200–500	FlowCam
		60–200	Dry weight	60–200	FlowCam
Triple Vertical	200	>200	Dry weight	>1000	Zooscan
				200–1000	Zooscan
	60	>60	Dry weight	>500	Zooscan
				200–500	FlowCam
				60–200	FlowCam
Manta	60	>300	Dry weight	>1000	Zooscan
				300–1000	Zooscan
		60–300	Dry weight	200–300	FlowCam
				60–200	FlowCam

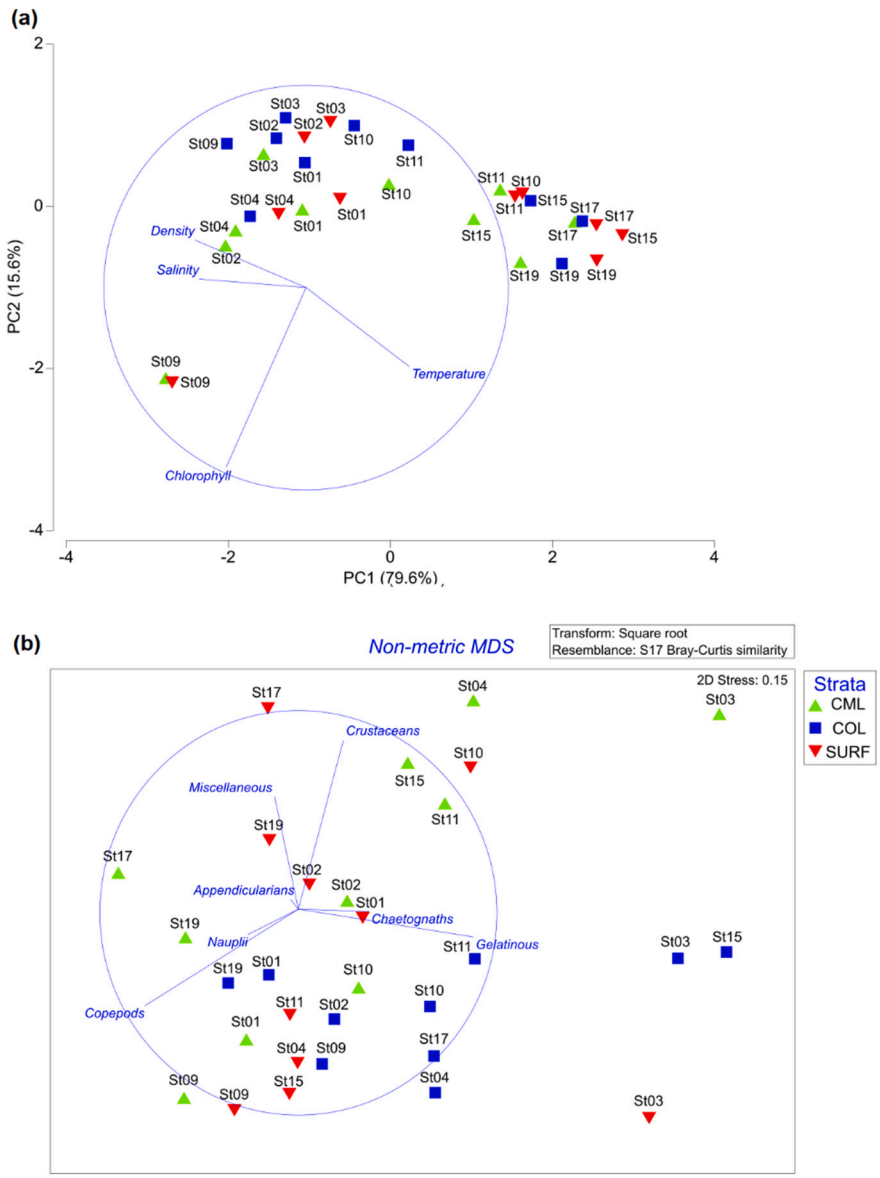


Fig. 2. (a) Principal component analysis (PCA) ordination of four environmental indicators: temperature, salinity, density and chlorophyll, and (b) Nonmetric Multi-Dimensional Scaling (NDMS) on zooplankton taxa relative biomass, for all sampled stations of the MERITE-HIPPOCAMPE cruise. Blue squares: Integrated water column values (COL) from the bottom depth (or 200 m depth) to the surface. Green triangles: values at the chlorophyll maximum layer (CML). Red triangles: values at the surface layer (SURF). (For interpretation of the references to color in this figure legend, the reader is referred to the web version of this article.)

almost homogenous temperature and salinity profiles. The fluorescence profile presents values around 0.2 mg Chl*a* m^{-3} at the surface and a maximum value of 0.93 mg Chla m^{-3} at 32 m (CML). Microalgae were found at CML only. For detritus, CML biomass is comparable to COL biomass (14.2 and 12.6 mg DW m^{-3}, respectively), whereas SURF biomass is weak (2.8 mg DW m^{-3}). The zooplankton biomass was twice as high at CML (10.4 mg DW m^{-3}) than in COL (5.5 mg DW m^{-3}) and three times higher than in SURF (3.5 mg DW m^{-3}). The contribution of zooplankton taxa differed between strata (Fig. 3a–c) with the highest percentage of crustaceans in CML (15 %), compared to SURF and COL (8 and 3 % respectively), and also in the case of appendicularians only present in SURF (10 %).

St03 is situated offshore of Marseille Bay, above the head of the Planier Canyon on the shelf break (Fig. 4c). The water column presents a homogeneous temperature profile, whereas salinity has low values at the surface. The fluorescence profile ranged between 0.08 mg Chla m^{-3} in SURF and 0.39 m^{-3} at CML (52 m). Microalgae were almost absent. The highest zooplankton and detritus biomass values were registered in COL (average ~ 85 m, 35 and 22 mg DW m^{-3}, respectively), and the lowest values in SURF (4.1 and 0.8 mg DW m^{-3}). Zooplankton biomass shows a strong dominance of gelatinous organisms in all strata (42.5 % in CML and 54.2 % in COL) (Fig. 3a–c). Crustaceans represent 30 % of zooplankton biomass in CML but were low in COL (4.6 %) and SURF (0.7 %).

St04 is within the Bay of Marseille (Fig. 4d). The water column presents a homogeneous temperature profile and a shallow halocline at 6 m. The fluorescence profile presents values of 0.6 mg Chla m^{-3} in SURF and a maximum of 0.83 mg Chla m^{-3} at CML (33 m). Higher biomass of detritus and microalgae were observed in the CML (50.5 and 30 mg DW m^{-3}, respectively) compared to SURF and COL. Inversely, zooplankton biomass was higher in COL (29.1 mg DW m^{-3} over the 48 m of the water column) compared to SURF and CML (26.9 and 19.6 mg DW m^{-3}, respectively). The zooplankton biomass was different among strata, characterized by highest contribution of gelatinous organisms and copepods in COL (20.3 and 74 %, respectively), whereas CML was dominated by crustaceans (55 %), and SURF by copepods (93 %) (Fig. 3a–c).

St09 is an offshore station in the north of the North Balearic Thermal Front (Fig. 4e). Both temperature and salinity profiles are homogeneous, although temperature displays a light thermocline at 22 m corresponding to the CML at the bottom of a surface mixed layer. The Chla profile shows high values (1.4 mg Chla m^{-3}) above the CML, and then

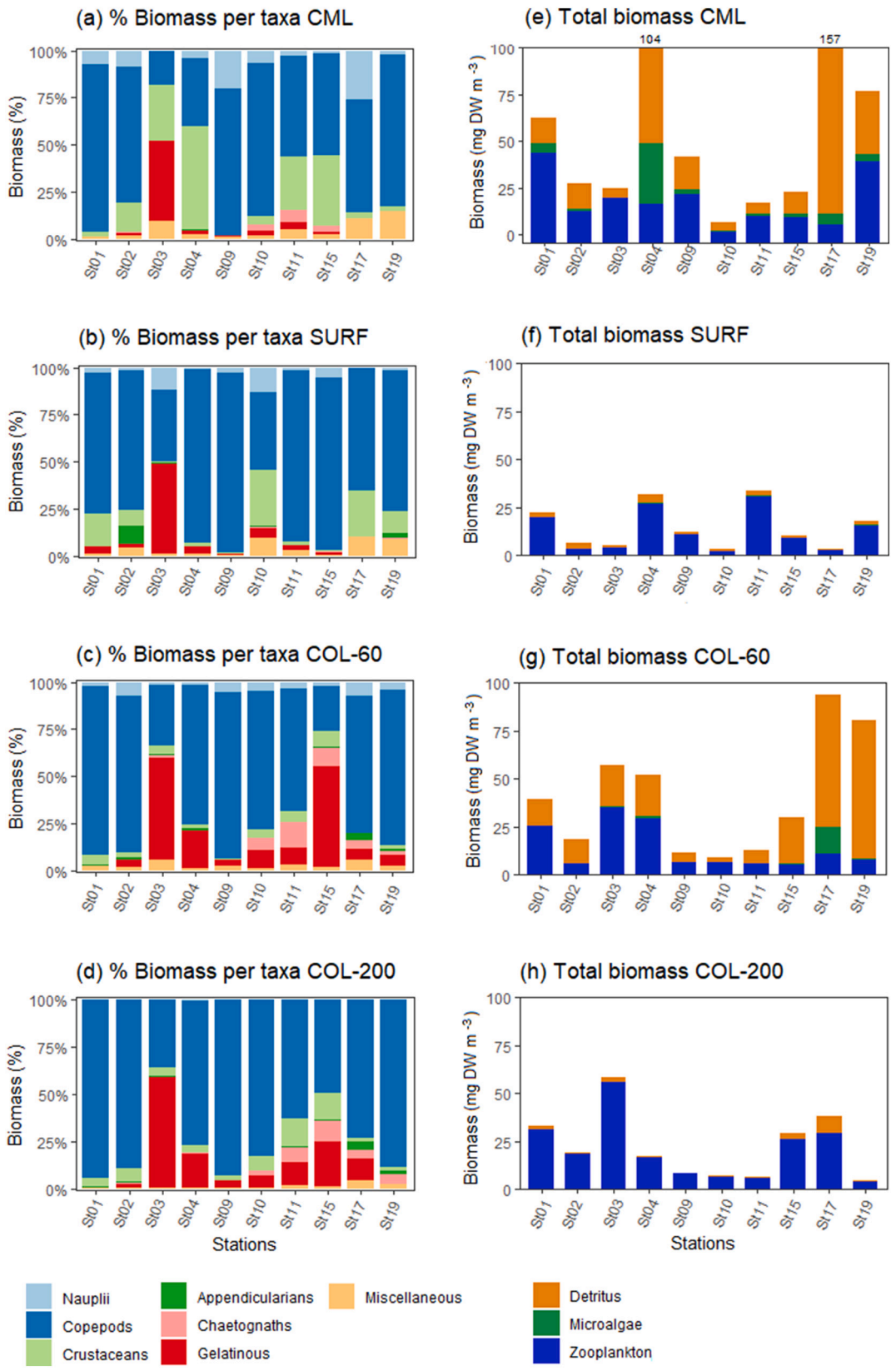


Fig. 3. *Left column*: Cumulated percentages of zooplankton taxa biomasses sampled at each station in the different strata (a) at the Chlorophyll maximum layer (CML), with the 60 μm mesh-size Hydro-Bios nets, (b) at the surface layer (SURF) with the 60 μm mesh-size Manta net, and in the whole water column with a vertical tow (c) of the 60 μm (COL-60) and (d) of the 200 μm (COL-200) mesh-size nets. *Right column*: Total biomass concentration (mg DW m^{-3}) (e) at the Chlorophyll maximum layer (CML), (f) at the surface layer (SURF), and for the integrated water column with (g) net 60 μm (COL-60) and (h) net 200 μm (COL-200). The colored bars, blue, green and orange, represent the cumulated contributions to the total biomass concentrations by zooplankton, microalgae and detritus, respectively. (For interpretation of the references to colo6r in this figure legend, the reader is referred to the web version of this article.)

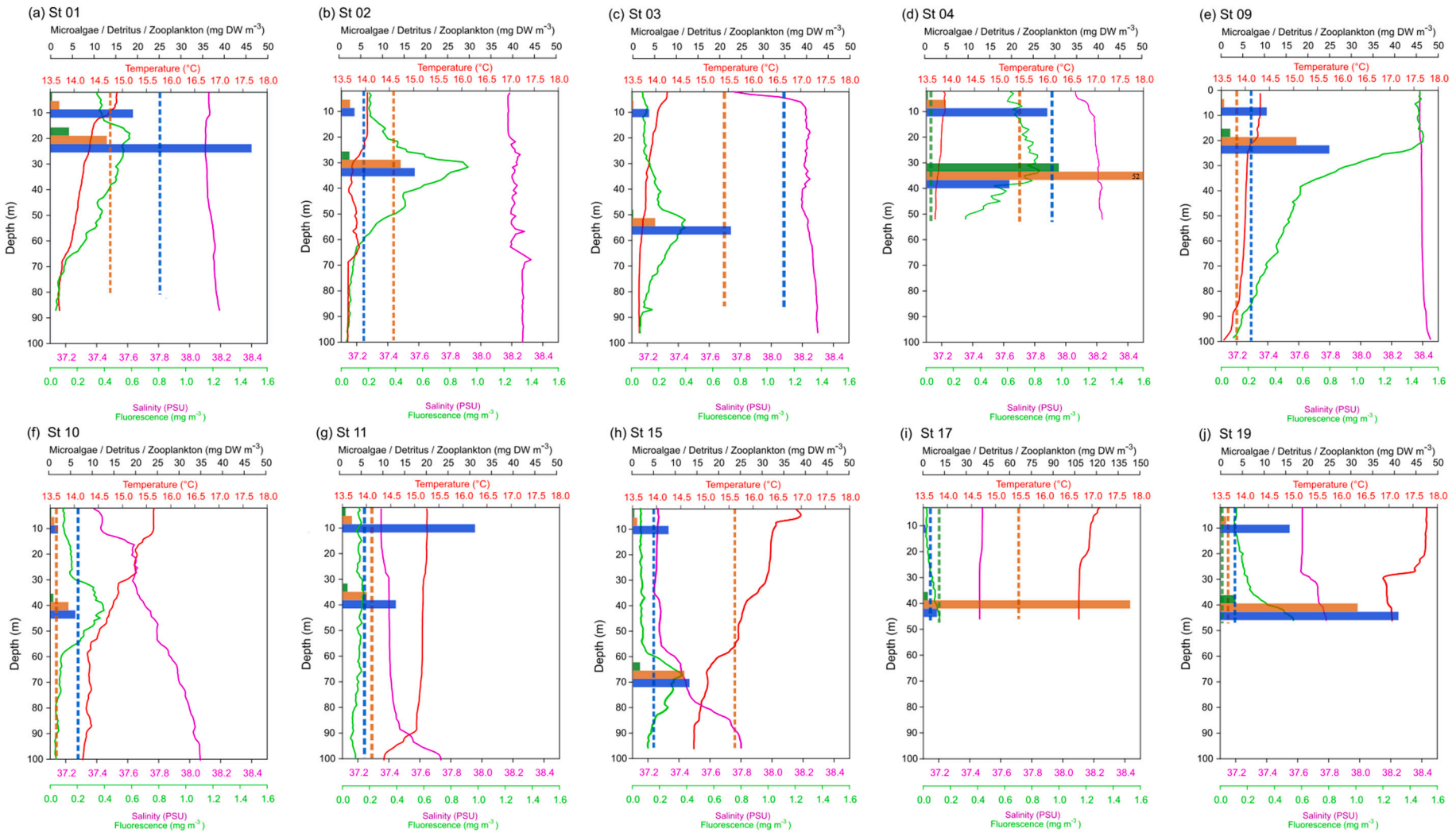


Fig. 4. Vertical profiles of oceanographic variables (temperature, red line; salinity, pink line; and chlorophyll, green line) for all stations (a to j) during the MERITE-HIPPOCAMPE cruise. Biomass of microalgae (green bars), detritus (orange bars) and zooplankton (blue bars) at the surface layer and at CML, and water column-averaged biomass (COL: bottom depth or 200 m deep to the surface) of microalgae (dotted green line), detritus (dotted orange line) and zooplankton (dotted blue line). (For interpretation of the references to color in this figure legend, the reader is referred to the web version of this article.)

sharply decreases down to 0.6 mg Chla m^{-3} at 39 m, and then to 0.1 mg Chla m^{-3} at 98 m. Very high biomass values of microalgae, detritus and zooplankton are recorded in the CML (respectively, 2.2, 16 and 25 mg DW m^{-3}). COL values (200–0 m averaged) for zooplankton and detritus biomass are more than twice as low as at CML. Although detritus and microalgae were negligible in SURF, SURF zooplankton was higher than the COL value. CML is characterized by high dominance of copepods and nauplii, with 78 and 20.3 % respectively, whereas SURF is dominated by copepods with 96 % (Fig. 3a–c).

St10 is situated southwards of the Balearic Front (Fig. 4f). The water column presents different strata with two thermoclines and haloclines respectively around 15 and 30 m, and a CML between 30 and 60 m (0.4 mg Chla m^{-3} at 42 m). Low biomasses of zooplankton, phytoplankton and detritus were found in all strata compared to other stations. COL presents higher zooplankton biomass (6.3 mg DW m^{-3}, on average over the upper 180 m) compared to CML (5.2 mg DW m^{-3}) and surface (2 mg DW m^{-3}). The detritus biomass at CML (4.2 mg DW m^{-3}) is twice as high as at SURF and COL. Microalgae were found only at the CML at a very low value. Zooplankton biomass composition appears different among strata (Fig. 3a–c). CML and COL are quite similar, with copepods dominating the biomass (81 and 74 % respectively). However, COL is differentiated by the contribution of gelatinous organisms and chaetognaths, with respectively 10 and 6 % of the biomass. SURF is characterized by the dominance of copepods, crustaceans, and nauplii (41, 30 and 13 %, respectively).

St11 is situated southwest of Sardinia (Fig. 4g). The water column presents a deep thermocline and a halocline around 88 m, and a homogeneous fluorescence profile with values between 0.1 and 0.2 mg Chla m^{-3}, with the maximum situated at 35 m. Low biomass values of microalgae were collected, with the highest value in the CML (1 mg DW m^{-3}). SURF surprisingly presents high values of zooplankton biomass (30.2 mg DW m^{-3}), more than twice as high as CML (13.8 mg DW m^{-3}) and six times higher than COL (5.8 mg DW m^{-3} averaged value over 182 m). Detritus biomass shows its highest values in COL (7.1 mg DW m^{-3}) compared to CML (5.4 mg DW m^{-3}), and low values at the SURF (2.6 mg DW m^{-3}). The zooplankton biomass presents high dominance of copepods at SURF (91 %) but not at the CML (54 %) due to a high proportion of crustaceans (28.3 %,), whereas in COL chaetognaths and gelatinous organisms were other major contributors (22.3 %) (Fig. 3a–c).

St15 is situated on the shelf of the Gulf of Hammamet on a 100 m depth sea floor (Fig. 4h). The vertical profiles show steps of decreasing temperature values with depth, associated with similar steps of increasing salinity, probably corresponding to different layers. The fluorescence profile shows a peak between 59 and 67 m, thus above the bottom boundary layer. Microalgae were found at the CML. The zooplankton biomass distribution is “classical”, with the highest biomass accumulated at the CML (13.1 mg DW m^{-3}), twice the average value of COL (5.25 mg DW m^{-3}, over the 85 m). Detritus biomass was higher in COL than in the CML (24.4 and 13 mg DW m^{-3}, respectively) and even higher compared to SURF (0.97 mg DW m^{-3}). Contributions of zooplankton taxa to biomass presented strong differences between the three strata (Fig. 3a–c). In CML, copepods and crustaceans dominate with 54 and 38 % respectively, whereas only copepods almost dominate SURF strata with 91 %. COL was characterized by the highest percentage of gelatinous organisms and chaetognaths, 54 and 9.2 %, respectively.

St17 is situated in the north of the Gulf of Gabès (Fig. 4i). The water column shows a light thermocline at 23 m and a homogeneous salinity profile. The fluorescence profile presents values of 0.02 mg Chla m^{-3} at the surface and a regular weak increase with depth down to the bottom. Microalgae are found at COL and CML. Comparable zooplankton biomasses are found in CML and COL (9.9 and 10.6 mg DW m^{-3}, respectively) whereas biomass is very weak in SURF. Very high detritus biomass cumulates in the CML (138.6 mg DW m^{-3}) in contrast with the lack of detritus in SURF (0.35 mg DW m^{-3}), whereas COL presented an intermediate value. The contribution of zooplankton taxa to biomass in the 3 strata slightly changed (Fig. 3a–c), although copepods dominate in all three. Gelatinous organisms and chaetognaths are recorded with 6 and 5 % for the COL but disappeared in SURF. The CML was characterized by a high presence of nauplii with 26 % and miscellaneous at 11 %.

St19 is the southern station in the Gulf of Gabès in shallow water (Fig. 4j). A thermocline and a halocline occur around 30 m. The fluorescence profile presents values of 0.11 mg Chla m^{-3} at the surface, and regularly increases down to the bottom 0.54 mg Chla m^{-3}. Microalgae were found at the CML. The detritus biomass at the CML (31.4 mg DW m^{-3}) is much higher than in COL (2 mg DW m^{-3}) and SURF. CML zooplankton biomass (41.6 mg DW m^{-3}) was double the biomass measured in SURF (16 mg DW m^{-3}) and was much higher than in COL. Copepods dominated zooplankton in all strata (Fig. 3a–c), whereas SURF differed by more crustaceans, CML by more miscellaneous, and COL by more gelatinous organisms.

3.4. Zooplankton and detritus biomass in different size-fractions in the CML

Fig. 5a shows the details of the distribution between sieved-size fractions of the biomass (see Section 3.2 and Table 2) collected with the Hydro-Bios net in the CML (Fig. 3e). In general, detritus were concentrated in the lowest size fractions, and absent above 1000 μm, and similarly, the Hydro-Bios net-retained microalgae accumulated in the smaller fractions, mostly in fraction 60–200 μm, plus in fraction 200–500 μm for St04 and 17. In contrast, zooplankton was distributed in all fractions with no clear pattern of dominance in a given size fraction among the stations. When detritus and microalgae biomasses were high in the first smaller fractions, zooplankton biomass was generally low in the largest fractions.

The percentages of zooplankton taxa biomasses (Fig. 5b) were dominated by copepods and nauplii in the first smaller fractions, except at stations St17 and St19 where other plankton (miscellaneous) contributed substantially. At all stations, except St04, the fraction 200–500 μm was strongly dominated by copepods (>71 %). At many stations, copepods still dominated the fraction 500–1000 μm (St01, 02, 03, 04, 09, 10, 19 > 80 %) and even the fraction 1000–2000 μm (St01, 02, 09, 10, 11). In the three largest fractions, crustaceans other than copepods could heavily dominate the biomass at some stations (St01, 02, 03, 09, 15 > 52 %), whereas at other stations, gelatinous organisms (St03, 10, 11, 19) and chaetognaths (St10, 11, 15) could make noticeable contributions. Appendicularians occur at some stations (St01, 04, 09) in the three smaller fractions, but with negligible biomass.

3.5. Comparisons of collected zooplankton and detritus biomasses in size fractions between CML and COL

In all stations, the contribution of the fraction 60–200 μm (Fig. 6a) to the total zooplankton biomass in COL-60 was weak, i.e., <9 %, except <17 % for St02, the biomass being distributed mostly in the fractions 200–500 μm and >500 μm but rather unequally and without a regular pattern between stations. The distribution patterns of zooplankton among size classes were not always entirely similar between COL-60 and CML (Figs. 6a and 5a), with the interesting exception of stations St03 and St15 where biomass concentrations increase with size-classes. It is noticeable that the contribution of the small fraction to the zooplankton biomass in CML was on average 2.5 times higher than in COL, and significantly different (Table 3).

In contrast to zooplankton distributions, detritus biomass in COL-60 (Fig. 6a) is concentrated in the two first size-classes, mainly the first one (60–200 μm), and a very low contribution for the fraction >500 μm (see average values on Table 3). This pattern is different from that of CML (Fig. 5a), where the contribution of the smaller fraction to biomasses was on average twice as low as in COL-60 (Table 2), whereas this contribution was much higher in the fractions above 200 μm. This shift

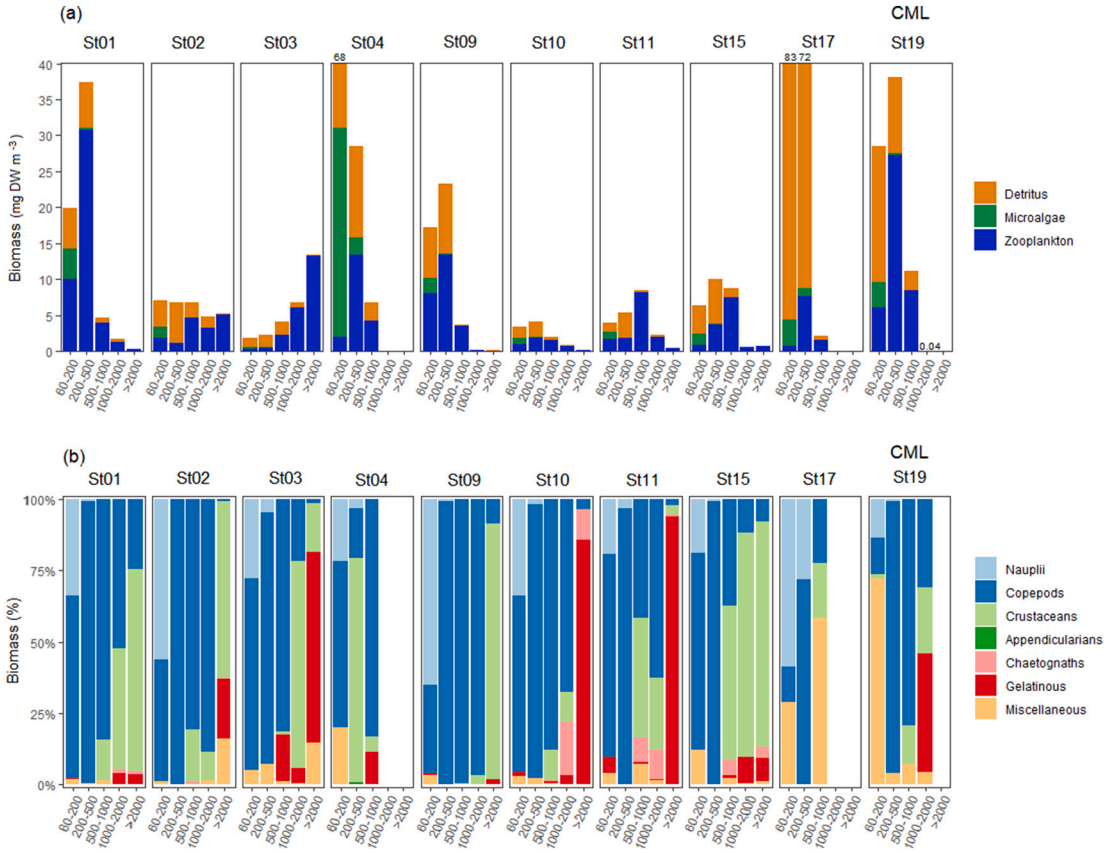


Fig. 5. Plankton and detritus biomasses collected with the Hydro-Bios tow using 60 μm mesh-size net at Chlorophyll Maximum layer (CML) at the different stations during the MERITE-HIPPOCAMPE cruise. (a) Cumulated biomass concentrations (mg DW m^{-3}) of zooplankton (blue), microalgae (green), and detritus (orange), and (b) cumulated percentages of zooplankton taxa biomasses, in the five size fractions. Note that: (1) fraction 1000–2000 μm is missing for stations St04 and St17, and the fraction >2000 μm is missing for stations St04, St17, and St19; (2) In the top panel for St04, 17, and 19 the numbers on the top of the bars the value reached by the cumulated biomass. (For interpretation of the references to color in this figure legend, the reader is referred to the web version of this article.)

in contributions of the detrital material in the successive size fractions was confirmed by significant differences between mean values (Table 3). In COL-60, when microalgae are collected, they are mostly present in the first class (Fig. 6a), a characteristic common with sampling in the CML.

In terms of taxonomic contributors to zooplankton biomass of COL-60 (Fig. 6b), nauplii and miscellaneous counterbalance, and sometimes dominate small copepods in the smaller fraction (60–200 μm). The fraction 200–500 μm is most often strongly dominated by copepods and completed by gelatinous organisms, excepted at St15 where gelatinous organisms dominate. Large copepods generally dominate the biomass in larger fractions (>500 μm), but some stations present high contributions of gelatinous organisms and crustaceans (St03, 10, 11, 15, and 17). The contribution of crustaceans is high in CML both for the total biomass and for the fractions above 500 μm. Inversely, the contribution of gelatinous organisms (and chaetognaths at a few stations) is much higher in COL-60 than in CML. These trends are confirmed by significant differences between mean values (Table 3).

3.6. Estimated zooplankton carbon demand and nitrogenous and phosphorous excretion

The daily carbon demand of zooplankton ranged from 0.6 to 6.9 mg C m^{-3} d^{-1} at the CML and from 0.5 to 5 mg C m^{-3} d^{-1} in COL, with the highest values at St19 for both strata (Fig. 7a–d). The mean values show no significant difference between the two strata (paired *t*-test; $p = 0.21$). When excluding the contribution of carnivorous forms (chaetognaths), this ZCD represented 2.7 to 22.7 % of the phytoplankton stock per day at the CML and between 3.1 and 25 % in COL, with no significant difference between the mean values of the two strata (paired *t*-test; $p = 0.29$). This grazing pressure showed no clear spatial trend at the CML, but in COL the values were on average significantly lower at the northern stations (St01 to St09; mean = 7.3 ± 3.3 %) than at the southern stations (St10 to St19; mean = 19.6 ± 6.0 %), in association with a parallel and significant decrease of the phytoplankton biomass from 27.4 ± 20.2 mg C m^{-3} in the north to 7.8 ± 6.1 mg C m^{-3} in the south (Mann-Whitney *U* tests; $p = 0.036$ and 0.0002, respectively).

The daily nitrogen and phosphorous excretion (Fig. 7b–e and c–f, respectively) varied between 4 and 908 μg N m^{-3} and between 0.5 and 131 μg P m^{-3}, respectively, and were not significantly different between the DCM and COL (paired *t*-test; $p > 0.3$). The zooplankton excretion represented a daily N and P recycling equivalent to 0.2 to 19 % of the DIN stock and to 0 to 21 % of the DIP stock. In both cases the highest values were found at the DCM of St01 in relation to the very high zooplankton biomass at this level (see Fig. 4a).

The contribution of the different size fractions to the ZCD was highly variable between stations and strata (Fig. 8). The contribution of the smaller fraction (<500 μm) to the ZCD is more often highly predominant or at least comparable to that of larger fractions (>500 μm), except at St19 for COL and at St03 in CML where most of the ZCD (>80 %) was from the larger fraction (>500 μm). On average, the relative contribution of the size-fractions to the ZCD showed no significant difference between CML and COL (paired *t*-test; $p > 0.1$).

Considering the whole size-fractions, copepods were the major contributors to the ZCD, except in the CML at St04 where other crustaceans made an equivalent contribution (46.9 % vs 47.3 % for copepods). Other crustaceans also made an important contribution to ZCD

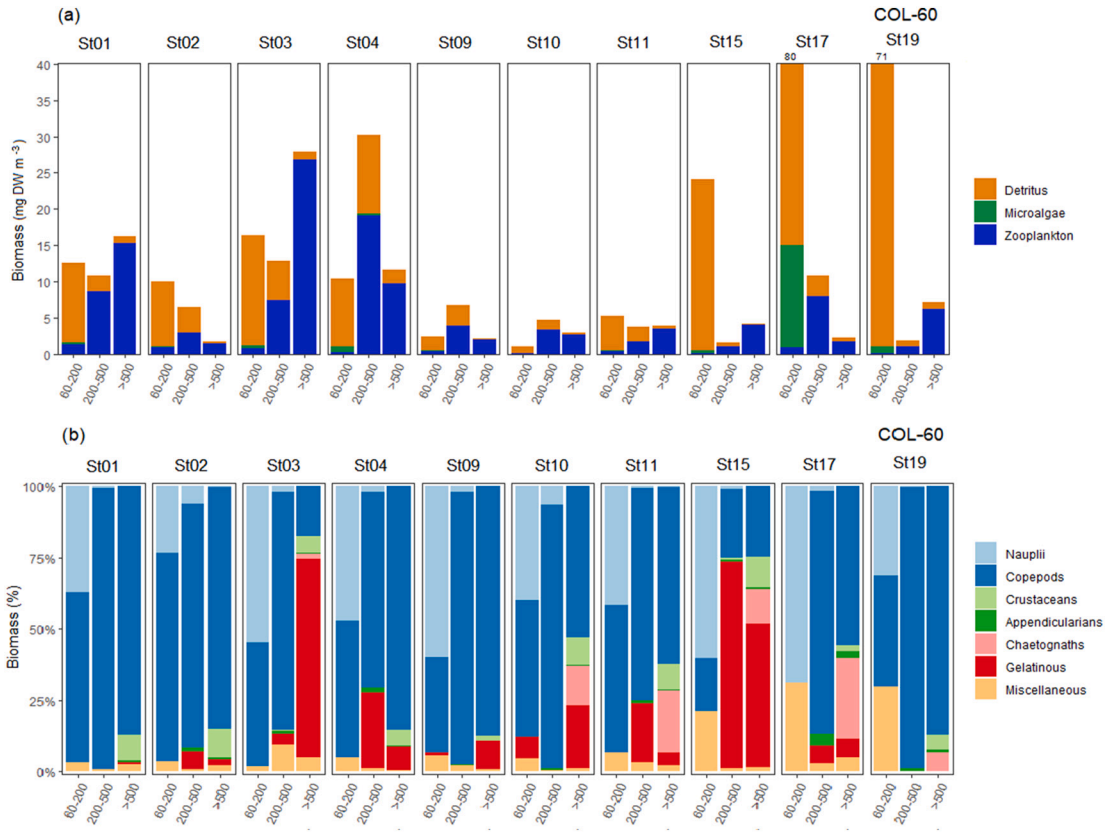


Fig. 6. Plankton and detritus biomasses collected with the vertical net tow using 60 μm mesh-size net (COL-60) at the different stations during the MERITE-HIPPOCAMPE cruise: (a) Cumulated biomass concentrations (mg DW m^{-3}) of zooplankton (blue), microalgae (green) and detritus (orange), and (b) cumulated percentages of zooplankton taxa biomasses, in the three size fractions. Note that: In the top panel for St17 and 19 the numbers on the top of the bars were the value reached by the cumulated biomass. (For interpretation of the references to color in this figure legend, the reader is referred to the web version of this article.)

in the CML at St15 (34.5 %) and St02 (25.4 %), whereas miscellaneous zooplankton was numerous in the CML at St19 (21.9 %) and gelatinous organisms in the COL at St03 (18.4 %) and St15 (28.5 %). On average, copepods contributed significantly more to the ZCD in COL than in CML, and the same trend was observed for gelatinous organisms and appendicularians, whereas nauplii contributed more to the ZCD in CML than in COL (paired *t*-test; $p < 0.05$). Overall, the total ZCD, and the contribution of size fractions or of taxa to this ZCD showed no clear spatial pattern.

The contributions of size-fractions or the taxa to N and P excretion rates were very similar to those of ZCD (i.e. similar to Fig. 8). All values for ZCD and excretion rates are presented in the supplementary material.

4. Discussion

4.1. Overview of the spatial patterns of environmental and biological variables during the MERITE-HIPPOCAMPE cruise

As the campaign took place over one month in the spring along a north-south transect with 10 stations sampled, either on the way out or on the way back, the environmental and biological characteristics of the stations did not enable a clear regional spatial pattern to be obtained, and local climatic and hydrodynamic conditions predominated over the spatial gradients. This means that the results obtained on the biotic compartment and ultimately in the contaminant studies must be interpreted in a mostly local context. Nevertheless, the present work contributes to broadening the characterization of plankton and detritus biomass distribution in the three different strata over several regions in the Mediterranean Sea.

We could highlight some global differences between the stations located north and south of the Balearic front, in terms of temperature and salinity values (see Fig. 2), in phytoplankton biomass in both COL and CML (see Fig. 7a and d), but only for COL in zooplankton grazing (see Fig. 7a). These patterns are probably linked to a late impact of the deep winter convection in the Gulf of Lion in 2019, a relatively convective and productive year (Margirier et al., 2020; Bosse et al., 2022), in the northern part of our transect (i.e. down to the Balearic front), whereas the generally low plankton productivity of the southern region can be increased by long-term mesoscale features isolated from the Atlantic current (Millot and Taupier-Letage, 2005), such as at our stations 10 and 11 (Rwawi et al., 2023), or by the impact of Saharan dust (Riandey et al., 2005; Feliú et al., 2020; Guieu et al., 2020) such as at our stations 10, 11 and 19 (Tedetti et al., 2023).

Some differences between coastal (St01, 03, 04, 15, 17, and 19) and open sea stations (St02, 09, 10, and 11) in terms of detritus and zooplankton biomasses (see Fig. 3g) could be linked in coastal stations to resuspension of sedimentary particulate matter induced by local wind-driven currents, and for zooplankton to limited deep vertical migration compared to open sea stations (since sampling was always performed during daylight, when most zooplankton are found in deeper water). However, the zooplankton biomass (total and in taxonomic contribution) does not show any specific gradient from north to south whatever the strata or the net considered (see Figs. 1b and 3). It is likely that the small number of sampled stations, especially in oceanic areas, as well as the long duration of our campaign do not allow identification of large north-south patterns that have nevertheless been widely documented for zooplankton in other studies (Mazzocchi et al., 2007; Siokou-Frangou et al., 2010; Nowaczyk et al., 2011; Saiz et al., 2014). Moreover, these studies have also mentioned that more local hydrodynamic or atmospheric conditions occur in addition to these large global patterns.

Table 3
Summary of the biomass for plankton and detritus, and size fractions during the MERITE-HIPPOCAMPE cruise. Mean and SD estimated of total biomasses for detritus, microalgae and zooplankton and percentage for size fractions and zooplankton taxa at CML and COL. Comparison between mean values based on paired *t*-test on non-transformed and log-transformed data (with respectively symbols * and ** for significant differences), and (1) significant but without reaching necessary conditions.

	CML		COL		*t*-Test on difference
	Mean	SD	Mean	SD	
Detritus (mg DW m^{-3})	29.08	42.26	20.23	20.52	
% 60–200	39.98	16.42	**69.52**	23.17	*, **
% 200–500	**47.07**	13.08	26.29	21.10	*
% >500 (n=7)	**16.47**	14.46	4.18	3.37	**
Microalgae (mg DW m^{-3})	5.26	9.36	5.81	16.95	
% 60–200	90.29	5.12	90.51	11.62	
% 200–500	9.71	5.12	9.49	11.62	
% >500 (n=7)	–	–	–	–	
Zooplankton (mg DW m^{-3})	20.40	13.33	13.69	11.46	
% 60–200	**13.53**	8.48	5.78	4.99	*, **
% 200–500	42.77	27.12	43.00	21.33	
% >500 (n=7)	54.22	31.58	51.22	23.50	
Total biomass in percentage					
Nauplii	**8.07**	8.54	3.57	2.54	(1)
Copepods	62.19	22.46	69.22	23.13	
Crustaceans	**17.98**	18.80	3.57	2.54	**
Chaetognaths	1.35	2.19	**4.01**	4.65	**
Appendicularians	0.06	0.17	**0.97**	1.01	(1)
Gelatinous	5.49	13.09	**16.04**	20.79	**
Miscellaneous	4.86	4.88	2.62	1.76	
Biomass fraction 60-200 in percentage					
Nauplii	34.84	18.57	46.33	14.42	
Copepods	48.94	22.87	41.57	20.67	
Crustaceans	0.14	0.44	0.01	0.03	
Chaetognaths	–	–	–	–	
Appendicularians	0.01	0.05	–	–	
Gelatinous	0.74	1.68	0.86	2.39	
Miscellaneous	15.33	22.03	11.23	11.44	
Biomass fraction 200–500 in percentage					
Nauplii	4.37	8.50	2.22	2.25	
Copepods	86.26	25.66	80.64	22.14	
Crustaceans	7.86	24.86	0.09	0.18	
Chaetognaths	–	–	–	–	
Appendicularians	0.08	0.25	**1.16**	1.19	(1)
Gelatinous	0.00	0.00	13.62	22.66	
Miscellaneous	1.43	2.44	2.26	2.74	
Biomass fraction >500 in percentage (n=7)					
Nauplii	0.02	0.04	0.03	0.04	
Copepods	59.19	28.82	64.51	26.69	
Crustaceans	**26.26**	18.14	6.87	3.35	**
Chaetognaths	3.08	3.53	8.40	10.27	
Appendicularians	0.01	0.01	**0.66**	0.67	(1)
Gelatinous	8.51	15.79	17.40	23.83	
Miscellaneous	2.94	3.41	2.13	1.73	

Bold characters indicate higher significant mean values.

For each station, our study strategy enabled us to identify vertical gradients provided that recent local climatic and hydrodynamic conditions did not lead to excessive mixing (see Fig. 4). Some stations (St01, 02, 03, 10, and 15) showed a rather typical stratification with clear vertical physical gradients and a maximum of chlorophyll, but this was not systematically reflected in the zooplankton biomasses. For various reasons, other stations did not show clear stratification. Station 04 had among the highest zooplankton biomass at the surface, probably related to a homogenization of the water column. Very shallow coastal stations in Tunisia showed accumulations of Chl*a* and zooplankton in a CML just above the bottom (St17 and St19). This phytoplankton biomass bulk above the bottom where zooplankton accumulates as well is a phenomenon also encountered in the Gulf of Lion (Espinasse et al., 2014). These Tunisian coastal stations (St15, 17, and 19) did not show high zooplankton concentrations in the water column compared to the northern coastal stations (St01, 03, and 04). This may be more related to their high detritus load than to differences in community structure when compared to the northern coastal stations. This detritus load may be a consequence of mixing and retention due to the high tidal currents in the Gulf of Gabès (Béjaoui et al., 2019).

The oceanic offshore stations presented a quite different pattern for the reasons explained below. Station 09 is located in the usual area of the deep-convection (Margirier et al., 2020). Although it was visited at the end of the survey (8–9 May), which was a little more than one month after the peak of the phytoplankton bloom observed at the end of March, it was the richest station in Chla, nitrate and silicate from the whole MERITE-HIPPOCAMPE cruise (Tedetti et al., 2023). Station 09 had a true mixed layer above the CML up to the surface, inducing higher Chla and zooplankton concentrations in CML and SURF, compared to COL (see Fig. 4e). Although the stratification appeared quite moderate (almost homogeneous temperature and salinity), the high chlorophyll in the layer 0–25 m might be due to previous steps of stratification and to mesoscale structures in this area in this period (Rwawi et al., 2023). Similar high zooplankton concentrations present in the upper layer in the post-bloom phase in the deep-convection area have already been described by Donoso et al. (2017). Station 02 is an oceanic station, situated in the broad periphery of the deep convection area (following Donoso et al., 2017), very close to the coast but also impacted by other different phenomena: intrusions of the northern current, hydrodynamic processes linked to the shelf break, and coastal impacts. This station sampled in the early phase of the cruise, under very bad weather conditions, presented a clear CML, despite a homogeneous physical structure. It is separated from the open ocean by the North Current and is not much affected by deep convection due to this natural barrier (Millot and Taupier-Letage, 2005). Zooplankton sampling at stations 10 and 11 in the western oceanic waters of Sardinia was performed with a time lag of one day and occurred respectively 2 and 3 days after a dust event (22 April). The zooplankton biomass and taxonomic structure showed an interesting contrast between these two stations, particularly with differences in surface (Figs. 3b and f; 4f and g), which could be consistent with zooplankton quick response to dust effect in a few days (Feliú et al., 2020). In contrast, differences in CML (Fig. 3a and e; Fig. 4f and g), not comparable to those observed at the surface, might be rather due to an additional specific 3D-mesoscale context of each station (Rwawi et al., 2023) impacting the vertical structure and differentiating the SURF and CML layers (see Fig. 4f and g), and the integrated values over the water column appeared buffered (Figs. 3c and g; 4f and g). For the oceanic station 11, the water column seems very homogeneous down to 90 m, with a very low Chla maximum, and the low zooplankton biomass from the vertical net in the upper 200 m is due to the very low biomass below 90 m. The very high value for zooplankton at the surface may be due to enhanced productivity since a high density of copepodites stages was observed (Makhlouf, pers. comm.).

4.2. Biological specificities of the CML

Due to the sampling strategy centered on the CML layer for measurements of contaminant contents in plankton, our focus on zooplankton characterization in the CML appears to be unique compared to previous regional studies in the Mediterranean Sea. Zooplankton net sampling is usually carried out by vertical net tows in the epipelagic zone (0–200 m) or just under the surface layer when studying the hyponeuston. These two types of sampling were also carried out during the MERITE-HIPPOCAMPE cruise to allow better characterization of the CML by comparisons with other strata.

At the scale of the basin, this comparison shows first of all an accumulation of detritus most often occurring at the CML, whereas SURF always presented the lowest detritus loads (see Fig. 4). Sometimes the CML was also a layer of accumulated microphytoplankton, mostly chain-aggregated and/or linked to detritus e.g. station 04 (see Fig. 4d). Among

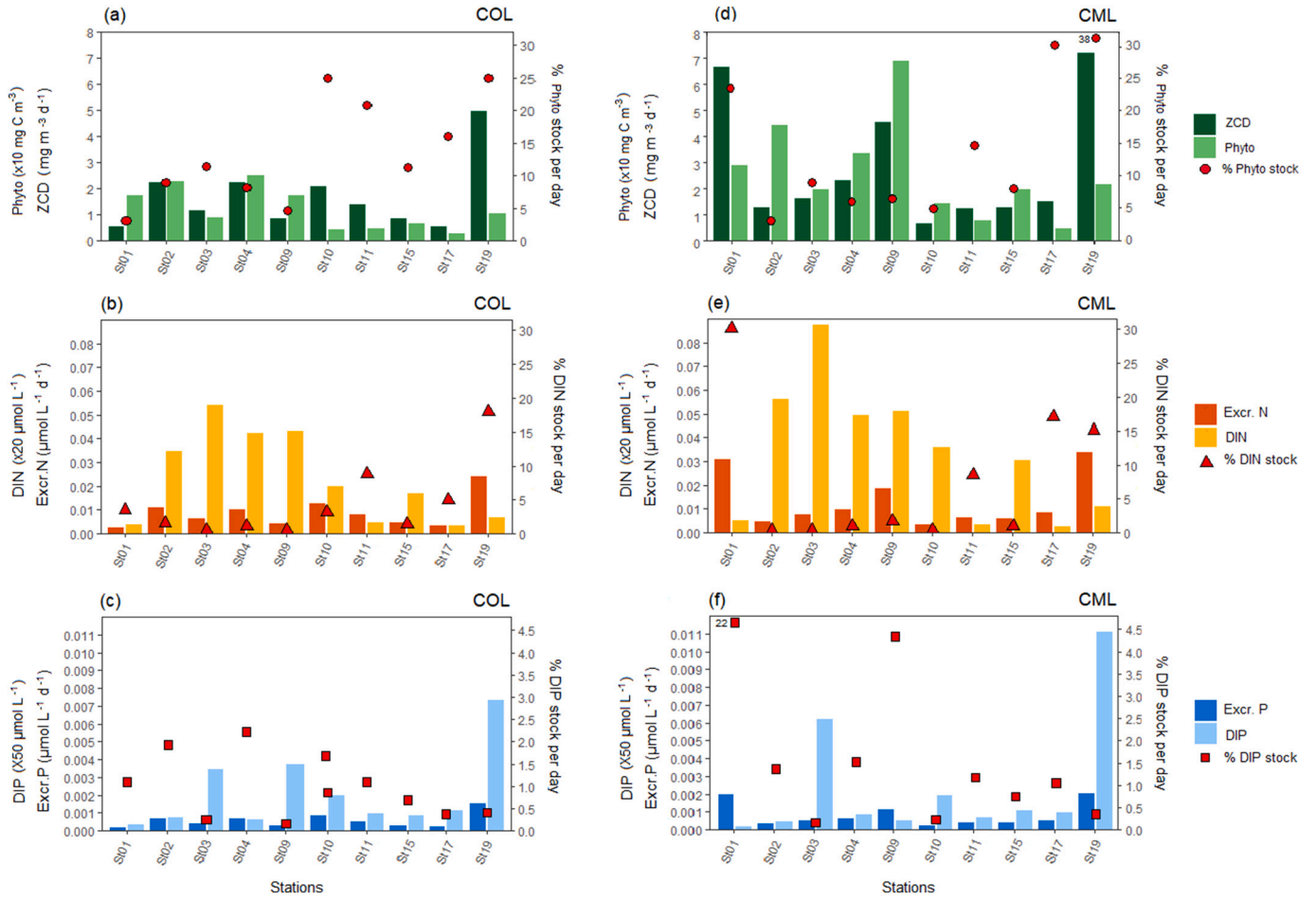


Fig. 7. Zooplankton carbon demand and phytoplankton stock, and percentage on the ratio (a, d), nitrogen excretion and DIN stock, and percentage on the ratio (b, e), phosphorous and DIP stock, and percentage on the ratio (c, f), respectively for COL (a, b, c) and CML (d, e, f). Note: In panel (f) the number for station 01 gives the value of %DIP stock out of scale.

all stations, zooplankton biomass was on average higher at the CML than in COL and SURF (respectively 1.5 and 1.7 times higher), but the differences between the 3 strata were not statistically significant due to very high variability. According to the stratification and the intensity of the chlorophyll peak around the identified CML in each station profile, we can indeed distinguish 4 cases: (1) no accumulation of zooplankton at the CML when the peak is not well-formed (St04, 11, and 17), (2) accumulation of zooplankton at the CML when the peak is well-formed (St01, 02, 15, and 19) but also (3) no accumulation despite a well-formed peak (St03 and 10), and finally (4) the case of station 09 is a bit different with a high concentration of zooplankton at the CML but with a 0–25 m layer quasi-uniformly rich in Chl*a*.

Our observations were not dedicated to the fine characterization of vertical profiles of phytoplankton, marine snow, and zooplanktonic groups, as shown in recent studies such as those described by several authors (e.g. Möller et al., 2012; Lombard et al., 2019; Briseño-Avena et al., 2020) using combinations of video sensors and net hauls enabling correlation of the aggregation layers to detrital and planktonic particles. However, our observations can be analyzed in the light of patterns described in these articles. Accumulation of detritus (marine snow) and large phytoplankton the most often slightly below the CML has been already documented in many situations. Very often, accumulation of zooplankton occurred as well (Nowaczyk et al., 2011; Möller et al., 2012; Espinasse et al., 2014; Saiz et al., 2014; Fender et al., 2019; Briseño-Avena et al., 2020), but was quite variable between taxa as shown by video observations (Möller et al., 2012; Briseño-Avena et al., 2020). In particular the aggregation of nauplii, copepodites and small copepods at the CML was already described during the stratification period in the Mediterranean (Alcaraz, 1985, 1988; Alcaraz et al., 2007; Sabatés et al., 2007, 2008; Olivar et al., 2010; Nowaczyk et al., 2011; Saiz et al., 2014), showing that this chlorophyll-rich layer constitutes a favorable habitat for the reproduction of copepods, particularly in oligotrophic conditions, where the CML can be considered as an "oasis" to sustain secondary production (Saiz et al., 2014). The high biomass of crustaceans recorded in the CML (mainly euphausiids larvae) may be explained by an adaptation of their vertical migration to track the most favorable trophic conditions, as reported in several studies (Sameoto, 1986; Guglielmo et al., 2011; Granata et al., 2020).

Inversely, gelatinous filter feeders (appendicularians, salps and doliolids) seem to avoid the CML, in agreement with many previous observations (Fenaux, 1968; Paffenhöfer et al., 1991; Briseño-Avena et al., 2020). In this layer, these filter-feeders might be disturbed by high accumulation of detritus and large algal cells leading to a decline in food quality (López-Urrutia et al., 2003) and/or to house clogging in the case of appendicularians (Tiselius et al., 2003; Feliú et al., 2020). The low abundance of chaetognaths and (presumably) of other gelatinous carnivorous organisms at the CML is rather surprising because we might have expected to high concentrations of these carnivorous organisms at a level where the stock of zooplankton prey would be more abundant. This could be related to day-night migration strategies, where these groups would be present in deeper waters during the day, thus avoiding larger predators (Granata et al., 2020). Their scarcity in our Hydro-Bios samples could be also linked to their active swimming out of the capture path of the net probably favored by a quicker net clogging compared to

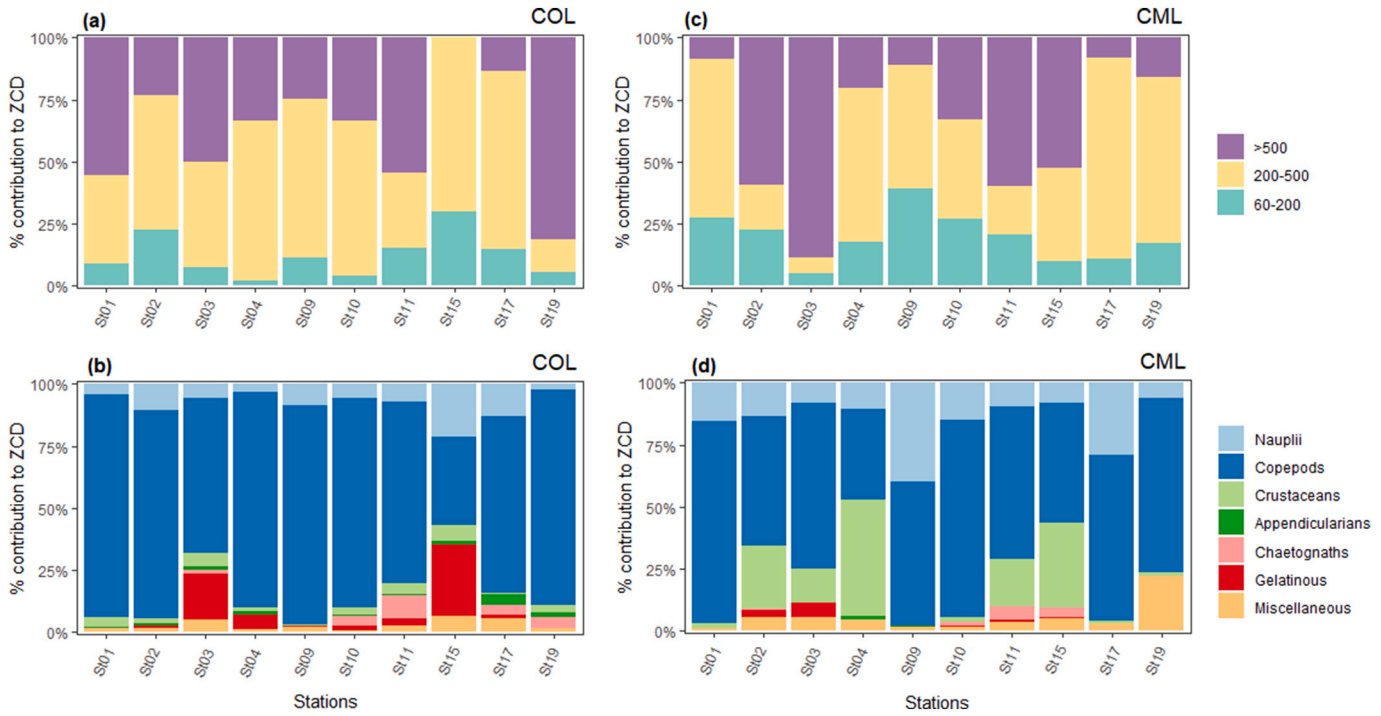


Fig. 8. Contributions in cumulated percentages of size-fractions (a, c) and zooplankton taxa (b, d) to the zooplankton carbon demand in COL (a, b) and CML (c, d).

the vertical net (Sameoto et al., 2000).

Such aggregation of matter and plankton linked to the CML has relevant implications for the functioning and structuring of the pelagic food web in the Mediterranean (Saiz et al., 2014). In our study, the high biomass of zooplankton over a wide size spectrum (from nauplii to large crustaceans) and its intense metabolic activity shown by high ZCD and excretion values are signs of increased trophic fluxes at this level. High densities of larvae of small pelagic zooplanktivorous fish such as anchovy have been reported as well (Sabatés et al., 2007, 2008; Olivar et al., 2010), showing the importance of CML for the trophic transfer of matter and contaminants towards higher trophic levels.

4.3. Characterizing the biota in size fractions to interpret biogeochemical and contaminant fluxes

The first characteristic of our Hydro-Bios samples is the high proportion of detritus, mainly in the size-fractions below 500 μm at all stations. Thus, the interpretation of contaminant levels in these fractions must be done cautiously to take account of a potential bias linked to these detritus content which may have various (mineral or organic) origins. In this paper, we have not gone into a detailed description of the nature of the detritus particles. These detritus probably have different sources and compositions in the coastal zone (resuspension of inorganic and organic particles from the sediment in addition to pelagic production of detritus particles) and the offshore zone (pelagic detritus particles to which may be added particles from atmospheric inputs). As mentioned in Section 4.2, patterns of vertical distributions of detrital particles which accumulate below the productive layer in the water column have already been well documented. This may have consequences for the biogeochemical cycles of contaminants and their accumulation/transfer processes in planktonic food webs in the Mediterranean Sea. Firstly, suspended particles (microphytoplankton and detrital particles) represent active surfaces for the adsorption and absorption of hydrophobic contaminants (Castro-Jiménez et al., 2021). Secondly, these suspended particles are also the site of intense microbial activity (Dolan and Marrasé, 1995; Azam and Long, 2001) which can certainly play a role in the accumulation and transfer of contaminants (da Fonseca et al., 2022; Chifflet et al., 2023), some components of which, such as ciliates, are known to be the preferred prey of mesozooplankton (Saiz and Calbet, 2011). And thirdly, a large part of these particles will sink (depending of their size and shape) and will export matter and contaminants into deeper layers (Bouloubassi et al., 2006; Bacosa et al., 2020) potentially integrated in the mesopelagic food-web (Romero et al., 2018). In the case of our MERITE-HIPPOCAMPE cruise, the fractions below 500 μm were much more impacted by detritus and microalgae at St04 and St17 (>90 %) than at St01 and St09 (~50 %), which clearly induced differences in biochemical compositions (see Fig. 3 in Tesán-Onrubia et al., 2023 and Fig. 3 in Guigue et al., 2023) and contaminant levels (see Fig. 5a,c in Guigue et al., 2023; see Table S4 in Chifflet et al., 2023).

The second characteristic concerns the trophic types of the dominant zooplanktonic species within the two smallest fractions (60–200 and 200–500 μm) which modulate the associated impacts on estimate fluxes. In MERITE-HIPPOCAMPE, when these fractions presented zooplankton biomass dominated by herbivorous and omnivorous types (small copepods and nauplii, or small pteropods), they showed isotope ratios $\delta^{13}C/\delta^{15}N$ confirming a trophic level around 2 (Tesán-Onrubia et al., 2023), relatively higher trophic fluxes (our Figs. 5 and 7) and contaminant contents (see Fig. 5c in Guigue et al., 2023; see Fig. 2 and Table S4 in Chifflet et al., 2023), such as for stations St01, 04, 09, and 19. This key role of herbivorous zooplankton in contaminant transfer has been already demonstrated in high latitude ecosystems where a few species massively dominate (e.g. Foster et al., 2012).

The third characteristic concerns the large fractions. First, the sampling of these fractions in our study was certainly impacted by clogging with detritus and microphytoplankton, favoring net avoidance of large organisms, and inversely explains their higher proportion for stations with low biomasses of detritus and microphytoplankton (e.g. St03). Moreover, it is also crucial to define the dominant trophic types in planktonic fractions >500 μm. During MERITE-HIPPOCAMPE, these fractions were either marked by the presence of typical carnivores, mainly chaetognaths, hydromedusae and siphonophores (St03, 10, 11, see Fig. 5b), or the presence of large crustaceans dominated by euphausiids and decapods (St01, 02, 09 and 15). Increased proportions of

carnivorous zooplankton in largest size fractions compared to smallest fractions (<500 μm) strongly dominated by herbivorous/omnivorous organisms, were already reported in the Gulf of Lion (Espinasse et al., 2014) and in the Bay of Marseille (Tiano et al., 2014). It is noticeable that ZCD and excretion rates calculated for St03, 10 and 11 were the lowest, linked to the lower weight specific-rates of the larger organisms. This increased proportion of carnivorous forms in the two largest fractions agree with the trophic level (TL) derived from isotopic analyses on the same fractions (Tesán-Onrubia et al., 2023): mean TL around 2.5, with highest values also found at St10 and 11 (TL of 3.6 and 2.8, respectively), suggesting a high proportion of secondary consumers.

Taxonomic determination by very large groups would merit being further refined, especially for copepods whose trophic characteristics vary from pure herbivory to carnivory (Kouwenberg, 1994; Espinasse et al., 2014), and gelatinous plankton, which covers very different trophic groups, from large herbivorous filter feeders (salps, doliolids) to carnivores (jellyfish, siphonophores, ctenophores).

5. Conclusion

The choice of sampling in the CML for this study regarding the role of plankton as a contaminant pump was guided by the aims of (1) collecting a high biomass of plankton from the same location to measure levels of a wide range of contaminants, and over a broad spectrum of planktonic size fractions, and (2) being located in an important area for pelagic trophic interactions in both the coastal and marine areas. The present paper has characterized the nature of the particles and zooplankton collected by the nets at depth and demonstrated the similarities and differences of this planktonic community to that of the water column.

The different distribution patterns of planktonic biomass encountered among the different stations during the MERITE-HIPPOCAMPE campaign should make it possible to compare contrasted situations of the accumulation or not of contaminants in the planktonic food web according to the pattern of these distributions.

By looking at the different size fractions of zooplankton that reflect different trophic levels (Tesán-Onrubia et al., 2023), we have shed new light on the processes of accumulation (or not) of contaminants, particularly in relation to studies where the zooplankton is either taken as a whole (Battuello et al., 2016, with the whole of the zooplankton caught by a mesh size net of 300 μm) or based on particular taxa but requiring their selective collection (Ndah et al., 2022). The method described in this paper, which characterizes successive fine size classes, provides an additional dimension for understanding the functioning of planktonic food webs in contaminant accumulation processes.

CRediT authorship contribution statement

All the authors who participated in the MERITE-HIPPOCAMPE project certify having contributed significantly to the work, to the preparation and sampling strategy, field work, laboratory analyses and/or data processing and interpretation, writing, or revision of the manuscript.

Conception and design of study: MP MT FC
Acquisition of data: PFG MP LG NM MT FC
Analysis and/or interpretation of data: PFG MP LG NM MT FC
Drafting the manuscript: PFG MP LG NM MT FC
Revising/editing the manuscript: PFG MP LG NM MT FC
Project administration and funding acquisition: MP MT FC

Declaration of competing interest

The authors declare that they have no known competing financial interests or personal relationships that might appear to influence the work reported in this paper.

Data availability

All data from the MERITE-HIPPOCAMPE cruise (doi:10.17600/18000900; Tedetti and Tronczynski, 2019) is stored in the MISTRALS-SEDOO database (https://mistrals.sedoo.fr/MERITE/) and will be made publicly accessible once all the articles related to the cruise are published in the present special issue. In the meantime, data can be obtained upon request from the corresponding author. In addition, navigation data and CTD profiles from the MERITE-HIPPOCAMPE cruise are available via the IFREMER/SISMER database (https://data.ifremer.fr/SISMER).

Acknowledgements

The MERITE-HIPPOCAMPE cruise was organized and supported by the French Oceanographic Fleet (FOF), CNRS/INSU, IFREMER, IRD, the Tunisian Ministry of Agriculture, Water Resources and Fisheries and the Ministry of Higher Education and Scientific Research of Tunisia. We are grateful to the captains and crew of the R/V Antea for their help and assistance during the cruise, as well as the scientific crew for help in collecting and processing net samples on board. Zooplankton analyses were realized on the Microscopy and Imaging platform of MIO, which is partly funded by the European FEDER Fund (project no. 1166-39417).

Our thanks to all the participants involved in the MERITE HIPPOCAMPE project, in particular those taking part in the cruise and/or sharing constructive discussions: Sirine Amri, Malika Bel Hassen, Daniela Banaru, Sana Ben Ismail, Nagib Bhairy, Ismail Boudriga, Nicolas Briant, Sandrine Chifflet, Mohamed Nejib Daly Yahia, Thibault de Garidel-Thoroni, Karine Desboeufs, Boris Espinasse, Cédric Garnier, Catherine Guigue, Joel Knoery, Deny Malengros, Marouan Meddeb, Olivier Pringault, Marianne Quemeneur, Olivier Radakovitch, Christophe Ravel, Asma Sakka Hlaili, Cherif Sammari, Bastien Thomas, Javier Angel Tesán Onrubia, Jacek Tronczynski, Nourredine Zaaboub. We also acknowledge contributions of the reviewer and the associate editor for their constructive comments and suggestions.

Pamela Fierro González was supported by a Becas-Chile N°72190675 PhD scholarship by the National Agency for Research and Development (ANID), Government of Chile.

References

Alcaraz, M., 1985. Vertical distribution of zooplankton biomass during summer stratification in the Western Mediterranean. In: Gibbs, P.E. (Ed.), Proceedings of the 19th European Marine Biology Symposium. Cambridge University Press, Cambridge, Plymouth, Devon, pp. 135–143.

Alcaraz, M., 1988. Summer zooplankton metabolism and its relation to primary production in the Western Mediterranean. In: Minas, H.J., Nival, P. (Eds.), Oceanographie Pelagique Mediterraneenne, Oceanologica Acta, 9, pp. 185–191.

Alcaraz, M., Calbet, A., Estrada, M., Marras, C., Saiz, E., Trepat, I., 2007. Physical control902 of zooplankton communities in the Catalan Sea. Prog. Oceanogr. 74 (2–3), 294–312. https://doi.org/10.1016/j.pocean.2007.04.003.

Alekseenko, E., Thouvenin, B., Tronczyński, J., Carlotti, F., Garreau, P., Tixier, C., Baklouti, M., 2018. Modeling of PCB trophic transfer in the Gulf of Lions; 3D coupled model application. Mar. Pollut. Bull. 128, 140–155. https://doi.org/10.1016/j.marpolbul.2018.01.008.

Alldredge, A., 1998. The carbon, nitrogen and mass content of marine snow as a function of aggregate size. Deep-Sea Res. I Oceanogr. Res. Pap. 45, 529–541. https://doi.org/10.1016/S0967-0637(97)00048-4.

Anderson, M.J., Gorley, R.N., Clarke, K.R., 2008. Guide to Software And Statistical Methods, p. 218.

Azam, F., Long, R.A., 2001. Sea snow microcosms. Nature 414, 495–498. https://doi.org/10.1038/35107174.

Bacosa, H.P., Kamalanathan, M., Cullen, J., Shi, D., Xu, C., Schwehr, K.A., Hala, D., Wade, T.L., Knap, A.H., Santschi, P.H., Quigg, A., 2020. Marine snow aggregates are enriched in polycyclic aromatic hydrocarbons (PAHs) in oil contaminated waters: insights from a mesocosm study. JMSE 8, 781. https://doi.org/10.3390/jmse8100781.

Battuello, M., Brizio, P., Mussat Sartor, R., Nurra, N., Pessani, D., Abete, M.C., Squadrone, S., 2016. Zooplankton from a North Western Mediterranean area as a model of metal transfer in a marine environment. Ecol. Indic. 66, 440–451. https://doi.org/10.1016/j.ecolind.2016.02.018.

Béjaoui, B., Ismail, S.B., Othmani, A., Hamida, O.B.A.-B.H., Chevalier, C., Feki-Sahnoun, W., Harzallah, A., Hamida, N.B.H., Bouaziz, R., Dahech, S., 2019.

Synthesis review of the Gulf of Gabes (eastern Mediterranean Sea, Tunisia): morphological, climatic, physical oceanographic, biogeochemical and fisheries features. Estuar. Coast. Shelf Sci. 219, 395–408.
Bosse, A., Testor, P., Coppola, L., Bretel, P., Dausse, D., Durrieu de Madron, X., Houpert, L., Labaste, M., Legoff, H., Mortier, L., D'Ortenzio, F., 2022. LION observatory data. In: SEANOE. https://doi.org/10.17882/44411.
Bouloubassi, I., Méjanelle, L., Pete, R., Fillaux, J., Lorre, A., Point, V., 2006. PAH transport by sinking particles in the open Mediterranean Sea: a 1 year sediment trap study. Mar. Pollut. Bull. 52, 560–571. https://doi.org/10.1016/j.marpolbul.2005.10.003.
Briseño-Avena, C., Prairie, J.C., Franks, P.J.S., Jaffe, J.S., 2020. Comparing vertical distributions of Chl-a fluorescence, marine snow, and taxon-specific zooplankton in relation to density using high-resolution optical measurements. Front. Mar. Sci. 7, 602. https://doi.org/10.3389/fmars.2020.00602.
Castro-Jiménez, J., Bănaru, D., Chen, C.-T., Jiménez, B., Muñoz-Arnanz, J., Deviller, G., Sempéré, R., 2021. Persistent organic pollutants burden, trophic magnification and risk in a pelagic food web from coastal NW Mediterranean Sea. Environ. Sci. Technol. 55, 9557–9568. https://doi.org/10.1021/acs.est.1c00904.
Chifflet, S., Briant, N., Tesán-Onrubia, J.A., Zaaboub, N., Amri, S., Radakovitch, O., Bănaru, D., Tedetti, M., 2023. Distribution and accumulation of metals and metalloids in planktonic food webs of the Mediterranean Sea (MERITE-HIPPOCAMPE campaign). Mar. Pollut. Bull. 186, 114384 https://doi.org/10.1016/j.marpolbul.2022.114384.
Chouvelon, T., Strady, E., Harmelin-Vivien, M., Radakovitch, O., Brach-Papa, C., Crochet, S., Knoery, J., Rozuel, E., Thomas, B., Tronczynski, J., Chiffoleau, J.-F., 2019. Patterns of trace metal bioaccumulation and trophic transfer in a phytoplankton-zooplankton-small pelagic fish marine food web. Mar. Pollut. Bull. 146, 1013–1030. https://doi.org/10.1016/j.marpolbul.2019.07.047.
da Fonseca, E.M., Gaylarde, C., Baptista Neto, J.A., Camacho Chab, J.C., Ortega-Morales, O., 2022. Microbial interactions with particulate and floating pollutants in the oceans: a review. Micro 2, 257–276. https://doi.org/10.3390/micro2020017.
Das, K., Debacker, V., Pillet, S., Bouquegneau, J.M., 2002. Heavy metals in marine mammals. In: Toxicology of Marine Mammals, pp. 147–179.
Dolan, J.R., Marrasé, C., 1995. Planktonic ciliate distribution relative to a deep chlorophyll maximum: Catalan Sea, N.W. Mediterranean, June 1993. Deep-Sea Res. I Oceanogr. Res. Pap. 42, 1965–1987. https://doi.org/10.1016/0967-0637(95)00092-5.
Donoso, K., Carlotti, F., Pagano, M., Hunt, B.P.V., Escribano, R., Berline, L., 2017. Zooplankton community response to the winter 2013 deep convection process in the NW Mediterranean Sea: zooplankton and winter deep convection. J. Geophys. Res. Oceans 122, 2319–2338. https://doi.org/10.1002/2016JC012176.
Espinasse, B., Harmelin-Vivien, M., Tiano, M., Guilloux, L., Carlotti, F., 2014. Patterns of variations in C and N stable isotope ratios in size-fractionated zooplankton in the Gulf of Lion, NW Mediterranean Sea. J. Plankton Res. 36, 1204–1215. https://doi.org/10.1093/plankt/fbu043.
Feliú, G., Pagano, M., Hidalgo, P., Carlotti, F., 2020. Structure and function of epipelagic mesozooplankton and their response to dust deposition events during the spring PEACETIME cruise in the Mediterranean Sea. Biogeosciences 17, 5417–5441. https://doi.org/10.5194/bg-17-5417-2020.
Fenaux, R., 1968. Distribution verticale de la fréquence chez quelques Appendiculaires. Rapports et Procès-verbaux des Réunions, Commission Internationale pour l'Exploration Scientifique de la Mer Méditerranée, 19, pp. 513–515.
Fender, C.K., Kelly, T.B., Guidi, L., Ohman, M.D., Smith, M.C., Stukel, M.R., 2019. Investigating particle size-flux relationships and the biological pump across a range of plankton ecosystem states from coastal to oligotrophic. Front. Mar. Sci. 6, 603. https://doi.org/10.3389/fmars.2019.00603.
Foster, K.L., Stern, G.A., Pazerniuk, M.A., Hickie, B., Walkusz, W., Wang, F., Macdonald, R.W., 2012. Mercury biomagnification in marine zooplankton food webs in Hudson Bay. Environ. Sci. Technol. 46, 12952–12959. https://doi.org/10.1021/es303434p.
Gorsky, G., Dallot, S., Sardou, J., Fenaux, R., Carré, C., Palazzoli, I., 1988. C and N composition of some northwestern Mediterranean zooplankton and micronekton species. J. Exp. Mar. Biol. Ecol. 124, 133–144. https://doi.org/10.1016/0022-0981(88)90116-5.
Gorsky, G., Ohman, M.D., Picheral, M., Gasparini, S., Stemmann, L., Romagnan, J.-B., Cawood, A., Pesant, S., Garcia-Comas, C., Prejger, F., 2010. Digital zooplankton image analysis using the ZooScan integrated system. J. Plankton Res. 32, 285–303. https://doi.org/10.1093/plankt/fbp124.
Granata, A., Bergamasco, A., Battaglia, P., Milisenda, G., Pansera, M., Bonanzinga, V., Arena, G., Andaloro, F., Giacobbe, S., Greco, S., Guglielmo, R., Spanò, N., Zagami, G., Guglielmo, L., 2020. Vertical distribution and diel migration of zooplankton and micronekton in Polcevera submarine canyon of the Ligurian mesopelagic zone (NW Mediterranean Sea). Prog. Oceanogr. 183, 102298 https://doi.org/10.1016/j.pocean.2020.102298.
Guglielmo, L., Minutoli, R., Bergamasco, A., Granata, A., Zagami, G., Antezana, T., 2011. Short-term changes in zooplankton community in Paso Ancho basin (Strait of Magellan): functional trophic structure and diel vertical migration. Polar Biol. 34, 1301–1317. https://doi.org/10.1007/s00300-011-1031-0.
Guieu, C., D'Ortenzio, F., Dulac, F., Taillandier, V., Doglioli, A., Petrenko, A., Barrillon, S., Mallet, M., Nabat, P., Desboeufs, K., 2020. Process studies at the air-sea interface after atmospheric deposition in the Mediterranean Sea: objectives and strategy of the PEACETIME oceanographic campaign (May–June 2017) (preprint). Biogeochem. Open Ocean. https://doi.org/10.5194/bg-2020-44.
Guigue, C., Tesán-Onrubia, J.A., Guyomarc'h, L., Bănaru, D., Carlotti, F., Pagano, M., Chifflet, S., Malengros, D., Chouba, L., Tronczynski, J., Tedetti, M., 2023. Hydrocarbons in size-fractionated plankton of the Mediterranean Sea (MERITE-HIPPOCAMPE campaign): concentrations and trophic transfer. Submitted, this special issue.
Khairy, M., Brault, E., Dickhut, R., Harding, K.C., Harkonen, T., Karlsson, O., Lehnert, K., Teilmann, J., Lohmann, R., 2021. Bioaccumulation of PCBs, OCPs and PBDEs in Marine Mammals From West Antarctica. Front. Mar. Sci. 8, 768715 https://doi.org/10.3389/fmars.2021.768715.
Kouwenberg, J.H.M., 1994. Copepod distribution in relation to seasonal hydrographics and spatial structure in the North-western Mediterranean (Golfe du Lion). Estuar. Coast. Shelf Sci. 38, 69–90. https://doi.org/10.1006/ecss.1994.1005.
Lehette, P., Hernández-León, S., 2009. Zooplankton biomass estimation from digitized images: a comparison between subtropical and Antarctic organisms: zooplankton biomass by digital images. Limnol. Oceanogr. Methods 7, 304–308. https://doi.org/10.4319/lom.2009.7.304.
Lombard, F., Boss, E., Waite, A.M., Vogt, M., Uitz, J., Stemmann, L., Sosik, H.M., Schulz, J., Romagnan, J.-B., Picheral, M., Pearlman, J., Ohman, M.D., Niehoff, B., Möller, K.O., Miloslavich, P., Lara-López, A., Kudela, R., Lopes, R.M., Kiko, R., Karp-Boss, L., Jaffe, J.S., Iversen, M.H., Irisson, J.-O., Fennel, K., Hauss, H., Guidi, L., Gorsky, G., Giering, S.L.C., Gaube, P., Gallager, S., Dubelaar, G., Cowen, R.K., Carlotti, F., Briseño-Avena, C., Berline, L., Benoit-Bird, K., Bax, N., Batten, S., Ayata, S.D., Artigas, L.F., Appeltans, W., 2019. Globally consistent quantitative observations of planktonic ecosystems. Front. Mar. Sci. 6, 196. https://doi.org/10.3389/fmars.2019.00196.
López-Urrutia, Á., Irigoien, X., Acuña, J., Harris, R., 2003. In situ feeding physiology and grazing impact of the appendicularian community in temperate waters. Mar. Ecol. Prog. Ser. 252, 125–141. https://doi.org/10.3354/meps252125.
Lovegrove, T., 1966. The determination of the dry weight of plankton and the effect of various factors on the values obtained. In: Some Contemporary Studies in Marine Science, pp. 407–420.
Margirier, F., Testor, P., Heslop, E., Mallil, K., Bosse, A., Houpert, L., Mortier, L., Bouin, M.-N., Coppola, L., D'Ortenzio, F., Durrieu de Madron, X., Mourre, B., Prieur, L., Raimbault, P., Taillandier, V., 2020. Abrupt warming and salinification of intermediate waters interplays with decline of deep convection in the Northwestern Mediterranean Sea. Sci. Rep. 10, 20923. https://doi.org/10.1038/s41598-020-77859-5.
Mazzocchi, M.G., Christou, E.D., Capua, I.D., Fernández de Puelles, M., Fonda-Umani, S., Molinero, J.C., Nival, P., Siokou-Frangou, I., 2007. Temporal variability of Centropages typicus in the Mediterranean Sea over seasonal-to-decadal scales. Prog. Oceanogr. 72, 214–232. https://doi.org/10.1016/j.pocean.2007.01.004.
Millot, C., Taupier-Letage, I., 2005. Circulation in the Mediterranean Sea. In: Saliot, A. (Ed.), The Mediterranean Sea, Handbook of Environmental Chemistry. Springer Berlin Heidelberg, Berlin, Heidelberg, pp. 29–66. https://doi.org/10.1007/b107143.
Möller, K., St John, M., Temming, A., Floeter, J., Sell, A., Herrmann, J., Möllmann, C., 2012. Marine snow, zooplankton and thin layers: indications of a trophic link from small-scale sampling with the Video Plankton Recorder. Mar. Ecol. Prog. Ser. 468, 57–69. https://doi.org/10.3354/meps09984.
Ndah, A.B., Meunier, C.L., Kirstein, I.V., Göbel, J., Rönn, L., Boersma, M., 2022. A systematic study of zooplankton-based indices of marine ecological change and water quality: application to the European marine strategy framework Directive (MSFD). Ecol. Indic. 135, 108587 https://doi.org/10.1016/j.ecolind.2022.108587.
Nowaczyk, A., Carlotti, F., Thibault-Botha, D., Pagano, M., 2011. Distribution of epipelagic metazooplankton across the Mediterranean Sea during the summer BOUM cruise. Biogeosciences 8, 2159–2177. https://doi.org/10.5194/bg-8-2159-2011.
Olivar, M.P., Emelianov, M., Villate, F., Uriarte, I., Maynou, F., Álvarez, I., Morote, E., 2010. The role of oceanographic conditions and plankton availability in larval fish assemblages off the Catalan coast (NW Mediterranean): larval fish assemblages off the Catalan coast. Fish. Oceanogr. 19, 209–229. https://doi.org/10.1111/j.1365-2419.2010.00538.x.
Paffenhöfer, G.-A., Stewart, T.B., Youngbluth, M.J., Bailey, T.G., 1991. High-resolution vertical profiles of pelagic tunicates. J. Plankton Res. 13, 971–981. https://doi.org/10.1093/plankt/13.5.971.
Riandey, V., Champalbert, G., Carlotti, F., Taupier-Letage, I., Thibault-Botha, D., 2005. Zooplankton distribution related to the hydrodynamic features in the Algerian Basin (western Mediterranean Sea) in summer 1997. Deep-Sea Res. I Oceanogr. Res. Pap. 52, 2029–2048. https://doi.org/10.1016/j.dsr.2005.06.004.
Romero, I.C., Sutton, T., Carr, B., Quintana-Rizzo, E., Ross, S.W., Hollander, D.J., Torres, J.J., 2018. Decadal assessment of polycyclic aromatic hydrocarbons in mesopelagic fishes from the Gulf of Mexico reveals exposure to oil-derived sources. Environ. Sci. Technol. 52, 10985–10996. https://doi.org/10.1021/acs.est.8b02243.
Rwawi, C., Hernandez-Carrasco, I., Tedetti, M., Rossi, V., 2023. Transport patterns and hydrodynamic context of the HIPPOCAMPE survey: implication for contaminant sources and distribution. In preparation for this special issue.
Sabatés, A., Salat, J., Palomera, I., Emelianov, M., Fernández De Puelles, M.L., Olivar, M. P., 2007. Advection of anchovy (Engraulis encrasicolus) larvae along the Catalan continental slope (NW Mediterranean). Fish. Oceanogr. 16, 130–141. https://doi.org/10.1111/j.1365-2419.2006.00416.x.
Sabatés, A., Zaragoza, N., Grau, C., Salat, J., 2008. Vertical distribution of early developmental stages in two coexisting clupeoid species, Sardinella aurita and Engraulis encrasicolus. Mar. Ecol. Prog. Ser. 364, 169–180. https://doi.org/10.3354/meps07461.
Saiz, E., Calbet, A., 2011. Copepod feeding in the ocean: scaling patterns, composition of their diet and the bias of estimates due to microzooplankton grazing during incubations. Hydrobiologia 666, 181–196. https://doi.org/10.1007/s10750-010-0421-6.
Saiz, E., Sabatés, A., Gili, J.-M., 2014. The zooplankton. In: Goffredo, S., Dubinsky, Z. (Eds.), The Mediterranean Sea. Springer Netherlands, Dordrecht, pp. 183–211. https://doi.org/10.1007/978-94-007-6704-1_11.

Sameoto, D., Wiebe, P., Runge, J., Postel, L., Dunn, J., Miller, C., Coombs, S., 2000. Collecting zooplankton. In: ICES Zooplankton Methodology Manual. Elsevier, pp. 55–81. https://doi.org/10.1016/B978-012327645-2/50004-9.

Sameoto, D.D., 1986. Influence of the biological and physical environment on the vertical distribution of mesozooplankton and micronekton in the eastern tropical Pacific. Mar. Biol. 93, 263–279. https://doi.org/10.1007/BF00508264.

Sieracki, C., Sieracki, M., Yentsch, C., 1998. An imaging-in-flow system for automated analysis of marine microplankton. Mar. Ecol. Prog. Ser. 168, 285–296. https://doi.org/10.3354/meps168285.

Siokou-Frangou, I., Christaki, U., Mazzocchi, M.G., Montresor, M., Ribera d'Alcalá, M., Vaqué, D., Zingone, A., 2010. Plankton in the open Mediterranean Sea: a review. Biogeosciences 7, 1543–1586. https://doi.org/10.5194/bg-7-1543-2010.

Strady, E., Harmelin-Vivien, M., Chiffoleau, J., Veron, A., Tronczynski, J., Radakovitch, O., 2015. 210Po and 210Pb trophic transfer within the phytoplankton–zooplankton–anchovy/sardine food web: a case study from the Gulf of Lion (NW Mediterranean Sea). J. Environ. Radioact. 143, 141–151. https://doi.org/10.1016/j.jenvrad.2015.02.019.

Tedetti, M., Tronczynski, J., Carlotti, F., Pagano, M., Sammari, C., Bel Hassen, M., Ben Ismail, S., Desboeufs, K., Poindron, C., Chifflet, S., Abdennadher, M., Amri, S., Bănarua, D., Ben Abdallah, L., Bhairy, N., Boudriga, I., Bourin, A., Brach-Papa, C., Briant, N., Cabrol, L., Chevalier, C., Chouba, L., Coudray, S., Daly Yahia, M.N., de Garidel-Thoron, T., Dufour, A., Dutay, J.-C., Espinasse, B., Fierro-González, P., Fornier, M., Garcia, N., Giner, F., Guigue, C., Guilloux, L., Hamza, A., Heimbürger-Boavida, L.-E., Jacquet, S., Knoery, J., Lajnef, R., Makhlouf Belkahia, N., Malengros, D., Martinot, P.L., Bosse, A., Mazur, J.-C., Meddeb, M., Misson, B., Pringault, O., Quéméneur, M., Radakovitch, O., Raimbault, P., Ravel, C., Rossi, V., Rwawi, C., Sakka Hlaili, A., Tesán Onrubia, J.A., Thomas, B., Thyssen, M., Zaaboub, N., Zouari, A., Garnier, C., 2023. Contamination of planktonic food webs in the Mediterranean Sea: setting the frame for the MERITE-HIPPOCAMPE oceanographic cruise (spring 2019). Mar. Pollut. Bull. 189, 114765 https://doi.org/10.1016/j.marpolbul.2023.114765.

Tesán-Onrubia, J.A., Tedetti, M., Carlotti, F., Tenaille, M., Guilloux, L., Pagano, M., Lebreton, B., Guillou, G., Fierro-González, P., Guigue, C., Chifflet, S., Garcia, T., Boudriga, I., Belhassen, M., Bellaaj-Zouari, M., Bănaru, D., 2023. Spatial variations of biochemical content and stable isotope ratios of size-fractionated plankton in the Mediterranean Sea (MERITE-HIPPOCAMPE campaign). Mar. Pollut. Bull. 189, 114787 https://doi.org/10.1016/j.marpolbul.2023.114787.

Tiano, M., Tronczyński, J., Harmelin-Vivien, M., Tixier, C., Carlotti, F., 2014. PCB concentrations in plankton size classes, a temporal study in Marseille Bay, Western Mediterranean Sea. Mar. Pollut. Bull. 89, 331–339. https://doi.org/10.1016/j.marpolbul.2014.09.040.

Tiselius, P., Petersen, J., Nielsen, T., Maar, M., Møller, E., Satapoomin, S., Tönnesson, K., Zervoudaki, T., Christou, E., Giannakourou, A., Sell, A., Vargas, C., 2003. Functional response of Oikopleura dioica to house clogging due to exposure to algae of different sizes. Mar. Biol. 142, 253–261. https://doi.org/10.1007/s00227-002-0961-z.

Van der Oost, R., Beyer, J., Vermeulen, N.P.E., 2003. Fish bioaccumulation and biomarkers in environmental risk assessment: a review. Environ. Toxicol. Pharmacol. 13, 57–149. https://doi.org/10.1016/S1382-6689(02)00126-6.

Weijs, L., Hickie, B., Blust, R., Covaci, A., 2014. Overview of the current state-of-the-art for bioaccumulation models in marine mammals. Toxics 2, 226–246. https://doi.org/10.3390/toxics2020226.

Wen, L.-S., Lee, C.-P., Lee, W.-H., Chuang, A., 2018. An ultra-clean multilayer apparatus for collecting size fractionated marine plankton and suspended particles. JoVE 56811. https://doi.org/10.3791/56811.